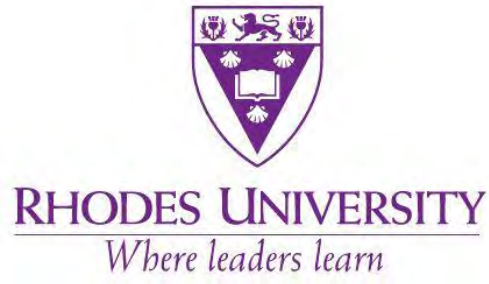

PETROGRAPHY, METAMORPHISM, DEFORMATION AND P-T CONDITIONS IN THE WESTERN ARM OF THE LUFILIAN ARC - ZAMBEZI, NORTHWESTERN ZAMBIA

By

Mwango Chilekwa

A thesis submitted in partial fulfillment of the requirements for the degree of

MASTER OF SCIENCE
(Exploration Geology Cwk/Thesis)

MSc Exploration Geology Program
Geology Department
Rhodes University
P.O. Box 94
Grahamstown 6140

South Africa

August, 2020

DECLERATION

I, MWANGO CHILEKWA, declare that this dissertation is my own work. It has not been submitted before for any degree or examination in any other University or tertiary institution. This is submitted as partial fulfilment of the Degree of Master of Science in Exploration Geology at Rhodes University.

Signature of the candidate……  ……

Date……21/08/2020……

DEDICATION

I wish to dedicate this to my wife Milimo Machila-Chilekwa and my son Mwango Musapa Chilekwa for their love and sacrifice throughout my study.

ABSTRACT

The Zambezi area in north-western Zambia is underlain by Neoproterozoic Katanga Supergroup and older, Archean to Mesoproterozoic Basement Supergroup rocks. The area lies within the Domes Region, which is a structural domain of the Lufilian Arc. The stratigraphic succession within Zambezi area is dominated by the Grand Conglomerate Formation (GC) and Mwashia Group which are the most extensive units, and the less abundant Lower and Upper Roan Groups of the Katanga Supergroup. They wrap around the domal Basement Supergroup units. The mineral assemblage of the Mwashia and the GC schists commonly contains garnet, anthophyllite and biotite. GC rocks show remnants of primary structures such as clasts and sedimentary features. Anthophyllite, garnet and biotite are the dominant Mg-Fe rich metamorphic minerals. However, these are iron rich for each mineral phase and has been attributed to iron rich protoliths.

The earliest recognised deformation episode (D1) formed NE-SW S1 foliations within GC which is consistent with the regional structural trend in the western Lufilian Arc. S1 was later affected by D2 that generated downward facing F2 folds and S2 foliations. The other associated feature to D2 is garnet that grew as the result of pro-grade metamorphism. The D3 deformation fabric is not developed and did not affect much of the structural geometry of the Zambezi area.

The peak assemblages of the Basement Supergroup and the Katanga Supergroup formed at mid-amphibolite facies conditions of 590 °C and 630 °C at an average pressure of 4.0 kbar. The Basement Supergroup has undergone retrograde metamorphism to greenschist facies condition indicated by presence of chlorite and also determined by biotite-anorthite isopleth in THERIAK DOMINO. At the eastern part of Zambezi area, the Katanga Supergroup rocks were retrogressed in the upper greenschist facies at about ~470°C and ~4.0 kbar due to isobaric cooling.

ACKNOWLEDGEMENTS

Professor Steffen Büttner is greatly appreciated for his supervision, encouragement and support throughout the course work and research.

Dr. Peter Mubanga Cheuka is greatly appreciated for correcting spellings and grammar.

It is a pleasure to thank my younger sister Chileshe Chilekwa-Silweya for the financial support rendered to me, to you I say thank you.

I wish to thank management for Anglo Exploration Zambia Limited for allowing me to use the geological data and support in for this work.

Professor Robin “Jock” Harmer, Ashley Goddard and the Geology Department team are greatly appreciated for the support and guidance before and from the onset of the program.

Lastly but not the least, I wish to thank the lab teams from Electron Microscopy Unit for the good work and support.

TABLE OF CONTENTS

LIST OF FIGURES

LIST OF TABLES

1. INTRODUCTION

1.1 GENERAL BACKGROUND

The Zambezi area, where the study was conducted lies within Zambia on the western arm of the Lufilian Arc (Figure 1). The Lufilian Arc is one of the Pan-African orogenic belts occurring between the Congo and Kalahari cratons (Figure 1). This belt formed during the Lufilian orogeny between the Neoproterozoic and the early Palaeozoic (Key et al., 2001). The Lufilian Arc has a convex shape and is approximately 850 km long (e.g. Kampunzu and Cailteux 1999; Cosi et al., 1992; Porada, 1989; Bumby and Guiraud, 2005), and it extends from Zambia in the east through the southern part of the Democratic Republic of Congo (DRC) and to northwest Zambia, and further south-westwards into Angola, Botswana and Namibia, where it links with the Damara Belt (Cosi et al., 1992).

The stratigraphy and geology of the western Lufilian Arc around the Zambezi area has not been studied before. The thesis presents the first information on the stratigraphy, geology, deformation and metamorphism of the Zambezi area. The study will show the stratigraphic correlation between the Zambezi area with the Katanga Supergroup described in the eastern and central parts of the Lufilian Arc.

Most of the deposits have mineralization occurring within 200 m interval of siliciclastic rocks from the base of the Katanga Supergroup which unconformably overly the granitic basement (Selley et al., 2005). A clear understanding of the geology and stratigraphy can be used for further exploration and discovery of similar deposits as those found on the eastern Lufilian Arc.

Metamorphism and deformation has great impact on the mineralisation style and occurrence. When units are metamorphosed and deformed, typical Copperbelt characteristics of the deposit are affected and sometimes obliterated. Hence, the exploration approach is done on new geological features as the result of metamorphism, alteration and deformation. The degree of metamorphism has been described to decrease eastwards from greenschist to amphibolite facies (Selley et al., 2005). The study will determine the condition of the regional metamorphism in the area using metamorphic mineral assemblages, thermodynamic modelling based on XRF analysis and mineral chemistry.

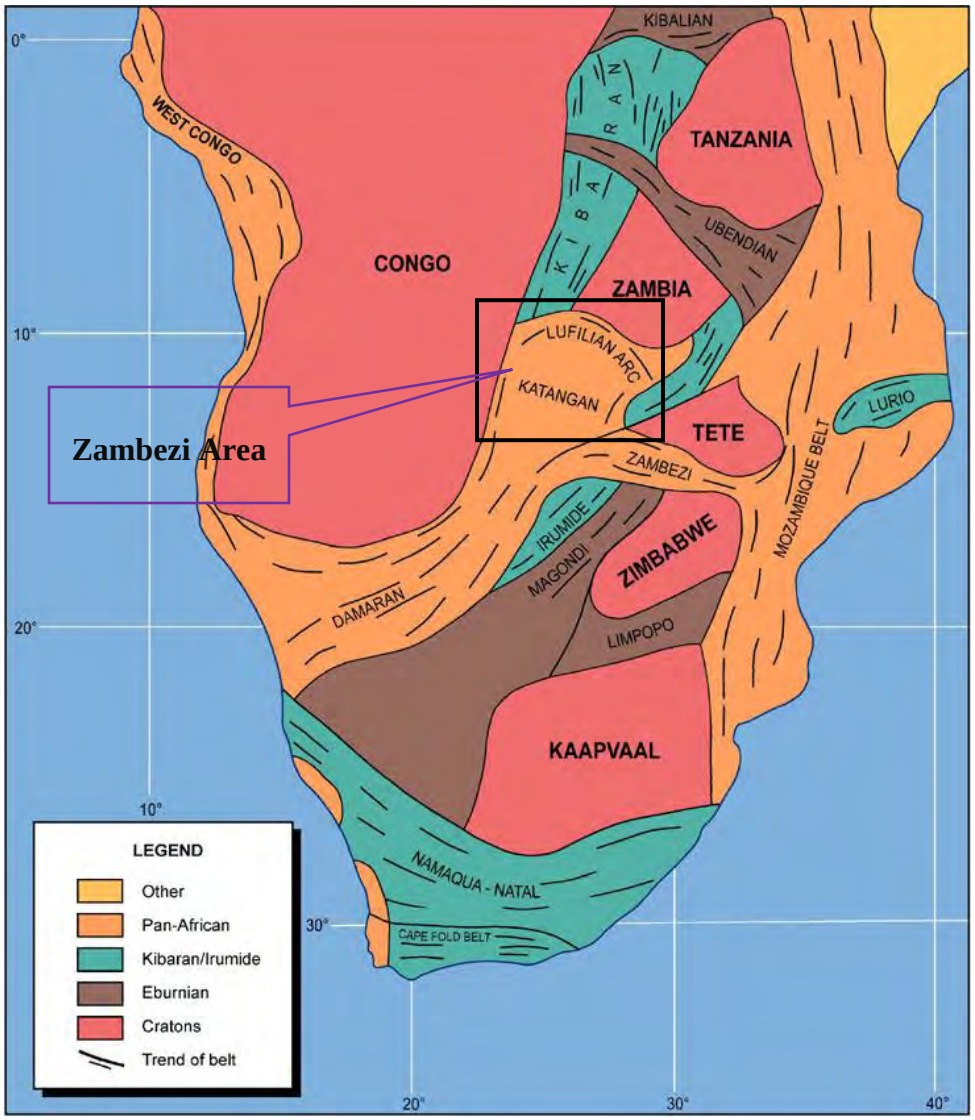

Figure 1: Pre-Pan-African cratons, Eburnian, Kibaran/Irumide and Pan-African mobile belts with the highlighted Lufilian Arc position in a black rectangular box and Zambezi area, after Porada, (1989).

The stratigraphic succession within the Lufilian Arc consists of the Archean to Proterozoic Basement Supergroup, the Neoproterozoic Katanga Supergroup and the Cenozoic Kalahari Group (Figure 2). Further details on the Lufilian Arc's geology, stratigraphy and evolution will be explained in subsequent sections.

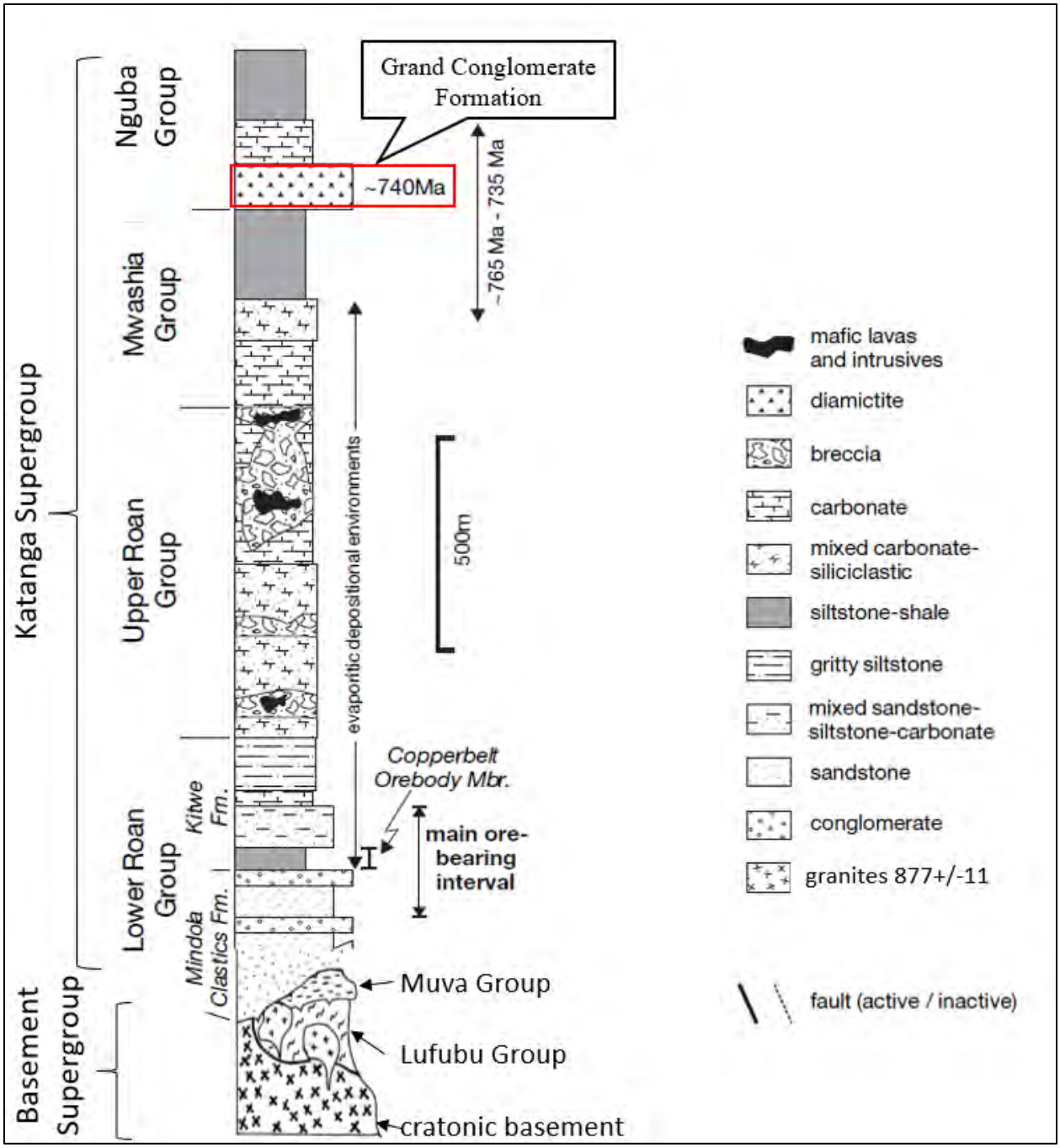

Figure 2: Simplified stratigraphic log of the cratonic basement (CB), the Basement Supergroup and the Katanga Supergroup. The Grand Conglomerate was deposited at ~740 Ma (modified after Selley et al., 2005).

The Basement Supergroup consists of the Lufubu Group, the Muva Group and granites (Figure 2; Mendelsohn, 1961). The Lufubu Group contains the oldest rocks of the Basement Supergroup which consist mainly of mica schists, amphibolites, quartzites and gneisses (Mendelsohn, 1961).

The Muva Group, overlying the Lufubu Group, consists of variable metasedimentary packages with mostly quartzites and shales. These have preserved sedimentary structures in places (Mendelsohn, 1961). The youngest Basement Supergroup rocks are several large granite masses (Figure 2) that intruded both the Lufubu and Muva Groups. Granites are variable in colour, textures, structure, and composition, and show different intrusive relationships to their country rocks (Mendelsohn, 1961; Armstrong et al., 1999).

The Katanga Supergroup unconformably overlies the Lufubu and Muva Groups and granites (Figure 2). The groups of the Katanga Supergroup are from the oldest to the youngest: Lower Roan, Upper Roan, Mwashia, Nguba and Kundelungu (Selley et al., 2005). These groups are divided further into subgroups and formations. The Grand Conglomerate Formation is a basal part of Nguba Group. The Grand Conglomerate is of importance for this study because of its abundance in the area and its metamorphic mineral assemblages consisting of garnet and biotite, which are phases suitable for thermobarometric analysis.

The Cenozoic Kalahari Group unconformably overlies both the Basement Supergroup and the Katanga Supergroup. The Kalahari Group is composed of unconsolidated and semi-consolidated sand with ferricrete, silcrete and calcrete. The underlying geology of the Zambezi area is mostly concealed by tens to hundreds of meters thick cover of the Kalahari Group (Downie, 1968). However, sporadic outcrops expose the Katanga and Basement Supergroups.

Anglo Exploration (Zambia) Limited's current exploration efforts present an opportunity that has provided insight into the structural geology, metamorphism, alteration, geology and stratigraphy of the area. The current research project was motivated by these recent findings. The overall goal for this research is to give a geological understanding and perspective which will improve the understanding of the geological history of the area. Section 1.5 explains the objectives of the study in more detail.

1.2 STRATIGRAPHY

The oldest rocks within the Lufilian Arc belong to the Archean to Mesoproterozoic Basement Supergroup (Key et al., 2001; Hanson, 2003; Selley et al., 2005), which essentially consists of metavolcanic rocks, migmatites, metasedimentary rocks and metagranites (Mendelsohn, 1961).

The three major groups within the Basement Supergroup are the Lufubu and the Muva Groups as well as the granites (Mendelsohn, 1961).

Cratonic granulite rocks of the Basement Supergroup are uncommon within the Lufilian Arc and where they occur are incorporated into the Lufubu Group. Key et al. (2001) dated several zircon in basement granulite samples of the northwest Zambia using $^{207}Pb/^{206}Pb$, all analyses combined give a concordant age of 2543 ±5 Ma. The dated granulite samples belong to the Congo Craton, and are referred to as part of the Kasai Shield (Key et al., 2001). These are the oldest known basement rocks within the Lufilian Arc in Zambia.

The Katanga rocks unconformably overlie the Basement Supergroup. They were deposited during the Neoproterozoic (Armstrong et al., 1999). The lowermost units belong to the Lower Roan Group (Figure 2). These are sequentially overlain by the Upper Roan, Mwashia, Nguba and Kundelungu Groups. The Lower Roan Group consists of predominantly conglomerates, sandstones, siltstones with shales and minor carbonates. A carbonate-dominated platform of the Upper Roan overlies the Lower Roan units. Above the Upper Roan is the Mwashia Group consisting of carbonaceous shales and siltstones. The Mwashia Group is overlain by the Nguba Group, the base of which is the Grand Conglomerate Formation (GC). The GC is overlain by, shales and carbonates. The Nguba Group is overlain by the Kundelungu Group consisting of the Petit Conglomerate Formation, carbonates, shales and breccias (Selley et al., 2005; Mendelsohn, 1961).

All core material shown in this chapter are drill core from the eastern part of the Lufilian Arc provided by Kalulushi Chamber of Mines in Kalulushi Town, Copperbelt Province in Zambia. This section shows the described rock types as they typically occur in the region.

1.2.1 BASEMENT SUPERGROUP: LUFUBU GROUP

The Lufubu Group forms part of the oldest Basement Supergroup rocks. These are mainly granulites, mica schists, amphibolites, quartzites and gneisses (Gray, 1929). Geochronology done by Rainaud et al. (2005) provided zircon age 1968±9 Ma ($^{207}Pb/^{206}Pb$) for Lufubu Group schists protolith. The schists are blastoporphyritic metavolcanic rocks derived from a hornblende quartz porphyry, which are common within Mufulira Town in the Copperbelt Province of Zambia. Other rocks dated by Rainaud et al. (2005) are meta-trachyandesitic porphyries with their igneous

protolith age of 1873.5 ± 8.3 Ma. A representative rock sample from the Lufubu Group (Figure 3) is a biotite amphibole schist. It is green, foliated, medium-grained and composed of biotite, amphibole, chlorite, minor quartz and feldspar.

Figure 3: Green medium-grained foliated biotite amphibole schist of the Lufubu Group2

1.2.2 BASEMENT SUPERGROUP: MUVA GROUP

The Muva Group consists of variable metasedimentary packages of mostly quartzites and siltstones, some with preserved sedimentary structures (Mendelsohn, 1961). The Muva Group uncomfortably overlies the Lufubu Group (Garlick, 1961). Detrital zircon ages between 1824 Ma and 1987 Ma (e.g., De Waele and Fitzsimons, 2004; Rainaud et al., 2005) may suggest the oldest possible sedimentation age of the Muva Group. However, Selley et al. (2005) suggest sedimentation of the Muva Group between ~1300 to 1100 Ma. Within the study area, the Muva Group outcrops 80 km north of Zambezi in the Chavuma area (Figure 11).

1.2.3 BASEMENT SUPERGROUP: GRANITES

Granites are the youngest rocks of the Basement Supergroup. They intruded both the Lufubu and Muva Groups. These granite masses vary widely in colour, textures, structure, composition and relationship to country rocks which they intruded (Mendelsohn, 1961; Armstrong et al., 1999). The largest granite bodies are the Nchanga, Chambishi, Mufulira and Muliashi granites, some of which are partially sheared (Mendelsohn, 1961; Armstrong et al., 1999). The emplacement of the

Nchanga granites has been dated ~880 Ma (Armstrong et al., 1999). The Nchanga granite's typical composition (Figure 4) is feldspar, quartz, biotite and muscovite. Biotite-rich layers define weak banding.

Figure 4: Pink coarse-grained meta-granite composed of feldspar, quartz, biotite and muscovite. It is weakly sheared with semi-continuous biotite bands.

1.2.4 KATANGA SUPERGROUP: LOWER ROAN GROUP

The Lower Roan Group overlies the Basement Supergroup above an angular unconformity (Armstrong et al., 1999). The Lower Roan Group is divided into two formations, the older is the Mindolo Clastics Formation conformably overlain by younger Kitwe Formation (Figure 2; Selley et al., 2005). The major rocks of the Mindolo Clastics Formation are immature conglomerates and sandstones whereas the Kitwe Formation comprises of dolomitic siltstones, carbonaceous shale/siltstone (Binda, 1994; Mendelson, 1961; Selley et al., 2005; Master et al., 2005). The base of the Kitwe Formation is marked by dolomitic siltstone, minor carbonaceous shale, argillaceous sandstone, and dolomite, which are principal host units for Cu-Co mineralization (Fleischer, 1984; Selley et al., 2005). Representative rocks of the Mindolo Clastics Formation (Figure 5) are interbedded conglomerate with sandstone. Clasts within the conglomerate are granite, sandstones and quartzites. Sandstone is reddish medium-grained with cross-beds marked by hematite bands.

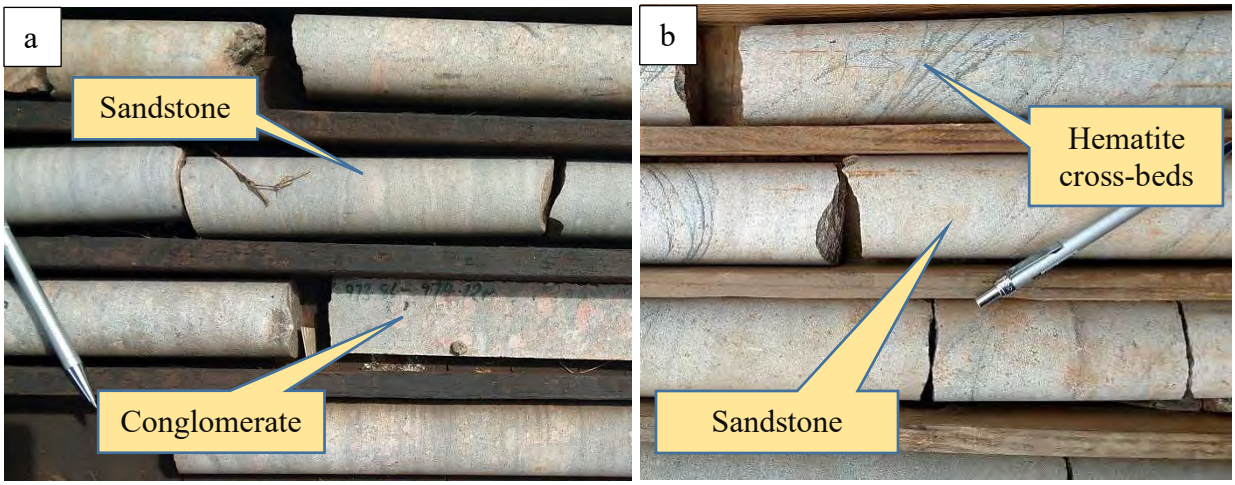

Figure 5: (a) Pink immature granitic pebble conglomerate interbedded with grey sandstones of the Mindolo Clastics Formation. (b) Reddish grey medium-grained cross-bedded sandstone of the Mindolo Clastics Formation; cross-beds are marked by grey hematite.

1.2.5 KATANGA SUPERGROUP: UPPER ROAN GROUP

The Upper Roan Group is marked by an appearance of a thick and lateral extensive carbonate sequence (Mendelsohn, 1961). The Upper Roan Group constitutes of dolomite, algal dolomite, local anhydrite and upward fining siltstones and sandstones (Selley et al., 2005). Figure 6 shows common occurrence of the Upper Roan rocks consisting of bands of dolomite and anhydrite with secondary phlogopite and talc commonly occurring within fractures. Other common rocks are breccias with rounded to angular intraformational fragments ranging from approximately millimetre size to several meters. The breccia fragments were formed by dissolution of anhydrite that resulted in voids and subsequent material collapse (Bull et al., 2011). The breccias are cemented by carbonate, albite, quartz and anhydrite (Jackson et al., 2003; Selley et al., 2005).

Figure 6: Banded Upper Roan carbonate unit with bands of phlogopite, anhydrite, dolomite and talc occurring along fractures.

1.2.6 KATANGA SUPERGROUP: MWASHIA GROUP

The Mwashia Group is a shale dominated sequence that is in cyclic sequence with minor carbonate beds (Selley et al., 2005). Selley et al. (2005) further describes the lower part of Mwashia Group to consist of dolomite, mixed dolomite-siltstone-mudstone sequences. The Mwashia Group has upwards increasing carbonaceous content with the upper Mwashia Group consisting of grey to black shales (Figure 7), which were deposited under increasingly anoxic conditions (Wendorff and Key, 2009). Basaltic volcaniclastic rocks and lavas form interlayers within the Mwashia succession. These mafic bodies have been dated as 745 ± 7.8 Ma and 765 ± 5 Ma, which is interpreted as the period of magmatism within the Mwashia Group and the associated basin rift (Master et al., 2005; Key et al., 2001).

Figure 7: Finely laminated grey shale interlayered with light grey carbonate and brown oxidized pyrite.

1.2.7 KATANGA SUPERGROUP: NGUBA GROUP

The Nguba Group is divided into two major formations, which are the basal Grand Conglomerate (GC) and the Kakontwe Limestone. The base of the Nguba Group is mostly defined by a thick succession of the GC, which was formed as the result of debris flow (Selley et al., 2005). The base is occasionally marked by massive or banded iron formation.

The constituents of the GC are poorly sorted polylithic fragments (few millimetres to several meters) within a shale-dominated matrix. The GC contains beds of laminated siltstones, coarse-grained sandstone and lithic sandstones (Binda and Van Eden, 1972; Wendorff and Key, 2009). The GC with polylithic fragments within the shale matrix (

Figure 8a) on the eastern Lufilian Arc is unmetamorphosed, whereas the GC on the western part, where the study is located in Zambezi, is metamorphosed, with developed red garnet porphyroblasts and matrix biotite (Figure 8b).

The Kakontwe Limestone is a thick limestone succession overlying the GC. The Kakontwe Limestone has impurities that characterize the limestone with a grey colour and have preserved

bedding structures (Wendorff and Key, 2009). The Kakontwe Limestone contains some shale layers with pyritic calcite veins in places.

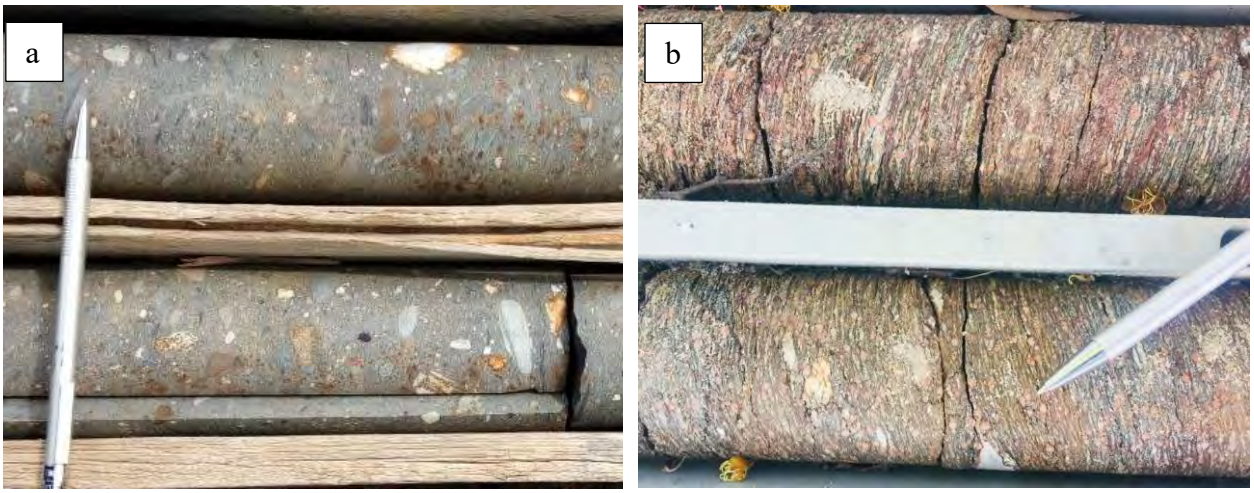

Figure 8: (a) Undeformed Grand Conglomerate with poorly sorted polylithic clasts of different shapes and sizes in a calcareous shale matrix. (b) Moderately weathered deformed Grand Conglomerate from the western part of the Lufilian Arc with polymictic sheared clasts in a garnet, biotite and calcite rich matrix.

1.2.8 KATANGA SUPERGROUP: KUNDELUNGU GROUP

The Kundelungu Group (KG) consists of conglomerates, carbonate, siltstones/shales and thick breccia units. The KG rests unconformably on the Nguba, Mwashia and Upper and Lower Roan Groups (Wendorff and Key, 2009). The Petit Conglomerate Formation defines the base of the Kundelungu Group. The Petit Conglomerate is similar to the GC and only distinguished by its sparsely distributed clasts, and the sequence is thinner than the GC (Wendorff, 2005). The Petit Conglomerate (Figure 9 a) has sparsely distributed shale and carbonate clasts within a dolomitic shale matrix. The upper rock units within the Kundelungu Group are composed of sandy shales, dolomites, and thick conglomerate complexes that are typically of the southern Lufilian Arc (Wendorff and Key, 2009). The distinctive rock unit above the Petit Conglomerate is a pink carbonate with minor matrix amphibole called the Cap Carbonate. The Cap Carbonate sequence is shown in Figure 9b. The Kundelungu Group has not received much attention in the existing literature.

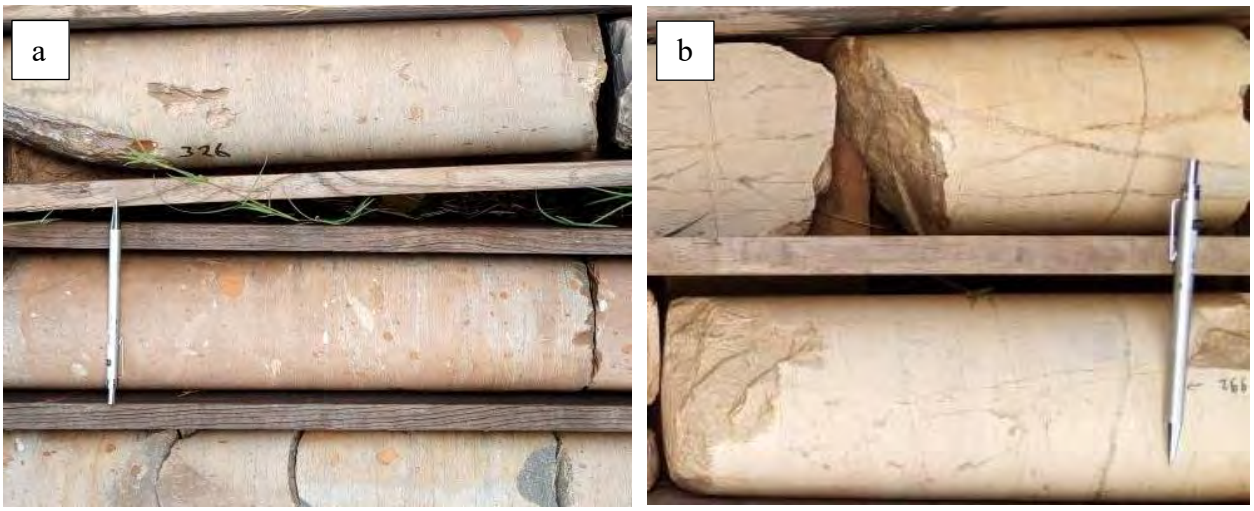

Figure 9: (a) Petit Conglomerate with sparse clasts within a dolomitic shale matrix. Clasts are composed of shale and carbonate, they range in size from few millimetres to a few centimetres. (b) Pink massive dolomites referred to the Cap Carbonate

1.3 KATANGA BASIN EVOLUTION

The Katangan basin, into which the Katanga Supergroup was deposited, formed as the result of rifting during Rodinia breakup (Porada and Berhorst, 2000). The intrusion of the Nchanga Granite, which is part of the youngest Basement Supergroup (dated at 877 ± 11 Ma; Armstrong et al., 1999), and the extrusion of the Kafue rhyolites (age 879 ± 19 Ma) which are also part of the Basement Supergroup are the earliest evidence of rift activity initiating the basin. This marks the beginning of Lower Roan sedimentation (Hanson et al., 1994). Sedimentation of the Katanga Supergroup lasted for ~300 m.y. and ended around 573 Ma (Armstrong et al., 2005; Master et al., 2005).

The Mindolo Clastics Formation (MCF) of the Lower Roan unconformably overlies the Basement Supergroup. The MCF was the first to be deposited after rift initiation (Figure 10) ~880 Ma (Armstrong et al., 1999; Johnson et al., 2007). The basal conglomerate within the MCF contains clasts that consist of granite material which probably eroded from the granites of the Basement Supergroup (Hancook, 1994). Due to limited preservation of lateral facies transition over short distances and the presence of asymmetric troughs, Hancook (1994) suggests deposition of the MCF in half-grabens.

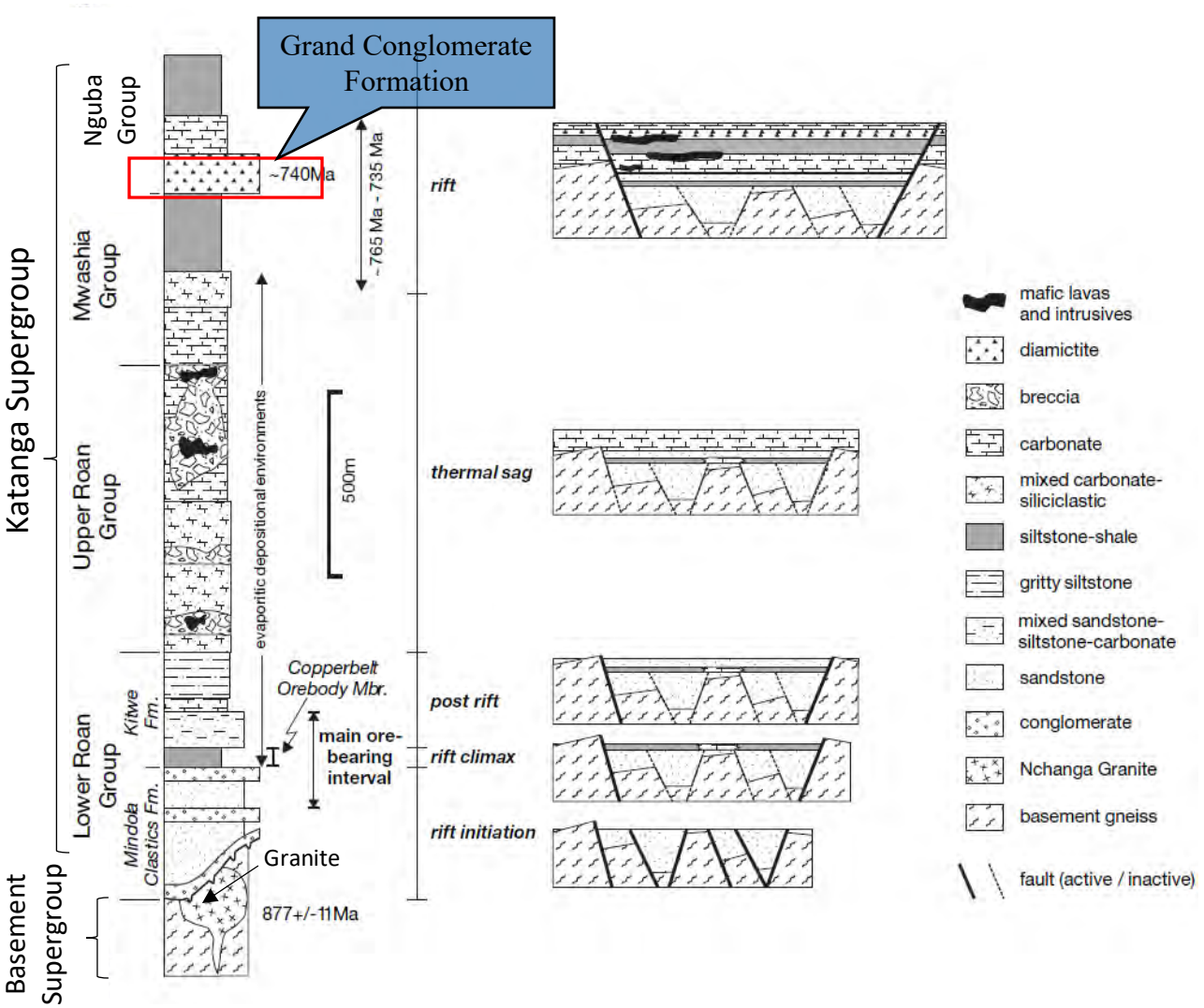

Figure 10: Simplified stratigraphic log of the Basement Supergroup (BSG) and the Katanga Supergroups. Interpreted schematic stages of basin development from initial rift initiation and deposition of the Lower Roan Group during the rift climax and post rift. Upper Roan Group deposition took place during thermal sagging, whereas the Mwashia and Nguba Groups where deposited during the second rifting episode. The Grand Conglomerate was deposited ~740 Ma (modified after Selley et al., 2005).

The Kitwe Formation conformably overlies the MCF. The Kitwe Formation is more laterally extensive than the MCF and consists of rocks that were deposited in lower energy environments (Selley et al., 2005). This suggests a significantly deeper basin, where major basin bounding faults led to basin subsidence, marking the rift climax, and resulting in marine transgression (Selley et al., 2005). The Kitwe Formation consists of a shale dominated sequence known as the Copperbelt Orebody Member, hosting most Cu-Co deposits. Overlying the shales are subsequent coarser-grained rocks postdating the rifting climax.

The Upper Roan Group, a carbonate and evaporite dominated sequence, and the lower Mwashia Group (Figure 10), were deposited when the basin had stabilized during thermal sag (Selley et al., 2005). This was the period when rifting had failed and due to sediment input into the basin, thermally-driven down-warping was initiated (Selley et al., 2005).

The deposition of the upper Mwashia, a shale-dominated sequence, is suggested to be the second rift within the Katanga Basin, where sediments were deposited in the transgressive environment (Selley et al., 2005). Basaltic volcaniclastic rocks and lavas, which only appear within the Upper Roan and Mwashia Groups (Figure 10), are marked as the beginning of extensional tectonism within the basin (Selley et al., 2005). Basaltic units dated at ~765 to 735 Ma by Key et al. (2001) are attributed to the deposition of the upper Mwashia Group.

The first glacial sedimentation within the Katanga basin was the diamictite (Grand Conglomerate Formation) of the lower Nguba Group, indicated in Figure 10. The Grand Conglomerate Formation (GC) has been correlated with global Sturtian glaciations ~740 Ma (Bodiselitsch et al., 2005). The GC is generally massive with poorly sorted clasts which are imbedded within a fine-grained and shale matrix. Clasts in the Grand Conglomerate GC are commonly composed of quartzites, gneisses, mica-schists, limestones, shales, sandstones, granites, porphyries and basic rocks (Master et al., 2005).

The Kakontwe Limestone Formation (KL) overlies the glaciomarine Grand Conglomerate. The KL is commonly a fine-grained grey limestone. It formed as a marginal marine stratum. The KL originated in a low-topography graded shelf during and immediately post-glacial period (Master and Wendorff 2011).

The Petit Conglomerate Formation (PC) is the lowest unit of the Kundelungu Group. It overlies the Nguba Group on an erosional unconformity (Wendorff 2003; Wendorff and Key, 2009). The PC is a second glaciogenic conglomerate like the Grand Conglomerate Formation. However, clasts within the PC are commonly sparse with faceted and striated surfaces of intrabasinal and extrabasinal origin (Master and Wendorff 2011). The PC matrix is dominantly shale with minor carbonate. Overlying the PC are thick, upward-deepening sequences of carbonates, siltstones, mudstones and breccias (Selley et al., 2005). These rock units overlying the PC were deposited during basin inversion from extensional to compressional tectonics of the Katanga Basin

(Batumike et al., 2006). The first unit above the PC is the Cap Carbonate Formation (CC) which is composed of pink massive dolomite and minor amphibole (Master and Wendorff 2011).

1.4 EVOLUTION OF THE LUFILIAN ARC

1.4.1 TECTONIC SETTING

The Lufilian Arc is bounded by several structural provinces, the Bangweulu Block northeast, Irumide Belt in the east, the Zambezi Belt in the south, and the Kibaran Belt in the north (Selley et al., 2005). The Lufilian Arc was primarily formed as the result of basin closure and inversion by collision of the Kalahari and Congo cratons (Cosi et al., 1992; Selley et al., 2005). The Lufilian Orogeny which affected the Lufilian Arc spans ~100 m.y with the oldest metamorphic ages provided by U-Pb monazite (592 ± 22 Ma) (Rainaud et al., 2002).

The Lufilian Arc is divided into four structural domains, from the southern Democratic Republic of Congo in the north down to Zambia in the south are (I) External Fold-Thrust Belt, (II) Domes Region, (III) Synclinorial Belt and (IV) Katanga High (Figure 11). The Kalahari Group largely conceals the Zambezi area on the western arm of the Lufilian Arc. The current study will focus on the metamorphism in rocks of this western part of the Lufilian Arc.

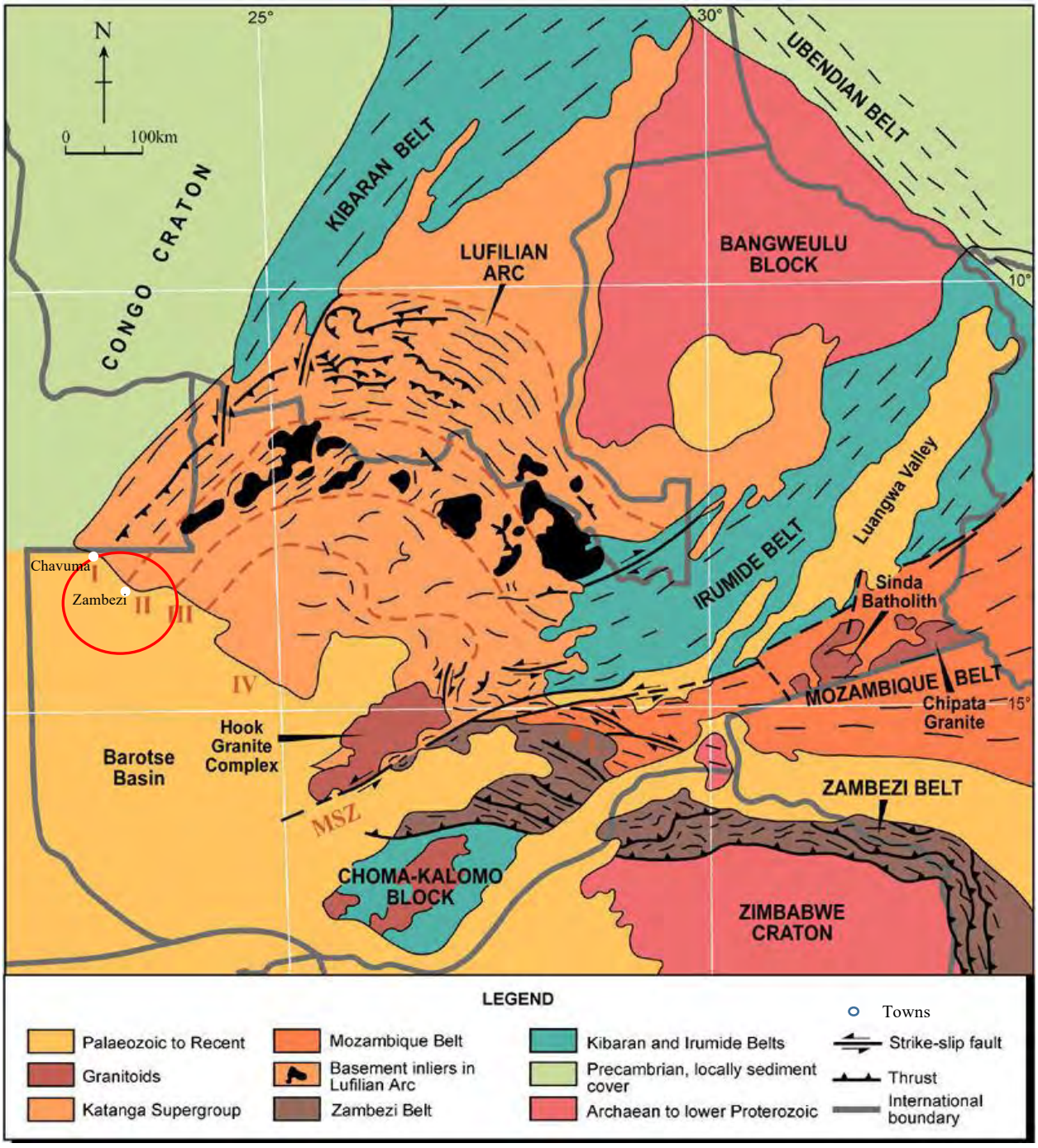

Figure 11: Tectonic structure of the Lufilian arc (after Porada, 1989; Kampunzu and Cailteux, 1999). I=External Fold and Thrust Belt, II=Domes Region III=Synclinorial Belt, IV=Katanga High, MSZ=Mwembeshi Shear Zone. The inserted red circle shows the study area.

1.4.2 TECTONIC DOMAINS

The northern outer part, referred to as the External Fold-Thrust Belt (I in Figure 11), occurs mostly within Democratic Republic of Congo (DRC), and consists of repeated upper Katangan stratigraphy (Key et al., 2001; Selley et al., 2005). The repetition of Katanga Group rocks reflects the northward thrusting of lower Katangan units, concealing the Basement Supergroup (Kampunzu and Cailteux, 1999). This domain is characterised by thin-skinned tectonics (Figure 12), repeating >50 m thick Katangan fragments, resulting in the Katangan stratigraphy of the southern DRC (Jackson et al., 2003; Key et al., 2001; Selley et al., 2005). Selley et al. (2015) suggested very low-grade metamorphism within the External Fold and Thrust Belt, with assemblages typical of the prehnite-pumpellyite facies.

The second domain from the north is the Domes Region (Figure 12), which is characterised by outcropping Basement Supergroup rocks 'domes', which are wrapped by Katanga rocks (Selley et al., 2005). The Domes Region units underwent thick-skinned deformation represented by antiformal stacks (Daly et al., 1984). Basement Supergroup 'domes' have similar petrological, structural and metamorphic features, and have been suggested to have been subjected to similar tectono-metamorphic events as Katanga rocks (Kampunzu and Cailteux, 1999). Though the Kalahari Group covers most of Zambezi area, the Domes Region rocks have been intersected by diamond drilling.

Katanga Supergroup and Basement Supergroup units within the Domes Region were deformed together, reaching up to amphibolite facies condition. The Katanga units of the Domes Region are distinguished from the northern domain by their higher metamorphic grade of greenschist- to upper amphibolite facies (Key et al., 2001; Selley et al., 2005). The metamorphism in the Domes Region of the eastern and central Lufilian Arc increases from the east to west from greenschist facies to upper amphibolite facies (Key et al., 2001; Selley et al., 2005). However, the nature of metamorphism and deformation is not known in the western part around Zambezi where this research is focused. The research will establish if metamorphism further increases, decreases or is constant towards the west.

The Synclinorial Belt (Figure 12) is thought to contain former deep-water sedimentary packages that have not been well studied; the belt is separated from the Domes Region by a thrust contact

(Selley et al., 2005; Cosi et al., 1992). Hanson et al. (1984) suggest decoupling along evaporitic horizons between the Domes Region and the Synclinoria Belt during the Lufilian orogeny at ~530 Ma. This resulted in several kilometers north-directed transport of Katanga High and Synclinorial Belt rocks. The transported units contained deep-water packages that were emplaced as multiple thrust sheets (Selley et al., 2005). The rocks within the Synclinorial Belt show large fold structures with lower metamorphic grade than the Domes Region (Loughlin, 1979).

The Katangan High is said to consist of uplifted Basement Supergroup rocks covered by thin former deeper water sedimentary packages (Figure 12 c). The Katanga High acted as the overriding plate during the Lufilian orogeny. The Lufilian orogeny affected the Lufilian Arc during the Pan-African orogenesis. The Pan-African orogenesis led to the assembly of East and West Gondwana during Neoproterozoic and early Paleozoic affecting all Pan-African belts whereas the Lufilian orogeny is attributed to the Lufilian Arc (Kampunzu and Cailteux, 1999). During the Lufilian orogeny, major events that affected the Katanga High were intrusions of granites dated as 570-530 Ma (Daly, 1986; Selley et al., 2005, Hanson et al., 1993). Rock units within the Katanga High are not as well studied as the northern domains.

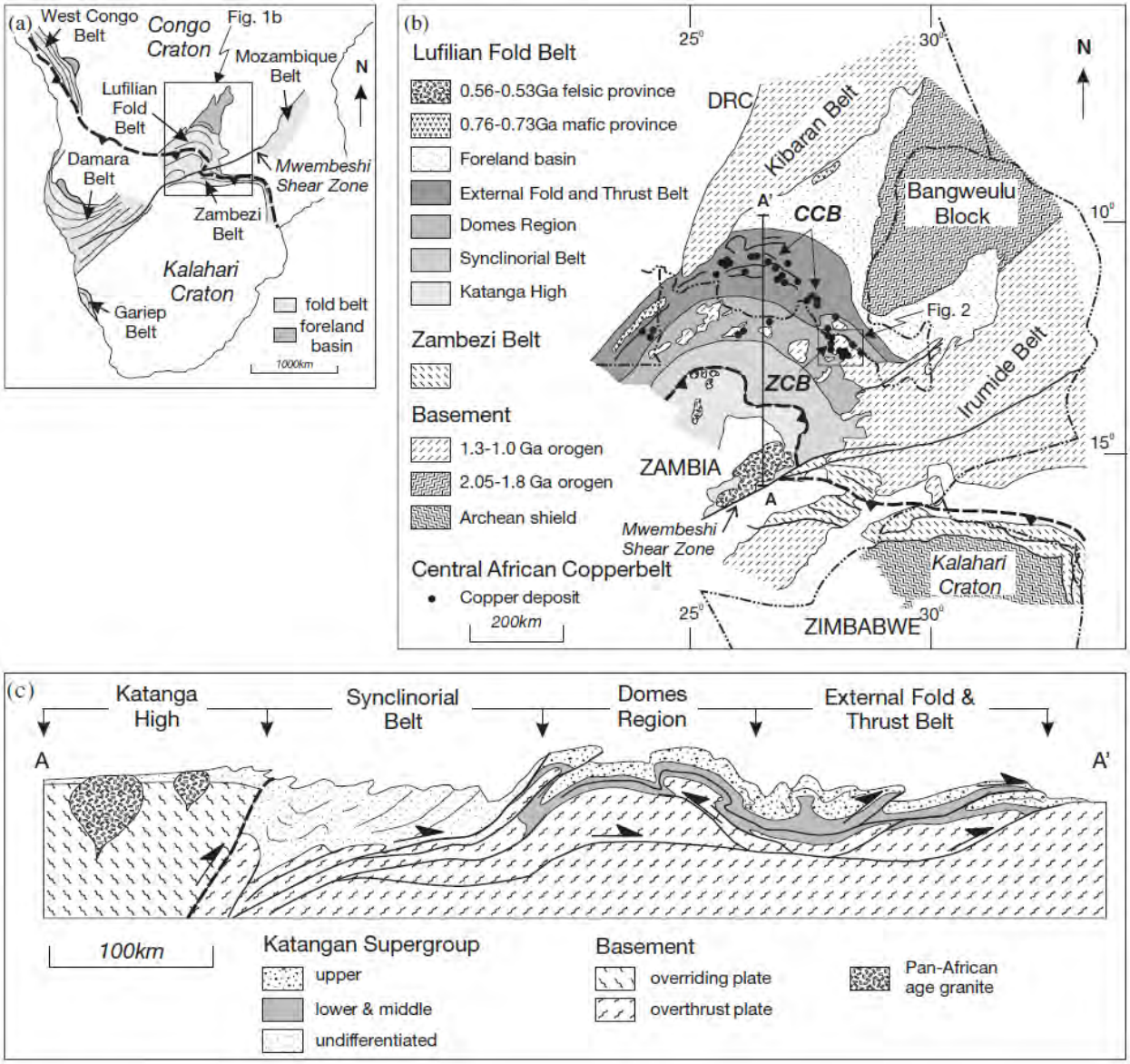

Figure 12: (a) Location of Lufilian Fold Belt within central Africa. (b) Lufilian Fold Belt location in Zambia and tectonic domains. (c) Schematic section of the Lufilian Fold Belt showing different tectonic domains (Selley et al., 2005).

1.4.3 DEFORMATION

The Lufilian Arc has undergone one major deformation phase during the Lufilian orogeny (~500 and 613 Ma). This deformation phase has been divided into three minor deformation episodes with different deformation features related to D1, D2 and D3 deformation episodes (Kampunzu and Cailteux, 1999).

Folding and thrusting observed throughout the Lufilian Arc has been attributed to the first deformation phase D1. The D1 event is characterized by northward trending upright and overturned folds associated with thrusts (Kampunzu and Cailteux, 1999). This deformation event of folding and thin-skinned thrusting did not result in significant internal deformation of the deformed units but formed repeated allochthonous sheets. D1 is also attributed to the formation of the NW-SE trending of the Lufilian Arc (Kampunzu and Cailteux, 1999; Figure 12).

The second deformation D2 was the major event within the Lufilian Arc, which resulted in the arcuate shape of the Lufilian Arc and formation of E-W trending of the Lufilian Arc (Kampunzu and Cailteux, 1999). This major deformation event is the result of clock-wise rotation of crustal blocks and strike-slip faulting. Within the central west of Lufilian Arc, basement rocks as well as those of the Katanga were refolded forming open N-trending antiforms (Key et al, 2001). Key et al. (2001) has also attributed local crenulation cleavage to D2. The crenulation cleavage that is axial planar to the folds created intersection lineation plunging south parallel to the fold axis.

The last deformation phase D3 is not well developed and is associated to transversal folding. These are large and open folds with hinges trending between NNE-SSW and ENE-WSW. These are cut by NS and EW striking faults (Kampuzu and Cailteux, 1999).

1.4.4 METAMORPHISM AND GEOCHRONOLOGY

The metamorphism within the Lufilian Arc is different in each tectonic domain. The highest grade of metamorphism has been recorded within the Domes Region (Figure 13). The least recorded metamorphism is in the External Thrust and Fold Belt (Cosi et al., 1992; Porada and Berhorst, 2000; Kampunzu and Cailteux, 1999; John et al., 2004).

There has been significant work on the metamorphic and geochronological evolution within the Katanga, which has led to understanding of Pan-African orogeny. The earliest metamorphic age within the Katanga Supergroup are those provided by Rainaud et al. (2002), with U-Pb monazite (592 ± 22 Ma) and Ar-Ar biotite (585.8 ± 0.8 Ma) ages within greenschist facies rocks of the eastern Lufilian Arc. Talc kyanite schist within the Domes Region have been attributed to peak metamorphic age dated ~530 Ma (John et al., 2004). During the main deformation of these rocks, the regional metamorphism temperature is estimated at ~620 °C (Turlin et al., 2016). This main

deformation is related to the orogenic phase (U-Pb zircon dating between ~560 and ~530 Ma) of syn-tectonic granites and rhyolite within the Katanga High (Hanson et al., 1993). The retrograde stage of metamorphism associated to post-orogenic cooling has been dated ~510 to 465 Ma using Ar-Ar system in biotite (Torrealday et al., 2000; Cosi et al., 1992; Rainaud et al., 2002).

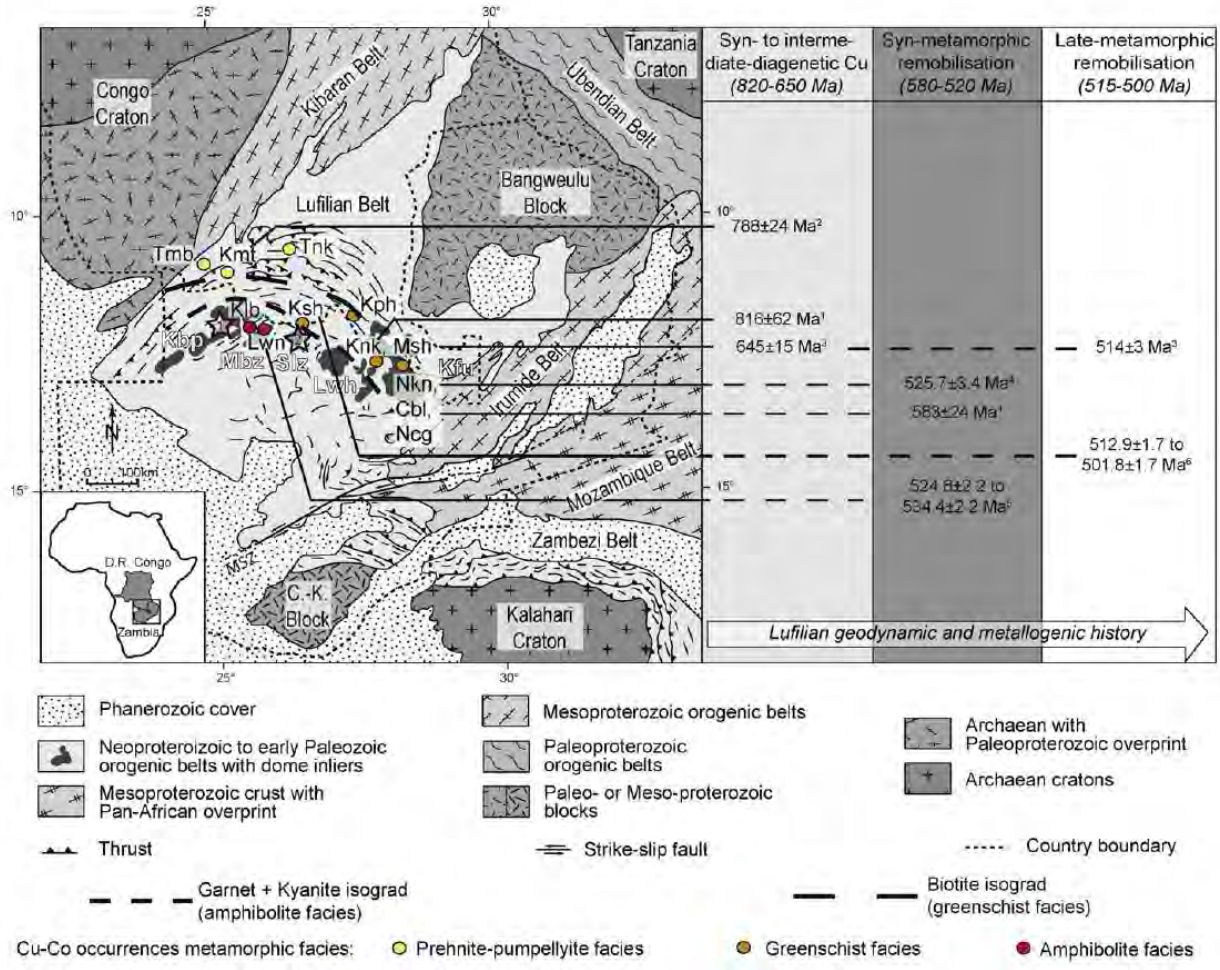

Figure 13: Lufilian Arc, other Pan-African mobile belts, cratons, associated geology, metamorphic facies and geochronological constraints, Cu-Co occurrences and their interpreted stage of emplacement (Turlin et al., 2016).

Table 1 outlines the key events that occurred within the Basement and Katanga rocks, modified from Key et al. (2001), Cosi et al. (1992), Selley et al. (2005), Rainaud et al. (2002), Porada, (1989) and Turlin et al. (2016). It shows the events from prior to the deposition of the Katangan rocks until the Pan-African event that resulted in the present-day metamorphic record and structure of the Lufilian Arc.

Table 1: Brief geological history of the Katanga basin and Lufilian Arc for both the Basement and Katanga Supergroups (modified after Key et al., 2001).

PERIOD (Ma)	EVENTS	BRIEF DESCRIPTIONS
465		The retrograde stage of metamorphism associated to post-orogenic cooling and D3 transversal folding
500-613	Pan-African orogeny	D2-Kalahari Craton pushing northward against the Congo Craton resulting in the formation of the present-day tectonic orientation of the Lufilian Arc (SW on the west, EW in the central and SE on the eastern)
		D1-Tectonothermal processes produced folding and thrusting observed within the Lufilian Arc.
<690		High-pressure and low-temperature regional metamorphism of rocks to amphibolite and greenschist facies.
735		Significant brecciation of the Kundelungu Group rocks and alteration of volcanic rocks within the Kundelungu basin in the western and central regions of the Lufilian Arc.
735-765	Sturtian Glaciation	The global Sturtian glaciation formed the extensive glaciomarine Grand Conglomerate formation. The Grand Conglomerate Formation (GC) occurs at the base of the Nguba Group. The GC is an extensive unit intersected in most drill holes in Zambezi and is thicker than the GC intersected in eastern and central Copperbelt on the eastern.
765	Rift reactivation	A second rift reactivation which led to Mwashia Group deposition and mafic volcanic eruptions. Most significant mafic rocks are in the northwest of Zambia. East-west extension and Rodinia fragmentation led to emplacement of mafic intrusions and other north-trending mafic dykes.
		Deposition of Upper Roan Group during the thermal sag of the basin
<880	Rifting and magmatism	880 Ma the age of Nchanga granites marks the onset of Lower Roan Group sedimentation. Formation of continental margins by northeast-trending basement shears which probably resulted from Rodinia breakup. Units belonging to the Katanga Supergroup were deposited in intracontinental rifts.
880		Emplacement of the Nchanga granites which are the youngest dated Basement Supergroup units known within the Katangan region.

1100-1300	Muva sedimentation	A period of sedimentation of the Muva Group (pelites and psammites). These are youngest Group of the metasedimentary Basement Supergroup. Muva Group outcrops 80 km north of Zambezi in the Chavuma area.
	Magmatism	NE-trending dolerite sheets intruded the Basement Supergroup
		The pre-Katangan Basement Supergroup underwent the NE-trending ductile sinistral shearing which was followed by multiple thrusting with significant NW tectonic displacement.
1873 to 2560	Eburnian Ubendian Orogeny	Porphyritic granite emplacement as well as minor granitic dykes of Kasai Shield (during the Archean to Palaeoproterozoic in northeast Zambia.
		Thermal event generating migmatite and later granite magmatic intrusion within the Congo Craton. This was followed by emplacement of dioritic stocks (metavolcanics) and deposition of sedimentary packages both belonging to the Lufubu Group.

1.5 OBJECTIVES

The purpose of this study is to evaluate the metamorphic history through analysis of fourteen samples from the Basement and the Katangan Supergroups. The rock units which are the primary focus of this study belong to the Mwashia and Nguba Groups of the Katanga Supergroup and the Basement Supergroup. Six drill holes were logged, and 14 samples selected for micro-petrography. Mineral chemistry has been studied and pressure-temperature (P-T) thermodynamic modelling was done to evaluate the metamorphic conditions and evolution.

The stratigraphy of the Zambezi area has not been coherently addressed. There are stratigraphic positions within the Katanga Supergroup which are commonly associated to deposits. Most of ore deposits in the Zambian Copperbelt occur within a 200 m stratigraphic interval above the basement (Selley et al., 2005). Those deposits that occur within stratigraphic positions above the Upper Roan Group have similar geological characteristics as those found in the lower stratigraphy. Understanding the stratigraphy of the Zambezi area will help identify the most prospective areas that would require further exploration.

The pressure-temperature (P-T) conditions, deformation episodes and metamorphism have not been documented in order to provide better understanding of any part of the Zambezi area. The Cu deposits in the Lufilian Arc are commonly hosted in sedimentary and metamorphic rocks. Primary

Cu mineralization is occasionally overprinted by a second syn-metamorphic Cu mineralizing event within the central copperbelt (Turlin., et al 2016). This mineralizing event is synchronous with the Pan-African metamorphism which affected both the basement and the Katanga metasedimentary sequence (Turlin., et al 2016). The metamorphism in the rocks and the new mineralising events have changed the primary occurrence of mineralisation. To discover deposits affected by deformation and metamorphism, new exploration methods are used.

The specific objectives of this study are three-fold:

- To determine if there is any stratigraphic correlation possible between Zambezi area with the Katanga Supergroup described for in the eastern and central parts of the Lufilian Arc and deformation episodes
- To identify the mineral phases of representative samples within the Zambezi area
- To determine the condition of the regional metamorphism in the area using metamorphic mineral assemblages, thermodynamic modelling based on XRF analysis and mineral chemistry

1.6 METHODOLOGY

Four historical drill cores stored at the Chamber of Mines in Kalulushi Copperbelt in Zambia were logged in order to correlate the local lithological units and the general Katanga Stratigraphy. These cores intersect both Basement Supergroup and Katanga rocks. Furthermore, geophysical surveys, field mapping data, aircore and diamond drilling results from Anglo Exploration Zambia Limited were used to generate a valid geological representation of northeast Zambezi area.

In additional to the four historical cores, six new diamond drill cores drilled in 2014 and 2016 by Anglo Exploration Zambia limited were selected for the study. Drill core selection was based on mineral assemblages, metamorphism, stratigraphy and drill hole locality distribution. 14 Samples from drill cores were selected for micro-petrographic studies based on metamorphic mineral assemblages, deformation patterns and stratigraphic representation within the Nguba and Mwashia Groups of the Katanga Supergroup and the Basement Supergroup. Samples selected were garnet biotite schists and banded gneisses. Samples for micro-petrography were cut in either quarter or

half using a core cutting machine. The minimum length for each sample was 20 cm. These samples were cut into thin sections and observed under a microscope.

Six samples dominated by zoned garnet, biotite, amphibole and plagioclase were then prepared for Energy Dispersive X-ray Spectrometry (EDS) analyses. This helped generate element maps to characterise elemental content of mineral phases and matrixes. EDS was also used for elemental analysis at selected mineral points. This was done in order to quantify elemental abundances. Oxide compositions were converted into normalised cation composition in order to assess the stoichiometric correctness of the obtained mineral composition and in order to produce X_{Mg} ratios and endmember proportions required for thermobarometry.

The six samples were polished and carbon-coated. EDS analysis was performed using an Oxford Instrument INCA Energy350 with a Si-Li detector, using an accelerating voltage of 20 kV. Cobalt was used as a standard for peak calibrations. The EDS data collected was from both point analysis on specific mineral phases and element mapping of specific garnet.

Material from six samples that were analysed by EDS were prepared for XRF analysis. Drill core samples were crushed into small pieces and later pulverized. After every sample, the pulveriser was cleaned with acetone in order to avoid contamination. Each sample was packed and labelled in a 100 ml container and later sent for XRF analysis at the Central Analytical Facility of Stellenbosch University. The major elements were analysed on a fused glass bead prepared by mixing 5 g of sample powder and flux. The Loss on Ignition (L.O.I) was determined by strongly heating a sample at a specified temperature, allowing volatile substances to escape, until its mass ceased to change. XRF results were used to model multiphase stability diagrams for each sample.

The thermodynamic modelling software used was THERIAK DOMINO (TD; de Capitani and Brown, 1987; v. 03.01.12) to estimate the temperature and pressure conditions. This method relies on the assumption of thermodynamic equilibrium of mineral phases, bulk compositions and thermodynamic datasets used. At fixed (P, T and composition), the result includes the stable mineral assemblage at these conditions.

Molar ratios from XRF data were used and TD calculated specific oxygen. The tcdb55c2d data set (Holland and Powell, 2011) was used as the data base for all calculations. The appropriate water

content during metamorphism and deformation was estimated based on calculations of pseudo-binary diagrams for variable water contents. This was done at specific pressure condition and temperature ranging between 200˚C and 600˚C. The appropriate water content were the ones that reflected assemblages similar to those observed in petrographic observations. In the multiphase equilibria diagrams, stable mineral assemblages and the positions of X_{Mg} (Mg/(Mg + Fe)) isopleths of garnet and biotite were plotted in P-T space for samples high in Mg and Fe. By comparison with observed paragenetic minerals and mineral compositions, the likely P-T condition of the analysed rocks were determined.

2. STRATIGRAPHY OF ZAMBEZI

2.1 STRATIGRAPHY

The following sections 2.1 to 2.5 describe the general results of the petrographic and stratigraphic investigation in the Zambezi area with the distribution of stratigraphic units in the field. Section 2.6 will describe the logs of selected drill cores. Section 2.7 will describe structural geology while Chapter 3 will describe micropetrography.

Figure 14 outlines the outcropping and subsurface geology below both the Kalahari Group and residual soils. The geological map of Zambezi (Figure 14) was generated from integrating geophysical data, mostly magnetics, aircore drilling results, diamond drilling results and geological mapping. The original data were provided from field mapping, aircore and diamond drilling results.

The Zambezi area is underlain by the Katanga and the Basement Supergroup rocks (Figure 2 and 14). The Basement Supergroup rocks are mostly schists, gneisses, feldspathic quartzites and meta-granites. Gneisses and schist are more abundant within the study area, few areas have outcropping gneisses and schists. Gneisses are generally banded and consists of biotite, quartz and feldspar. Schists are biotite rich and rarely contain scapolite. Occasionally, schists are altered by retrograde chlorite growth. Feldspathic quartzites and granites of the Basement Supergroup have been concealed by thin units of the Katanga Supergroup. Descriptions of various rocks belonging to the Basement Supergroup will be provided in subsequent sections.

The contacts between the Basement Supergroup (BS) and rocks belonging to the Katanga Supergroup (KS) are different. Thrust faults characterise most contacts, which in some cases are indicated by presence of massive ironstones. Other contacts are unconformities marked by sudden change from rocks of the Katanga Supergroup and the Basement Supergroup.

Overlying the Basement Supergroup units are thin layers of the Lower and Upper Roan, the Mwashia and the Nguba Groups, which usually consist of garnet biotite schists, amphibole schists, dolomitic marbles, meta-sandstones and basaltic rocks. Some units belonging to the Katanga Supergroup have preserved primary structures which make it easier to correlate them with rocks in the weakly deformed eastern part of the Lufilian Arc.

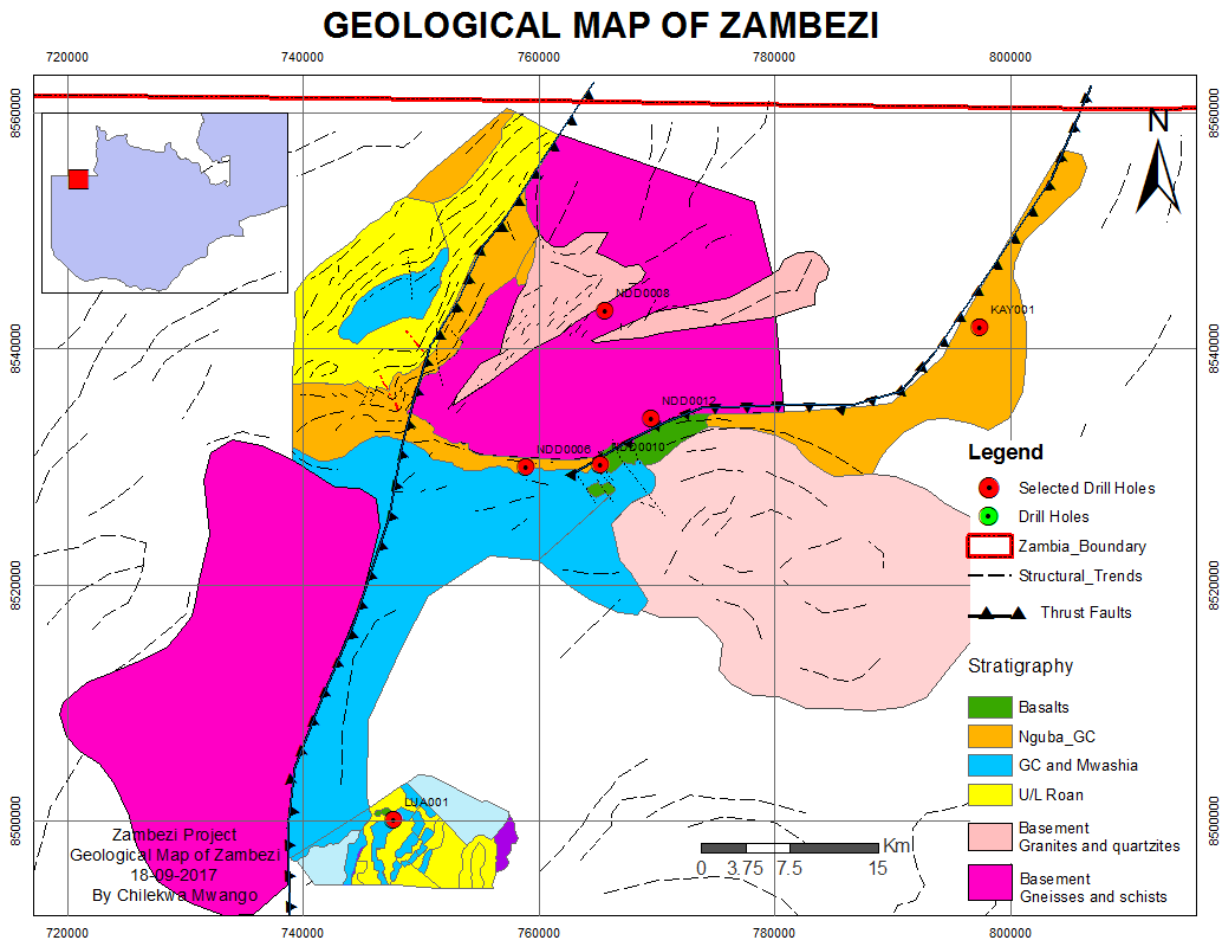

Figure 14: Geological map of Zambezi, showing Basement Supergroup schists, gneisses, quartzites and granites. Overlying the Basement Supergroup are Upper/Lower (U/L) Roan Groups chiefly composed of carbonates and sandstones. The Mwashia Group is occasionally grouped with Grand Conglomerate, consisting of garnet +/- amphibole biotite schists. The Nguba Group is predominated by the Grand Conglomerate, consisting commonly garnet biotite schist with clasts. Red points show drill hole positions relevant for this study (LUA001, KAY001, NDD0006, ND0008, NDD0010 and NDD0012).

Figure 15 shows various units intersected in diamond drilling just below Kalahari Group cover. Rocks just below Kalahari cover are brecciated, transitioning into unfragmented rocks of the Basement Supergroup. This breccia is interpreted as a paleo-surface unit onto which Kalahari Group sands were deposited. Basement Supergroup units (Figure 15c, e and f) are feldspathic quartzite, biotite feldspar quartz gneiss and muscovite feldspar quartz schist respectively. Figure 15a shows biotite schist with stretched pebbles. Figure 15b, g and h are garnet biotite schist with stretched pebbles all belonging to the Grand Conglomerate.

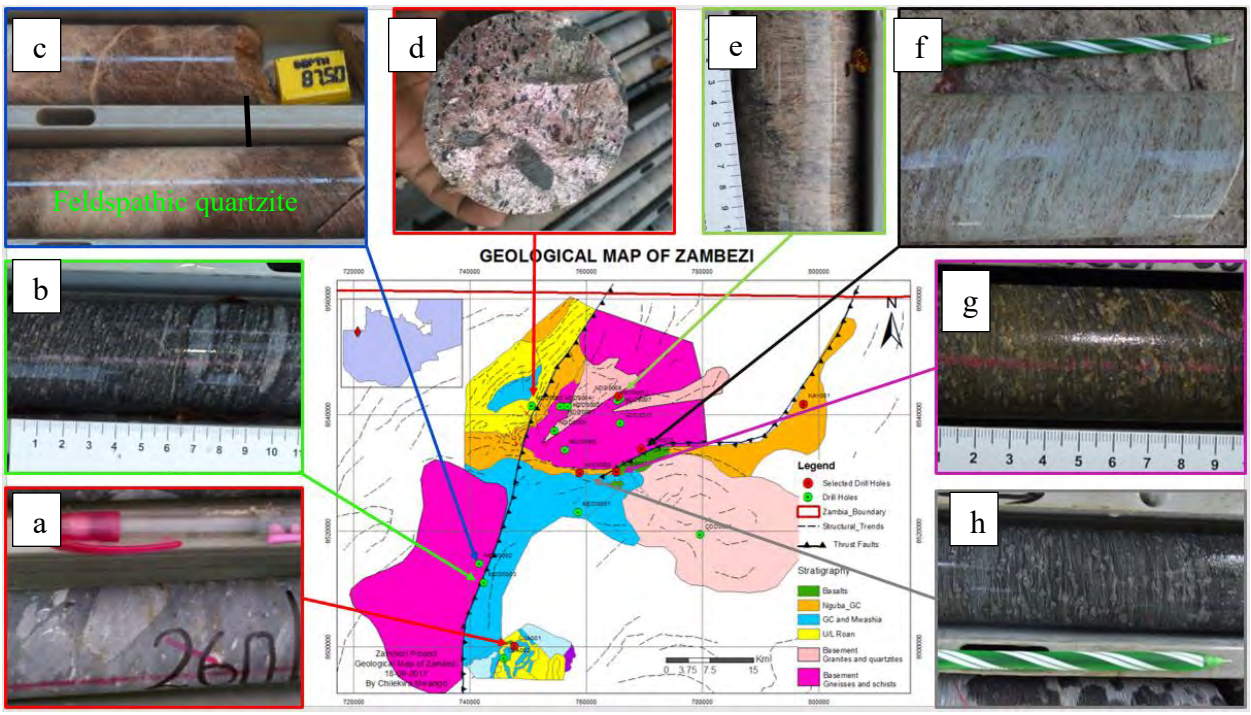

Figure 15: Various units underlying the Kalahari sand cover marking the bedrock from where the geological map was produced. (a) Grey pebble biotite schist from hole LUA001 belonging to the Grand Conglomerate. Grey foliated rock composed of biotite, calcite and quartz matrix. Garnet porphyroblasts and pebble polymictic clasts are cemented within a biotite and carbonate rich matrix. (b) Garnet biotite schist with stretched polymictic clasts intersected within MDD0003 belonging to the Grand Conglomerate Formation. (c) Feldspathic quartzite of the Basement Supergroup. Pink coarse-grained weakly foliated fabric composed of feldspar and quartz. Light pink quartz-feldspar veins cross-cut rock. (d) Hornblende biotite schist of the Lower Roan Group from hole NDD0003. Up to 2 cm long hornblende porphyroblasts within a biotite, quartz, calcite and hematite rich matrix. (e) Biotite feldspar quartz gneiss, which is part of the Basement Supergroup from NDD0008. (f) Muscovite quartz schist from the Basement Supergroup intersected within NDD0012. (g) Moderately weathered grey pebbly garnet biotite schist from hole NDD0010 belonging to the Grand conglomerate. (h) Grey pebbly garnet biotite schist from NDD0006 belonging to the Grand Conglomerate Formation. Grey to brown garnet porphyroblasts and stretched clasts within a foliated biotite, calcite, quartz and feldspar matrix

2.2 BASEMENT SUPERGROUP

The Basement Supergroup is mainly characterised by gneisses, schists, quartzites and meta-granites. Gneisses and schists are the most abundant rocks within the study area, though also feldspathic quartzites are present. Contacts of Basement Supergroup rocks with those of Katanga sequences are marked by major thrust faults and an angular unconformity. The western margin has unclear contacts, but the appearance of coarse biotite schists and gneisses below hematitic meta-sandstone usually marks the Lower Roan and Basement Supergroup contact. Basement

Supergroup rocks (Figure 14) NE-SW trend, which also is characteristic of the other surrounding rocks of the Katanga Supergroup.

2.2.1 CHLORITE MUSCOVITE SCHIST

Figure 16 shows a rare surface geological profile exposed within a pit of chlorite muscovite schist of the Basement Supergroup. The chlorite muscovite schist is medium-grained, light green with up section increase of mottled appearance marked by quartz and feldspar. The foliation is the prominent structure within the rock, defined by aligned chlorite, muscovite and biotite. The unit dips at 30° to the southeast parallel to the regional trend. Above the chlorite muscovite schist, there is secondary laterite and ferricrete-cemented young conglomerate.

Chlorite muscovite schist occurs in the central of the north east Basement Supergroup block (Figure 14). Chlorite muscovite schist was also observed within diamond-drilled hole (NDD008); a summary will be provided in further sections below.

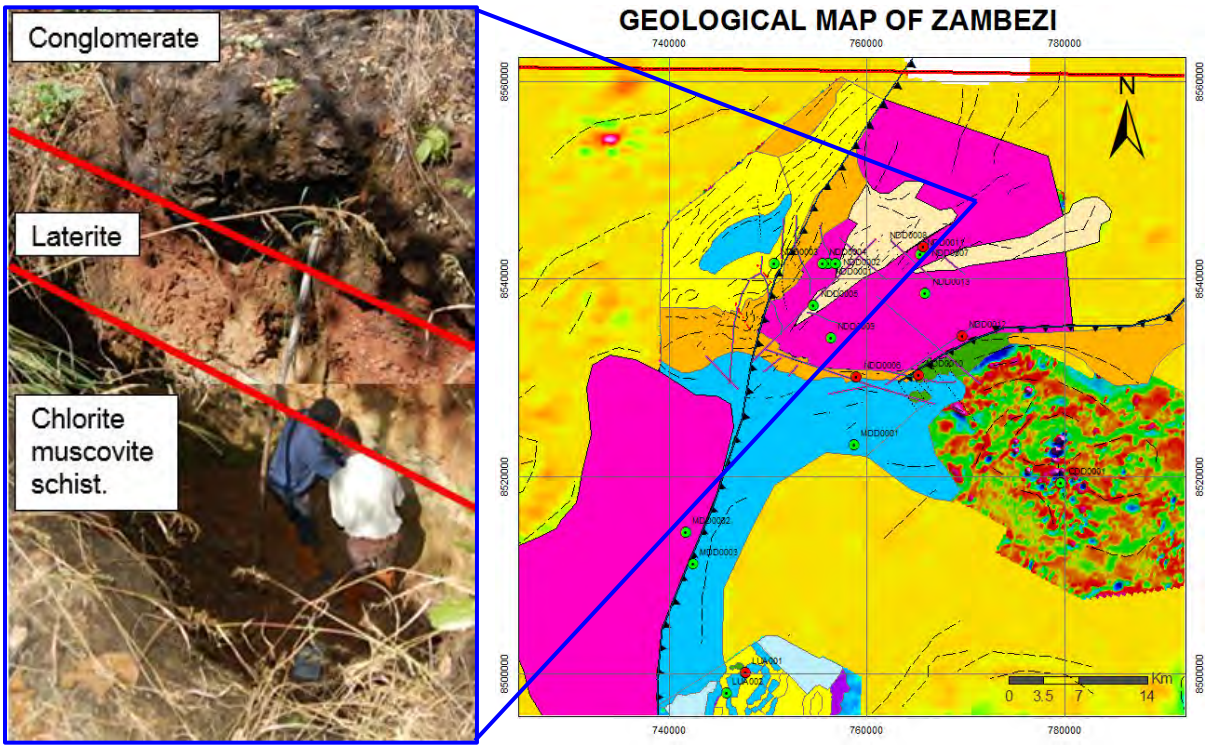

Figure 16: Geological profile within a pit and its location on the geological map. The lowest unit is chlorite muscovite schist, above it is laterite and ferricrete-cemented conglomerate.

2.2.2 BIOTITE FELDSPAR GNEISSES

The rocks intersected within diamond drilled holes NDD012 and NDD008 (see locations in Figure 14) are predominantly pink biotite feldspar gneiss and grey banded gneiss both belonging to the Basement Supergroup (Figure 17). Basement Supergroup gneisses vary in mineral composition, structure and alteration.

Figure 17 (a) is a grey and pink coarse-grained feldspar biotite gneiss. The dominant mineral compositions are K-feldspar and biotite while quartz and muscovite are minor. Minor chlorite alterations also occur along fractures and biotite enriched zones. The rock has variable biotite and feldspar concentrations in different sections. Those that are biotite rich have more pronounced foliation and banding than the feldspar rich. The dominant foliation fabrics developed in a less competent part of the rock are deflected on competent feldspar rich zones.

The pink K-feldspar portions of the gneisses have a strong pervasive potassic alteration of sericite which also is characterised by weakly developed foliation. However, sericite alteration is more pervasive along veins and also characterise weak zones and fractures of the rock. There are also minor portions rich in clay suggesting being weathering of feldspar, and when exposed to air they swell and disintegrate.

Figure 17 (b) shows a grey and pink coarse-grained banded biotite feldspar quartz gneiss. The gneiss is chiefly composed of biotite rich bands alternating with quartz-feldspar rich bands. Biotite band thicknesses range from a few mm to ~1 cm. The bands are dominated by biotite rich bands with minor interstitial quartz and feldspar, which alternate with felsic bands. Felsic bands are composed of sericite, quartz and feldspar with minor biotite. Felsic zones occasionally occur as uniform thin bands. Occasionally, augen and lenses ranging from <1 cm up to 4 cm are wrapped by thin bands. The quartz-feldspathic augen porphyroblasts exhibit weak rotation and are wrapped by biotite rich bands.

Medium-grained greenish grey amphibole biotite feldspar quartz gneiss occurs as thin layers (~50 cm) crosscutting the banded biotite feldspar gneiss. Biotite amphibole band thicknesses are variable.

The gneissic banding in the host and crosscutting rock are parallel to each other with sharp contacts. Amphibole biotite feldspar quartz gneiss might have been part of dyke swarms within the host rock that have been deformed with host rock.

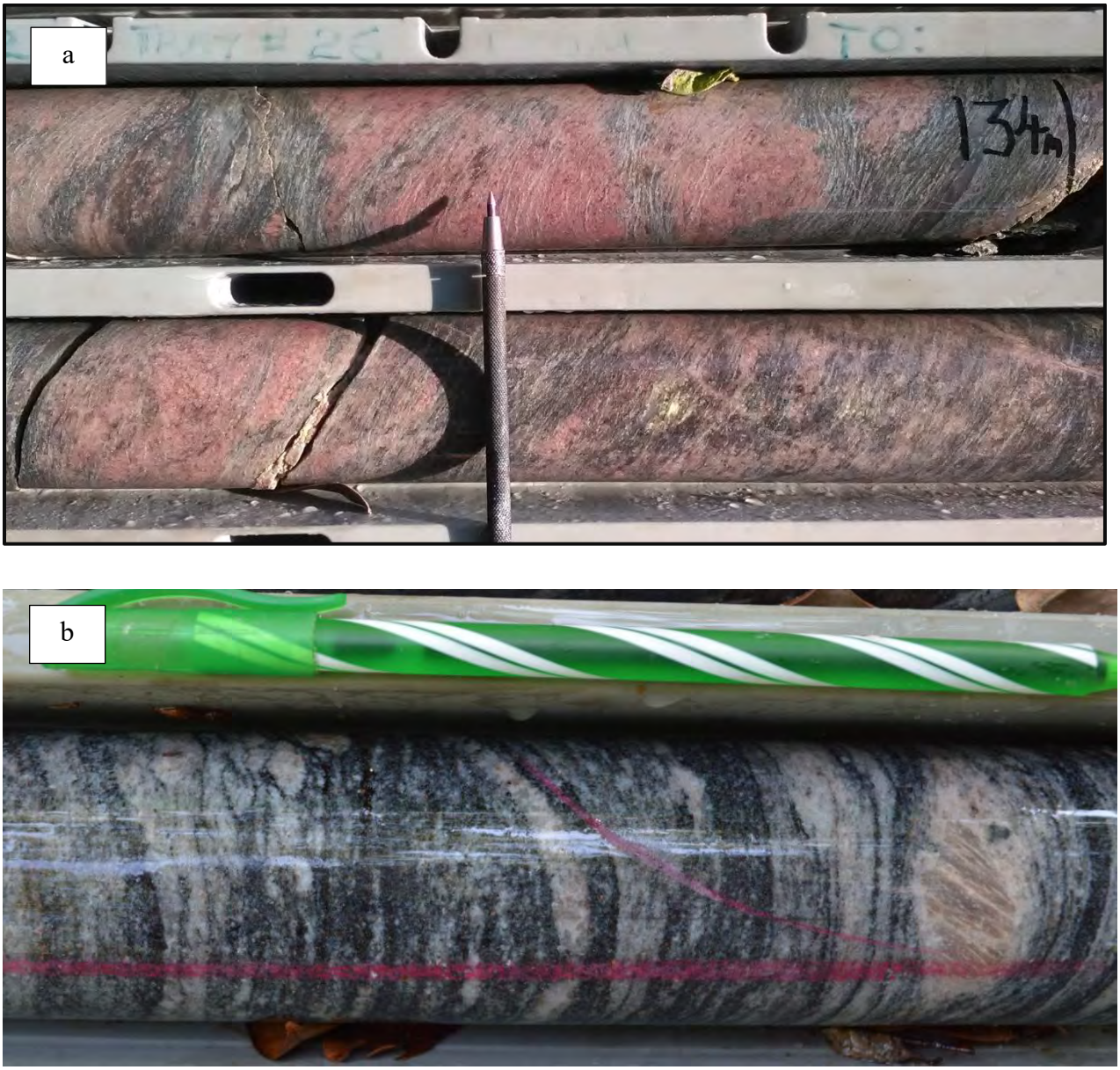

Figure 17: Gneisses of the Basement Supergroup (a) Pink and grey coarse-grained feldspar biotite gneiss. (b) Banded biotite feldspar gneiss composed of biotite rich bands alternating with quartz-feldspar rich bands.

2.3 KATANGA SUPERGROUP: UPPER AND LOWER ROAN GROUPS

The Lower Roan Group (LRG) in Zambezi consists of banded quartzites with hematite while the Upper Roan Group (URG) has carbonate layers and breccias. The LRG in the Zambezi area has rare conglomerates, which are observed in the eastern part of the Katanga Supergroup (Selley et al., 2005). The hematite content is variable though it is the most distinguishing feature of the LRG. The URG is a carbonate dominated sequence and carbonate rich breccias are abundant rock units.

2.3.1 BANDED QUARTZITE

Banded quartzite belongs to the Lower Roan Group. The quartzite consists of thick quartz rich bands alternating with hematite rich bands. The rock occasionally outcrops in the southern portion of the study area, and rarely in the central. The quartzite is in contact with the Basement Supergroup rocks as shown on Figure 18 and Figure 20.

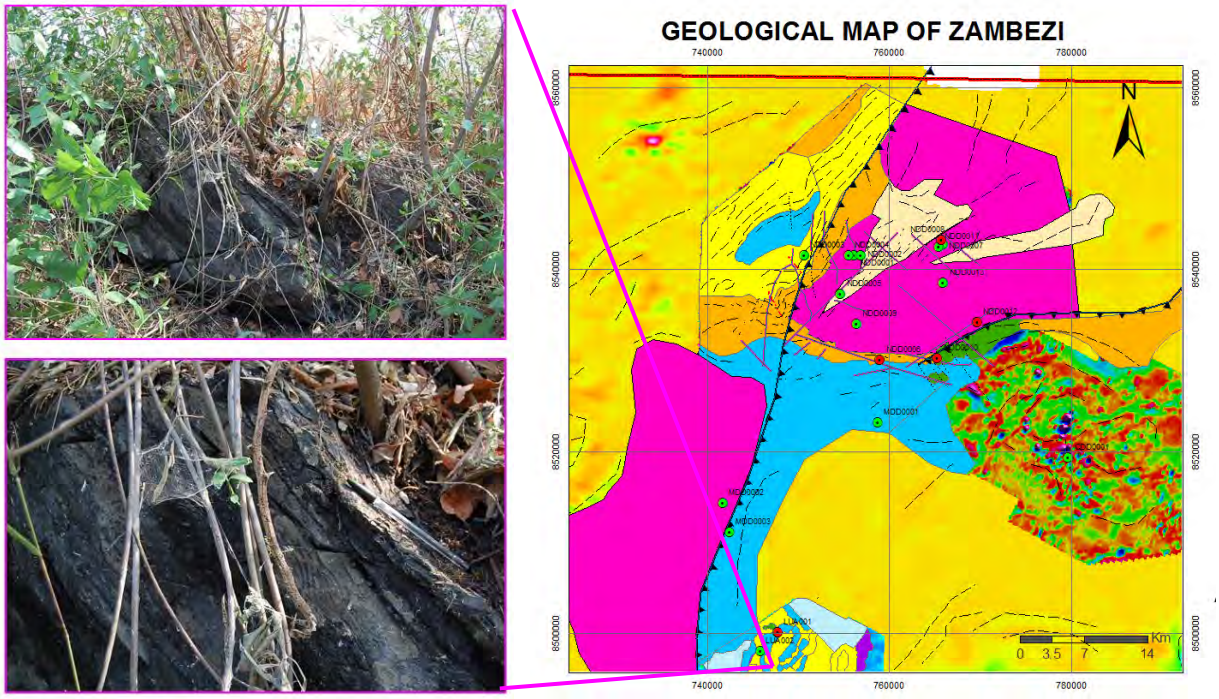

Figure 18: Grey medium-grained banded quartzite with hematite and its location on the geological map.

Banded hematite quartzite is a grey coarse- to medium-grained rock with variable hematite compositional band thicknesses. Thicker crystalline quartzite bands alternate with thinner hematite bands (1 mm to ~8 mm) at irregular intervals.

Banded hematite quartzite is correlated with the rock unit intersected towards the base of diamond drill hole KAY001 section 2.6.2 KAY001 DRILL HOLE. In this hole, the Lower Roan occurs as a medium-grained, interbedded quartzite with biotite schist. The unit is also hematitic with calcite veins concordant to banding and foliations.

However, unlike the eastern Lufilian Arc, there are no conglomerates within the Lower Roan Group to suggest proximity to major fault scarps or sub-basin boundaries. Thrust faults are present along the contacts of the Upper and Lower Roan Groups with the Basement Supergroup on the northwest margin of the basement block (Figure 14).

2.3.2 BRECCIAS

The carbonate rich breccia are the major rocks that characterise the Upper Roan Group with other carbonate rocks. Figure 19 shows a brown outcrop breccia in contact with the quartzite of the Lower Roan Group.

The breccia has quartzite fragments within a fine-grained calcite, hematite and silica rich matrix. Some clasts have a jig-saw structure suggesting in-situ brecciation. Other clasts occasionally show a semi-continuous and broken quartzite bands that have undergone brittle deformation and are recrystallized. The breccia fragments are commonly cemented by hematite with calcite and silica. The fragments consist of calcite and quartz, which is similar to the unfragmented rock that hosts the breccia. The unit is ~50 m thick extending ~500 m along strike along. The breccia occurs along a stream and consist of parts with pits, vugs and cavities.

Figure 19 shows a breccia with sandstone and quartzite fragments in a hematite, silica and carbonate matrix. Closer to this breccia are quartzites, containing oxidised pyrite cubes. The structural trend could not be identified.

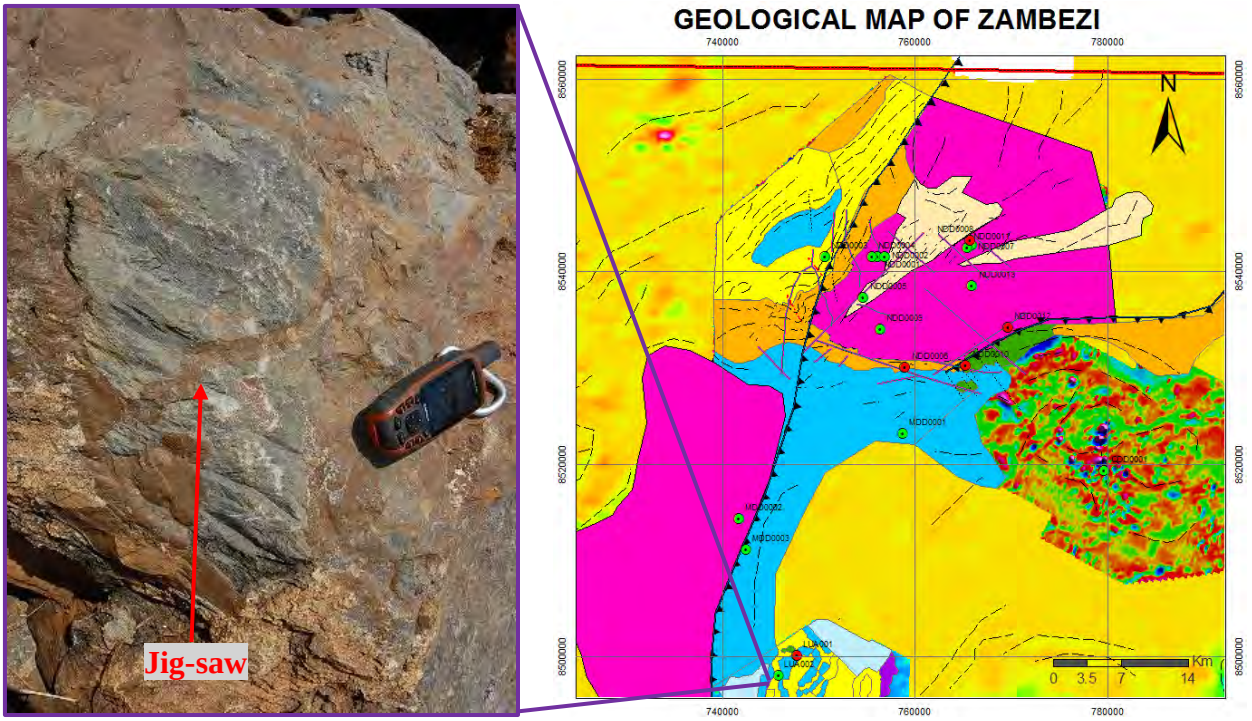

Figure 19: (a) Breccia with semi-continuous grey quartzite fragments that can fit together and are separated by the matrix. Fragments are cemented by brown fine-grained silica, carbonate and hematite matrix.

Different breccia units are intersected within diamond drill holes. The breccias are distinguished based on the composition, clast size and distribution. Figure 20 shows brown breccia with carbonate and quartz clasts within a hematite and carbonate matrix. Clast sizes are variable from ~1 mm within the ground mass to 20 mm. The brown breccia transition into a grey breccia composed of carbonate clasts which are randomly distributed within a biotite dominated matrix with minor carbonate.

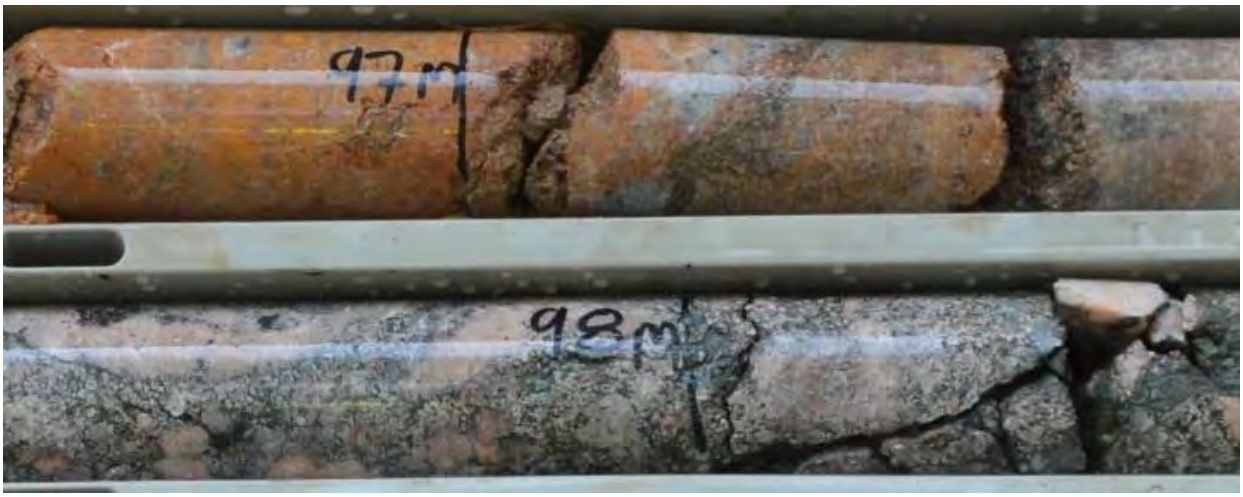

Figure 20: Carbonate breccia consists of two different compositional breccia. The brown breccia with carbonate clasts cemented by carbonate and iron oxide matrix while the grey breccia has carbonate clasts cemented by biotite rich matrix.

2.4 MWASHIA GROUP

The Mwashia Group within Zambezi has been metamorphosed to schists which consist mainly of muscovite and biotite. The Mwashia Group is extensive within the central and southern part of Zambezi area. The Mwashia Group has similarities with the Grand Conglomerate Formation and are in contact with each other. These units have been grouped as one on the geological map in Figure 14. Contacts of the Grand Conglomerate Formation and the Mwashia Group are transitional and can in some places be over 100 m thick.

2.4.1 MUSCOVITE SCHIST

Muscovite schist belonging to the Mwashia Group is commonly brown and weathered muscovite schist. It has preserved schistose fabric defined by muscovite. The muscovite schist exposure has foliations with shallow south easterly dip. The weathered muscovite schist lies west of the breccia indicated in Figure 21.

The schist is brown medium-grained rock composed of muscovite, quartz, feldspar and calcite with hematite alteration. Muscovite defines the wavy schistose fabric of the rock. Along the schistose fabric are minor quartz and feldspar within coarser portions.

Two sets of calcite veins cut across the schist concordantly and discordant to foliation fabric. The schist has also been cross-cut perpendicular to foliations by ~5 cm thick fragmented quartz vein.

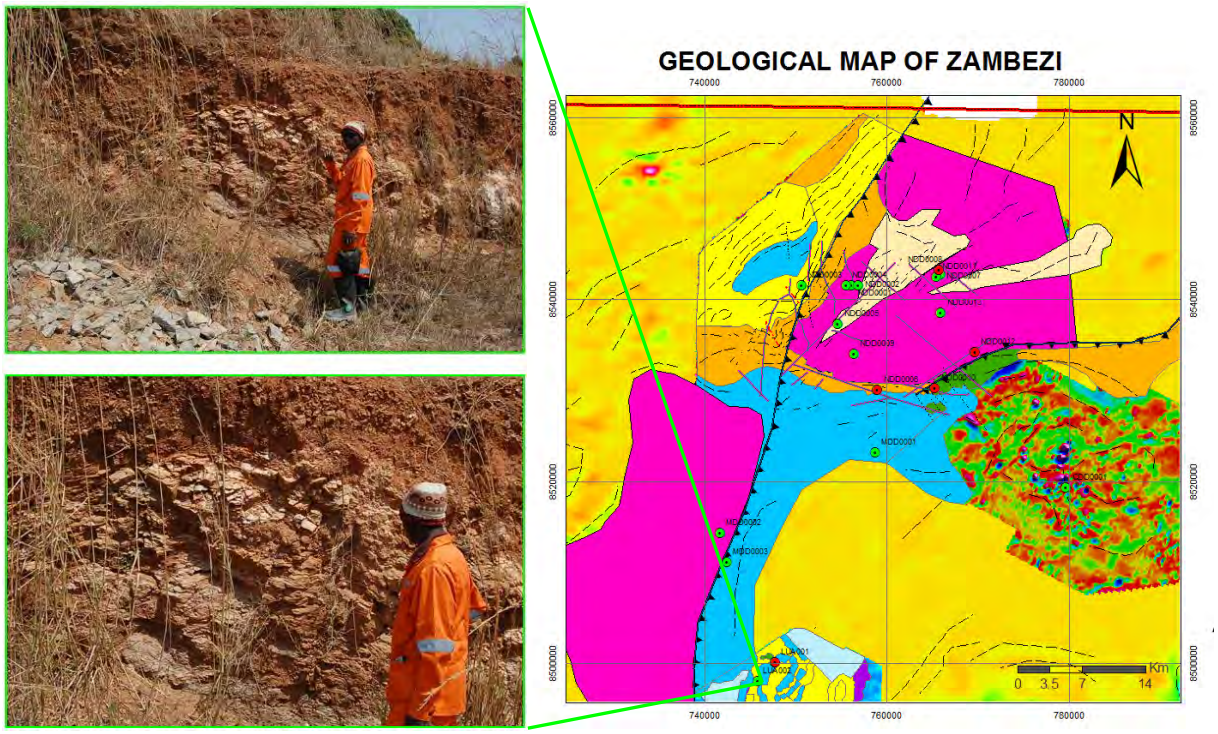

Figure 21: Weathered foliated muscovite schist and its location on a geological map with foliation dipping eastwards.

2.4.2 GARNET BIOTITE SCHIST

Garnet biotite schist (Figure 22) characterizes the Mwashia Group. Garnet biotite schist is commonly grey and medium-grained. The major compositions are biotite, quartz and calcite with garnet porphyroblasts. Amphibole is present in places.

The pervasive foliation is defined by dark grey biotite in variable abundance. The light grey bands are composed of calcite and quartz. Pinkish to brown garnet porphyroblasts are ~5 mm in size and are randomly distributed within the biotite, quartz and calcite matrix.

In places, the Mwashia Group schists occur, and where they are present they show magnetite and pyrrhotite alteration along the schistose fabric.

Figure 22: Medium-grained grey foliated garnet biotite schist showing garnet porphyroblasts within a biotite and calcite rich matrix. The foliation is defined by fine-grained dark grey biotite; light grey bands are calcite and quartz.

2.5 NGUBA GROUP

2.5.1 GRAND CONGLOMERATE FORMATION

The distinct and common formation within the Nguba Group is the Grand Conglomerate (GC). The GC consist commonly of garnet biotite schist containing stretched polymictic clasts within a foliated biotite rich matrix. The GC schist is generally medium-grained and composed of biotite, garnet, amphibole, calcite, and feldspars forming the matrix of polylithic clasts.

The major matrix composition is biotite, quartz, feldspar, calcite with minor muscovite. Biotite defines the foliation fabric, it is continuous and pervasive throughout the rock unit. Quartz and feldspar occur along foliation. Calcite matrix is whitish grey occurring more as bands along biotite foliation trend (Figure 23). When sulphides are present, they occur as part of matrix along the foliation fabric.

Porphyroblasts commonly are garnet and amphibole, which are randomly distributed within the matrix. ~1 mm to ~8 mm sized garnet porphyroblasts are reddish-pink and euhedral in shape

(Figure 23). Garnets have been rotated, as indicated by asymmetrical trails curving into foliation trend.

Amphibole porphyroblasts within the GC are rare. They are greyish green, euhedral and are rarely aligned with matrix. This suggests amphiboles to be post deformation.

Clasts within the GC are composed of dolomite, granite, quartz, sandstones and argillite rich rocks. Clast sizes range from pebble to cobble. Clast shapes are variable from sub-rounded to angular while others are lencoidal following foliation fabric. Some clasts contain pyrite and pyrrhotite and such sulphides are more abundant on the rims and less common towards the core. Competent clasts are commonly wrapped by deflected matrix foliation. Less competent clasts are stretched, forming lenses. They commonly exhibit weak foliation concordant to the matrix foliation trend.

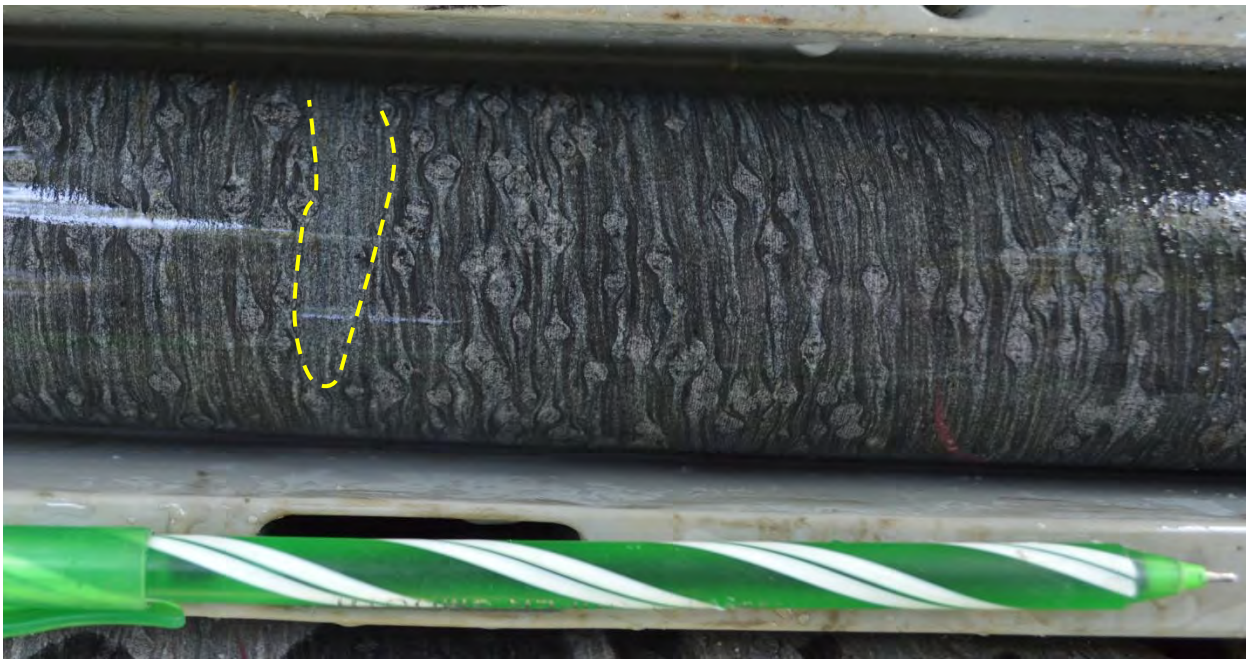

Figure 23: Grey garnet biotite schist of the GC Formation with a clast outlined with a yellow hashed line. Garnets show rotation and trails.

The Mwashia Group (MG) is not easily distinguished from the Grand Conglomerate (GC) in drill cores. The two groups have similar mineral assemblages and metamorphic fabric. Commonly, the contact between the GC and MG is transitional with clasts that become less abundant towards the MG. Absence of clasts is interpreted as the beginning of the MG. The other distinguishing feature

separating the GC and the MG are occasional banded iron formations and massive magnetite and hematite ironstones that are present in the MG but not in the GC.

2.6 DRILL HOLE STRATIGRAPHIC SECTIONS

The stratigraphic succession of drill holes in Zambezi area is based on interpretation of mapping, aircore and diamond drill holes in comparison to the typical stratigraphy of eastern Zambia. The units within selected drill holes in Zambezi have been metamorphosed, and identification of marker stratigraphic units like the Grand Conglomerate was key to the placement and understanding of the stratigraphic succession.

Six drill holes were selected for detailed study: LUA001, KAY001, NDD0006 NDD0008, NDD0010 and NDD0012. The drill hole positions are indicated on the map in Figure 14. These drill holes intersected different lithologies that have been interpreted and placed in their stratigraphic position within the Katanga and Basement Supergroups. The Katangan units within these drill holes include distinctive biotite pebble schists interpreted to represent the Grand Conglomerate (GC) Formation; banded iron formation and garnet biotite schists are interpreted as part of the Mwashia Group. Quartzites with hematite bands and meta-sandstones with schists belong to the Upper Roan Group. Thick dolomites and breccias were generally interpreted as Upper Roan Group. There are other units which are interpreted as Basement Supergroup, which include quartzite, gneisses and schists. Generally, the degree of metamorphism and to a lesser extent deformation is high in the Zambezi area which complicates the stratigraphic analysis as well as correlation.

2.6.1 LUA001 DRILL HOLE

LUA001 was collared within sands of the Kalahari Group, the pebble biotite schist below of which is interpreted as Grand Conglomerate Formation (Table 2). The hole starts from 0 m and terminates at 490.5m. The hole intersects the GC Formation, the last 60 m consisting of phlogopite schist with stretched clasts into thin lenses.

The drill hole summary log (Table 2) shows the stratigraphy and the various units intersected. In summary, the hole consists of unconsolidated sand and sandstones of the Kalahari Group underlain by a pebble schist. The schist consists of sub-rounded to angular and lencoidal polymictic clasts

in a biotite, muscovite, carbonaceous and calcitic foliated matrix. Clasts composition include sandstones, carbonates, siltstones, shales, and quartzite, which are randomly distributed and are wrapped by the matrix foliations. Pyrite and pyrrhotite crystals occur along the clasts rim and become more disseminated towards the core. The foliated matrix is dominated by biotite, muscovite and phlogopite with quartz, feldspar and calcite forming. From all the holes drilled and logged, this was the least deformed and metamorphosed sequence within Zambezi area. The sample MC004 of biotite schist with shale and carbonate clasts was sampled from LUA001 between 265.5 and 265.8 m.

Table 2: Summary geology and stratigraphy of LUA001, included are photographs, summary of rock descriptions, strip log and stratigraphy.

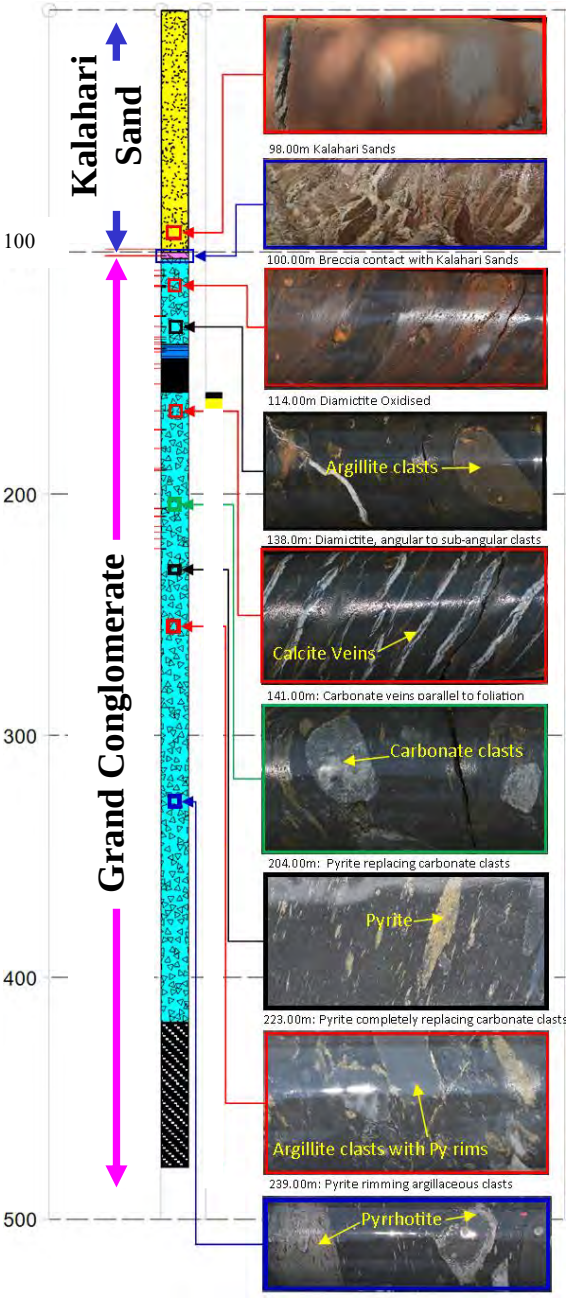

0-98 m Brown patched consolidated, massive Kalahari sandstone consist mainly medium-grained quartz.

98-102 m Weathered argillic hematite rich breccia cemented by fine-grained clay, quartz and calcite. Fragmented and weathered indicating base of Kalahari and top of bedrock contact. Clasts are foliated and elongate, there are pebble to cobble sized clasts oriented along foliation trend.

102-130 m Moderately foliated, oxidised brown pebble schist below of which is a carbonaceous schist with few pebbles.

130-415 m Medium to coarse-grained, sub-rounded to angular and lencoidal polymictic clasts in a grey muscovite, carbonaceous and calcitic foliated matrix. Clasts have oxidized pyrite growth within and along the rims. Clasts commonly have deflecting and wrapping of foliations around them.

141-149 m Matrix is dark grey to black (carbonaceous), muscovite with calcareous material and calcite occurring as veins along foliation.
204-216 m Fine-grained and moderately foliated calcareous phyllitic matrix with clasts sheared together with matrix and have lencoidal porphyroclasts texture with rotated clasts. The unit has granule-size clasts with minor being pebbly, some are partially replaced by pyrrhotite and pyrite. Clasts shapes vary from subrounded to augen, lencoidal and flat lenses.
223-230 m Pyrite mineralization occurs as blobs, disseminations and striations following planar S1 foliation direction with some pyrite replacing clasts. (Clasts are sheared and elongate).
239-244 m Pyrrhotite is more massive than pyrite though occurring as massive bands
Sulphide mineralization is zoned, from 150 to 250 m is pyrite. From 250 to 340 m is a mixed zone of pyrite and and pyrrhotite while from 340 to 490 m is a pyrrhotite zone.

415-490.5m Phlogopite schist with minor clasts. The schist has phlogopite defining the foliation fabric with minor calcite. Clasts are sparsely distributed and range from ~2 to 10 mm

LUA001 Key

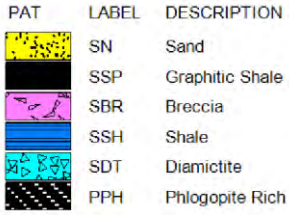

2.6.2 KAY001 DRILL HOLE

KAY001 primarily intersected four Katangan stratigraphic units, which are the Grand Conglomerate Formation of Nguba Group, the Mwashia Group, the Upper Roan Group and the Lower Roan Group (Table 3). Overlying the Katangan stratigraphic units is the Kalahari Group consisting of loose sands and sandstones with calcrete. The contact between Kalahari Group and the Katanga Supergroup is marked by a thin ~1 m breccia that have fragments with similar composition as the unit below it.

The Lower Roan Group is characterized by grey interbedded quartzite with biotite schist. Occasionally, hematite pervasively alters the rock and gives a reddish color. Calcite veins are commonly discordant to foliation fabric.

The Upper Roan Group consists of medium-grained foliated calcite rich grey biotite schist. The rock easily breaks along foliation planes.

Overlying the Upper Roan Group is the Mwashia Group, which consists of a bleached silty calcareous phyllite with preserved primary lamination that is cut by the foliation at high angle.

The Grand Conglomerate of the Nguba Group overlies the Mwashia Group. The contact between these two consists of banded ironstones. The Grand Conglomerate has a foliated matrix composed of biotite quartz, calcite and feldspar. Within the matrix are randomly distributed garnet and amphibole porphyroblasts. Primary clasts ranging in size from 2 mm to 40 mm are composed of quartz, siltstone, carbonates and shale. These are randomly distributed within the matrix.

Three rock samples were taken from KAY001 which include MC001, MC002 and MC003. These were taken from intervals 170.0 to 170.2 m, 242.0 to 242.2 m and 351.2 to 351.4m respectively.

Table 3: The summary geological description of KAY001. This includes a strip log, photographs and summary of intersected lithologies and the stratigraphic succession on the left.

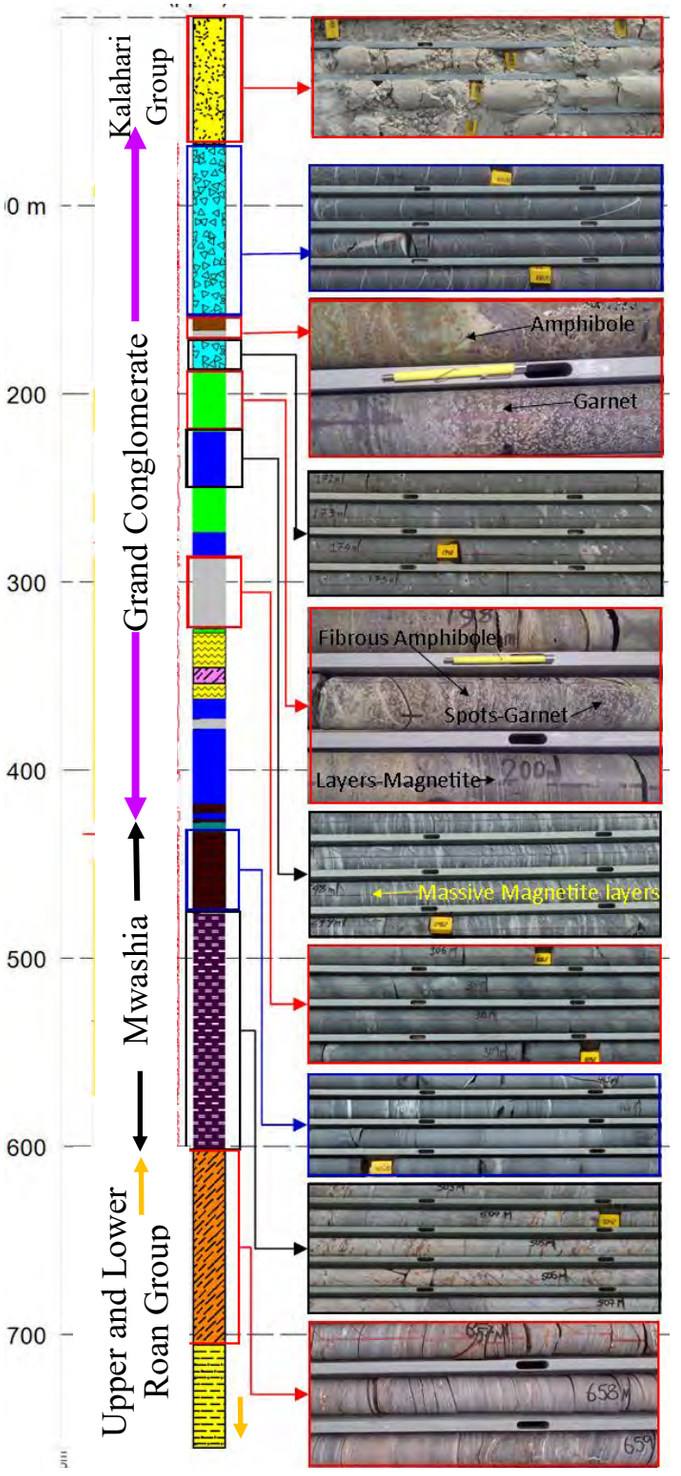

0-65 m Grey medium-grained massive, friable Kalahari Group sandstone.

65-188 m Grand Conglomerate (GC) composed of interbedded biotite schist and amphibole-garnet schist. The GC is metamorphosed and has blackish grey carbonaceous phyllitic shale with sub-angular poorly sorted matrix-supported clasts. Clasts include different lithic fragments like carbonates, quartzites, shales, sandstones and granites. The unit is moderately foliated and cut by parallel calcite veins that are ~1mm thick. The amphibole-garnet schist has coarse radiating actinolite clusters along the foliation and some disseminated medium to coarse magnetite/hematite crystals.

188-287 m Interbedded amphibole-garnet-magnetite schist with thick banded iron with quartz. The unit has interbedded magnetite-actinolite layers which in places show garnet and massive bands of magnetite. Pyrite occurs along fractures and calcareous veins.

287-324 m Altered amphibole garnet schist. The garnets porphyroblasts are coarse-grained within an actinolite rich groundmass with pyrite in fractures.

324-362 m Mixed zone dominated by amphibole-garnet schist with calcite rich zones; variable banded hematite/magnetite intervals.

362-430 m Magnetite rich zone. Representative unit is amphibole garnet magnetite schist. Magnetite and garnet concentration vary on different intervals.

430-470 m Amphibole-garnet schist. An altered unit with magnetite and pyritic shale with minor calcite. An increase of pyrite within deformed zones and increased calcite veins from 468.2 m.

470-600 m Bleached silty calcareous shale. Weak laminations are cut by foliation at 60°.

600-705 m Calcite rich, medium-grained grey biotite schist. Rock easily breaks along foliation planes.

705-760 m Medium-grained, interbedded quartzite with biotite schist and shows poorly preserved cross beds within the quartzite. Hematite alteration and calcite veins vary in places.

PAT	LABEL	DESCRIPTION
	SN	Sand
	MQT	Quartzite
	MA	Amphibolite
	SSH	Shale
	SDT	Diamictite
	ACT	Amphibole-Iron Oxide Altered Unit
	AGM	Amphibole-Garnet-Magnetite Altered Unit
	AGS	Amphibole-Garnet altered Shale
	ALT	Altered Unit
	AMG	Amphibole-Garnet Altered Unit
	BSH	Bleached Shale
	MAA	Magnetite-Amphibole Altered Unit
	MAG	Magnetite-Amphibole-Garnet Altered Unit
	XB	Biotite Schist

2.6.3 NDD0006 DRILL HOLE

NDD0006 intersects 60.5 m thick sand and sandstones of the Kalahari Group underlain by 64.5 m garnet biotite schist of the Grand Conglomerate (GC), below which is the 53 m thick Mwashia Group consisting of pyritic shales and meta-siltstones (Table 4).

The lowermost unit intersected is 83 m grey garnet biotite schist belonging to the GC. The Mwashia Group is in between beds of pyritic meta-siltstones and shales. The upper contact is gradational while the lower contact with the GC is sharp. The conglomerate is massive with poorly preserved sedimentary structures. However, it exhibits strong biotite dominated foliation with sheared clasts such as shale and carbonates. Some clasts such as granites and quartzites are not sheared and the biotite matrix wraps around them.

Two sets of foliations are observed, in some portions foliation overprints other earlier foliation structures, which suggests multiple deformation phases. The GC has pyrrhotite and pyrite sulphide mineralisation that occurs along foliation fabric and within clasts. The rock sample was taken from 252.2 to 252.4 m and consist of a grey garnet biotite schist. The unit has sheared lens-shaped clasts stretched along foliation fabric.

In the north of NDD006, a hole NDD0018 was collard in the Grand Conglomerate and intersects subsequent stratigraphic units belonging to the Mwashia, Upper and Lower Roan Groups.

Table 4: Summary geological descriptions of NDD0006, included are strip log, stratigraphy and representative photographs.

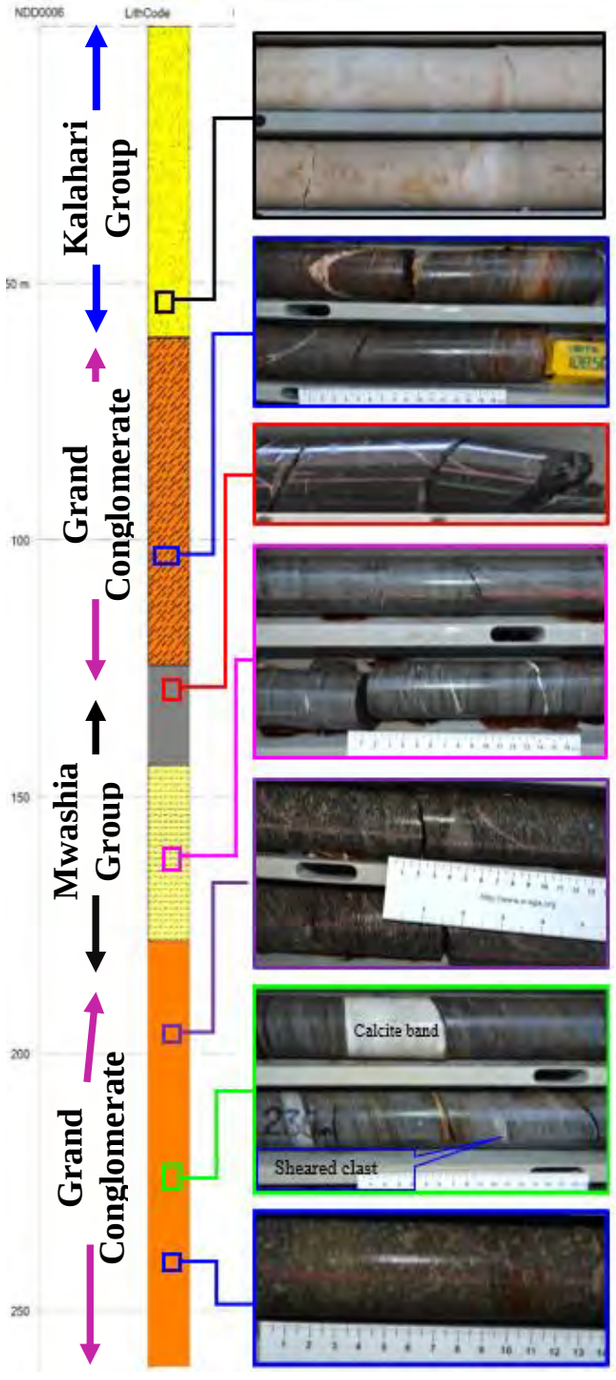

0-60.5 m Whitish grey consolidated Kalahari sands. They are ferrugenised and calcretised patches within the unit.

60.5-125 m Foliated dark grey biotite schist. The unit has brown alteration along foliation with calcite veins discordant to foliations trend. Unit is matrix supported polymictic clasts meta-conglomerate. Some clasts are sheared and elongate, ranging in size from 1 to 80 mm composed of mostly carbonate, sandstone and shale.

125-144 m Carbonaceous grey and black phyllitic shale, finely foliated, pyrite-rich, minor pyrrhotite with calcite-rich bands in places. The unit has some tight folds and sheared portions with minor chloritic alterations along fractures.

144-178 m Grey argillaceous meta-siltstone. The unit is slightly foliated though the siltstone protolith is also distinct. They are calcite veins and easily breaks within the foliation planes.

178-261 m Grey garnet biotite schist. The unit has sheared lens shaped clasts stretched along foliations, there are also calcite bands and veins within. Garnets are euhedral ranging up to 5mm in size. Garnets have white calcite and biotite around them. Garnet composition is variable, some intervals don't have developed garnets.

PAT	CODE	DESCRIPTION
	SSL	Siltstone
	SSH	Shale
	XB	Biotite Schist
	SAN	Sand
	XBG	Biotite Garnet Schist

2.6.4 NDD0008 DRILL HOLE

NDD0008 intersects 69 m of Kalahari Group underlain by 174.6 m of Basement Supergroup (Table 5). Basement rocks intersected include gneisses, schists and quartzites. Major gneisses include banded biotite-rich feldspar quartz gneiss and pink K-feldspar rich gneiss. However, amphibole biotite feldspar quartz gneisses occasionally occur as bands within the main unit. Schists include biotite feldspar schist and scapolite chlorite schist with occasional feldspathic quartzite bands. Feldspathic quartzite is coarse-grained and fragmented, it occasionally occurs as bands within schists and gneisses.

Three samples for petrography were taken from NDD0008 and include MC007, MC008 and MC012. MC007, a biotite feldspar quartz gneiss was sampled from 209.3 to 209.5 m. MC008, an amphibole biotite feldspar quartz gneiss was sampled from 214.2 m to 214.4 m while MC012 an amphibole biotite feldspar quartz schist was sampled from 178.4 to 178.7m.

Table 5: Summary geology descriptions, pictures, strip log and stratigraphic section of NAC0008

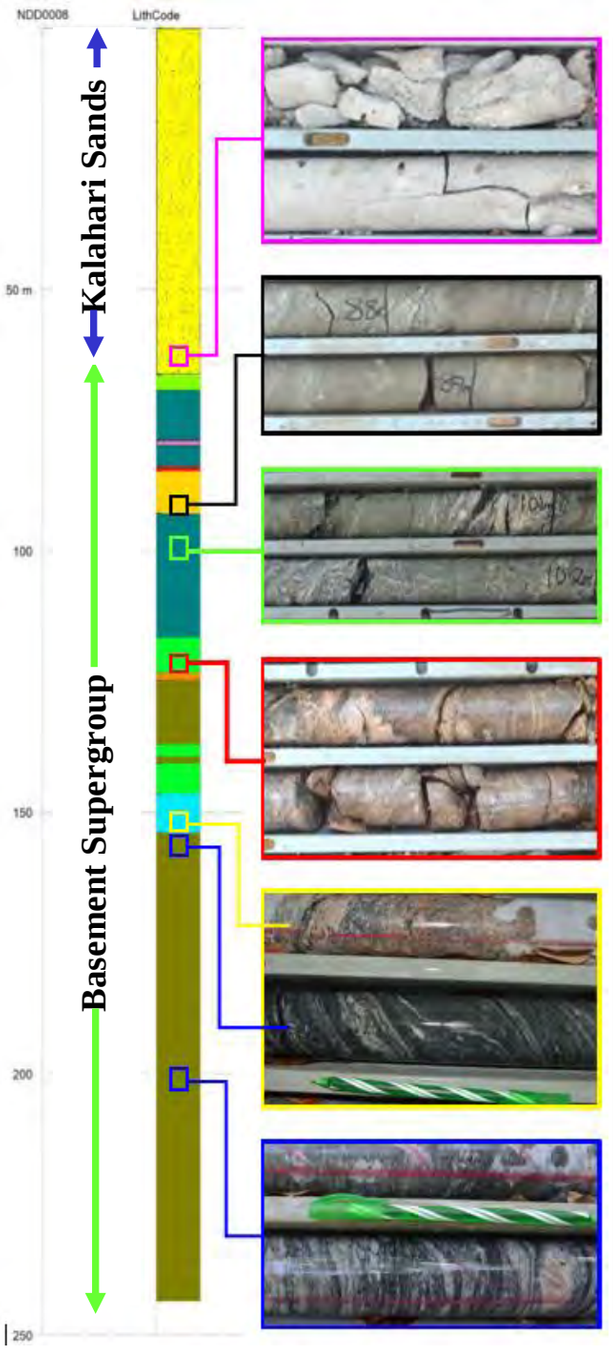

0-69 m Grey Kalahari Group consisting sands with various degree of oxide alteration stains

69-71 m Fractured and weathered feldspathic quartzite occurring as paleo-surface breccia.

71-79 m Brecciated feldspathic quartzite supported by a weathered and altered feldspar and biotite rich matrix. Unit becomes more biotite rich with increase in depth and becoming more sheared. It has talcose feel on joint surfaces.

79-93 m Biotite feldspar schist with some feldspathic quartzite bands.

93-123 m Greenish medium-grained K-feldspar rich biotite chlorite feldspar quartz gneiss. Dominant minerals are feldspar and quartz with minor biotite and chlorite. They are bands of biotite chlorite schist at sparse intervals within the unit.

123-137 m Feldspathic quartzite with greyish and pink coarse-grained biotite feldspar quartz gneiss. There are minor biotite scapolite chlorite schist bands.

137-146 m Pink, coarse-grained K-feldspar biotite gneiss. Dominant minerals are feldspar and quartz with some very minor biotite.

146-154 m Biotite quartz feldspar gneiss with interlayers of biotite scapolite chlorite schist.

154-243.6 m Banded biotite feldspar quartz gneiss. There are pink K-feldspar and quartz felsic bands interlayered with biotite rich schists. Minor augen feldspar in places with sigmoidal trails. There are amphibole biotite feldspar quartz gneiss occurring as bands.

PAT	CODE	DESCRIPTION
	SAN	Sand
	XBS	Biotite Sericite Schist
	SFQ	Feldspathic Biotite Quartzite
	NBFQ	Biotite Feldspar Quartz Gneiss
	NBQF	Biotite Quartz Feldspar Gneiss
	NFQ	Feldspar Quartz Gneiss
	TLS	
	XBF	Biotite Feldspar Schist
	XBSE	Biotite Scapolite Epidote Schist
	XEF	Epidote Feldspar Schist

2.6.5 NDD0010 DRILL HOLE

NDD0010 intersects 30.5 m of grey loose sands and sandstones of the Kalahari Group. Underlying the Kalahari Group is a 219.5 m of metamorphosed Grand Conglomerate Formation with abundant variable garnet biotite schist, dolomite, meta-siltstones and limestone (Table 6).

Garnet biotite schist is the dominant rock unit within the GC, it is grey when fresh and brown when oxidised and weathered. It consists of red garnets within a foliated biotite rich matrix, other matrix compositions include calcite, quartz and feldspar. Clasts are embedded within the matrix and are elongate along foliation fabric, abundant clasts consist of carbonates and clay. Grey dolomite is massive with weak banding, within are massive pyrite mineralization along fractures and as veins parallel to banding. Meta-siltstones are weakly foliated with abundant disseminated pyrite and rare specks of chalcopyrite. Limestone is interlayered with rare pyritic shale. Limestone is grey with weak fabric that have concordant calcite veins.

There were three samples for petrography that were taken from NDD0010. These include MC005, MC006 and MC013 all being garnet biotite schists and belonging to the GC. These were sampled from 127.0 to 127.2 m, 144.3 to 144.5 m and 114.9 to 115.3 m respectively.

Table 6: Summary geological descriptions, representative pictures, strip log and stratigraphic profile of NDD010.

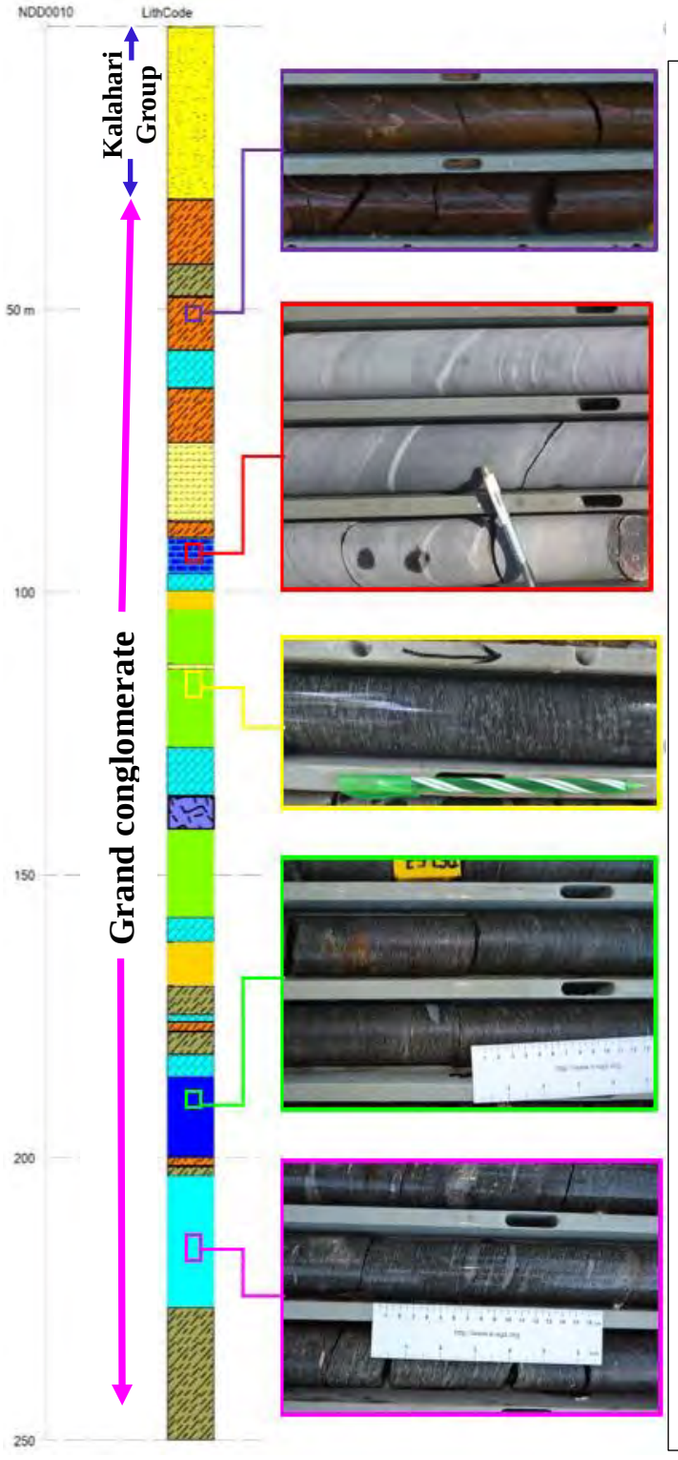

0-30.5 m Sandstones and sands of Kalahari Group.

30.5-89 m Brown ferruginized biotite schist. Minor quartz in places. 57-63 m silicified and iron stained dolomite with pyrite completely oxidised. 73-87 m bands of siltstones and quartz biotite schist, they are minor pyrite and carbonate veins.

89-100 m Whitish grey limestone unit rich in calcite underlain by a pinkish brown to orange brown silicified dolomite.

100-170m Grand Conglomerate comprising of grey garnet biotite schist with some dark grey to black metamorphosed clasts with carbonate rims. Garnet porphyroblasts are range from 3 to 6 mm in sizes.

170-181m Whitish grey garnet biotite schist. Garnets existing as pinkish euhedral clasts aligned parallel to foliation embedded in a biotite foliation. Minor dolomite bands within.

181-200 m Biotite scapolite schist. Scapolite occurs as pale white rounded spots, grey to black foliated biotite schist with carbonates as matrix.

200-250 m Grey garnet biotite schist medium to euhedral coarse-grained garnets with pyrite mineralization along foliation fabric. From 226 to 250 m, there is a whitish grey garnet biotite schist. Euhedral garnet porphyroblasts are pinkish red and aligned parallel to the biotite foliation.

PAT	CODE	DESCRIPTION
	SSL	Siltstone
	SD	Dolomite
	XB	Biotite Schist
	SAN	Sand
	SL	Limestone
	XBC	Biotite Carbonate Schist
	XGB	Garnet Biotite Schist
	XQBC	Quartz Biotite Chlorite Schist
	XGBC	Garnet Biotite Chlorite Schist
	XBCS	Biotite Carbonate Scapolite Schist
	XBGC	Biotite Garnet Carbonate Schist

2.6.6 NDD0012 DRILL HOLE

NDD0012 intersected 41.5 m of Kalahari Group consisting of grey sands and patched grey and brown sandstones. This is underlain by 162.5 m of schists and gneisses of the Basement Supergroup (Table 7).

Two types of schists were intersected, these include medium-grained grey to brown foliated muscovite feldspar quartz schist with hematite alteration. Their upper portion is fractured with rare weathered portions in places. Another rare occurrence includes schists with spotted muscovite along foliation fabric. The other schists are grey, coarse-grained biotite chlorite schists with minor muscovite, feldspar and quartz biotite muscovite schists. Gneisses include a greyish pink coarse-grained biotite feldspar banded gneiss. It is composed of K-feldspar, quartz, biotite and muscovite with a weak chlorite alteration and strong pervasive potassic alteration of sericite. The unit is cut by quartz-feldspar veins that have altered walls of host rock. Another common gneiss is a coarse-grained grey banded biotite quartz feldspar gneiss interlayered with quartz muscovite schist.

Three samples for petrography were taken from NDD0012 which include MC009, MC010 and MC014. MC009, a muscovite feldspar quartz schist was sampled from 72.3 to 72.5 m. MC010, a feldspar biotite gneiss was sampled from 138.4 to 138.6 m while MC014, a biotite quartz feldspar gneiss was sampled from 188.0 m to 188.2m.

Table 7: The table shows from left to right the stratigraphy, strip log, corresponding pictures and intersected lithologies.

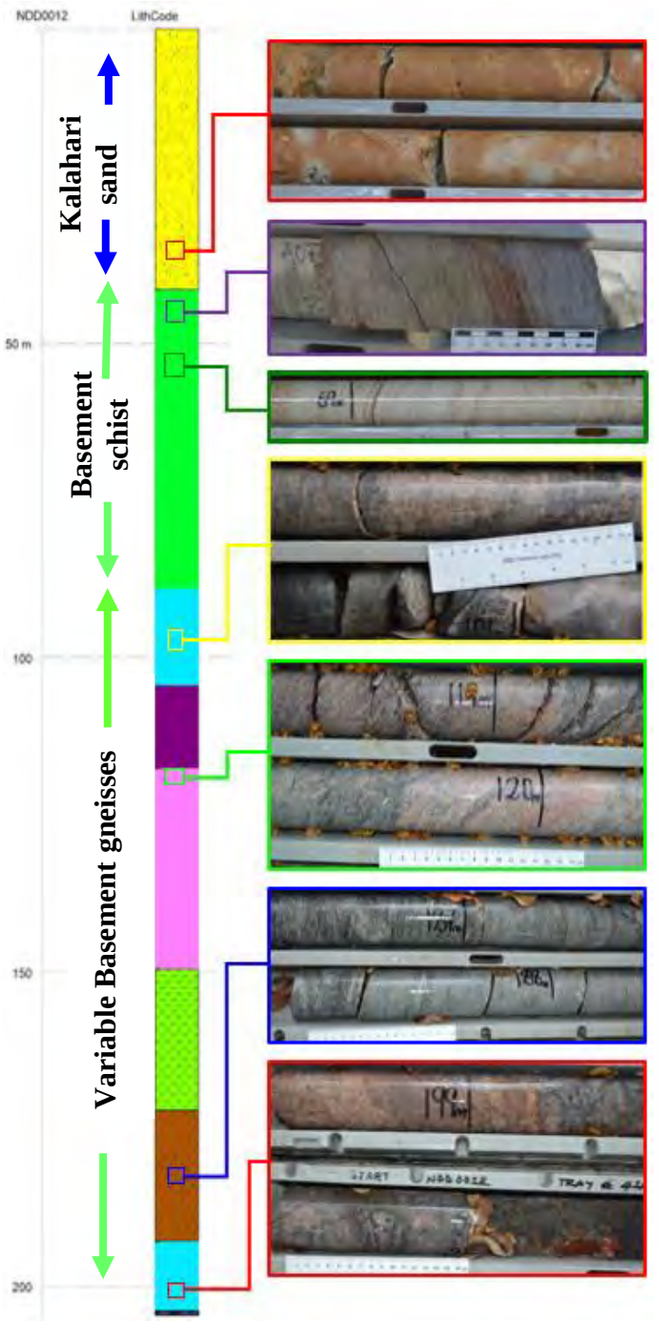

0-41.5 m Poorly consolidated medium-grained grey and brown Kalahari Group sands.

41.5-89 m Medium-grained grey to brown strongly foliated muscovite feldspar quartz schist with hematite alteration. Unit is fractured with rare weathered portions.

89-104 m Greyish pink coarse-grained biotite feldspar banded gneiss composed of K-feldspar, quartz, biotite, muscovite. The section has weak chlorite alteration and strong pervasive potassic alteration. They are minor portions rich in clay derived from weathering of feldspar, when exposed to air they swell. Quartz-feldspar veins are fragmented and have altered walls of host rock.

104-117 m Pink greenish grey, coarse-grained biotite muscovite feldspar quartz gneiss. Consist of minor quartz/chlorite and strong pervasive potassic alteration. There are common portions rich in clay resulting from weathering of feldspar and when exposed to air they swell.

117-149 m. Greyish pink, coarse-grained banded feldspar, quartz, biotite, muscovite gneiss. This unit is the repetition of interval between 89 to 104 m.

149-192 m Coarse-grained grey sheared and foliated interbanded muscovite quartz schist with biotite quartz feldspar gneiss. There are minor portions altered with feldspar, chlorite and silica. From 172 m, the biotite content decreases.

192-204 m Grey, coarse-grained sheared feldspar quartz biotite muscovite schist.

204-204.5 m Medium-grained greenish black biotite chlorite schist. The unit has minor coarse-grained quartz and feldspar.

PAT	CODE	DESCRIPTION
	SAN	Sand
	XQM	Quartz Mica Schist
	XBC	Biotite Carbonate Schist
	XQBM	Quartz Biotite Muscovite Schist
	XFQB	Feldspar Quartz Biotite Schist
	XFQM	Feldspar Quartz Muscovite Schist
	XMF	Muscovite Feldspar Schist
	XMFQ	Muscovite Feldspar Quartz Schist

2.7 STRUCTURAL GEOLOGY

There are different phases and styles of deformation attributed to different events that have affected the Lufilian Arc. Structural deformation and metamorphism within the Lufilian Arc is not uniform. Different areas and domains of the Lufilian Arc have undergone different extent of metamorphism. The structural geology of the Zambezi area on the western Lufilian Arc will be described qualitatively with few examples of limited rock samples from drill cores and outcrops. Deformation structures are dominant within the Grand Conglomerate Formation and the Mwashia Group suggesting that this rock type was susceptible to undergo deformation and to preserve the generated structural inventory. Preserved deformation fabric within rocks such as foliations, folds, veins and clasts have been used as aid to assess the deformation history and relate it to the regional metamorphism.

2.7.1 FOLIATIONS AND FOLDS

The rocks in the Zambezi area show three major episode of fabric development that are attributed to the evolution of the Lufilian Arc. These are manifested in foliations, folding and associated thrusting in both the Katanga and the Basement Supergroups. Some of the structures seen in the examined material can be correlated to those established in the eastern Lufilian Arc.

S0 fabrics are commonly parallel to lithological contacts and are weakly preserved in foliated rocks. S0 fabrics are preserved primary sedimentary bedding of the metasedimentary rocks defined by contacts between quartz rich layers and those of biotite schists (Figure 24). S0 fabrics occasionally exhibit disjointed banding within less competent biotite and calcite rich layers. However, there are commonly overprinted by deformation fabrics, which have been used to identify further deformation episodes.

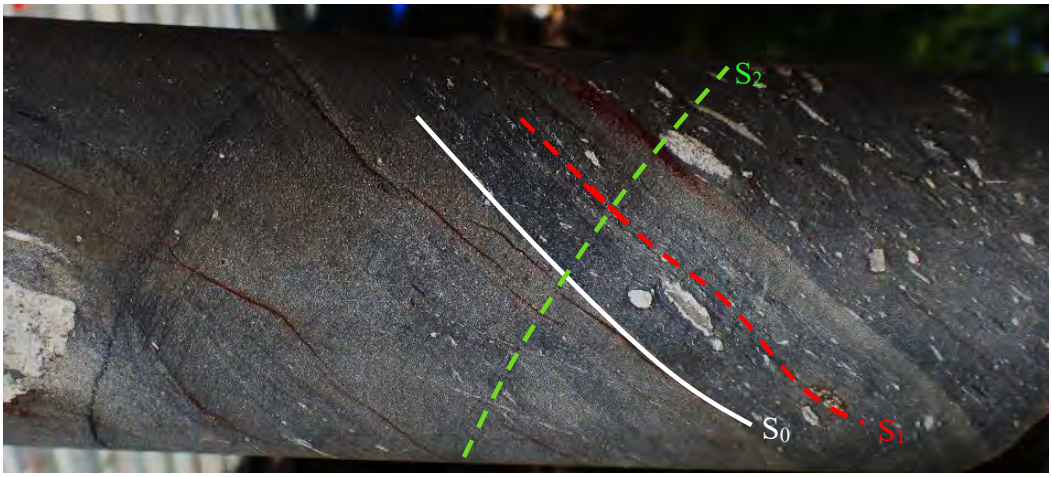

Figure 24: Sub-parallel S0 and S1 foliation within the Grand Conglomerate. S1 is defined by clast alignment and growth of metamorphic biotite while S0 is defined by preserved sedimentary contacts and layering within the Grand Conglomerate. S2 foliation planes defined by biotite transect S0 and S1 at ~90°.

Parallel to S0 is S1, which is related to the first identifiable deformation episode D1. D1 is characterised by aligned metamorphic biotite +/- garnet and clasts defining the S1 foliation fabric. The domain within S1 foliation is defined is defined by aligned biotite and stretched clasts of up to 3 cm length (Figure 25). The other features are calcite-rich bands which are commonly discontinuous suggesting to be affected by flattening and stretching during D1 deformation event.

In places, the S1 foliations are folded and truncated during a subsequent deformation episode D2. This formed a younger foliation, referred to as S2, which is commonly parallel to the F2 axial surface (Figure 25). F2 folds have unequal limbs and are generally gentle folds. S2 foliation is most prominent where it is oriented at high angle with the S1 and the D1 layering. S2 foliation fabric slightly offsets boundaries of the clasts, it also disrupts earlier foliation fabric within the rock (Figure 25). Some clasts and D1 layers show minor offset along S2 planes.

The S2 foliation planes, defined by aligned biotite, transect the layering and S1 at high angle (Figure 25). S2 is also seen in association with small-scale folds and crenulations (see images in sections 3.1 and 3.9). Most likely S2 forms as axial cleavage during F2 folding of S0 and S1, but the genetic relationship of S2 and F2 is not always evident in the drill core material.

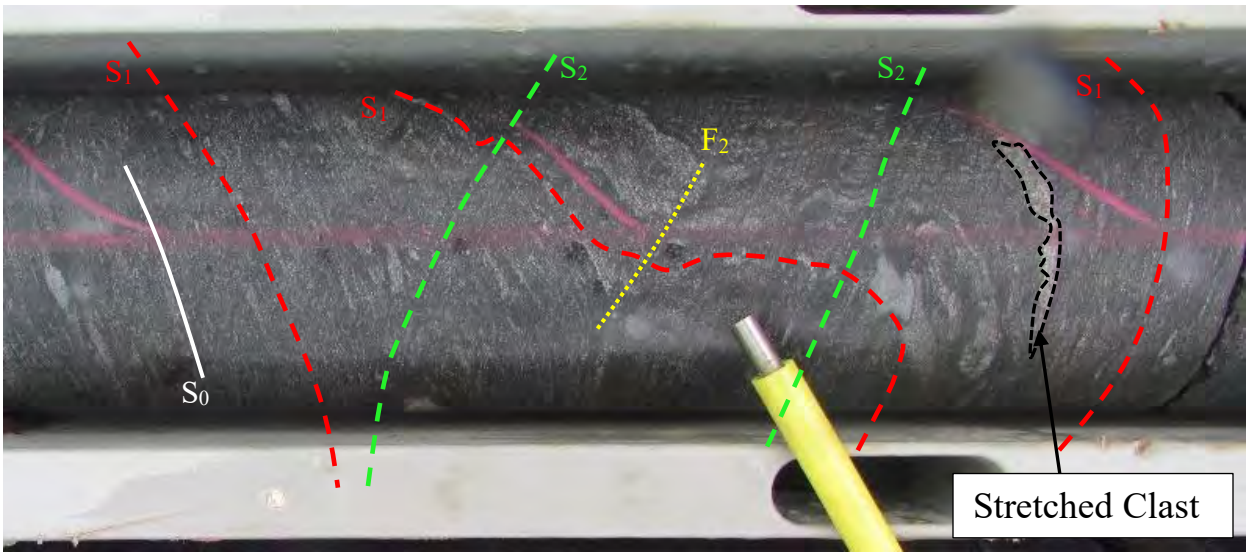

Figure 25: Different fabrics S0, S1 and S2 within the pebble phlogopite schist from the Grand Conglomerate. S0 and S1 are sub-parallel to each other along which are stretched clasts. S2 foliation truncates and offsets both S1 and clasts while F2 fold hinge lines are sub-parallel to S2 foliation.

Folding is also characterised by moderately inclined tight to open folds. Structures associated with F2 folds are S2 crenulation cleavages that are defined by biotite and occasionally with chlorite. S2 crenulation cleavage is sub-parallel to F2 axial surfaces and folds are northwest verging. Figure 26a shows the closure of a relatively high amplitude fold in the middle of the banded iron formation section within KAY001. Figure 26b shows an outcrop of folded quartzite. Folds in the quartzite are asymmetrical gentle folds with convoluted folds within limbs. The axial surface trends nearly east-west, while the fold hinge line plunges in the westerly direction.

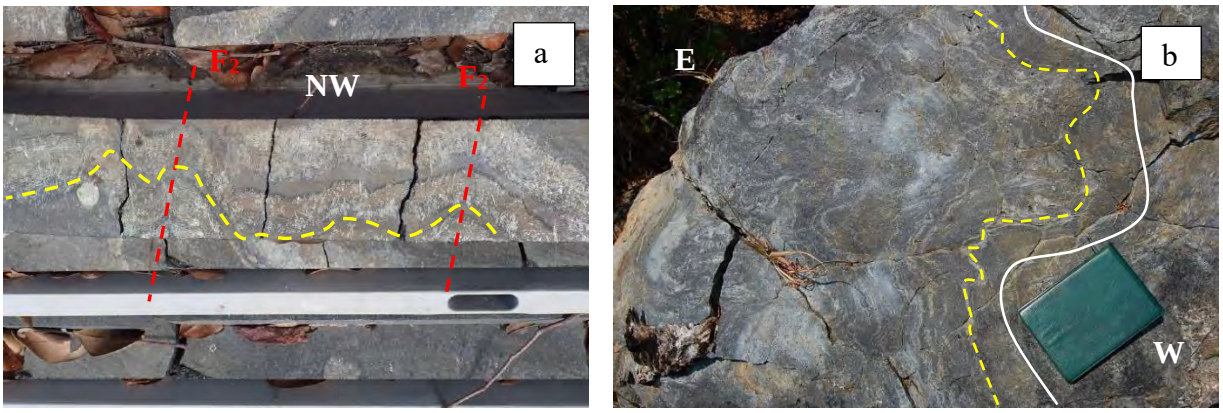

Figure 26: (a) Folding of banded iron formation within KAY001, F2 folds verging northwest with axial surfaces defined by oriented amphiboles; the red dashed lines indicate the trace of the F2 axial surface (b) West plunging fold hinge line within a quartzite exposure, convolute folds are poorly developed within fold limbs.

2.7.2 VEINS AND PODS

Hydrothermal veins vary in thickness from ~1 mm to several meters. The veins vary in shapes between pod-like to lenses. The dominant composition of veins is calcite, quartz, feldspars and pyrite. They cut across pre-existing foliation fabric in varying orientation and occasionally occurs subparallel to axial surfaces of fold structures.

Veins within gneisses of the Basement Supergroup are commonly parallel to zones with potassium alteration. These have light pink vein cores that become dark towards the contacts with the country rock. Occasionally, veins within schists of both the Katanga and the Basement Supergroups are folded and stretched. Some veins show internal fragmentation that has poorly healed by similar cementing material as the veins.

Figure 27 shows potassium rich hydrothermal vein in biotite feldspar gneiss. Contacts between vein and biotite feldspar gneiss are sharp. The biotite concentration within biotite feldspar gneiss increases towards the contact boundary with quartz feldspar vein. The biotite matrix foliation that truncates on quartz feldspar veins are curved (Figure 27). This suggests displacement occurring during or after vein formation.

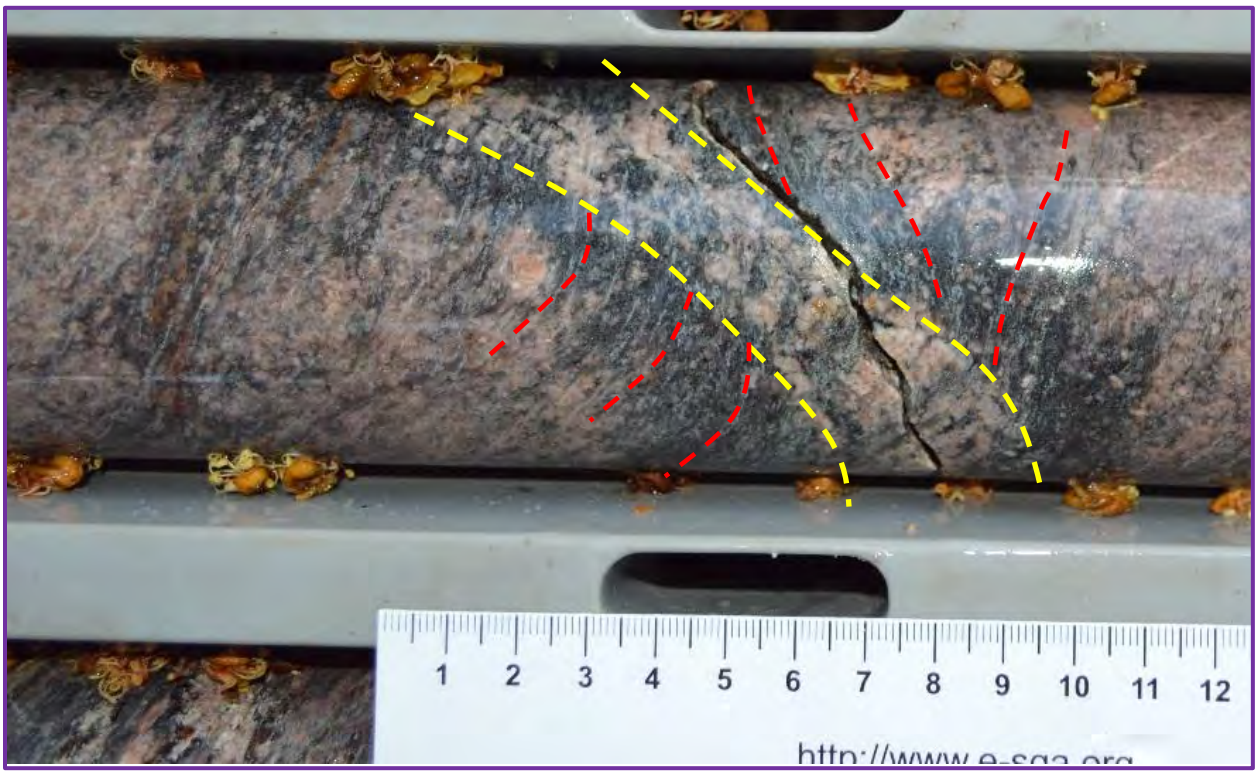

Figure 27: Vein consisting of K-feldspar and sericite is outlined yellow. Foliation within the biotite feldspar gneiss is curved towards the vein contacts. Biotite matrix increases towards vein contact within the biotite feldspar gneiss.

Figure 28 shows hydrothermal quartz pods with minor secondary fragmentation. The pod on the left (Figure 28) from NDD0012 occurs occasionally within Basement Supergroup rocks. The pod is irregular shaped and truncates S1 foliation. It has the longest axis vaguely subparallel to S2 foliation.

The pod on the left (Figure 28) may have been a vein that was folded and then disrupted. The vein on the right (Figure 28) formed during hydrothermal activity early in the deformation episode forming S1-parallel veins. This may have been related to dissolution creep with veins forming along the surface that most easily could be dilated S1.

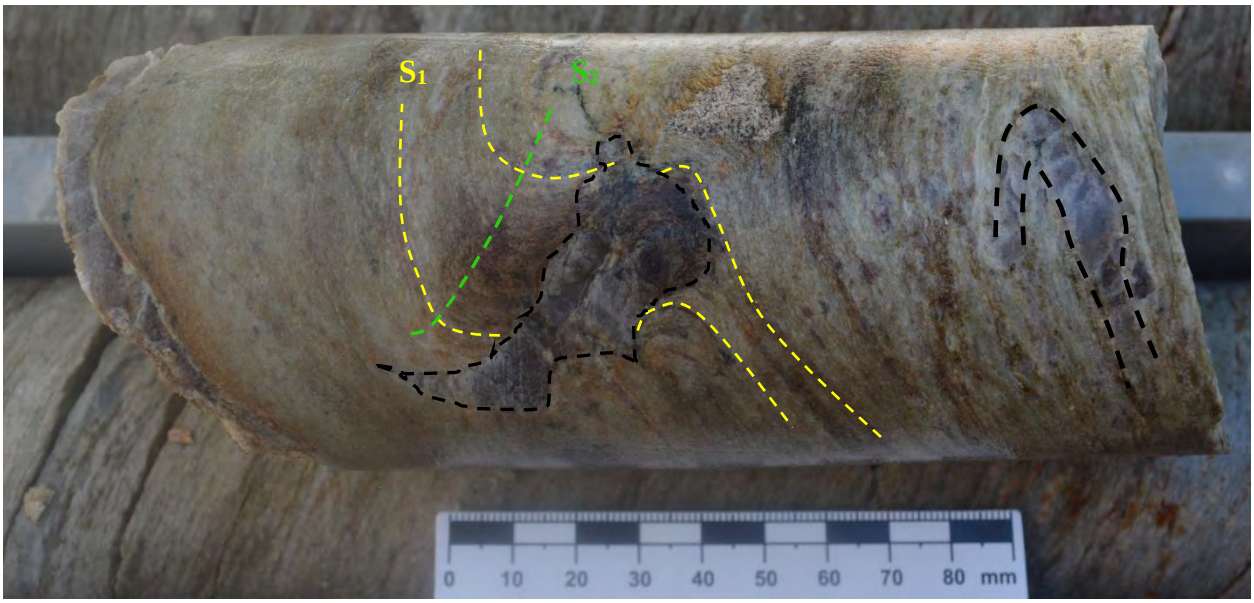

Figure 28: Internally fragmented quartz pods outlined black with S1 and S2 foliation. S1 foliation truncates at right angle to pods longest axis. S1 foliations are indicated in yellow outline with poorly defined S2 in green.

2.7.3 PINCH-AND-SWELL STRUCTURES

The other common features within Grand Conglomerate Formation schists are pinch-and-swell structures (Figure 30). These are commonly composed of quartz and have biotite wrapping around them. Pinch-and-swell structures commonly occur parallel to S2 foliations and F2 axial surfaces.

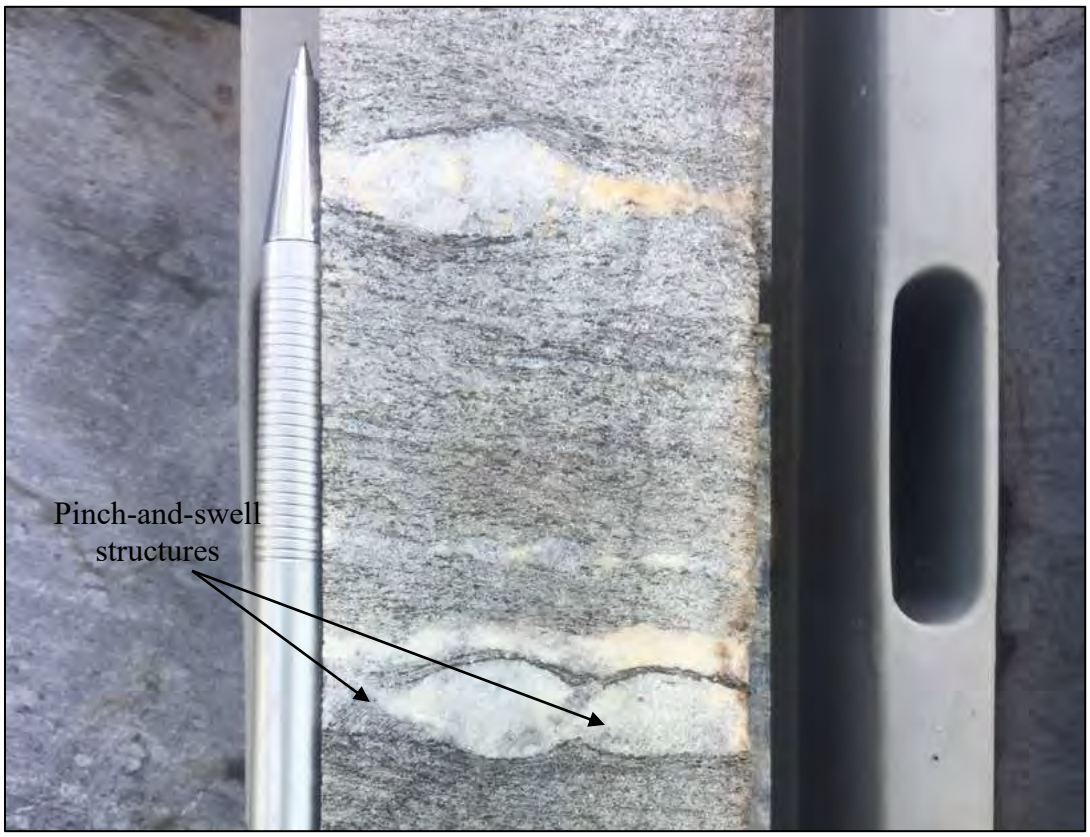

Figure 29: Pinch-and-swell structures of a quartz vein with narrowly spaced biotite foliation along the rims. This structure usually occurs in less competent veins that have been stretched within ductile biotite rich matrix.

2.7.4 CLASTS

Clasts are composed of quartz, granite, carbonate, shale, sandstones and siltstones are dominant within the Grand Conglomerate Formation. Less competent clasts that are composed of shales, carbonates and siltstones are stretched along foliations into lenses. More quartz and granite clasts resit flattening and stretching, suggesting that they were more competent during deformation than shale, carbonate and siltstone clasts (Figure 30).

These clasts are interpreted as primary features composed commonly of quartzites, sandstones, granites, shales, carbonate and quartz pebbles.

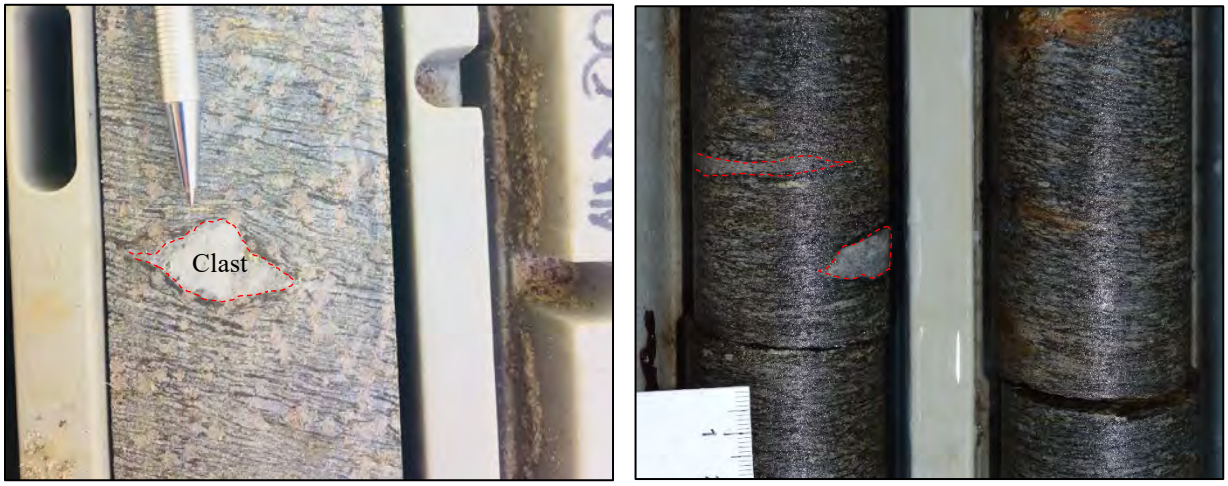

Figure 30: (a) Competent quartz clast within matrix of biotite, calcite and quartz. Pink porphyroblasts within the matrix are garnets. The biotite rich foliation is deflected around the quartz clasts. (b) Competent quartz clast and stretched dolomite clasts within matrix of biotite, calcite, quartz and feldspar.

3. MICROPETROGRAPHY

This section focuses on the petrographic description of selected samples. 14 fresh samples (Figure 31 and Figure 32) from six different diamond drill holes were selected for petrographic analysis based on metamorphic mineral assemblages, stratigraphy and structures present. Drill hole identity, depth, sample number and rock names for selected samples for petrography are shown in Table 8.

Table 8: Summary information of drill hole identity, sample depth and identity, rock name, group and Supergroup of selected samples for petrography.

Hole ID	From (m)	To (m)	Sample ID	Rock Name	Groups	Supergroups
KAY001	170.0	170.2	MC001	Garnet Biotite schist	Nguba	Katanga
KAY001	242.0	242.2	MC002	Garnet amphibole biotite schist	Nguba	Katanga
KAY001	351.2	351.4	MC003	Amphibole biotite schist	Nguba	Katanga
LUA001	265.5	265.8	MC004	Biotite schist	Nguba	Katanga
NDD0010	127.0	127.2	MC005	Garnet biotite schist	Nguba	Katanga
NDD0010	144.3	144.5	MC006	Garnet biotite schist	Nguba	Katanga
NDD0008	209.3	209.5	MC007	Biotite feldspar quartz gneiss	Lufubu	Basement
NDD0008	214.2	214.4	MC008	Biotite feldspar quartz gneiss	Lufubu	Basement
NDD0012	72.3	72.5	MC009	Muscovite feldspar quartz schist	Lufubu	Basement
NDD0012	138.4	138.6	MC010	Feldspar biotite gneiss	Lufubu	Basement
NDD0006	252.2	252.4	MC011	Garnet biotite schist	Nguba	Katanga
NDD0008	178.4	178.7	MC012	Amphibole biotite feldspar quartz schist	Lufubu	Basement
NDD0010	114.9	116.3	MC013	Garnet biotite schist	Nguba	Katanga
NDD0012	188.0	188.2	MC014	Biotite quartz feldspar gneiss	Lufubu	Basement

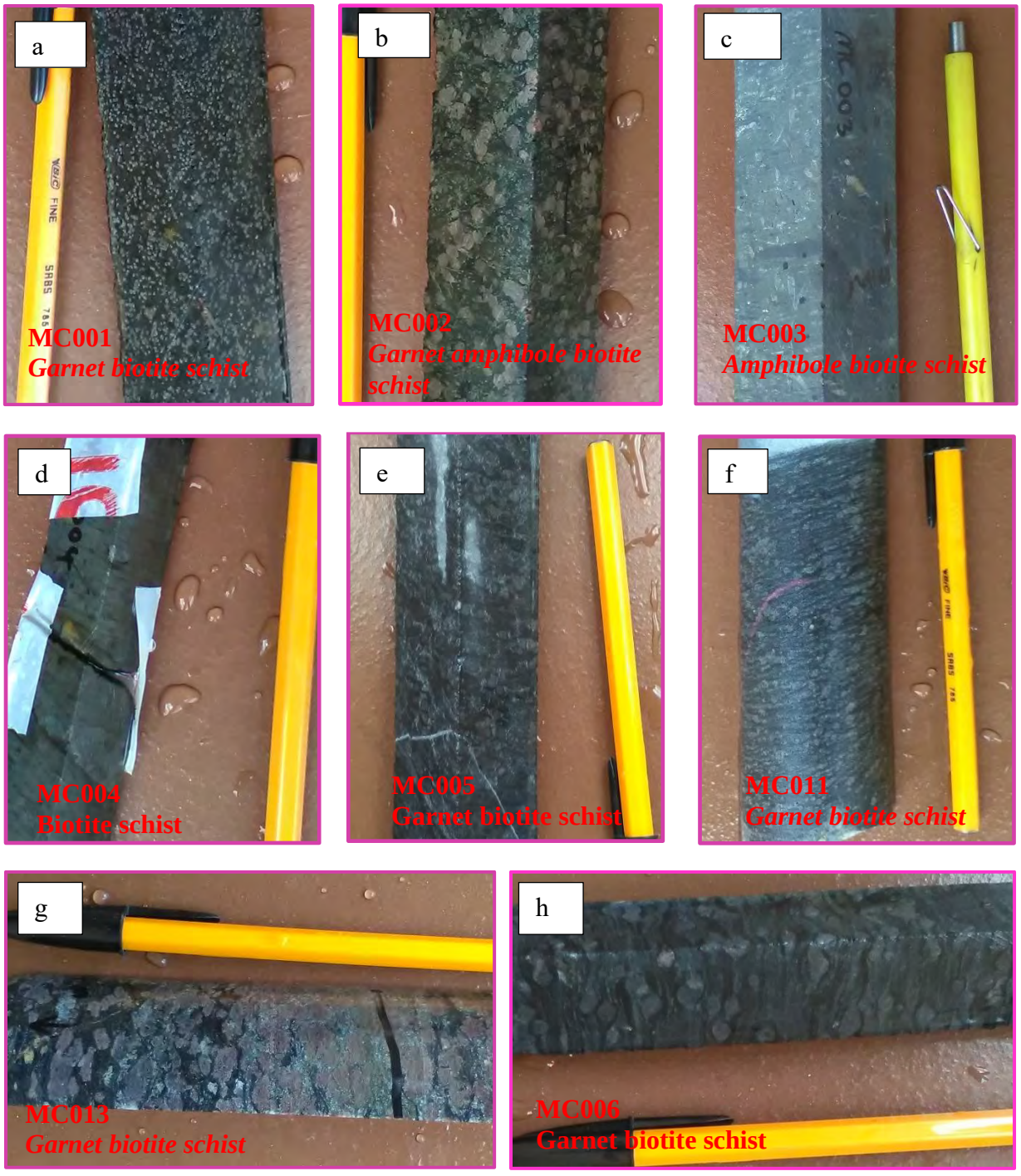

Figure 31: Core samples from different holes of various biotite schists and garnet biotite schists selected for petrographic analysis. All samples belong to the Grand Conglomerate Formation. (a) Weakly foliated grey garnet biotite schist composed of biotite and calcite matrix with randomly distributed pink ~1 mm garnet porphyroblasts. (b) Porphyroblastic garnet amphibole biotite schist. Matrix is fine-grained grey biotite and calcite with pink garnet and grey amphibole porphyroblasts. (c) Massive grey amphibole biotite schist, amphiboles are randomly oriented within a calcitic

matrix. (d) Grey biotite schist, matrix is composed of biotite and contains grey clasts elongated along foliation. (e) Weakly foliated grey garnet biotite schist. Matrix is biotite dominated with garnet porphyroblasts. (f) Garnet biotite schist with garnet porphyroblasts within a biotite and calcite rich matrix (g) Garnet biotite schist, consist ~6 mm pink garnets randomly distributed in the biotite matrix. Garnet abundance varies across the length of the core. (h) Grey garnet biotite schist, biotite is fine-grained dark grey defining foliation with grey calcite. Pinkish grey garnet porphyroblasts range from 5 to 10 mm.

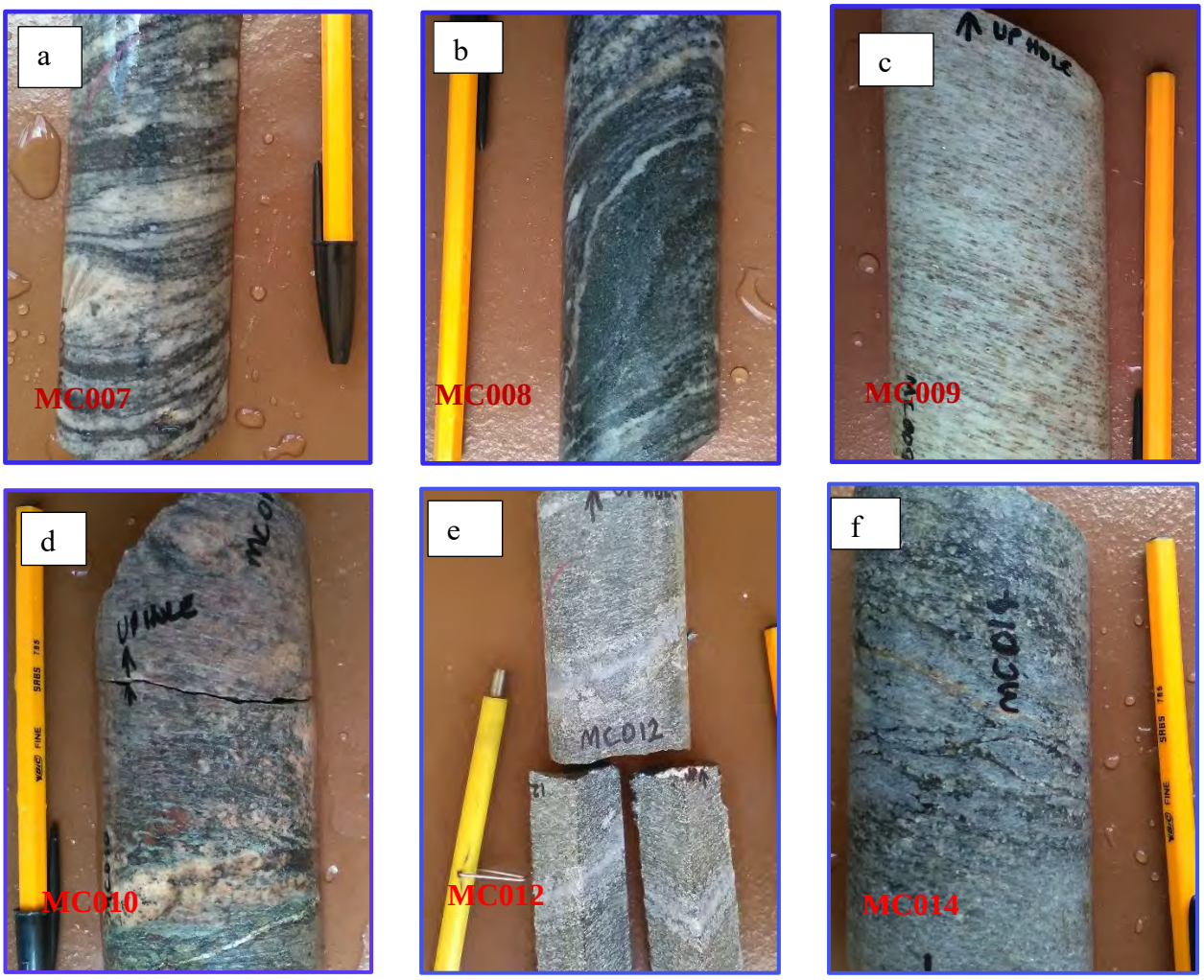

Figure 32: Gneisses and schists from the Basement Supergroup selected for petrographic analysis. (a) Coarse-grained banded biotite feldspar quartz gneiss. Pink K-feldspar and quartz felsic bands are interlayered with dark biotite rich bands. (b) Greenish grey biotite feldspar quartz gneiss, the colour is dominated by biotite and amphibole. (c) Medium-grained light grey strongly foliated muscovite feldspar quartz schist with hematite alteration. (d) Coarse-grained pink with grey feldspar biotite gneiss. (e) Foliated grey medium-grained amphibole biotite feldspar quartz schist. (f) Grey biotite quartz feldspar gneiss, felsic bands are dominant composed of feldspar and quartz.

3.1 MC001: GARNET BIOTITE SCHIST

MC001 is from the Grand Conglomerate Formation and was sampled from KAY001 at the depth of ~170 m (Table 8; Figure 30.a). The rock shows well-developed foliations with interstitial coarser brown biotite, white calcite and quartz grains following the foliation trend (Figure 33). The rock also shows randomly distributed garnet porphyroblasts wrapped by matrix material. The matrix is dominated by biotite oriented along foliations, biotite vary in abundance at different sections relative to other matrix phases of quartz and calcite.

Euhedral and zoned grey garnet are randomly distributed within the matrix. Garnet shapes are commonly hexagonal with occasional curved faces. Garnet porphyroblast sizes range from ~0.6 to ~1 mm diameter. There are two zones within garnets; a thin (~0.05 mm) lighter rim zone and a thicker (~0.8 mm) darker core. The thin rim zone shows few if any matrix inclusions whereas the inner core of the garnet shows abundant crystal inclusions. At higher magnifications, the inclusions can be identified as quartz, biotite and calcite which is the same assemblage that form the matrix in which the garnet formed.

Fractures in garnet are more pronounced in the rim zones commonly showing a radial orientation towards the core. However, often these fractures are terminated before they reach the centre of the garnet. Other fractures transect the entire crystal (Figure 34). Some garnets appear to have conjoined during growth. Garnet porphyroblasts' internal structures hardly show inclusion trail alignment. Garnets have finely disseminated inclusions that increase from the rim to the core.

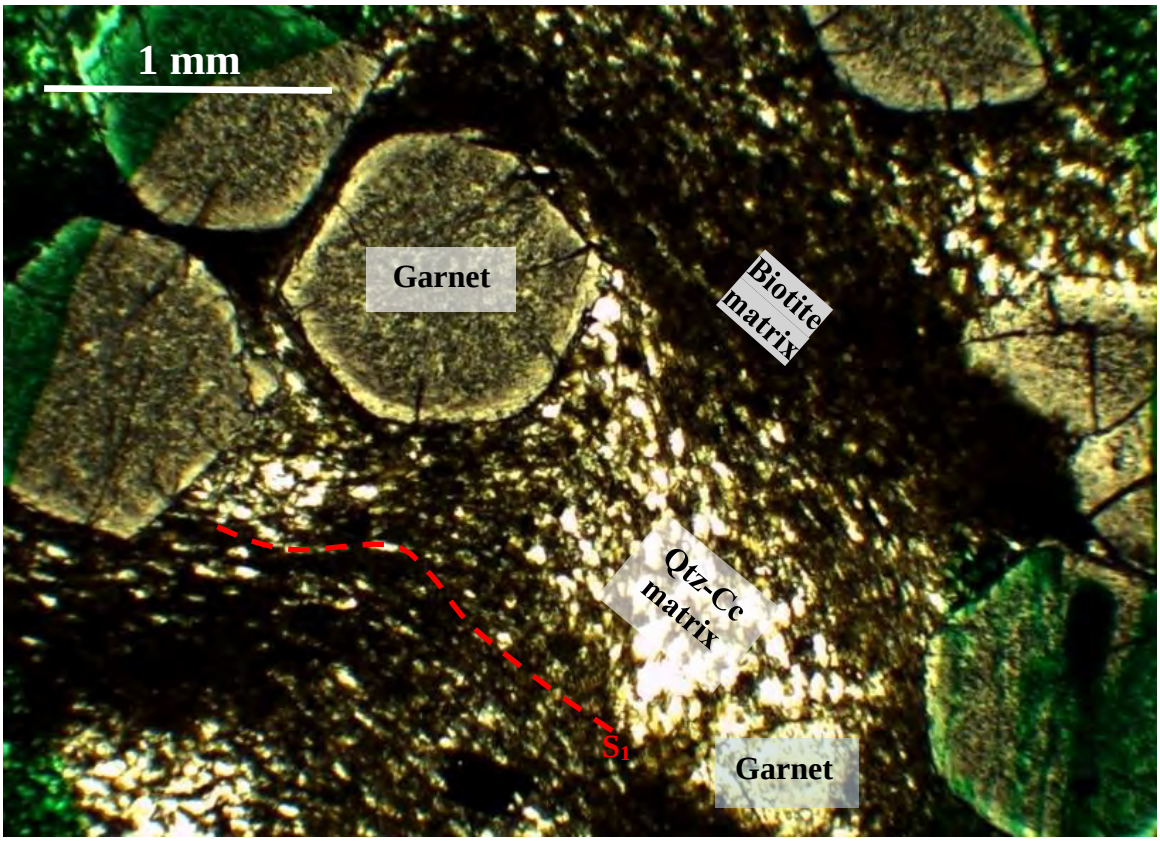

Figure 33: Photomicrograph of euhedral garnet porphyroblasts randomly distributed within a biotite, quartz and calcite dominated matrix. S1 is deflected around the garnet porphyroblast. The green colour on the edges of the photomicrograph is an artefact of a marker outline.

The internal textural variation of a garnet porphyroblast and its matrix are shown in Figure 34. The garnet boundary with the matrix is sharp. Two zones within the garnet are clearly visible: a lighter thin outer rim with thickness of ~ 0.05 mm that is free of matrix inclusions. The inner zone, containing the bulk of the garnet, contains abundant small mineral phases as inclusions. This core of the garnet is darker and spotted with matrix material.

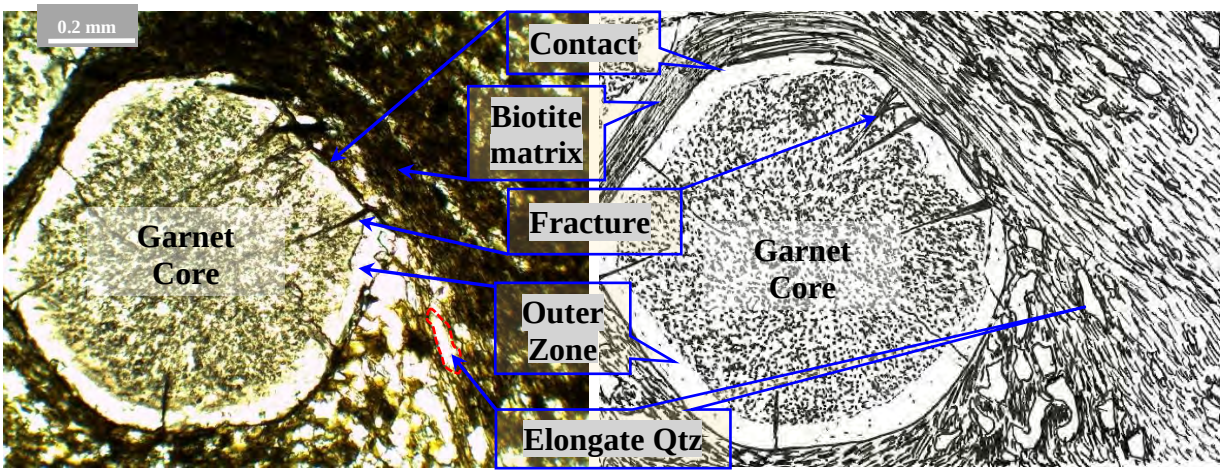

Figure 34: Photomicrograph and a sketch highlighting distinct features of garnets and matrix. Hexagonal zoned garnet with inclusions of quartz, calcite and biotite matrix composition. Garnets have fractures which are mostly wedge-shaped tapering towards the core of the garnet. The matrix shows oriented biotite grains forming the bulk composition. Other matrix materials include quartz and calcite that are elongated along foliation trend.

The matrix minerals are elongate biotite, quartz and calcite grains. The matrix shows coarse-grained portions chiefly composed of quartz and calcite and finer-grained biotite-dominated portions (Figure 35). The matrix shows a weak crenulation cleavage which intersect S1 at around 120°. The presence of S1 and crenulation cleavage indicates the transposition of foliations and hence the overprint of earlier deformation structures by a subsequent younger crenulation cleavage.

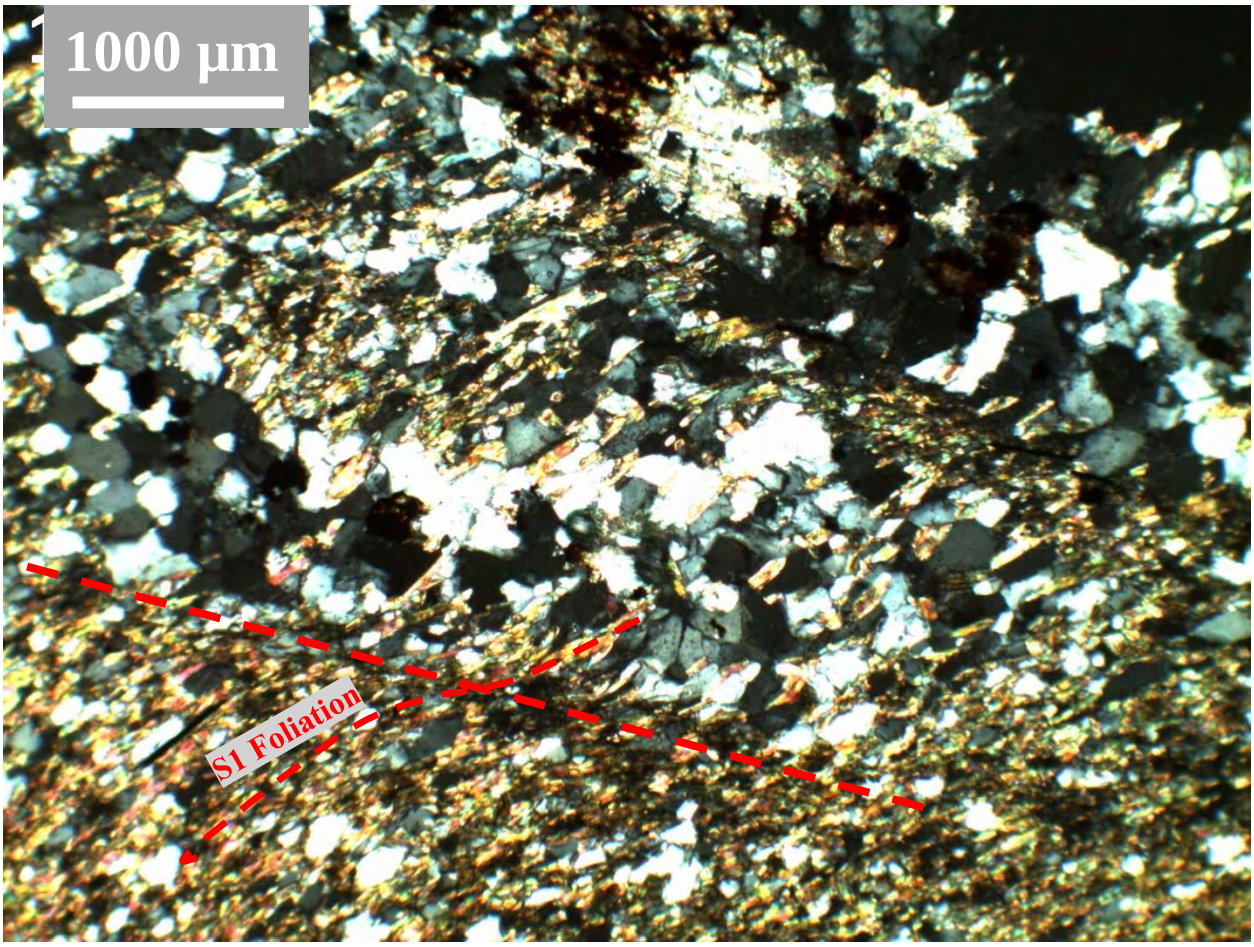

Figure 35: Matrix material of MC001 composed of muscovite, biotite, chlorite, quartz, feldspar and calcite. Biotite alignment is dominant along S1 foliation and weak crenulation cleavage intersects S1 at around 120°.

3.2 MC002: GARNET AMPHIBOLE BIOTITE SCHIST

Garnet amphibole biotite schist belongs to the Grand Conglomerate Formation. It has a weakly developed foliation with randomly distributed garnet and amphibole porphyroblasts (Figure 36). The rock was sampled from KAY001 at the depth of ~242 m (Table 8). The sample has euhedral trapezium shaped amphiboles and hexagonal garnet porphyroblasts within a fine-grained carbonate and biotite dominated matrix. Other matrix minerals include hematite, quartz and feldspar.

The trapezium shaped amphibole porphyroblasts are randomly oriented in the matrix and their abundance is variable in different parts of the rock, suggesting clustered distribution. However, amphiboles also occur as inclusions within the garnet porphyroblast. The amphiboles have variable

sizes ranging up to 2 mm along the longest section. These amphiboles show the typical mineral cleavage intersecting at ~ 120°.

Garnet porphyroblasts are euhedral and range up to 6 mm in size. Garnet porphyroblasts are randomly distributed within the carbonate rich matrix. Garnets have inclusions of amphibole, carbonate, biotite and quartz, the phases that form the matrix. Some garnet parts are concealed by overgrown amphibole inclusions. Garnets are weakly optically zoned, but the zonation is not as distinct as in sample MC001. Zonation is evident by minor color variations with somewhat darker cores than rims (Figure 36). The garnets show randomly oriented fractures.

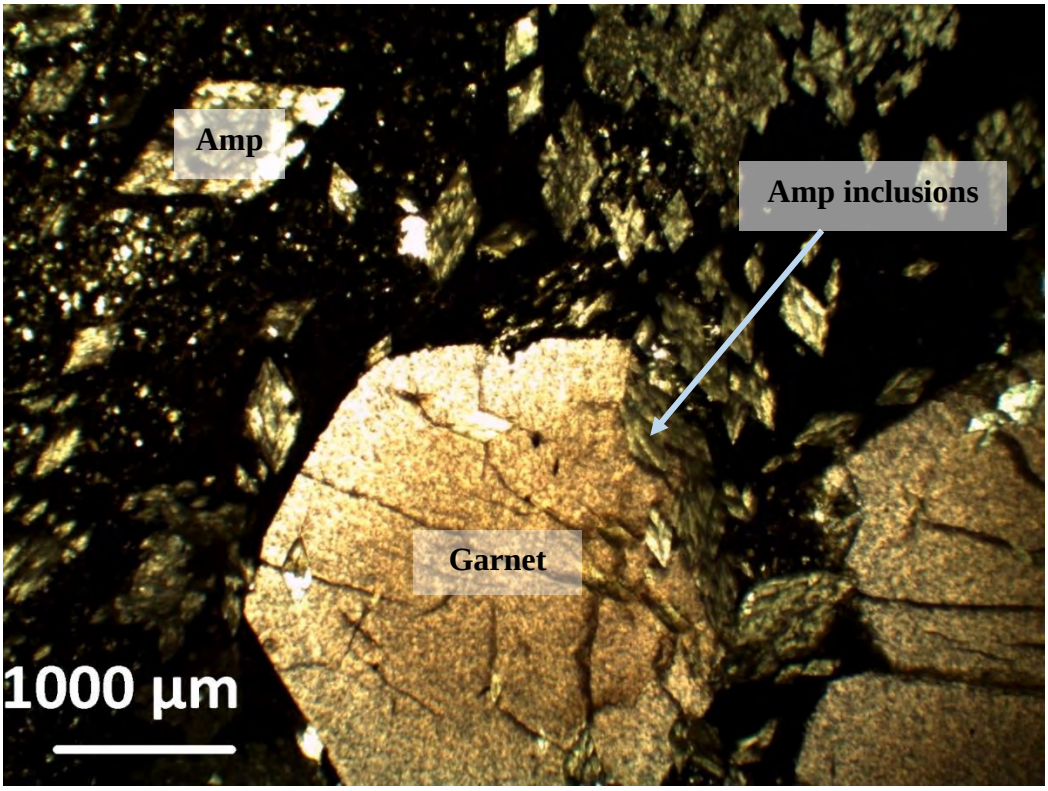

Figure 36: Garnet amphibole biotite schist in plane polarized light. Zoned euhedral garnets with amphibole inclusions within a biotite-carbonate rich matrix with abundant euhedral amphibole.

3.3 MC003: AMPHIBOLE BIOTITE SCHIST

MC003 consists of amphibole and garnet porphyroblasts within a biotite and carbonate dominated matrix (Figure 37 and Figure 38). Porphyroblasts are randomly distributed within the matrix, their abundance is variable with some sections having more garnet than amphibole.

Large (~3 mm long) trapezium shaped amphibole porphyroblasts occur within a foliated biotite and carbonate rich matrix (Figure 37). They exhibit rims around them and show aligned inclusions that display minor folding but in general is parallel to the external foliation in the matrix. Foliations within amphibole porphyroblasts are dominantly defined by biotite and calcite. Smaller (~0.5 mm) amphibole occurs within the matrix and is elongate along the foliation. The smaller amphibole porphyroblasts are trapezium shaped and relict foliation within them is barely visible.

Amphiboles show twinning along the longest section of the porphyroblasts and they are zoned around boundaries. Zoning on the face of the amphibole tapers towards the apex of the porphyroblast crystal.

The foliation runs continuously through amphibole porphyroblasts without deflection (Figure 37). This indicates post-tectonic amphibole growth. When rotating the stage, amphiboles are anisotropic, and twinning is also distinctive when stage is rotated under cross-polarized light.

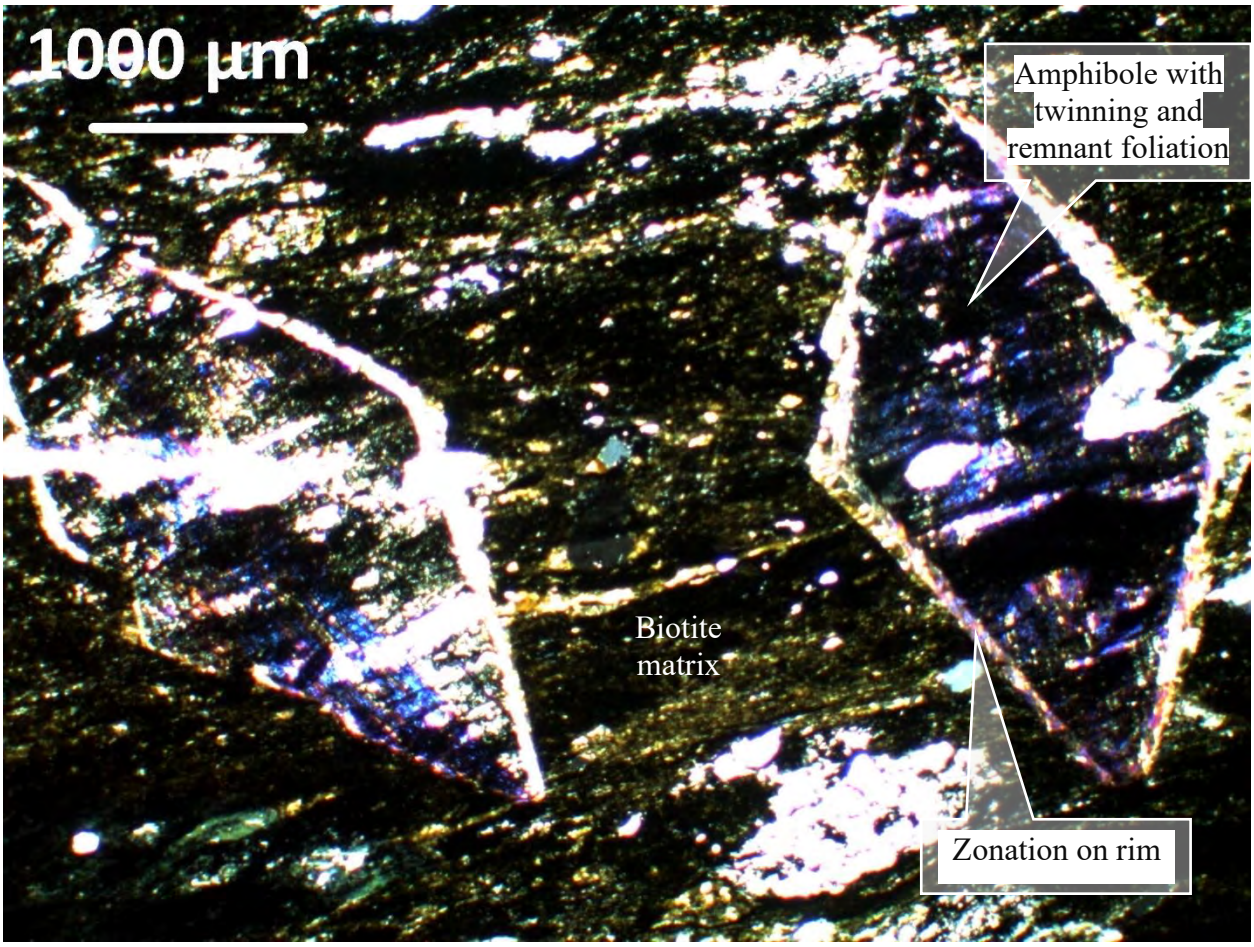

Figure 37: Photomicrograph of amphibole biotite schist showing weakly defined twinning of amphibole porphyroblasts within a biotite and calcite dominated matrix. Biotite defines the orientation of the foliation in the matrix, matrix foliation is concordant to that observed in the porphyroblast.

There are ~0.5 to ~1 mm garnet porphyroblasts within the matrix with subhedral shapes in other sections of MC003 (Figure 38). Like amphiboles, garnet contains inclusion trails that display a foliation parallel to the foliation in the matrix. Hence, also the garnet is likely to have overgrown the external foliation post-kinematically.

The matrix is dominated by calcite and biotite. Other matrix materials include quartz, feldspar and minor chlorite and hematite. Amphibole is randomly distributed within a biotite and carbonate dominated matrix.

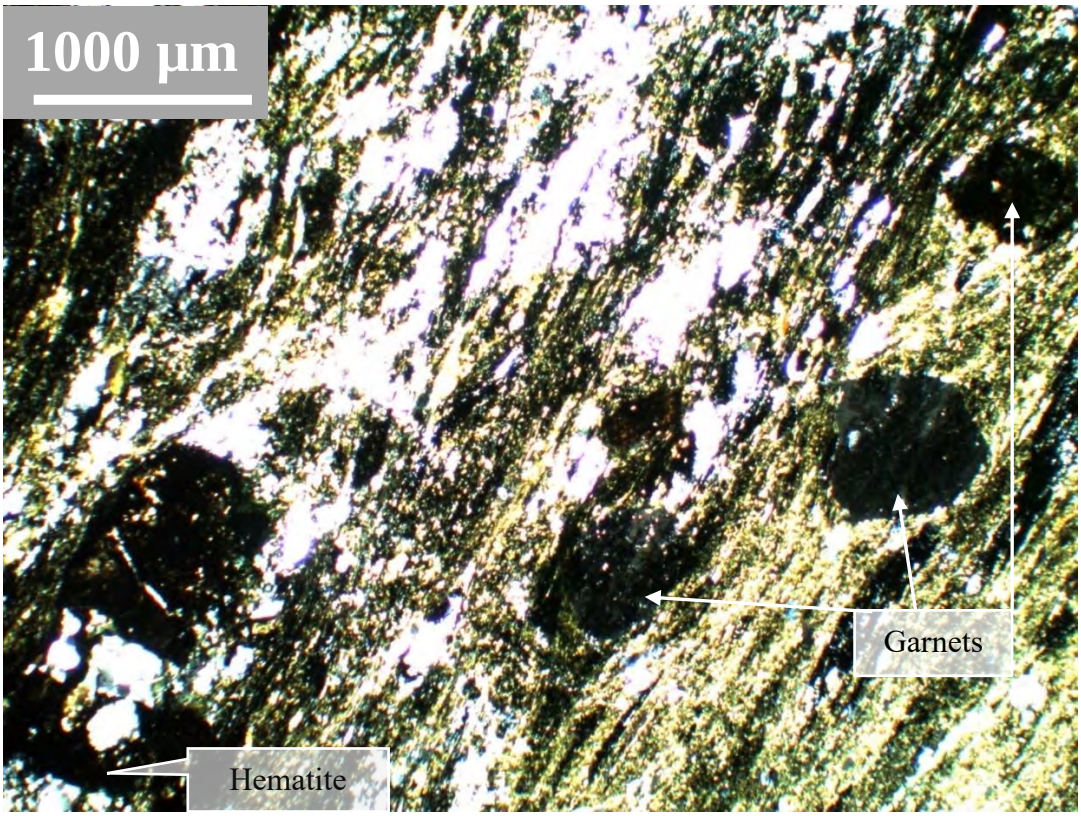

Figure 38: Photomicrograph showing amphibole biotite schist with garnet porphyroblasts. Garnet is subhedral and consist of inclusion trails that display a foliation parallel to the foliation in the matrix.

3.4 MC004: BIOTITE SCHIST

MC004 was sampled from hole LUA001 at depth between 265.5 and 265.7 m (Table 8). The rock belongs to the Grand Conglomerate Formation. The hand sample is grey weakly foliated biotite schist. The matrix is fine-grained and consists of biotite, quartz, calcite and feldspar. The matrix has clasts that are stretched and randomly distributed. Clasts are composed of sandstone, quartzite, marble and shale ranging in sizes from 5 to 10 mm. Clasts are flattened along foliation fabric and have flat lenses. Clasts commonly show pyrrhotite and pyrite around the rim boundaries, occasionally they are completely replaced by pyrrhotite and pyrite.

The rock shows a weakly foliated matrix under microscope study (Figure 39). The schist is cut by quartz and calcite dominated veins which occasionally consists of pyrite (Figure 39). The matrix is foliated consisting commonly of muscovite and minor biotite. Calcite and quartz occur along foliation trends. Schistosity is poorly developed, it becomes clearly defined with abundance of

micas. However, there are some portions with less mica that are dominated by calcite, quartz and feldspar.

Veins are commonly concordant to foliation trend consisting of coarse-grained mineral grains of quartz and calcite with minor elongate muscovite (Figure 39). The vein boundaries are irregular and exhibit pinch-and-swell structures.

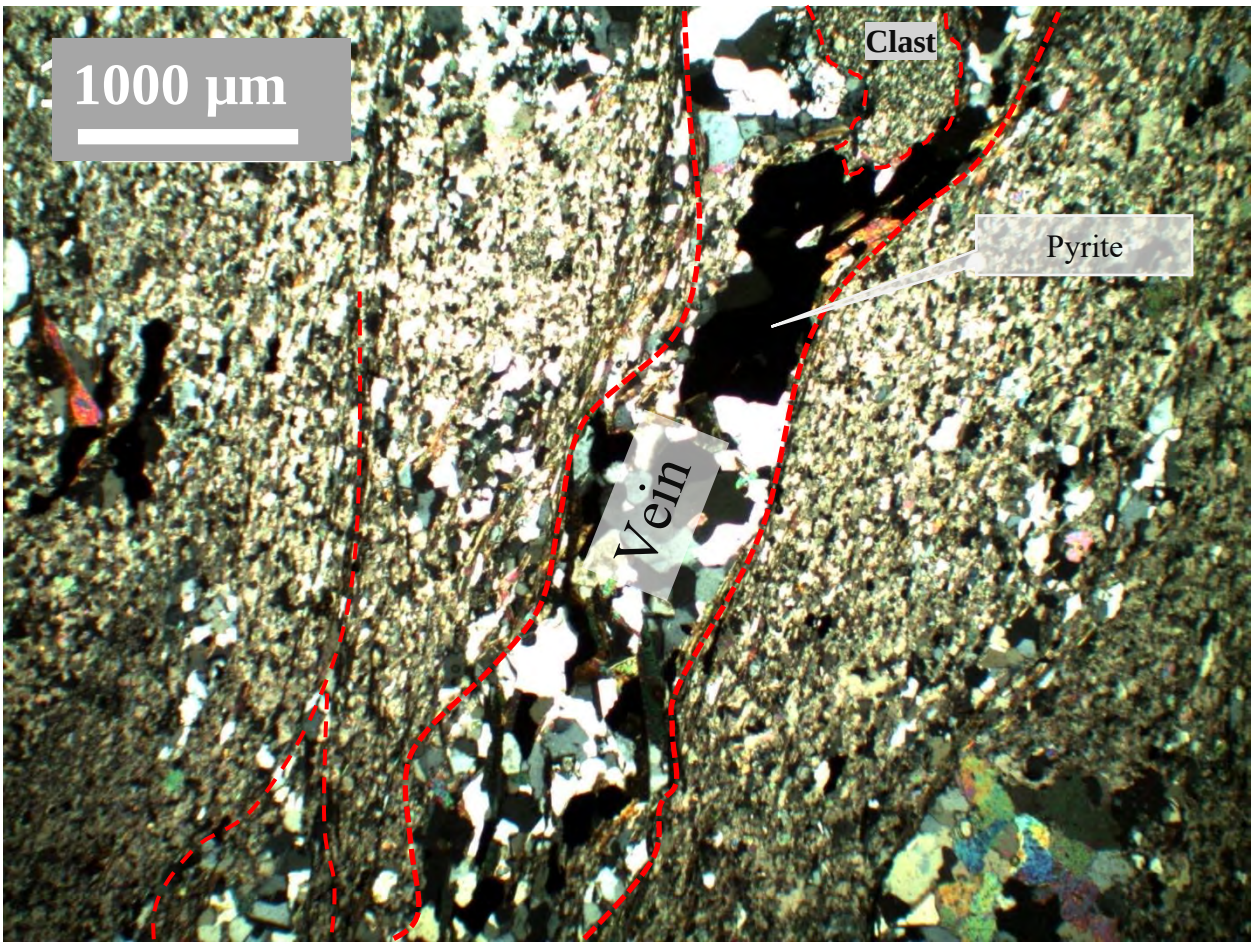

Figure 39: Photomicrograph showing foliated matrix with quartz-calcite-pyrite vein indicated by red hashed line.

Clasts are finer-grained and exhibit a very weak foliation, they are elongate along foliation trend. The clasts are distributed within a foliated muscovite, calcite and quartz matrix. Clasts commonly have coarse-grained calcite-quartz rim with minor pyrite. Foliation commonly wraps around the clasts while occasionally, foliation truncates into the clast boundary. Pyrite commonly occurs

along foliation and also on the rim boundary of the clasts. Figure 40 shows a ~3 mm elongate clast within a foliated matrix, the rock belongs to the Grand Conglomerate Formation.

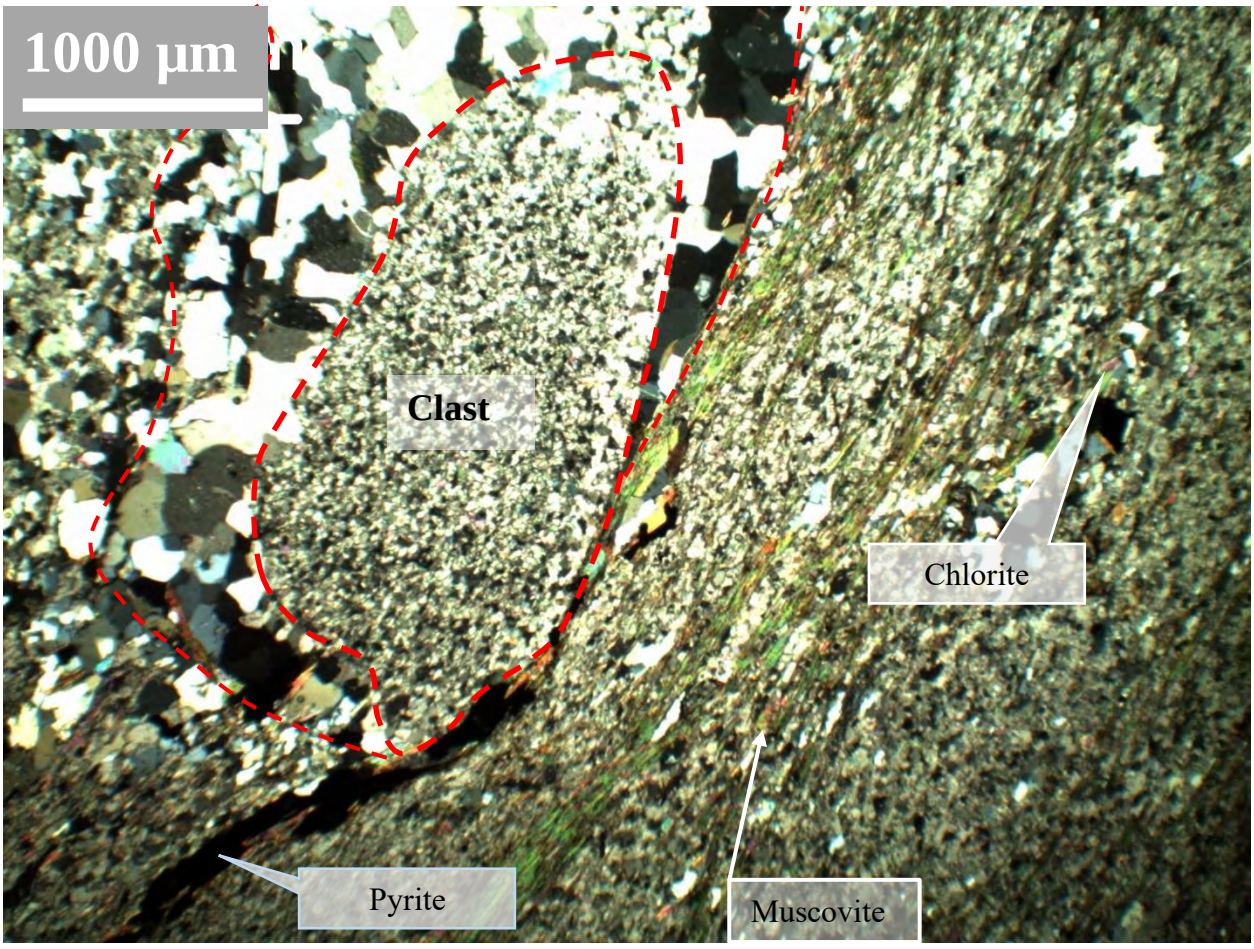

Figure 40: Preserved weakly deformed clast with calcite, quartz and pyrite rim. Clast with red outline is within a foliated matrix composed of muscovite, calcite, quartz and minor pyrite and chlorite. Coarse-grained rim around the clast is indicated by an outer red outline.

Foliation within the matrix is deflected around the boundary of a rigid clast and veins. Clasts are elongate along foliation trend which could imply flattening during deformation. There are also undeformed clasts wrapped around by foliation. This suggests clasts to consist of more rigid material than matrix composition.

3.5 MC005: GARNET BIOTITE SCHIST

Sample MC005 was sampled from hole NDD0010 at depth intervals between 127.0 m and 127.2 m within the Grand Conglomerate Formation. The hand sample is grey with porphyroblasts of

garnet ranging in sizes from 2 to 5 mm. Garnets are randomly distributed within foliated grey matrix which consist essentially of biotite, quartz and calcite. There are minor 1-2 mm thick veins that are discordant to foliation at ~110°.

The matrix is composed of biotite, calcite, quartz, plagioclase and opaque minerals. The matrix has both fine-grained and coarse-grained layers. The finer matrix is defined by continuous and penetrating foliation mostly defined by aligned biotite with finer quartz and plagioclase. Coarse-grained bands are mostly parallel to the foliation trend (Figure 41). The coarse-grained layering parallel to foliation is defined plagioclase feldspar and quartz, probably a thin vein. Veins cut across foliation and have elongate minerals which are subparallel to foliation suggesting veins to have been emplacement of pre-deformation.

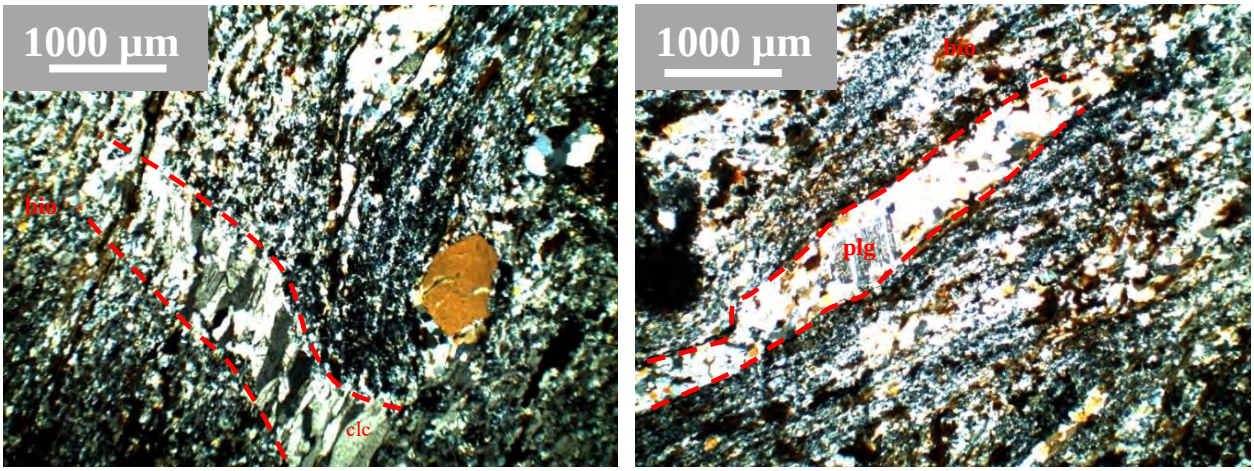

Figure 41: Photomicrograph of MC005 showing matrix phases composed of plagioclase, calcite and biotite. Two veins concordant and discordant to foliation trend marked by red hashed lines on the left and right respectively.

Garnet porphyroblasts are brown with sizes ranging from ~0.5 to ~3 mm. They have a euhedral-rhombododecahedron shape and are zoned (Figure 42). There are three zones within garnet porphyroblasts (Figure 42) with poorly defined zonal contacts. Under plane-polarised light, the core is light brown with inclusion and does not entirely have a hexagonal shape. The second zone is greyish brown with curvy and poorly defined hexagonal outer boundary. The outer zone is lighter brown with hexagonal inner and outer boundaries. The outer garnet zone contains small mineral inclusion at variable abundance, in different parts of this zone.

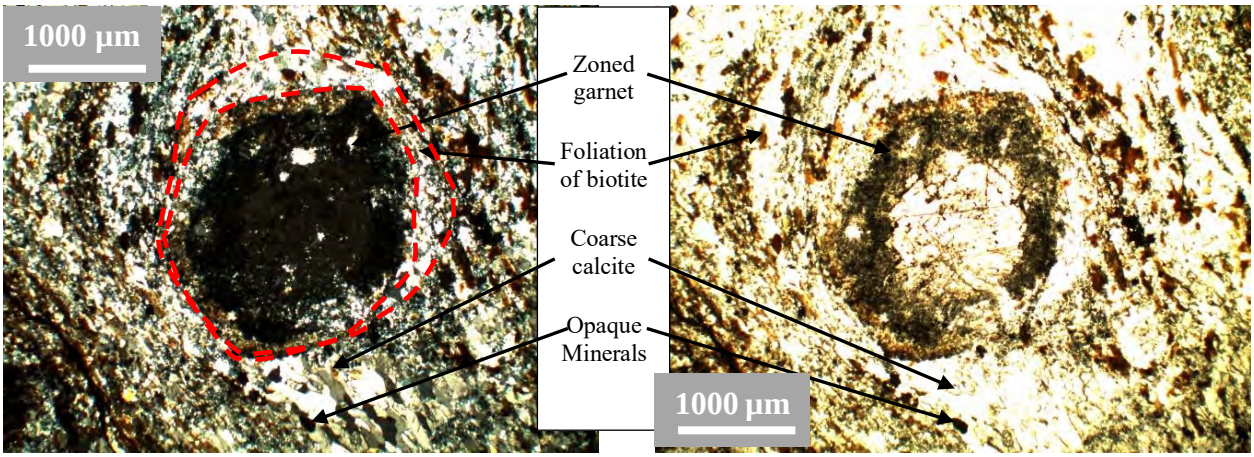

Figure 42: Thin section micrograph showing both cross- and plane-polarised light of garnet. The matrix is foliated and composed of biotite, quartz and feldspar. Garnet is zoned, the outer zone is strongly retrogressed to biotite.

Garnet porphyroblasts are wrapped by foliated biotite rich matrix. The garnets have fine-grained matrix material suggesting to have grown from matrix (Figure 42). There is a weakly defined outer zone composed mostly of retrogressed biotite and minor quartz. This may suggest that the garnet underwent retrogression and forming biotite within the outer zone.

3.6 MC006: GARNET BIOTITE SCHIST

Garnet biotite schist sample MC006 was taken from a diamond drill core NDD0010 at depths between 144.3 m and 142.5 m within the Grand Conglomerate Formation. MC006 was sampled just below sample MC005, and these two samples have similar mineralogy. The hand sample is a grey garnet biotite schist. It consists of randomly distributed dark grey and black sheared clasts which have minor carbonate rims. The macroscopic hand sample is distinctly defined by garnets randomly spaced within a strongly foliated biotite and carbonate rich matrix.

Garnet porphyroblasts are euhedral with sizes ranging from ~1 mm to ~4 mm. Garnets are wrapped by deflected biotite foliation and also exhibit pressure shadows (Figure 43). The deflection of the foliation around garnet indicates pre-kinematic growth. Accordingly, these garnets, although they might have grown as porphyroblasts, are now porphyroclasts.

Garnet shows inclusions of calcite, quartz and biotite, an assemblage identical to that in the matrix. This suggests garnet growth from the matrix in which they are present. Inclusions in garnets vary in sizes and may reach up to 0.2 mm (Figure 43 and Figure 44).

Microscopically, there are euhedral garnet porphyroclasts within a well foliated matrix (Figure 43). The matrix is composed of fine-grained biotite commonly defining the foliation domains and coarse-grained microlithons composed of quartz, feldspar and calcite. The foliation domains and microlithons are separated by variable biotite dominance relative to quartz, calcite and feldspar. The coarse-grained bands are poorly foliated with grains that are less than ~0.2 mm size of quartz, calcite, feldspar and minor biotite. The minor biotite within microlithons defines the poorly developed foliation.

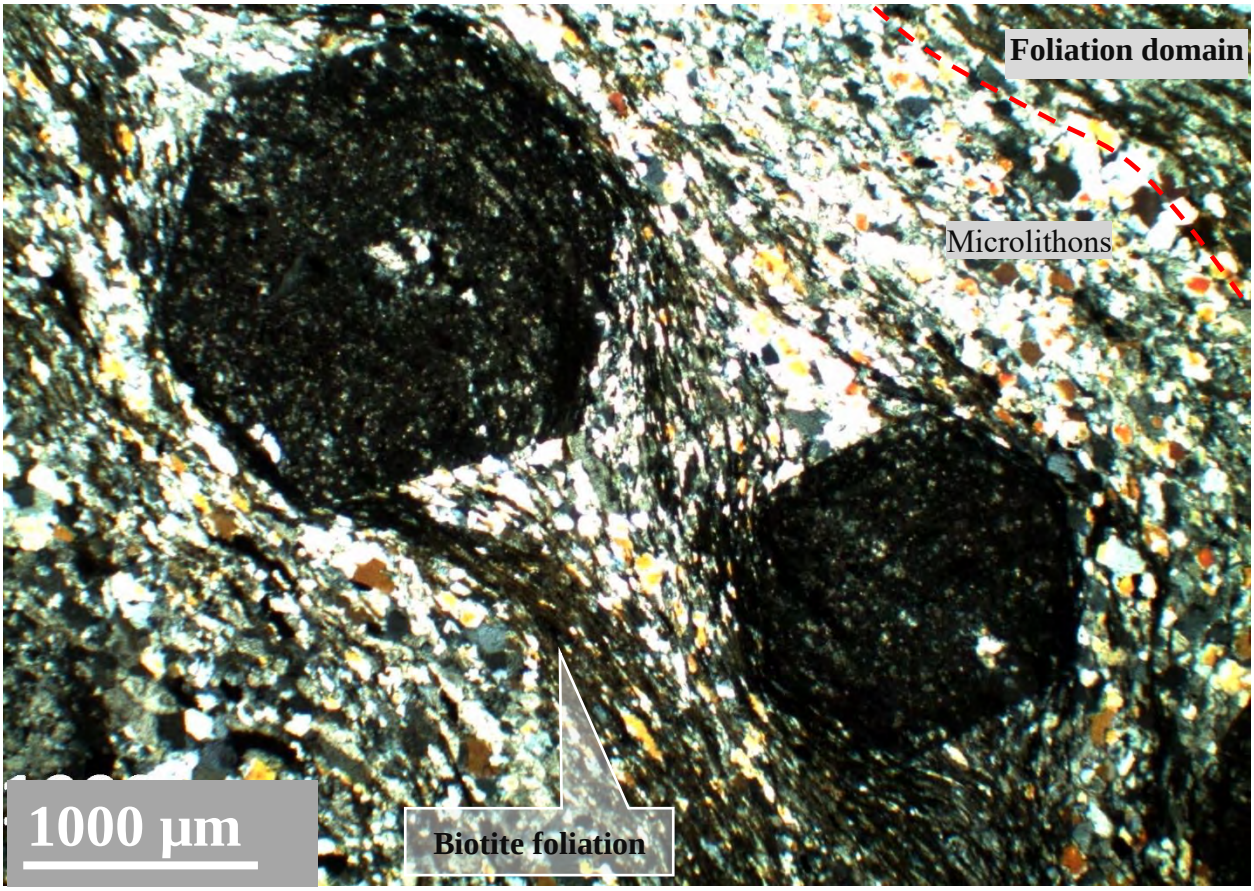

Figure 43: Photomicrograph of MC006 showing garnet porphyroclasts with a foliated matrix under crossed polarized light. Brown biotite defines foliation domain which wraps around garnet porphyroclasts. Other matrix phases are microlithons which include feldspar, quartz and calcite. Garnet porphyroblasts are euhedral, zoned and have matrix inclusions.

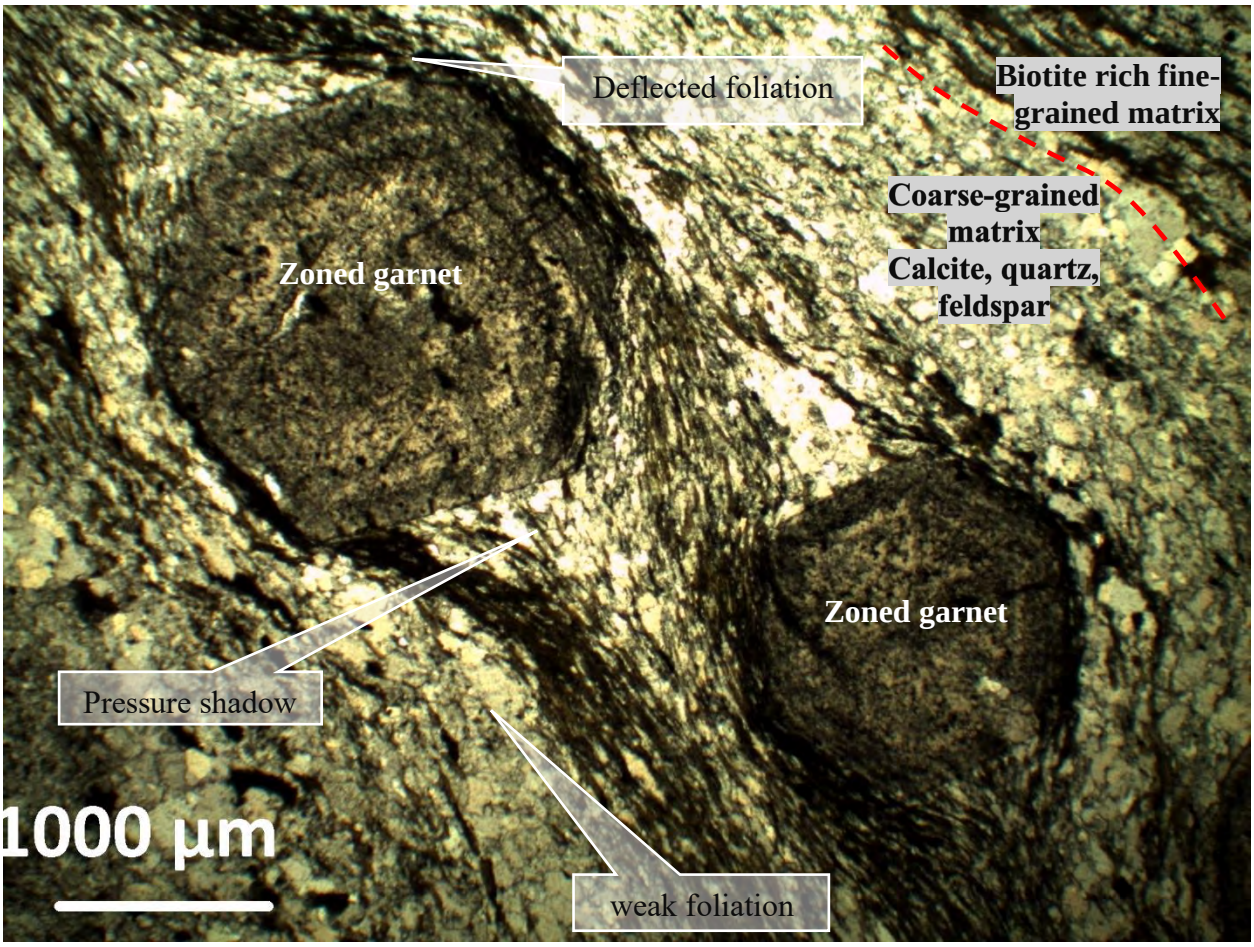

Figure 44: Photo micrograph of MC006 showing garnet porphyroclasts with a foliated matrix under plane polarized light. Foliation domains are biotite rich while microlithons are composed of coarse-grained calcite, quartz and feldspar.

Garnets are generally zoned with six zones. The zones alternate between light colour and dark colour. The zonation of garnets is texturally repetitive, alternating between light brown colour and grey to black colour. The core is grey rimmed by the light brown ring which indicates the first growth episode. This repeats outwardly to the second and third phases (Figure 45). The zonal euhedral shape gets more defined further away from the core of the garnet.

Garnet porphyroblasts are commonly within a foliated biotite rich matrix. Some garnet are euhedral with unequal faces. The foliation preserved within garnets is commonly wavy. The foliation in the matrix generally wraps around the garnet porphyroclast indicated by red line, though it also rarely truncates into garnet boundary (Figure 45).

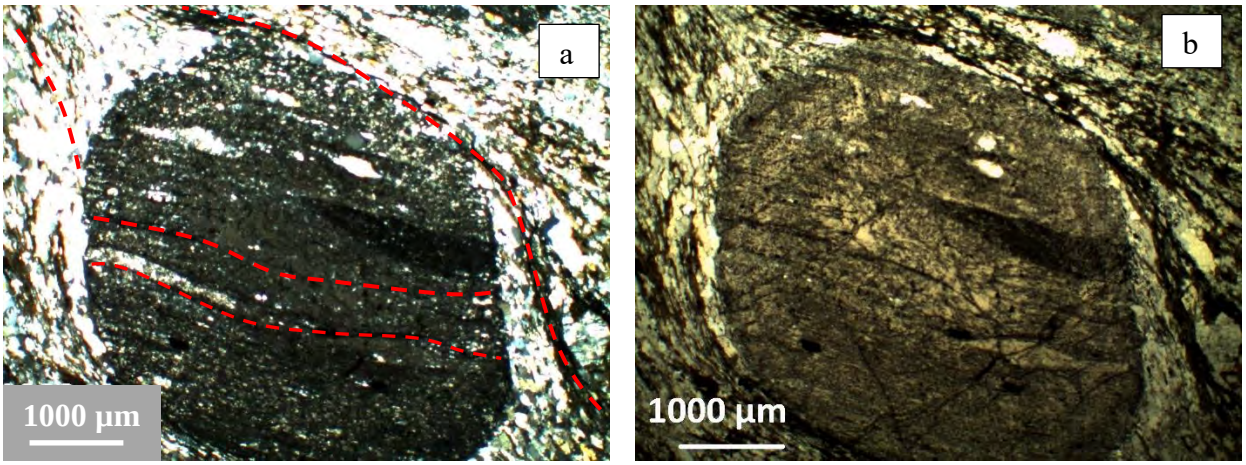

Figure 45: A zoned garnet porphyroblast within foliated matrix showing three cycles of light and dark rims. (a) cross-polarised light. (b) plane-polarised light. Garnet internal foliations are highlighted red.

Foliation in the matrix is generally discordant to preserved foliation in the garnet suggesting a post deformation growth. Garnets porphyroclast show rare fractures which are filled with calcite. Fractures offsets the continuity of preserved fabric within garnet. The filled structure is a micro fault zone within a garnet porphyroblasts (Figure 46). The external foliation trend wrapping around garnet porphyroclast. The internal foliation trend within the garnet is cut off at the garnet margin.

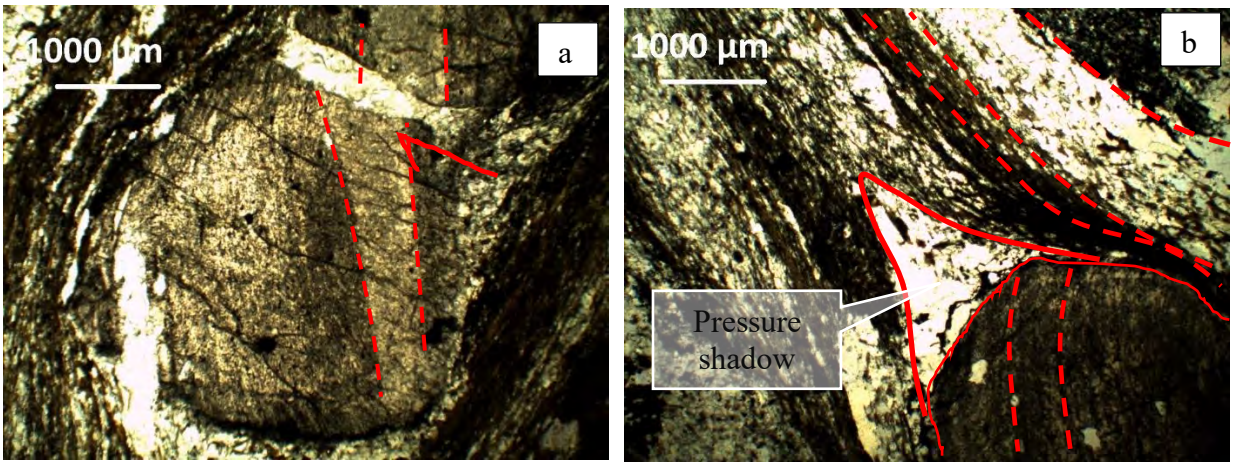

Figure 46: (a) Garnet porphyroclasts with a joint filled with calcite. The garnet has traceable continuous internal fabric suggesting a joint. (b) Pressure shadow, foliation within garnet and matrix foliation deflecting on the garnet porphyroclast. Light coloured microlithons and pressure shadows are marked by solid and dotted red lines respectively. The darker portions are foliation domains defined by deflected biotite.

Garnet porphyroclasts have preserved foliation trends with inclusion composition similar to those of the matrix. The foliation trails in garnet are not concordant to those of the matrix. Matrix foliation wraps around garnet suggesting the garnet porphyroclasts being pre-tectonic. The matrix fabric was developed after garnets had already grown as suggested by fabric and preserved matrix material in the garnet.

3.7 MC007: BIOTITE FELDSPAR QUARTZ GNEISS

MC007 was sampled from NDD0008 at depth intervals between 209.3 and 209.5 m. The rock unit belongs to the Basement Supergroup described in sections 1.2.2 and 2.6.4. The hand sample is a banded biotite feldspar quartz gneiss. The rock consists pink K-feldspar and quartz bands which alternate with biotite rich bands forming a gneissic texture. There are minor augen feldspar porphyroblasts along felsic bands with some showing sigmoidal trails.

Microscopically, the rock is a coarse-grained, weakly banded granoblastic gneiss (Figure 47). Felsic composition dominates the gneiss with minor interstitial biotite. The dominant felsic minerals are quartz, plagioclase and anhedral microcline crystals which are up to ~1 mm size. Microcline commonly exhibits hatch twinning and is occasionally weakly altered to sericite. Quartz is second most abundant mineral characterised by sutured contacts. Plagioclase feldspar has anhedral shape and size is up to ~1 mm. Plagioclase exhibits polysynthetic twinning as its distinguishing feature. The dark biotite is commonly oriented parallel to weak foliation. Brown elongate biotite is randomly and sparsely oriented within the coarser-grained felsic bands.

Due to the abundance of coarse-grained microcline, plagioclase and quartz, the assemblage may suggest a protolith of granitic rocks or its mineralogically equivalent unit.

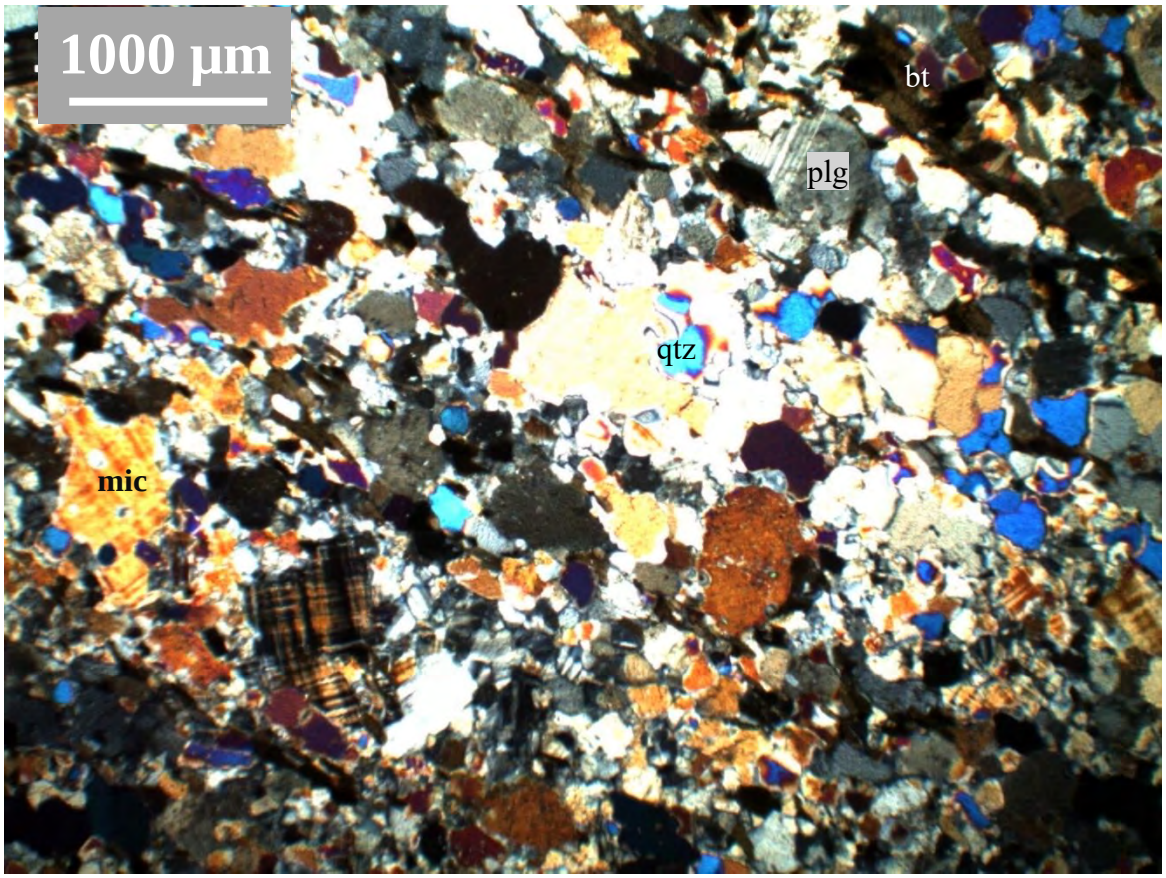

Figure 47: Photomicrograph for MC007 showing mineral phases and weak banding composed of biotite, plagioclase, quartz and microcline.

Quartz, feldspar and biotite alignment in both plane- and cross-polarized lights show S-C fabric (Figure 48). The biotite bands separate the crystalline portions of felsic minerals such as quartz and feldspar. Biotite foliation bands have two orientations marked in Figure 48b. The first biotite foliation trend is indicated by a purple line. The second well-defined foliation is marked red which cuts the first foliation at ~135°.

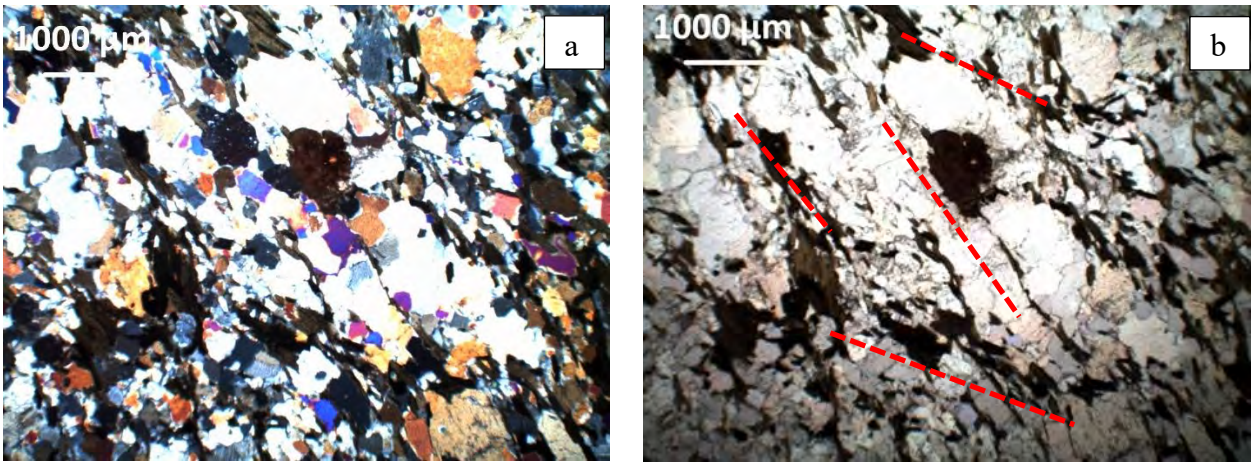

Figure 48: Photomicrographs showing S-C fabric defined biotite bands which are indicated by red and purple lines. (a) cross polarized light (b) plane polarised light shows marked foliation trends.

3.8 MC008: BIOTITE FELDSPAR QUARTZ GNEISS

MC008 was sampled from NDD0008 at depth between 214.2 m and 214.4 m. The hand sample is grey banded biotite feldspar quartz gneiss belonging to the Basement Supergroup described in sections 1.2.2 and 2.6.4. It consists of mafic bands composed of dark green amphibole with brown biotite. The felsic bands are composed of pink K-feldspar and quartz. The rock is folded. The sample is similar to sample MC007 though bands dominated by mafic minerals are more prominent in MC008.

The rock is dominated by mafic minerals which are interlayered with minor felsic minerals (Figure 49). The mafic bands are composed of biotite, chlorite and amphibole. The felsic bands are composed of feldspars and quartz. Biotite is brown elongate platy mica mostly in contact with amphibole and plagioclase. Amphibole is commonly subhedral with sizes ranging from 0.2 to 1 mm. The amphibole is dark green and brown commonly associated with biotite and chlorite. Chlorite is green and commonly associated to amphiboles.

Felsic minerals are plagioclase, alkali feldspar and quartz. Plagioclase shows undulose extinction and occurs rarely twined with grain boundaries marked by curvilinear surfaces. Plagioclase occasionally shows inclusions and alterations along grain boundaries and fracture zones. Quartz is curvilinear and shows sutured grain boundaries. Plagioclase occasionally exhibits hatch twinning which is observed in microcline. This might be a combination of albite and pericline.

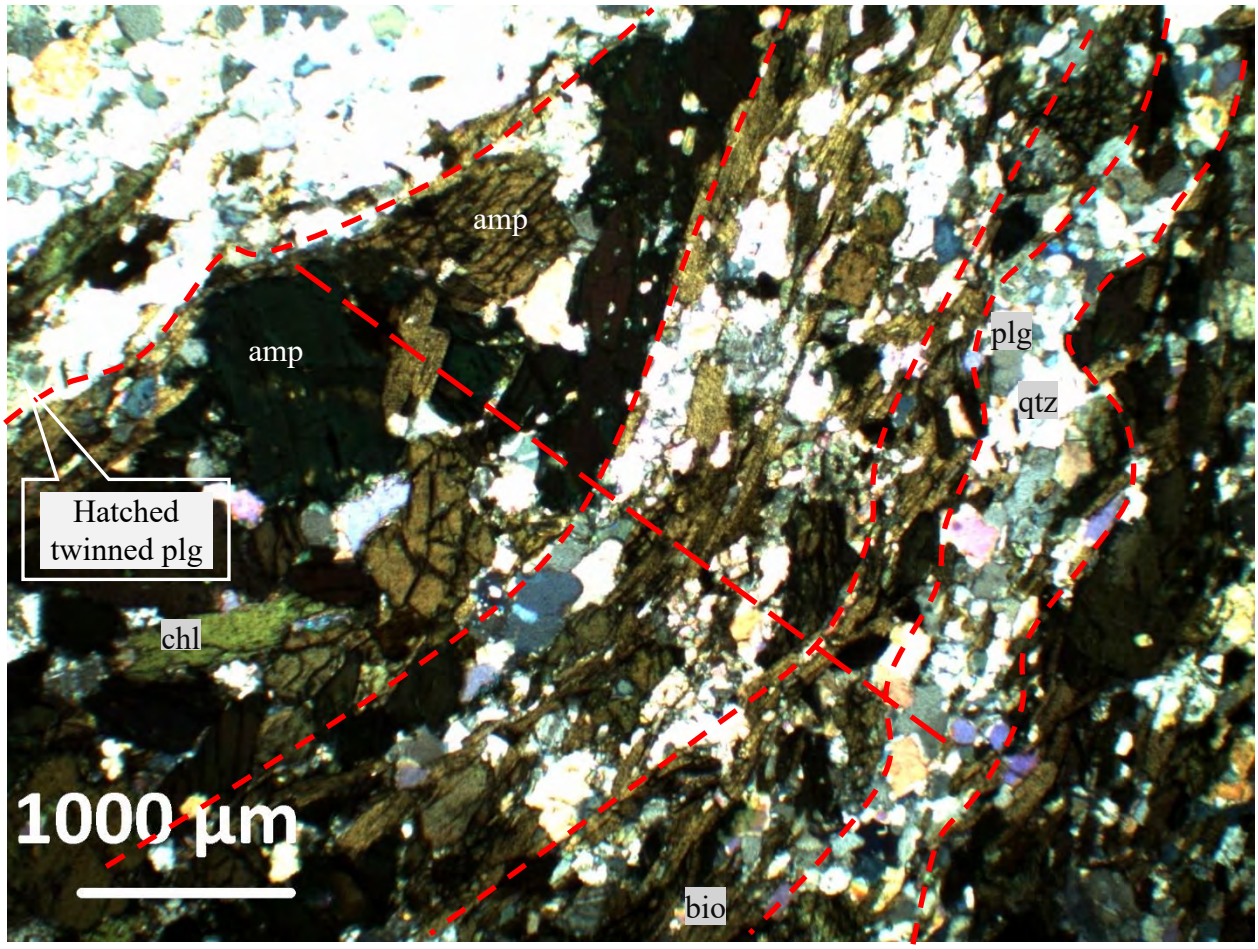

Figure 49: Photomicrograph of MC008 showing mafic and felsic bands that have been folded. The composition is biotite, plagioclase, quartz, chlorite and amphibole. Red lines show the contact between the felsic and mafic bands. The red lines also show curving of internal layering.

3.9 MC009: MUSCOVITE FELDSPAR QUARTZ SCHIST

MC009 was sampled from drill hole NDD0012 at depths between 72.3 and 72.5 m. The sample is interpreted as part of the Basement Supergroup. The hand sample is medium-grained, light grey to silky and is a strongly foliated schist. It is composed of muscovite, feldspar and quartz with minor hematite. The unit rarely has a soapy feel along foliation surfaces and joints interpreted to be feldspar alteration to clay. There are minor brecciated zones interlayered with strongly foliated zones.

The muscovite feldspar quartz schist exhibits strong foliation dominated by mica and minor muscovite (Figure 50 and Figure 51). The mica is greenish brown with a set of cleavage planes

along the elongate direction. Muscovite ranges in size from 100-1000 µm in length and 50-120 µm in width and has set of cleavage planes along the elongate direction. Muscovite is suhedral and occurring mostly along one foliation domain commonly associated to other mica. Muscovite and other mica define the foliation domain while coarse-grained microlithons are quartz and feldspar dominant with minor sericite. Plagioclase is not twined, it is commonly anhedral and occurs in contact with quartz, mica and muscovite (Figure 51). Quartz is anhedral to rounded and shows undulose extinction. Quartz also exhibits sutured grain contacts with other quartz and feldspar.

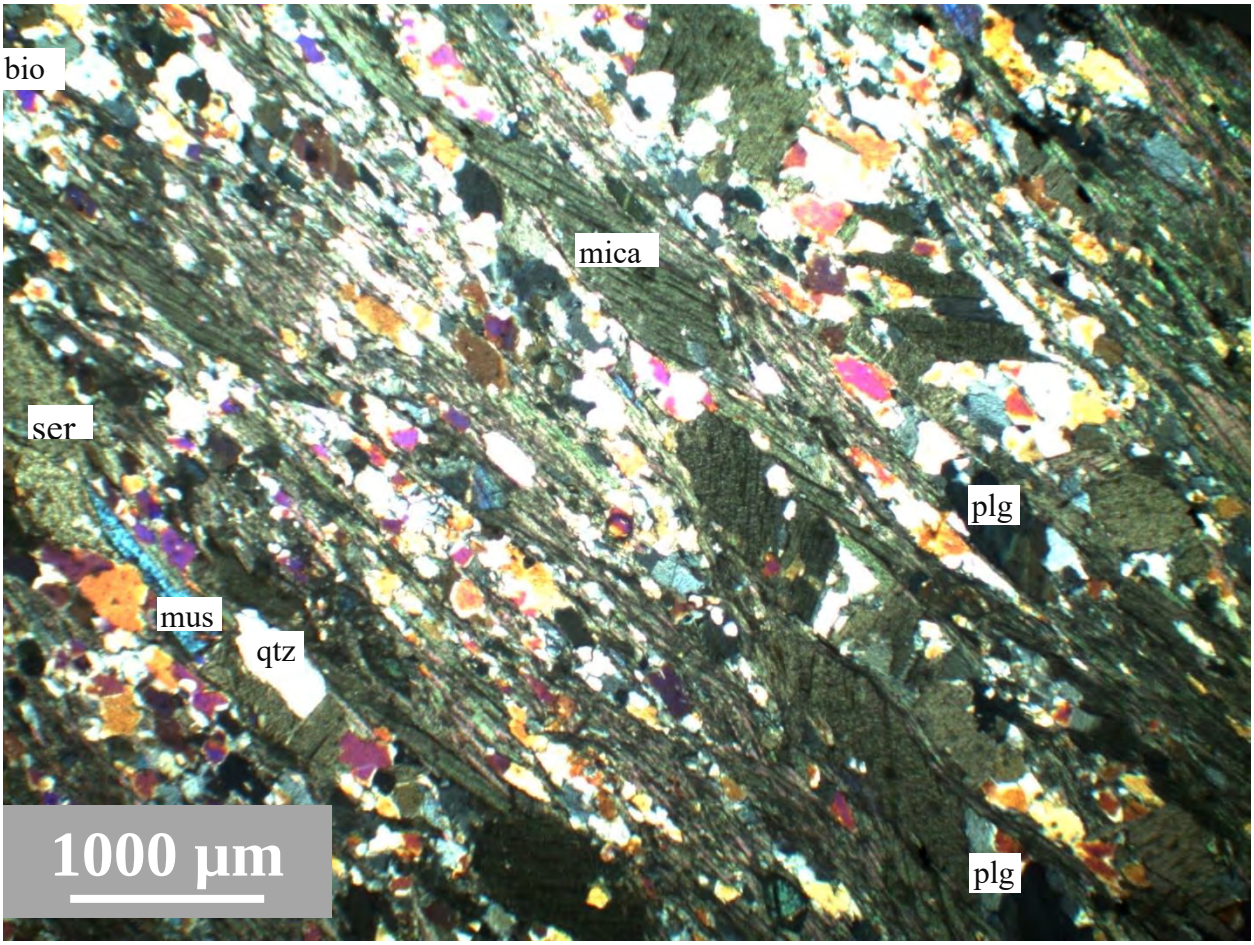

Figure 50: Photomicrograph of MC009 showing strongly foliated schist with muscovite (mus), quartz (qtz), plagioclase (plg), biotite (bio), mica and sericite (ser).

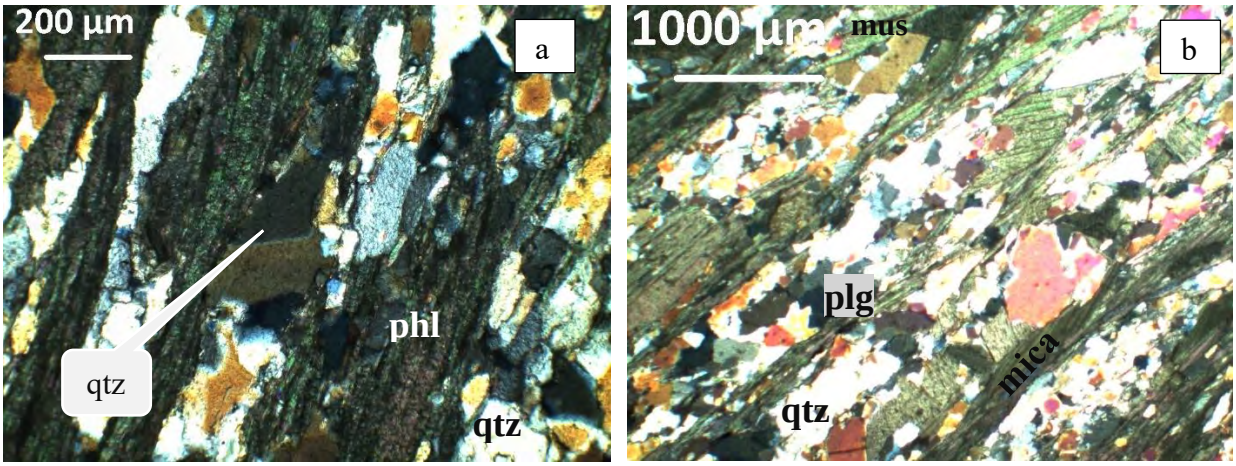

Figure 51: (a) Two quartz crystals sharing a straight boundary with mica and quartz crystals. (b) Foliated schist composed of plagioclase, quartz, muscovite and mica.

Foliations are marked by elongate muscovite and phlogopite which are more dominant along trend marked by hashed purple lines in Figure 52. The photomicrograph shows a disrupted and wavy foliation fabric marked in red. The wavy foliation marked by red hashed lines can be interpreted to be the earlier S1 fabric. This has been truncated by another foliation S2 marked in purple. The rock exhibits crenulation cleavage. Micas exhibit two grain shape orientations, one being elongate along S2 foliation trend while the other is subhedral and discordant to S2 fabric (Figure 48).

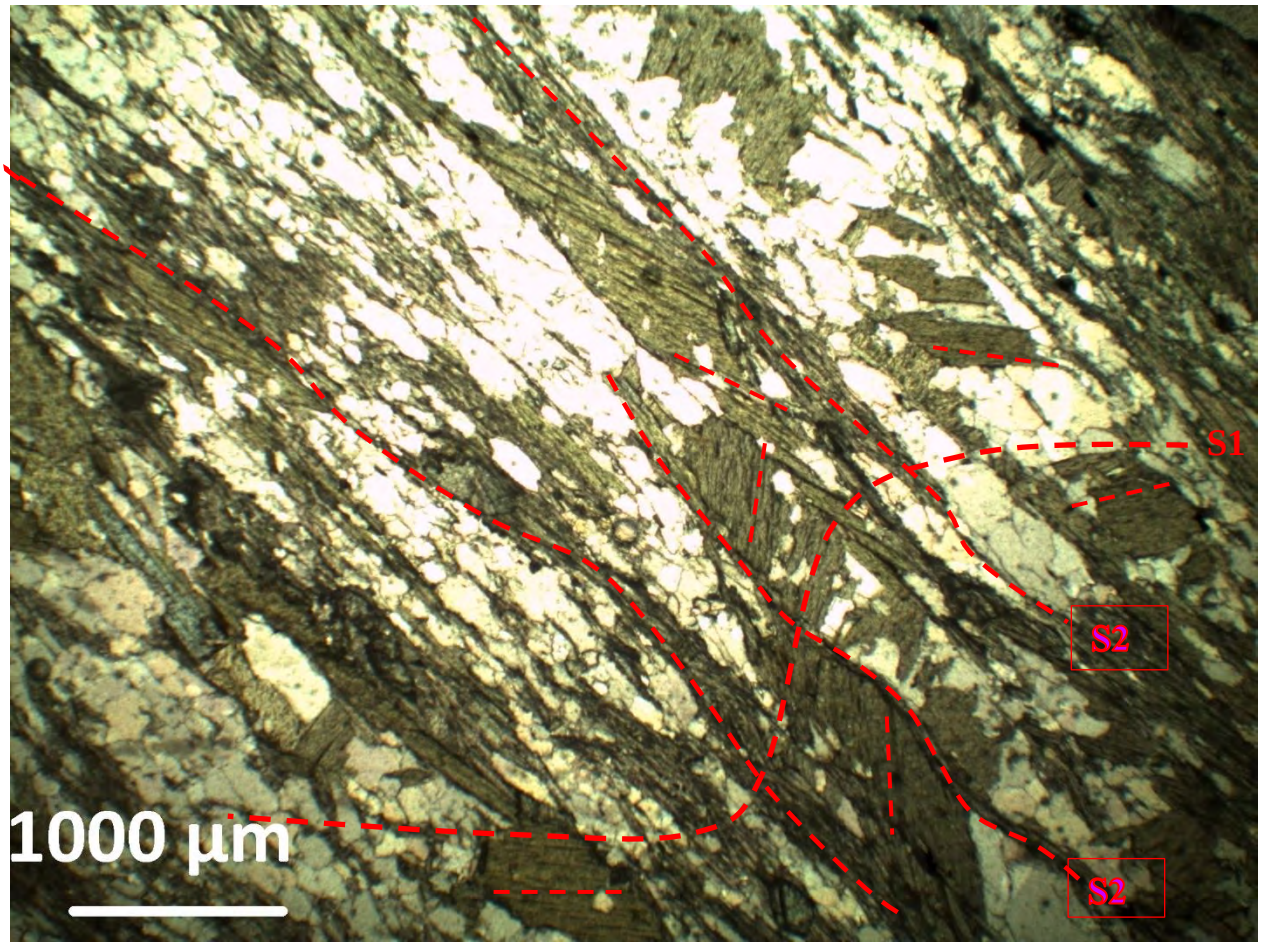

Figure 52: MC009 shows crenulation cleavage with S1 foliation defined by wavy and disrupted mica dominated foliation trend. S2 foliations forms well-defined foliation fabric marked by red hashed lines.

3.10 MC010: FELDSPAR BIOTITE GNEISS

MC010 was sampled from NDD0012 at depth between 138.4 and 138.6 m. The hand sample is greyish pink coarse-grained banded biotite feldspar gneiss. The sample is interpreted as part of the Basement Supergroup. It is composed of K-feldspar, quartz, biotite and minor muscovite. Pink K-feldspar and quartz occur as bands alternating with foliated biotite rich foliation domain. The rock has a very weak chlorite alteration and strong pervasive potassic alteration defined by sericite and muscovite. Potassic alteration is dominant along joints and shear zones. Minor clay rich portions resulting from weathering of feldspar swell when exposed to air. There are light pink quartz-feldspar veins cutting rock layering. Veins are commonly fragmented and have altered the walls of host rock.

The thin sections (Figure 53 and Figure 54) show muscovite and biotite defining foliation domain and wrapping around feldspars rich porphyroclasts. Muscovite is fine-grained elongate platy mineral defining the foliation domain. Biotite is also elongate, brown, platy and coarse-grained occurring along foliation trend.

Porphyroclasts are commonly composed of plagioclase and microcline. Microcline is more abundant and has multiple shades of colour, it can be easily distinguished by its hatched twinning (Figure 53). Microcline porphyroblasts range in size from 1 to 4 mm with subhedral and lencoidal shape marked by red outline in Figure 53a. Hatched microcline occasionally has sutured contacts with other granular minerals. Plagioclase feldspar porphyroblasts have been slightly altered to sericite.

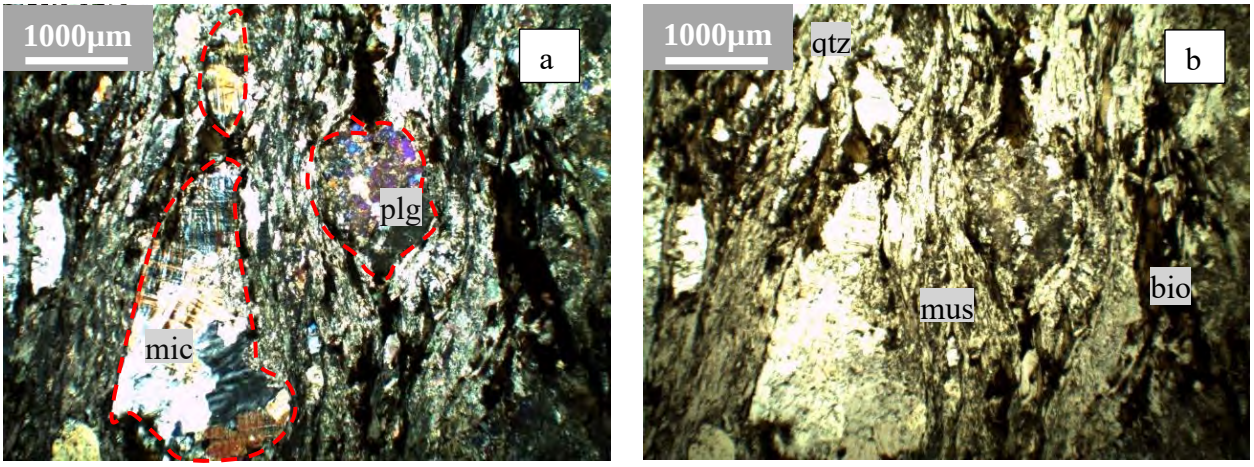

Figure 53: Photomicrograph showing microcline and plagioclase and quartz porphyroblasts within muscovite and biotite matrix (a) cross-polarized light and (b) plane-polarized light.

Augen feldspar porphyroclasts are commonly sericitised with microcline showing weak hatched twining (Figure 54). The porphyroclasts are elongated along foliation trend. The matrix composed of muscovite and minor biotite wraps around porphyroclasts (Figure 54). The dominant foliation trend is marked by pink in Figure 54. Another poorly defined set of foliations intersect the dominant foliation at low angles of ~30°.

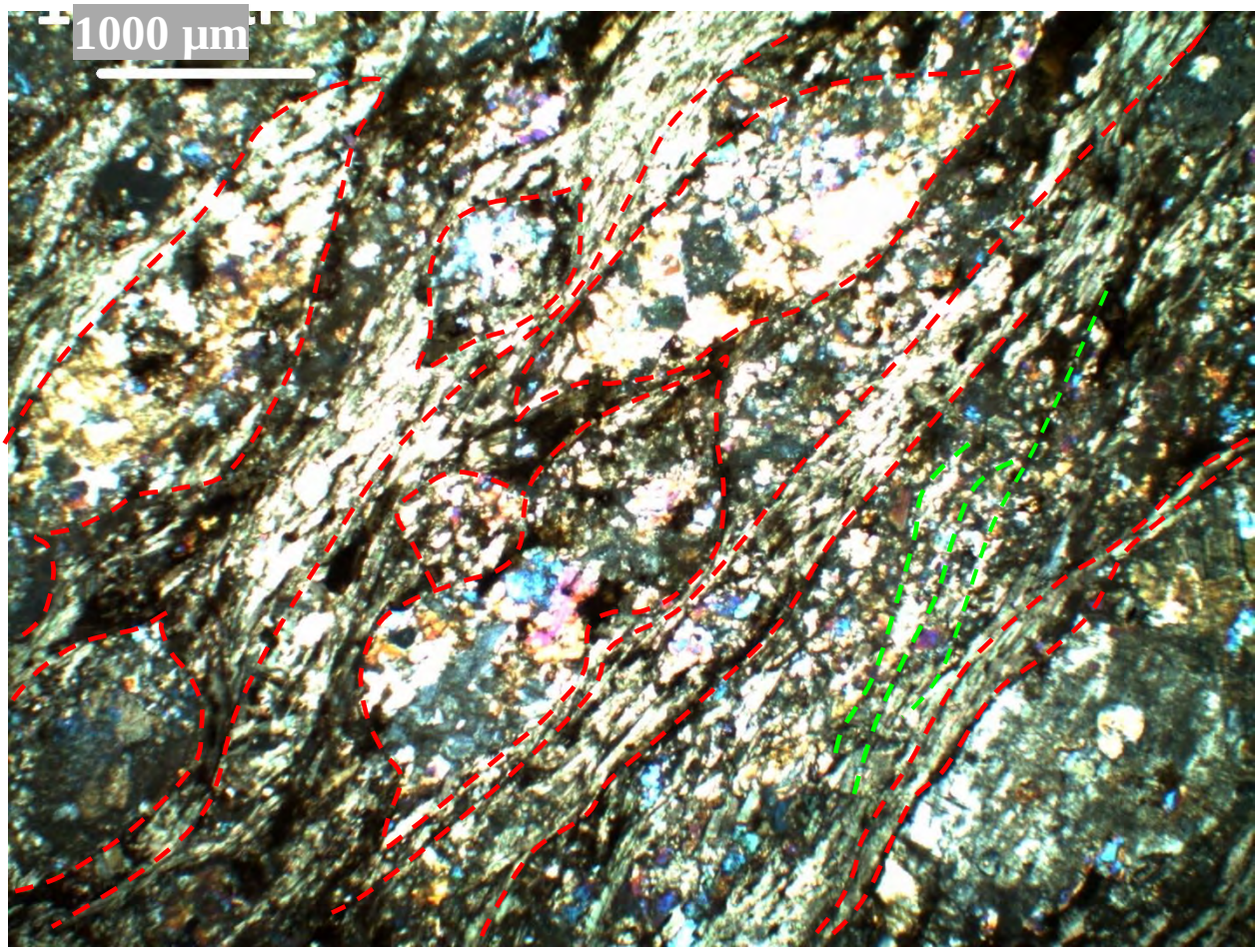

Figure 54: Photomicrograph showing augen shaped altered feldspar porphyroblasts within a foliated matrix. Matrix is dominated by muscovite with minor biotite marked by red long hashed lines. Green hashed lines indicate weak foliation trend bounded by dominant foliation marked by red hashed lines.

3.11 MC011: GARNET BIOTITE SCHIST

MC011 was sampled from NDD0006 at depths between 252.2 and 252.4 m. The hand sample is a grey biotite garnet schist with stretched clasts. The rock is interpreted to belong to the Grand Conglomerate Formation. Garnet porphyroblasts are randomly distributed within foliated biotite, calcite and quartz matrix. Garnets are euhedral and occasionally rimmed with calcite and biotite. The unit has stretched clasts which are elongated along foliation direction. There are calcite bands and veins cross cutting foliations at different angles.

The rock under cross-polarized light (Figure 55a and b) show a mixed medium- and fine-grained strongly foliated matrix with garnet porphyroblasts. Matrix composition is muscovite, biotite, quartz, calcite and feldspar. Muscovite is elongate mineral occurring along foliation trend. Muscovite abundance is variable on different sections, it is commonly associated with elongate brown biotite both defining the foliation domain. Minor biotite grains are rarely discordant to dominant foliation trend. The coarser microlithons of the matrix are composed of anhedral to rounded quartz, calcite and feldspar that are up to 0.5 mm. The anhedral calcite is randomly distributed within the matrix.

The matrix has randomly distributed subhedral and rounded garnet porphyroclasts. Garnet porphyroclasts show inclusions of quartz and biotite assemblage identical to that in the matrix (Figure 55). The inclusions within garnet form S shape marked in red lines in Figure 55. Some garnets show randomly oriented fractures filled with calcite and quartz (Figure 55). Garnet is commonly in contact with foliated matrix consisting of biotite and muscovite while others have quartz and calcite rims.

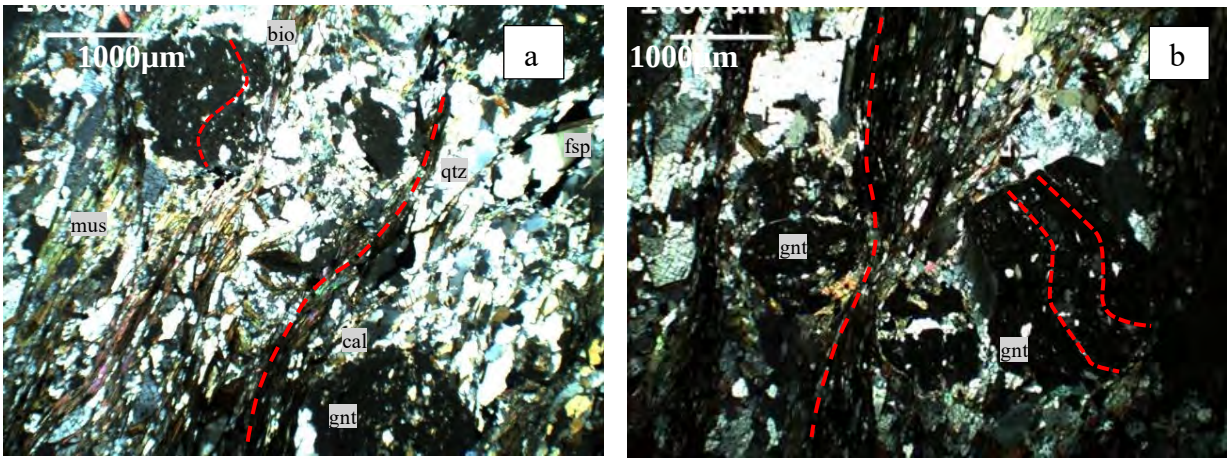

Figure 55: Garnet porphyroclasts randomly distributed in foliated matrix of muscovite, biotite, quartz, calcite and feldspar. Garnets have S trails defined by matrix material which is marked in red lines. Foliation marked in red hashed line is mostly defined by biotite and muscovite.

The matrix foliation is deflected around garnet porphyroclasts which suggests that the garnets were there when shearing took place along the foliation. The garnets may suggest former cleavage within a schist which had developed earlier during deformation. The inclusion and preserved

foliation within the garnet forming an S-shape rotational trail suggest a syn-tectonic growth of garnet which are now porphyroclasts.

3.12 MC012: AMPHIBOLE BIOTITE FELDSPAR QUARTZ SCHIST

MC012 was sampled from diamond drill core NDD008 at depths between 178.4 to 178.7 m. The rock is amphibole biotite feldspar quartz gneiss. The sample is interpreted as part of the Basement Supergroup. It consists of pink K-feldspar and quartz felsic bands alternating with amphibole and biotite rich bands. Feldspar commonly shows augen shape wrapped by biotite rich foliation.

Microscopically, amphibole phase in sample MC012 is pleochroic exhibiting brown and green colour. Other mineral phases include biotite plagioclase and quartz (Figure 56). Amphibole phase is greenish anhedral crystal that vary in sizes from 0.2 mm to 1 mm. It is randomly distributed within the rock and commonly occur with biotite and plagioclase. Biotite occurs as brown, platy and elongate mineral defining foliation fabric with size ranging from 0.1 mm to 1.2 mm. Biotite has one set of cleavage along the elongate direction. Some biotite grains show slight alteration to chlorite. Quartz is fine- to medium-grained crystals commonly associated to plagioclase.

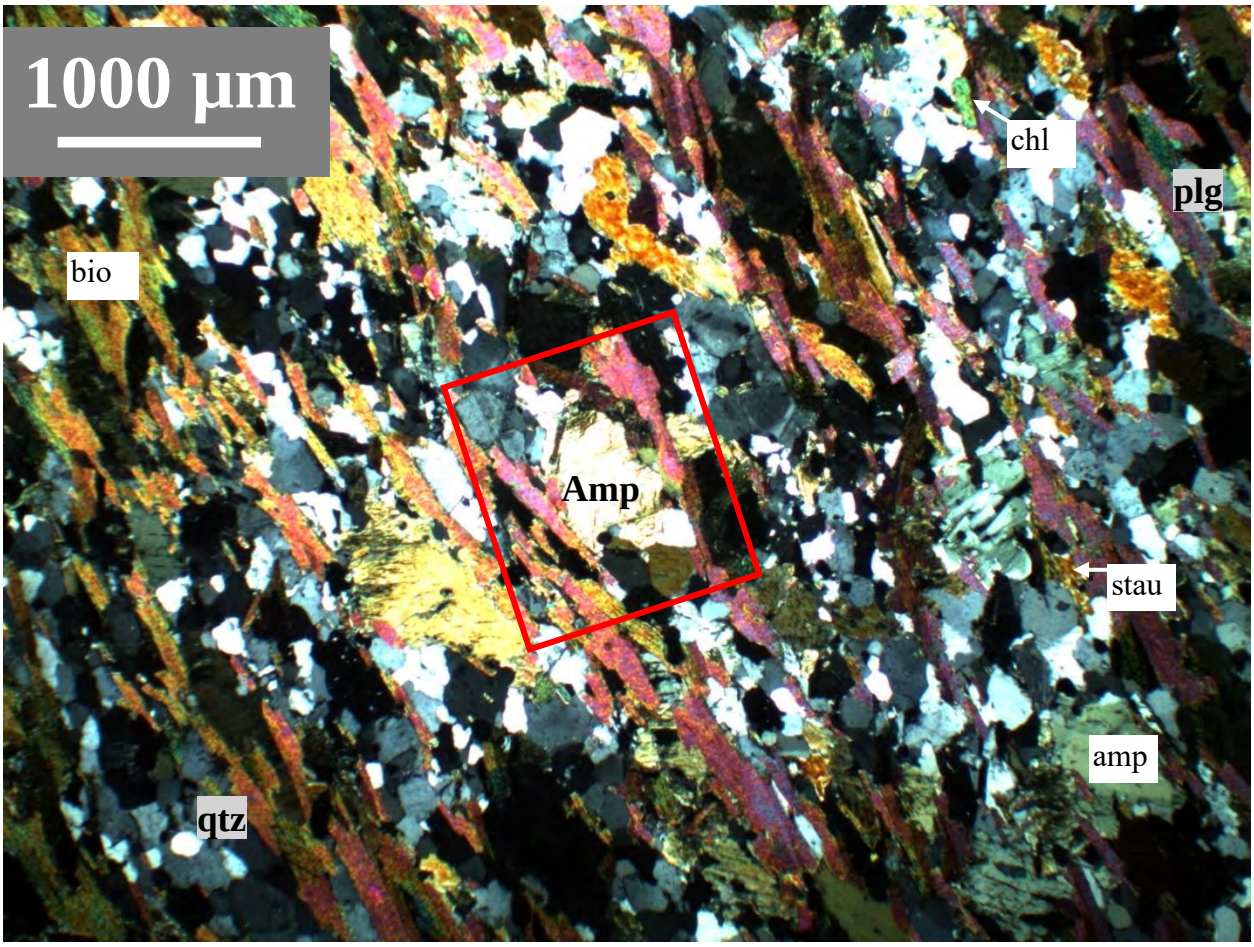

Figure 56: Cross-polarized photomicrograph showing foliation defined by biotite. Other mineral assemblages include pleochroic brown and green amphibole, plagioclase, chlorite, staurolite and quartz. The red rectangular outline consists of brown amphibole with biotite, quartz and feldspar and has been magnified in Figure 57.

Mineral phases include amphibole, quartz, biotite and plagioclase (Figure 57). Plagioclase feldspar is anhedral with twinning, it generally ranges in length from 0.1 to 0.5 mm with common size being 0.2 mm. Quartz is commonly subhedral, it is associated with plagioclase feldspars. Amphibole is brownish and subhedral, its size ranges from 0.2 mm to 1 mm in length. It is usually distinguished commonly by its cleavage and extinction angle.

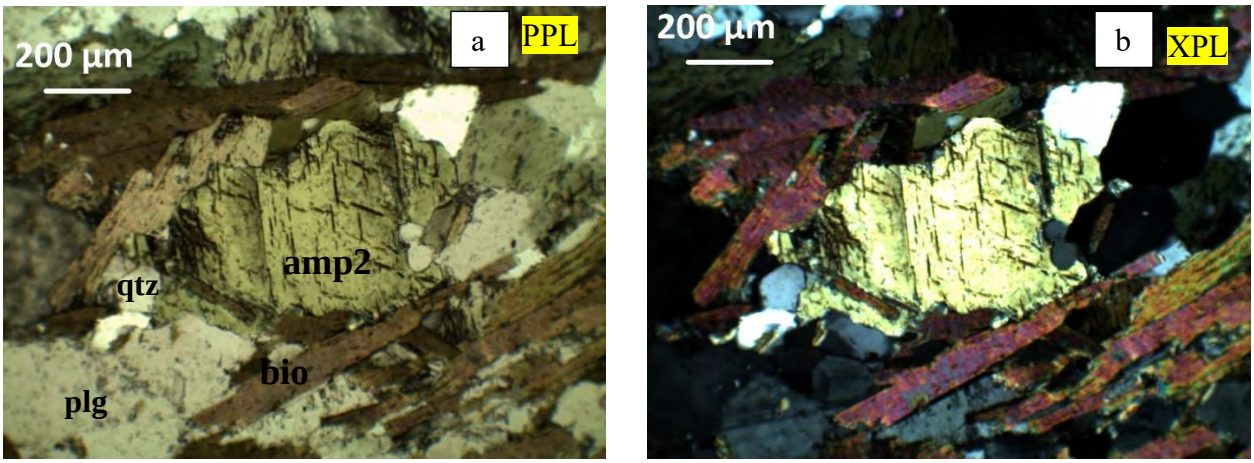

Figure 57: Photomicrograph showing amphibole, quartz, plagioclase and biotite in plane- and cross-polarized light. PPL: plane-polarized light and XPL: cross-polarized light.

3.13 MC013: GARNET BIOTITE SCHIST

MC013 was sampled from diamond drill core NDD0010 at depths between 114.9 to 116.3 m. The rock sample is grey garnet biotite schist composed of large garnet (~10 mm), biotite with minor quartz and calcite. The rock sample belongs to the Grand Conglomerate Formation. The rock has large (~10 mm) garnets. The unit comprises of dark grey to black stretched clasts with pyrite and calcite rims around them.

Microscopically, garnet biotite schist consists of garnet, biotite, quartz, calcite and feldspar (Figure 59 and 59). Garnet porphyroblasts range in sizes from 4 mm to 7 mm long. Garnet is anhedral with boundaries commonly defined by coarser matrix composition. Garnet porphyroblasts have inclusions similar to those of the matrix such as biotite, quartz, calcite and feldspar. There is foliation fabric preserved within garnet, this foliation has similar direction as the shape of the garnet.

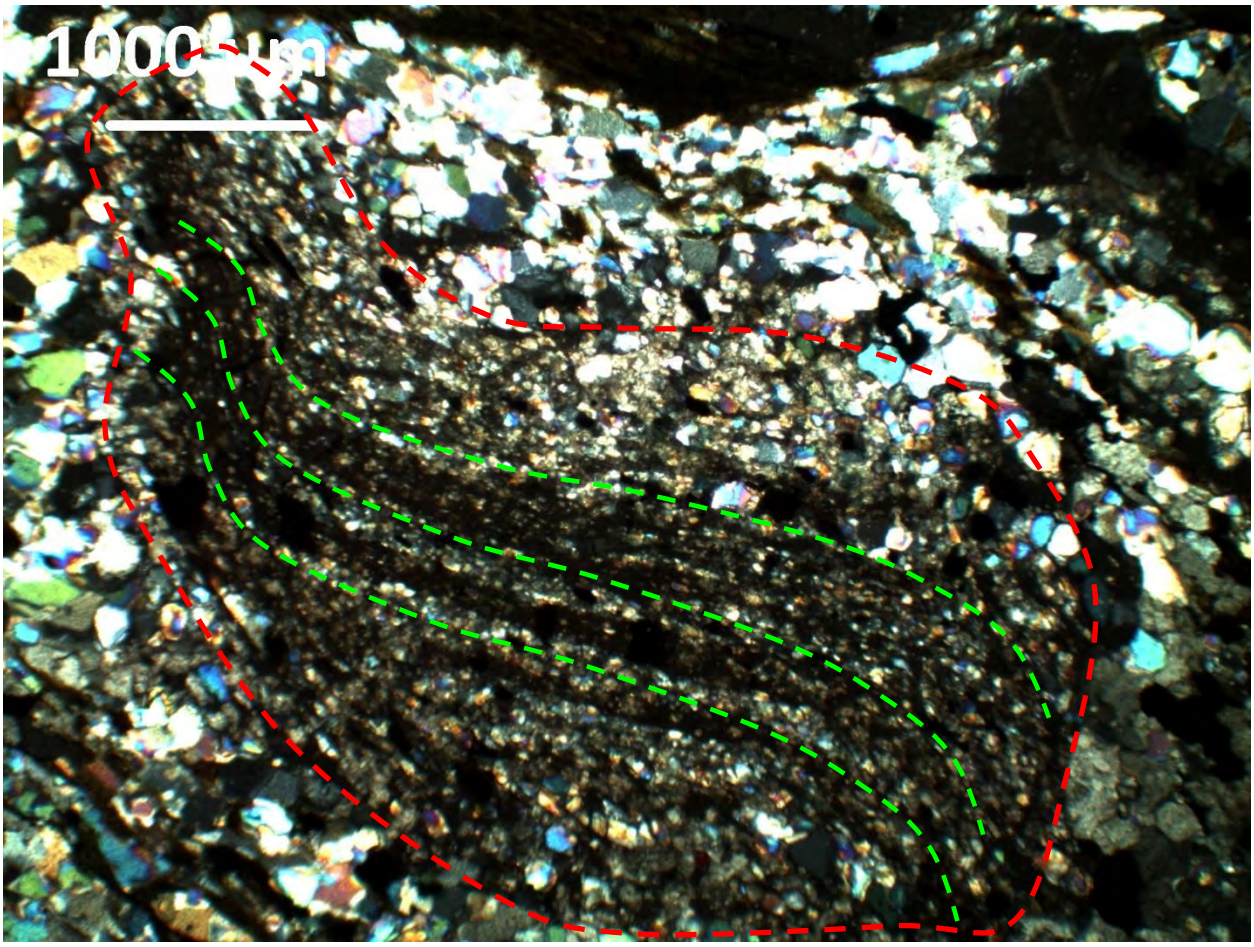

Figure 58: CPL photomicrograph showing a ~7 mm long garnet porphyroblast within a biotite, calcite, feldspar and quartz matrix. The garnet boundary is in red hashed line. Inclusions within garnet show an S shape alignment documenting internal foliation (highlighted in green). The red outline shows the garnet boundary.

The matrix is composed of quartz, calcite, biotite and minor plagioclase feldspar (Figure 59). Biotite is brown, platy and elongate while calcite is grey and anhedral. Feldspar is anhedral commonly associated with quartz. Feldspar crystals ranges in size from 0.1 mm to 0.3 mm. Quartz is rounded and anhedral crystals that vary in size from 0.1 mm to 0.3 mm. Within the matrix are randomly distributed garnet porphyroblast. They have preserved internal foliation trends marked in green dashed lines in (Figure 59). The internal foliation within the garnet is discontinuous with the external matrix foliation. Garnet exhibits helicitic texture suggesting syn-kinematic growth.

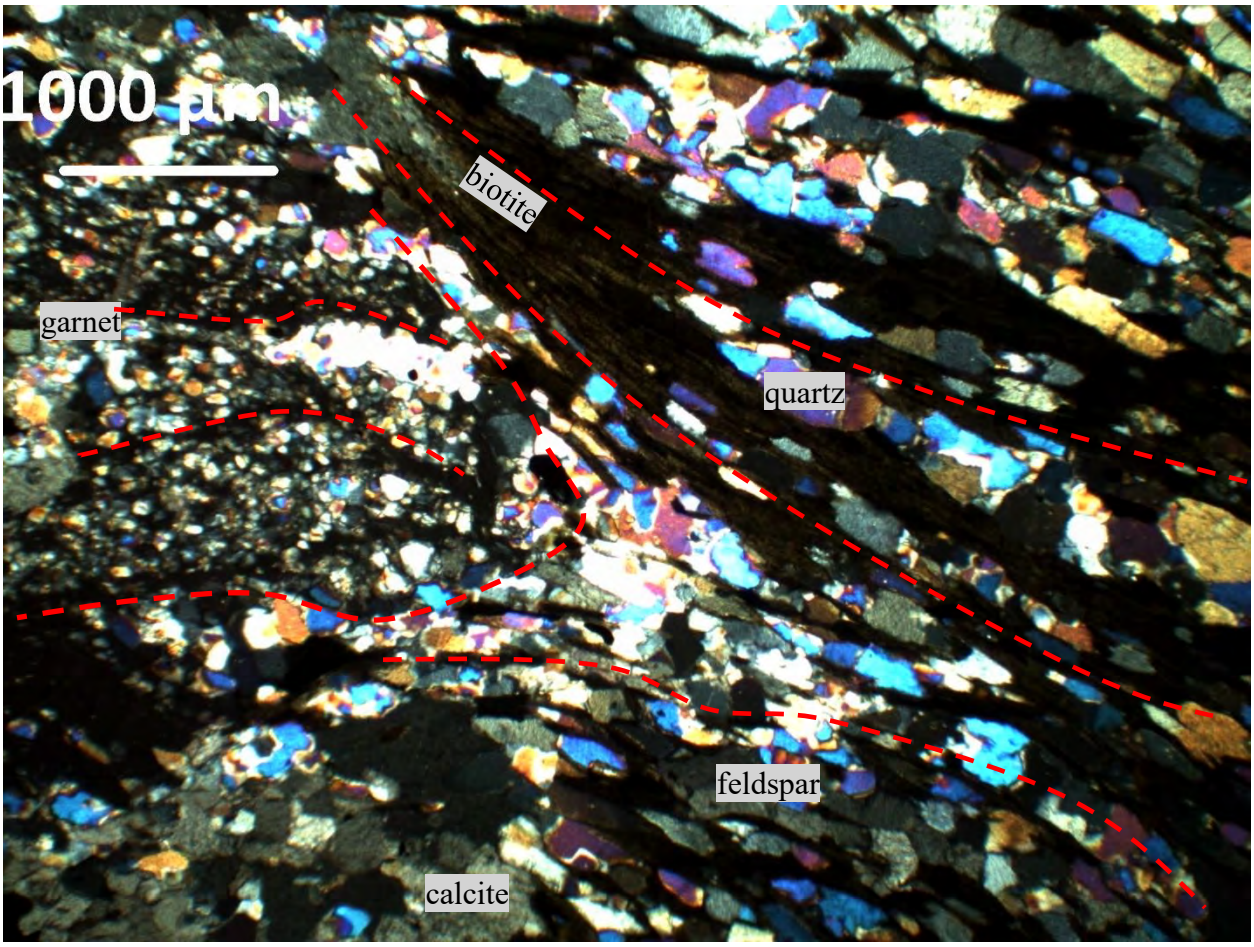

Figure 59: Garnet porphyroclast within matrix foliation composed of biotite, quartz, calcite and feldspar. Foliation fabric truncates into garnets and also wraps around the garnet porphyroclasts. Internal garnet foliation is discontinuous with the matrix foliation.

The foliation in garnets suggests being initial S1 foliation. The S1 was later overprinted by S2 foliation within the matrix which wraps around the garnet porphyroclast. The deflection of the foliation around garnet indicates that the garnet was there when S2 shearing took place along the foliation. However, garnets are syn-tectonic. In the current case there might be a younger overprint that rotated the garnet with its inclusion trails. The garnet has finer-grained foliations and inclusions than the matrix foliation. MC013 and MC006 are similar, they both have developed garnet porphyroclasts with S trail.

3.14 MC014: BIOTITE QUARTZ FELDSPAR GNEISS

MC014 was sampled from hole NDD0012 at depth between 188.0 to 188.2 m. The sampled is within biotite quartz feldspar gneiss belonging to the Basement Supergroup. The rock is composed

of biotite, quartz, feldspar, chlorite and epidote. The hand sample is medium-grained, grey banded gneiss with layers of quartz muscovite schist. Feldspar composition is variable at different sections.

Microscopically, biotite feldspar quartz gneiss shows feldspar porphyroclasts wrapped by muscovite and biotite foliation (Figure 60). Porphyroclasts have augen shape with size ranging from 1 to 4 mm. Some feldspar porphyroclasts have been altered to sericite (Figure 60). Microcline rarely shows hatch twinning and sutured contacts with other granular minerals. Quartz is medium-grained anhedral crystals and has sutured contacts with feldspar. Matrix composition is mostly muscovite, biotite and chlorite which define the foliation domain. The matrix material are commonly elongate micas which wrap around porphyroclasts.

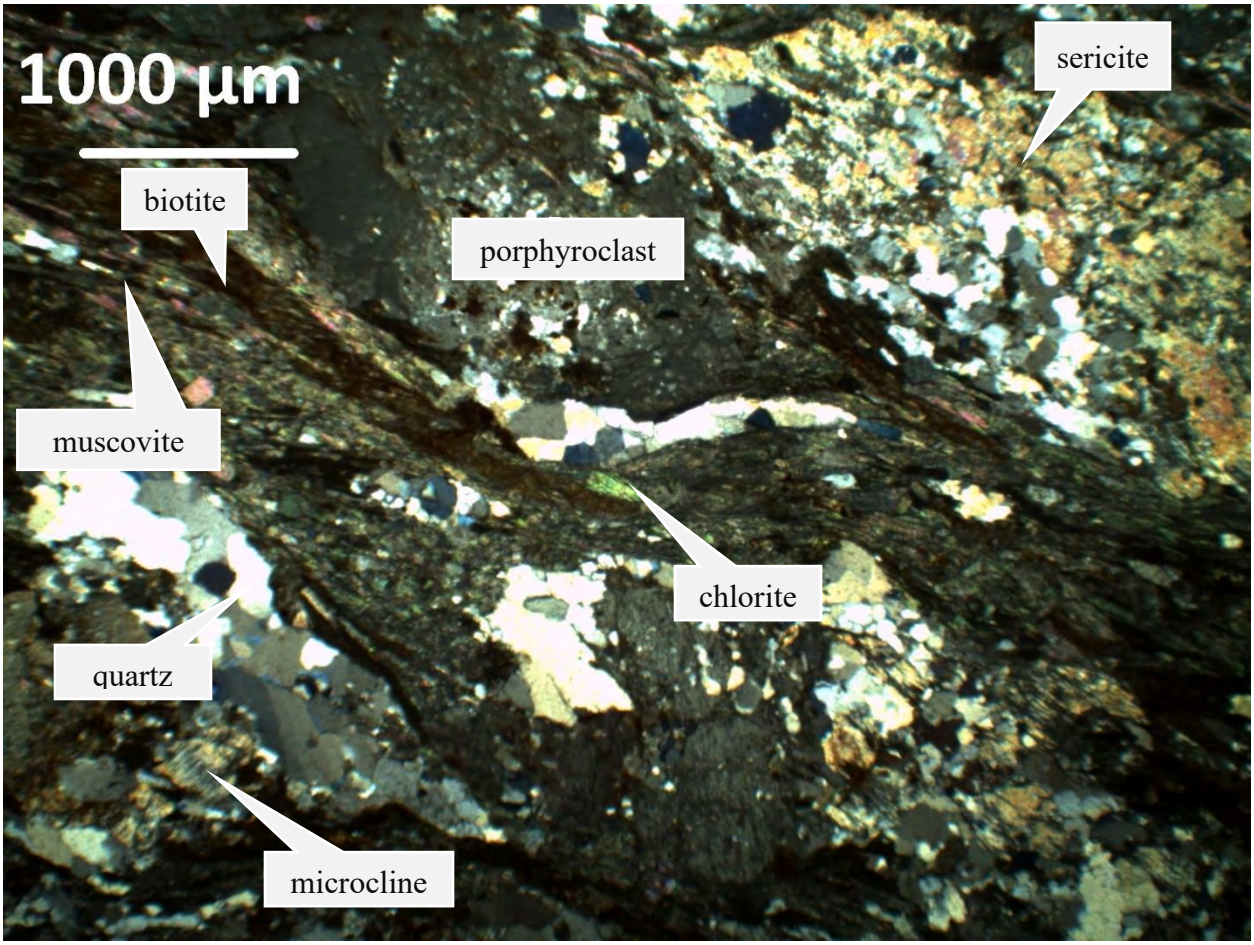

Figure 60: Porphyroclasts composed commonly of feldspar and sericite are wrapped by biotite and muscovite foliation.

4. MINERAL AND BULK CHEMISTRY

Six samples were selected for Energy Dispersive X-ray Spectrometry (EDS) analysis based on micro-petrographic features of minerals such as garnet zoning and other mineral phases. This method was employed in order to confirm the identity of mineral species and to obtain chemical compositions and cation ratios of solid solutions (e.g., garnet, plagioclase, amphibole) required to refine pressure-temperature estimated of the regional metamorphism.

The analyses were done at Rhodes University using an Energy Dispersive X-ray Spectrometry (EDS) machine at an accelerating voltage of 20kV. Thin section samples were coated with carbon before analysis. The MS Excel software (Büttner, 2012) was used to calculate number of cations with specific oxygen cation using EDS oxide results. The actual mineral phases were identified using pdf online hand book of mineralogy by Anthony et al. (1995).

4.1 GARNET

The merged element maps of sample MC001 show different element composition for garnet porphyroblast and matrix (Figure 61). Generally, different elemental concentration in each garnet zone is slightly different. It is also noted that garnets exhibit variety of element zoning patterns that are useful in determining metamorphic history.

The rim of the garnet (Figure 61) has high Fe content which reduces towards the core. Mg concentration is uniformly low throughout the garnet porphyroblast. Mn concentration is highest within the core of the garnet and decreases towards the rim. Ca concentration is high, it reduces towards the garnet rim. The very thin outer rim (<10 μm) in contact with the matrix is slightly higher in Ca and Mn.

There are anhedral garnet inclusions with sizes less than 10 μm. Inclusions within garnet are commonly quartz as evident by high silica content and absence of Fe, Mg, Mn and Ca. Biotite and calcite are occasional. Garnets and matrix show minor mineral trend within Fe and Si element maps (Figure 61).

The matrix is high in Fe, Mg and Si while higher Ca is occasionally occurring as specs. The composition of the matrix is commonly biotite (high Mg and Fe), quartz (only Si) and minor calcite (only Ca present).

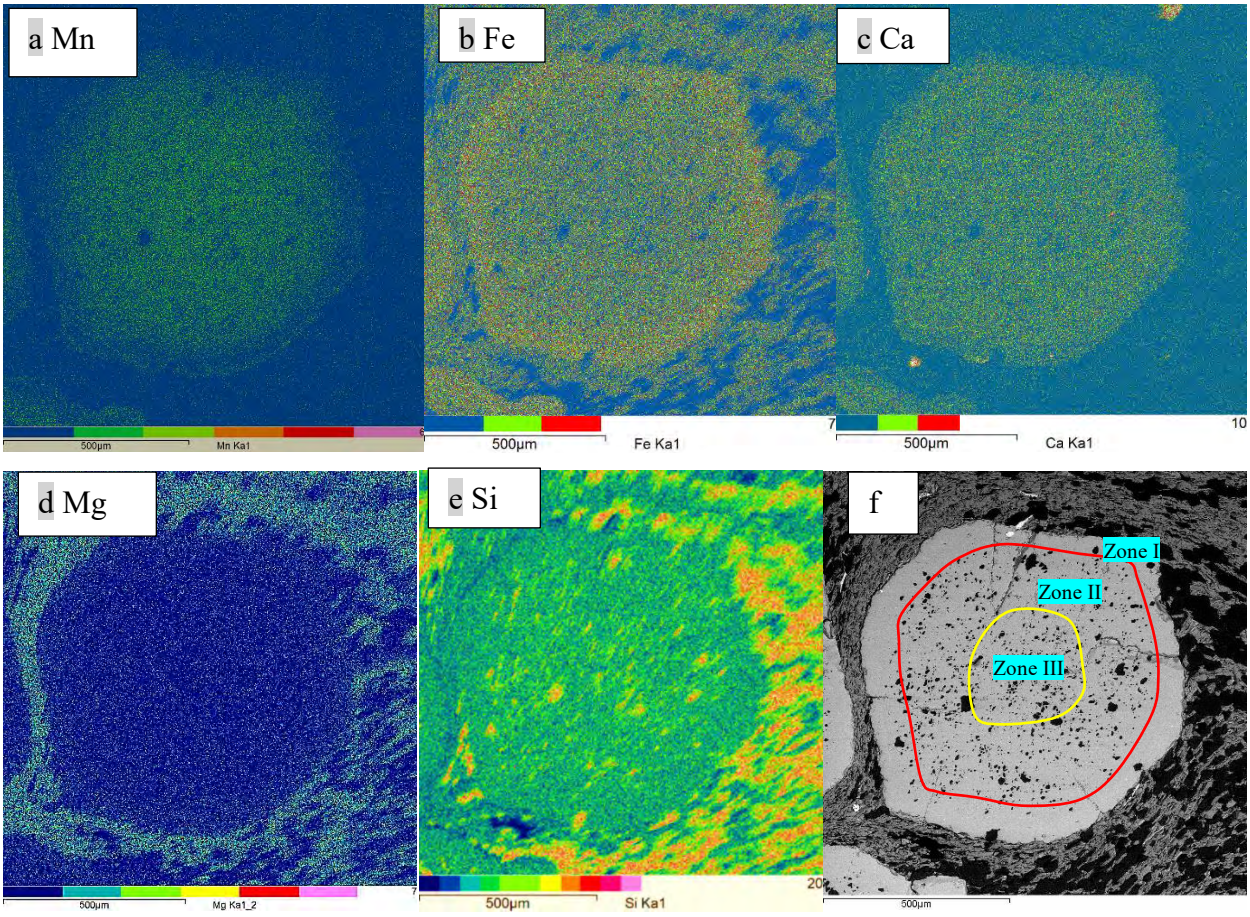

Figure 61: Merged maps of (a) Mn, (b) Fe, (c) Ca, (d) Mg and (e) Si showing relative element concentration of the garnet porphyroblasts and matrix; (f) distinguished garnet zones I, II and III, different shades of grey, black and white indicates different mineral phases.

The small white specs within the matrix (Figure 61f) is ilmenite and hematite. Quartz is black while different shades of grey represent biotite and minor calcite. The brown biotite matrix indicated earlier (Figure 34) is medium grey in Figure 61f.

Electron Dispersive X-ray Spectrometry (EDS) analyses were done on different zones of garnet labelled Zone I, II and III (Figure 61f). Table 9 below shows results for different analyses within specified zones of the garnet. There were little or no Cr and Ti compositions hence results only

included Si, Al, Mg, Fe, Ca and Mn. These results were calculated using MS Excel software by Büttner (2012) and garnet endmembers were averaged for different zones as shown in Table 9.

The garnet porphyroblast show zonal variations in Mg, Fe and Mg, and to a minor extent also in Ca (Table 9). The variable composition results in different endmember proportions for different zones. The rim (zone I) of the garnet is dominated by almandine (X_{Alm}) ranging from ~0.67 to 0.72 and averaging at ~0.70. The grossular content (X_{Grs}) ranges from ~0.11 to 0.15 and spessartine (X_{Sps}) between ~0.06 and 0.09. The pyrope content (X_{Prp}) ranges between 0.04 and 0.07 while andradite content (X_{And}) is 0.03.

The middle zone (zone II) commonly shows matrix inclusions and has decreased almandine and pyrope contents compared to zone I. The almandine content ranges from ~0.49 to 0.53 while the pyrope contents are negligible 0.02. The grossular content ranges from ~0.14 to 0.15. The spessartine content has significantly increased by on average 200% and is between ~0.27 and 0.31 while andradite content (X_{And}) is 0.04.

Within the garnet core (zone III), almandine and spessartine contents are high and range from ~0.38 to 0.39 and ~0.42 to 0.44 respectively. The grossular content is almost the same as that of zones I and II ranging from ~0.11 to 0.15. The andradite content is 0.04 while the pyrope content is negligible being ~0.01. The spessartine content has increased from zone I through to zone III while almandine and pyrope have decreased.

Table 9: Representative garnet analyses within different zones ($X_{Mg} = Mg/(Mg+Fe^{2+})$

Sample	MC001	MC001	MC001	MC001	MC001	MC001	MC001	MC001	MC001	MC001
Zone	I	I	I	I	II	II	III	III	III	III
Analysis	1-11	2-8	2-1	1-3	1-5	2-4	1-2	2-7	2-6	2-5
SiO2	37.40	37.29	37.63	37.42	37.91	37.17	37.59	37.81	37.52	37.62
TiO2	0.00	0.00	0.00	0.00	0.00	0.00	0.00	0.00	0.00	0.00
Al2O3	21.14	21.06	20.95	21.09	21.38	21.31	21.32	21.18	21.36	21.19
Cr2O3	0.00	0.00	0.00	0.00	0.00	0.00	0.00	0.00	0.00	0.00
Fe2O3	1.02	1.02	0.99	1.07	1.28	1.22	1.34	1.35	1.37	1.37
MgO	1.25	1.20	0.89	1.58	0.37	0.38	0.28	0.32	0.29	0.24
CaO	5.80	5.23	5.91	4.96	5.97	6.14	6.25	5.68	4.96	5.85
MnO	3.63	4.44	4.82	2.67	11.23	12.85	17.26	17.54	18.09	17.34
FeO	29.75	29.76	28.81	31.21	21.86	20.92	15.97	16.14	16.41	16.39
Total	100.00	100.00	100.00	100.00	100.00	100.00	100.00	100.00	100.00	100.00
Number of cations on the basis of 24 O										
Si	6.010	6.006	6.051	6.012	6.074	5.998	6.036	6.070	6.038	6.049
Ti	0.000	0.000	0.000	0.000	0.000	0.000	0.000	0.000	0.000	0.000
Al	4.003	3.998	3.970	3.994	4.038	4.053	4.035	4.008	4.050	4.015
Cr	0.000	0.000	0.000	0.000	0.000	0.000	0.000	0.000	0.000	0.000
Fe^{3+}	0.124	0.124	0.120	0.130	0.154	0.089	0.161	0.163	0.166	0.166
Mg	0.300	0.288	0.214	0.378	0.088	0.092	0.066	0.076	0.071	0.058
Ca	0.999	0.903	1.019	0.854	1.025	1.061	1.076	0.977	0.854	1.008
Mn	0.494	0.606	0.656	0.363	1.524	1.757	2.348	2.385	2.465	2.361
Fe^{2+}	3.997	4.008	3.875	4.194	2.929	2.882	2.145	2.167	2.209	2.204
Cation Tot	15.93	15.93	15.90	15.93	15.83	15.93	15.87	15.84	15.85	15.86
X_{Mg}	0.07	0.07	0.05	0.08	0.03	0.03	0.03	0.03	0.03	0.03
Endmembers										
X_{And}	0.03	0.03	0.03	0.03	0.04	0.04	0.04	0.04	0.04	0.04
X_{Grs}	0.14	0.12	0.15	0.11	0.14	0.15	0.15	0.13	0.11	0.13
X_{Alm}	0.69	0.69	0.67	0.72	0.53	0.49	0.38	0.39	0.39	0.39
X_{Sps}	0.09	0.10	0.11	0.06	0.27	0.31	0.42	0.43	0.44	0.42
X_{Prp}	0.05	0.05	0.04	0.07	0.02	0.02	0.01	0.01	0.01	0.01

The average constituent for different zones is shown in Table 10. Zone I has X_{Alm} of 0.69, which is the most dominant endmember within the outer zone, while X_{Grs} is 0.13. The negligible contents with less than 0.18 combined are X_{Sps} (0.09), X_{Prp} (0.05) and X_{And} (0.03). Toward the core of the garnet crystal within Zone II, there is decrease in the X_{Alm} and X_{Prp} content which are on average 0.51 and 0.02 respectively. X_{Sps} content increases towards the core to 0.29 while X_{Grs} and X_{And} contents slightly increase by 0.01 for each endmember. The core (zone III) of the garnet has X_{Sps} content being 0.43 while X_{Alm} content is averaged at 0.39. The X_{Grs} is averaged at 0.13 which is similar to zone I. The smallest contents in zone III are X_{And} and X_{Prp} which are on average 0.04 and 0.01 respectively.

Table 10: Average garnet endmember composition within MC001

Garnet endmember	Zone I	Zone II	Zone III
Andradite (X_{And})	0.03	0.04	0.04
Grossular (X_{Grs})	0.13	0.14	0.13
Almandine (X_{Alm})	0.69	0.51	0.39
Spessartine (X_{Sps})	0.09	0.29	0.43
Pyrope (X_{Prp})	0.05	0.02	0.01

Element maps of Mn, Fe, Ca, Mg, Si, K and Al with EDS and micro-petrographic image of MC002 are shown in Figure 62. Colours such as green, orange and pink represent higher concentration while colours such as blue and black represent lower concentration. The garnet porphyroblast is euhedral and some rim portions are masked by amphiboles (Figure 62). The garnet has higher content of Mn and Fe whereas Mg and Ca is lower relative to amphibole, biotite and calcite in the matrix. Al content is higher within the garnet than the matrix while Si is higher in the matrix as shown in Figure 62. The garnet porphyroblast in MC002 shows no zonal element variations as the case of sample MC001. Matrix materials can be separated based on variable compositions of elements. Within the matrix, Ca-rich crystals are commonly calcite. Si rich crystals in both the matrix and garnet porphyroblasts are quartz. K-rich zones in the matrix are commonly biotite.

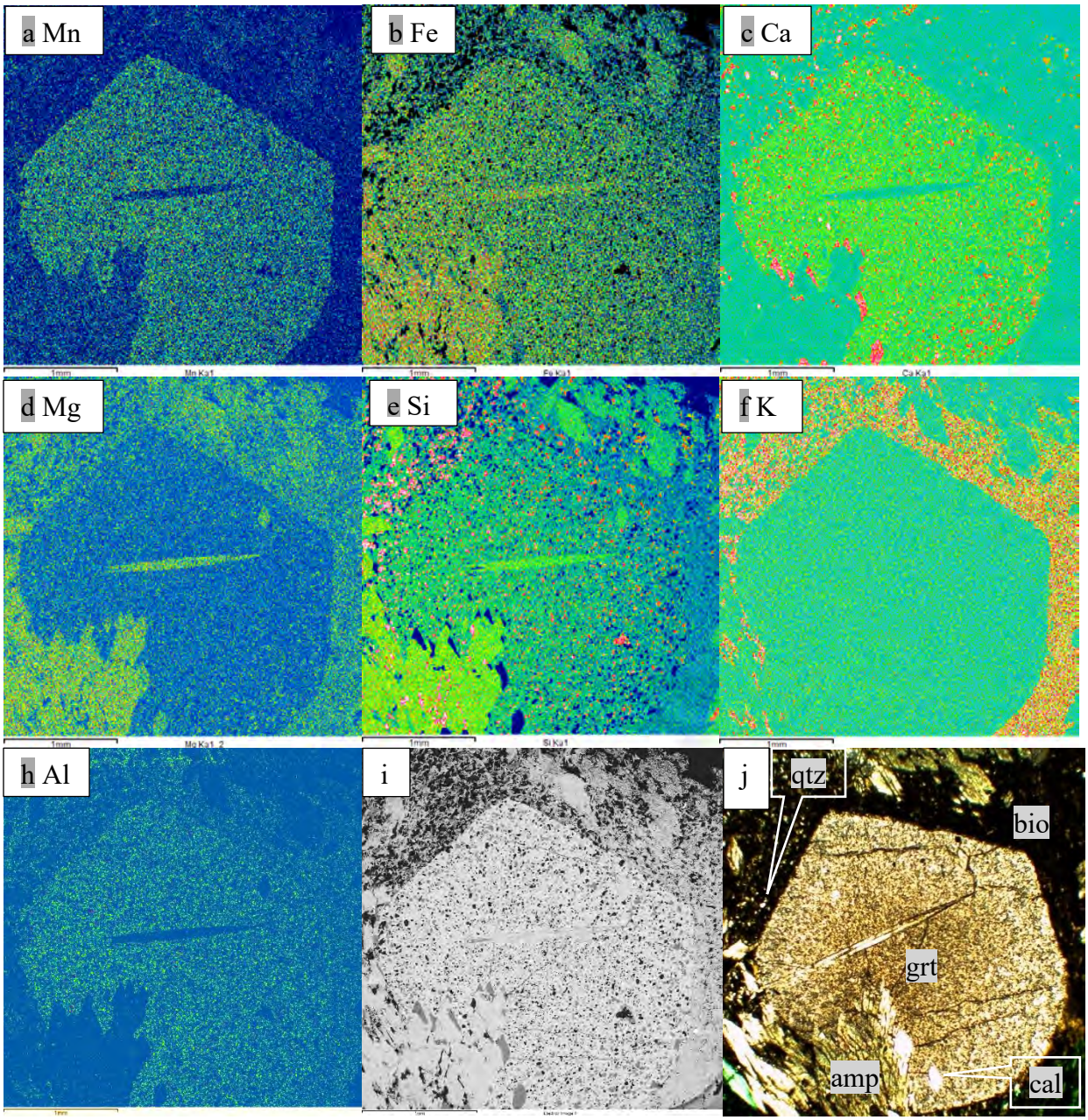

Figure 62: Element distribution maps of (a) Mn, (b) Fe, (c) Ca, (d) Mg, (e) Si, (f) K and (h) Al. (i) BSE image of the garnet grain and (j) CPL image for sample MC002 showing garnet porphyroclasts and matrix consisting of quartz, biotite, amphibole and calcite.

Table 11 shows EDS results for garnet in samples MC002 and MC013. The cations are calculated from 24 Oxygen anions. Analyses are representative of the garnet core and the rim. Almandine contents in both samples are high ranging from ~0.73 to 0.79.

Grossular and andradite endmembers in MC002 are similarly abundant with contents of X_{Grs} ranging from ~0.04 to 0.07 and X_{And} being ~0.06. Pyrope is negligible with highest contents being less than 0.04. The almandine contents are the highest ranging from ~0.73 to 0.77. The spessartine contents are relatively uniform ranging from 0.10 to 0.12. The garnet is an almandine-spessartine solid solution. The garnet does not show zonal composition variations.

Two representative analyses of the garnet in sample MC013 are shown in Table 11. Generally, the garnet composition is similar to that of MC002. Within MC013, the almandine content (X_{Alm}) is high between ~0.77 and 0.79. The grossular content ranges from ~0.07 to 0.09. Spessartine (X_{Sps}), andradite (X_{And}) and pyrope (X_{Pyp}) contents are the smallest with totals < 0.07 (X_{Sps} ~0.03, X_{And} ~0.06 and X_{Pyp} ~0.05). The X_{Mg} content is low at ~0.06. Garnet is an almandine-grossular solid solution with minor andradite and pyrope.

X_{Mg} contents in garnet are very low for both samples. They range between 0.02 and 0.04 in MC002 while MC013 is 0.06.

Table 11: Representative garnet analyses for MC002 and MC013 X_{Mg} = Mg/(Mg+Fe^{2+})

Sample	MC002	MC002	MC002	MC002	MC002	MC013	MC013
Mineral	Garnet	Garnet	Garnet	Garnet	Garnet	Garnet	Garnet
Analysis	1-12	2-11	2-12	1-13	1-14	1-2	1-3
SiO2	37.30	37.38	36.96	37.03	36.91	37.12	36.96
TiO2	0.00	0.00	0.00	0.00	0.00	0.00	0.00
Al2O3	21.18	21.20	20.97	20.63	20.37	20.95	21.04
Cr2O3	0.00	0.00	0.00	0.00	0.00	0.00	0.00
Fe2O3	1.77	1.84	1.83	1.82	1.85	1.94	1.91
MgO	0.49	0.74	0.51	0.44	0.43	1.21	1.24
CaO	4.10	3.31	3.80	4.19	4.09	4.48	4.84
MnO	4.92	4.00	4.58	4.80	4.76	1.15	1.32
FeO	30.24	31.53	31.35	31.09	31.60	33.15	32.69
	100.00	100.00	100.00	100.00	100.00	100.00	100.00
Number of cations on the basis of 24 O							
Si	6.024	6.032	5.994	6.013	6.010	5.989	5.963
Ti	0.000	0.000	0.000	0.000	0.000	0.000	0.000
Al	4.030	4.032	4.007	3.948	3.909	3.984	4.001
Cr	0.000	0.000	0.000	0.000	0.000	0.000	0.000
Fe3+	0.215	0.224	0.224	0.222	0.226	0.235	0.232
Mg	0.118	0.178	0.123	0.106	0.104	0.290	0.297
Ca	0.710	0.573	0.661	0.729	0.714	0.774	0.836
Mn	0.673	0.547	0.629	0.660	0.656	0.157	0.180
Fe2+	4.084	4.255	4.252	4.223	4.302	4.473	4.410
Cation total	15.85	15.84	15.89	15.90	15.92	15.90	15.92
X_{Mg}	0.03	0.04	0.03	0.02	0.02	0.06	0.06
Endmembers							
X_{And}	0.06	0.06	0.06	0.06	0.06	0.06	0.06
X_{Grs}	0.07	0.04	0.06	0.07	0.06	0.07	0.09
X_{Alm}	0.73	0.77	0.75	0.74	0.74	0.79	0.77
X_{Sps}	0.12	0.10	0.11	0.12	0.11	0.03	0.03
X_{Prp}	0.02	0.03	0.02	0.02	0.02	0.05	0.05

4.2 ANTHOPHYLLITE

Anthophyllite in samples MC002 and MC003 occurs commonly as trapezium shaped crystal and is associated with biotite, quartz, garnet and feldspar. Representative analyses are shown in Table 12. Anthophyllite show slight variation in X_{Mg} ratio for individual samples. Anthophyllite in

MC002 has low X_{Mg} ratio ranging between 0.28 and 0.31 while MC003 X_{Mg} ranges between 0.37 and 0.40. Mn content is lower (1.01-1.53 w%), however, there are trace amounts of Ca, Al and Na which is typical of most anthophyllite.

Table 12: Representative analyses of anthophyllite within MC002 and MC003 and crystal Temperature of formation estimated based on method by Holland and Blundy (1982).

Sample	MC002	MC002	MC002	MC002	MC002	MC003	MC003	MC003	MC003	MC003
Mineral Group	Amphibole	Amphibole	Amphibole	Amphibole	Amphibole	Amphibole	Amphibole	Amphibole	Amphibole	Amphibole
Mineral	Anthophyllite	Anthophyllite	Anthophyllite	Anthophyllite	Anthophyllite	Anthophyllite Rim	Anthophyllite Rim	Anthophyllite rim	Anthophyllite core	Anthophyllite core
Analysi	1-2	1-3	1-10	2-1	2-2	1-2	1-3	1-11	1-1	1-7
Al_2O_3	0.39	0.23	0.37	0.19	0.50	0.32	0.21	0.10	0.22	0.23
CaO	0.31	0.30	0.23	0.26	0.03	0.30	0.20	0.26	0.35	0.30
K_2O	0.03	0.00	0.08	0.00	0.00	0.00	0.00	0.00	0.00	0.00
SiO_2	50.57	51.05	50.84	51.01	50.43	51.99	52.13	51.53	51.98	51.99
MgO	8.46	8.92	8.52	8.48	8.12	11.86	11.82	11.01	11.54	11.63
FeO	36.67	36.12	36.80	36.95	37.04	32.15	32.08	32.77	32.39	32.17
Fe_2O_3	0.48	0.00	0.00	0.00	0.86	0.00	0.00	0.66	0.00	0.05
MnO	1.04	1.20	1.11	1.01	1.10	1.13	1.42	1.53	1.33	1.48
Cr_2O_3	0.00	0.00	0.00	0.00	0.00	0.00	0.00	0.00	0.00	0.00
TiO_2	0.00	0.00	0.00	0.00	0.00	0.00	0.00	0.00	0.00	0.00
Na_2O	0.14	0.26	0.13	0.18	0.00	0.29	0.18	0.19	0.23	0.19
H_2O	1.92	1.92	1.92	1.92	1.91	1.96	1.96	1.95	1.96	1.96
Total	100.00	100.00	100.00	100.00	100.00	100.00	100.00	100.01	100.00	100.00
Number of cations on the basis of 23 O										
Si	7.912	7.955	7.945	7.970	7.903	7.960	7.958	7.924	7.951	7.948
Al	0.072	0.042	0.068	0.035	0.092	0.040	0.038	0.018	0.040	0.041
Ti	0.000	0.000	0.000	0.000	0.000	0.000	0.000	0.000	0.000	0.000
Cr	0.000	0.000	0.000	0.000	0.000	0.000	0.000	0.000	0.000	0.000
Fe^{3+}	0.056	0.000	0.000	0.000	0.102	0.000	0.000	0.077	0.000	0.006
Fe^{2+}	4.797	4.707	4.809	4.828	4.855	4.111	4.095	4.215	4.143	4.113
Mn	0.138	0.158	0.147	0.134	0.146	0.146	0.184	0.199	0.172	0.192
Mg	1.973	2.072	1.985	1.975	1.897	2.671	2.690	2.524	2.631	2.651
Ca	0.052	0.050	0.039	0.044	0.005	0.049	0.033	0.043	0.057	0.050
Na	0.042	0.079	0.039	0.055	0.000	0.086	0.053	0.057	0.068	0.056
K	0.006	0.000	0.016	0.000	0.000	0.000	0.000	0.000	0.000	0.000
X_{Mg}	0.29	0.31	0.29	0.29	0.28	0.39	0.40	0.37	0.39	0.39
OH	2.00	2.00	2.00	2.00	2.00	2.00	2.00	2.00	2.00	2.00
Temp (°C)	445	445	445	445	445	445	445	445	445	445

$X_{Mg} = Mg/(Mg+Fe^{2+})$

4.3 BIOTITE

Biotite occurs in both Katanga and Basement Supergroups. It is commonly within the matrix and defines foliation trend. Biotite is associated to most mineral phases such as quartz, amphibole, plagioclase, garnet, calcite, microcline and chlorite.

4.3.1 KATANGA SUPERGROUP-BIOTITE

Biotite occurs as fine- to medium-grained elongate mineral. It defines the orientation of the foliation in the matrix. Biotite is commonly associated to quartz, feldspar, calcite and anthophyllite. Other biotite grains are associated to garnet porphyroblasts. The biotite analyses are shown in Table 13.

X_{Mg} of biotite ranges widely for different samples. For MC001, the X_{Mg} is moderate ranging between 0.40 and 0.53. The X_{Mg} in biotite within MC002 is lower ranging from 0.37 and 0.38. Sample MC003, X_{Mg} in biotite is 0.37 while that of MC013 it ranges between 0.43 and 0.45. Ti content is relatively low in all samples ranging between 1.43 and 2.29 wt% TiO_2 while MC003 has Ti concentrations below the detection limit.

Table 13: Representative water free biotite analyses within the Katanga Supergroup normalised to 96%. (X_{Mg} = Mg/(Mg+Fe).

Sample	MC001	MC001	MC001	MC001	MC002	MC002	MC002	MC003	MC013	MC013
Mineral	Biotite	Biotite	Biotite	Biotite	Biotite	Biotite	Biotite	Biotite	Biotite	Biotite
Analysis	1-7	2-8	2-9	2-11	1-4	1-1	1-19	1-4	1-6	1-4
Al_2O_3	16.78	18.46	17.94	17.05	16.57	16.59	16.40	15.73	15.56	17.06
CaO	0.09	0.00	0.00	0.06	0.00	0.00	0.00	0.00	0.27	0.09
K_2O	9.50	9.26	9.17	9.54	9.43	9.43	9.48	9.27	9.67	9.48
SiO_2	35.53	35.59	35.98	35.33	35.44	35.78	35.31	36.29	34.69	34.86
MgO	12.21	10.82	8.31	12.66	8.11	8.22	8.05	8.61	10.19	10.05
FeO	19.86	20.08	22.70	19.95	24.52	23.93	24.52	25.70	23.59	22.17
MnO	0.31	0.00	0.00	0.00	0.00	0.00	0.36	0.24	0.00	0.06
Cr_2O_3	0.00	0.00	0.00	0.00	0.00	0.00	0.00	0.09	0.09	0.01
TiO_2	1.62	1.69	1.82	1.37	1.91	1.99	1.83	0.00	1.87	2.20
Na_2O	0.09	0.10	0.07	0.04	0.02	0.07	0.05	0.07	0.08	0.04
Total	96.00	96.00	96.00	96.00	96.00	96.00	96.00	96.00	96.00	96.00
Number of cation on the basis of 22 O, OH, F										
Si	5.410	5.389	5.508	5.375	5.504	5.535	5.498	5.662	5.404	5.366
Ti	0.186	0.192	0.211	0.157	0.224	0.231	0.215	0.000	0.219	0.254
Al	3.012	3.295	3.237	3.057	3.033	3.025	3.010	2.891	2.857	3.096
Cr	0.000	0.00	0.00	0.00	0.00	0.00	0.00	0.011	0.011	0.002
Mg	2.772	2.443	1.897	2.872	1.876	1.896	1.870	2.004	2.364	2.304
Ca	0.014	0.00	0.00	0.010	0.00	0.00	0.00	0.000	0.044	0.014
Mn	0.039	0.00	0.00	0.00	0.00	0.00	0.046	0.032	0.000	0.008
Fe	2.529	2.544	2.906	2.538	3.183	3.094	3.194	3.354	3.072	2.853
Na	0.025	0.028	0.022	0.012	0.007	0.021	0.015	0.021	0.024	0.010
K	1.846	1.790	1.788	1.852	1.866	1.861	1.884	1.846	1.920	1.860
X_{Mg}	0.52	0.49	0.40	0.53	0.37	0.38	0.37	0.37	0.43	0.45

4.3.2 BASEMENT SUPERGROUP-BIOTITE

Biotite is coarse-grained elongated mineral commonly occurring within the darker bands in sample MC012. It is commonly associated with amphiboles, plagioclase, chlorite and quartz.

X_{Mg} is consistently high ranging between 0.63 and 0.64. (Table 14). The Mg oxide content ranges between 15.52 and 16.21 wt% with moderate TiO_2 content of 1.51 to 1.98 wt%. The Fe oxide content is similar Mg oxide ranging between 15.51 to 16.26 wt%. The biotite from the Basement Supergroup has higher Mg molar content. Mn is typically below the detection limit with just one sample (MC012 analysis 5-9) with MnO of 0.32 wt%.

Table 14: Representative water free biotite analyses from the Basement Supergroup normalized to 96%. (XMg = Mg/(Mg+Fe).

Sample	MC012	MC012	MC012	MC012	MC012	MC012
Mineral	Biotite	Biotite	Biotite	Biotite	Biotite	Biotite
Analysis	3-10	3-11	5-9	5-10	7-6	7-9
Al_2O_3	16.37	16.07	17.12	17.31	17.04	17.16
CaO	0.00	0.00	0.00	0.00	0.00	0.00
K_2O	9.98	10.01	9.97	9.82	9.98	9.72
SiO_2	37.28	37.28	36.36	36.67	36.48	36.78
MgO	15.16	15.15	14.90	15.17	15.29	15.56
FeO	14.89	15.59	15.54	15.57	15.61	15.32
MnO	0.00	0.00	0.33	0.00	0.00	0.00
Cr_2O_3	0.44	0.00	0.00	0.00	0.00	0.00
TiO_2	1.88	1.90	1.79	1.46	1.58	1.45
Na2O	0.00	0.00	0.00	0.00	0.00	0.00
Total	96.00	96.00	96.00	96.00	96.00	96.00
Number of cation on the basis of 22 O, OH, F						
Si	5.533	5.547	5.423	5.450	5.434	5.456
Ti	0.209	0.213	0.200	0.163	0.178	0.162
Al	2.862	2.818	3.009	3.032	2.992	3.001
Cr	0.052	0.000	0.000	0.000	0.000	0.000
Mg	3.352	3.361	3.312	3.359	3.395	3.441
Ca	0.000	0.000	0.000	0.000	0.000	0.000
Mn	0.000	0.000	0.041	0.000	0.000	0.000
Fe^{2+}	1.847	1.941	1.939	1.935	1.944	1.901
Na	0.000	0.000	0.000	0.000	0.000	0.000
K	1.889	1.900	1.897	1.862	1.897	1.841
X_{Mg}	0.64	0.63	0.63	0.63	0.64	0.64

4.4 FELDSPAR

Feldspar within the Basement Supergroup is commonly subhedral and associated to quartz, biotite and amphibole. Table 15 shows representative feldspar analyses for sample MC012. The plagioclase is more dominant in the felsic bands, it is rarely twinned and weakly zoned with Ca richer rim. Few EDS analyses where deliberately done on grain contact between feldspar and amphiboles for metal cation exchange.

The anorthite composition (X_{an}) ranges from 0.19 to 0.25 while albite composition (X_{ab}) is between 0.71 and 0.81. Orthoclase (X_{or}) composition is negligible with composition ranging from 0.00 to 0.08. The X_{an} and X_{ab} contents indicate the mineral to be oligoclase.

Table 15: Representative feldspar analyses

Sample	MC012	MC012	MC012	MC012	MC012	MC012	MC012	MC012	MC012
Mineral	Feldspar	Feldspar	Feldspar	Feldspar	Feldspar	Feldspar	Feldspar	Feldspar	Feldspar
Position	core	rim	rim						core
Analysis	3-2	3.3	3-12	5-1	5-2	5-3	5-4	5-13	7-1
SiO_2	64.98	64.70	64.32	64.91	64.21	63.91	63.59	63.21	65.35
Al_2O_3	21.89	22.11	22.18	22.07	22.53	22.51	22.01	22.63	21.79
MgO	0.00	0.00	0.00	0.00	0.00	0.00	0.48	0.00	0.00
CaO	3.85	4.12	4.55	4.11	4.50	4.99	4.78	4.69	3.95
FeO	0.00	0.00	0.00	0.00	0.00	0.00	0.37	0.00	0.00
Na_2O	9.28	8.90	8.80	8.90	8.76	8.40	8.30	8.00	8.91
K_2O	0.00	0.17	0.15	0.00	0.00	0.19	0.47	1.48	0.00
Total	100.00	100.00	100.00	100.00	100.00	100.00	100.00	100.00	100.00
Number of cation on the basis 8 O									
Si	2.86	2.85	2.84	2.85	2.83	2.82	2.82	2.81	2.87
Al	1.14	1.15	1.15	1.14	1.17	1.17	1.15	1.18	1.13
Mg	0.00	0.00	0.00	0.00	0.00	0.00	0.03	0.00	0.00
Ca	0.18	0.19	0.22	0.19	0.21	0.24	0.23	0.22	0.19
Fe	0.00	0.00	0.00	0.00	0.00	0.00	0.01	0.00	0.00
Na	0.79	0.76	0.75	0.76	0.75	0.72	0.71	0.69	0.76
K	0.00	0.01	0.01	0.00	0.00	0.01	0.03	0.08	0.00
Cation Total	4.97	4.96	4.97	4.94	4.96	4.96	4.98	4.98	4.95
Endmembers									
Xan	0.19	0.20	0.23	0.20	0.22	0.25	0.24	0.23	0.21
Xab	0.81	0.78	0.77	0.78	0.77	0.74	0.73	0.71	0.79
Xor	0.00	0.01	0.01	0.00	0.00	0.01	0.03	0.08	0.00

4.5 AMPHIBOLE

The amphibole group within the Basement Supergroup is the magnesio-hornblende which is a calcic-amphibole (Table 16). The magnesio-hornblende amphibole (Table 16) has Mg oxide content ranging from 12.78 to 15.52 wt% while Fe total oxide content ranges from 9.65 to 15.73 wt %. There are rare amphiboles with higher Fe total oxide content than Mg, however, commonly Mg content is higher. The X_{Mg} ratios is high ranging from 0.59 to 0.75. All analyzed amphiboles in sample MC012 have high Al2O3 and CaO contents which range from ~6.95 to 10.28 wt% and

11.75 to 15.38 wt% respectively. Mn and Ti contents are in trace amounts. The magnesio-hornblende typically shows low oxide concentrations of K, Na, Fe and Al.

Table 16: Representative analyses of water free magnesio-hornblende (mag-hornblende) normalized to 98%. Temperature of formation estimated based on method by Holland and Blundy (1982).

Sample	MC012	MC012	MC012	MC012	MC012	MC012	MC012	MC012	MC012	MC012	MC012	MC012	MC012	MC012	MC012	MC012
Mineral Group	Amphibole	Amphibole	Amphibole	Amphibole	Amphibole	Amphibole	Amphibole	Amphibole	Amphibole	Amphibole	Amphibole	Amphibole	Amphibole	Amphibole	Amphibole	Amphibole
Mineral	Mag-hornblende	Mag-hornblende	Mag-hornblende	Mag-hornblende	Mag-hornblende	Mag-hornblende	Mag-hornblende	Mag-hornblende	Mag-hornblende	Mag-hornblende	Mag-hornblende	Mag-hornblende	Mag-hornblende	Mag-hornblende	Mag-hornblende	Mag-hornblende
Analysi	3-4	3-6	5-5	5-6	5-8	5-11	5-12	6-1	7-5	7-7	7-8	7-2	7-3	5-7	6-2	6-3
SiO_2	47.75	49.35	48.77	49.69	46.72	49.38	47.04	49.65	47.11	46.11	48.13	51.29	51.30	50.84	51.06	50.70
TiO_2	0.36	0.55	0.46	0.48	0.55	0.42	0.44	0.00	0.00	0.45	0.45	0.00	0.51	0.00	0.00	0.41
Al_2O_3	9.56	7.22	8.79	8.16	10.01	8.11	10.07	8.30	6.27	10.68	9.37	6.82	6.81	6.94	6.84	7.49
Fe_2O_3	1.57	0.00	2.24	0.94	3.12	1.62	3.02	1.19	0.00	3.99	0.28	1.63	1.29	1.39	1.83	0.79
FeO	11.57	12.69	10.60	10.96	10.59	10.58	10.65	11.06	15.42	10.12	12.68	9.76	9.46	10.06	8.92	10.34
MnO	0.00	0.00	0.00	0.00	0.33	0.00	0.31	0.35	0.00	0.31	0.00	0.32	0.00	0.30	0.59	0.00
MgO	13.00	13.87	13.47	14.01	12.61	14.03	12.52	13.63	12.48	12.34	12.82	14.75	15.21	14.73	15.07	14.63
CaO	11.93	12.69	11.85	12.09	11.85	11.83	11.54	11.96	15.07	11.52	11.91	12.05	11.88	12.22	11.81	12.01
Na_2O	1.23	0.88	0.98	0.94	0.98	1.12	1.22	1.07	0.82	1.30	1.31	0.81	0.91	0.74	0.94	0.87
K_2O	1.02	0.74	0.83	0.73	1.23	0.90	1.18	0.79	0.82	1.17	1.05	0.57	0.64	0.77	0.94	0.76
Total	98.00	98.00	98.00	98.00	98.00	98.00	98.00	98.00	98.00	98.00	98.00	98.00	98.00	98.00	98.00	98.00
No of Cations on the basis of 23 O																
Si	6.933	7.158	7.035	7.144	6.806	7.114	6.843	7.159	7.024	6.722	6.997	7.329	7.308	7.288	7.300	7.252
Al	1.636	1.236	1.497	1.384	1.719	1.377	1.727	1.411	1.102	1.836	1.604	1.148	1.144	1.172	1.153	1.263
Ti	0.040	0.060	0.050	0.052	0.060	0.046	0.048	0.000	0.000	0.049	0.049	0.000	0.055	0.000	0.000	0.044
Fe3+	0.172	0.00	0.243	0.101	0.341	0.175	0.331	0.129	0.000	0.438	0.031	0.175	0.139	0.150	0.197	0.085
Fe2+	1.405	1.541	1.279	1.318	1.292	1.275	1.296	1.328	1.922	1.234	1.541	1.166	1.126	1.206	1.067	1.237
Mn	0.000	0.000	0.000	0.000	0.041	0.000	0.039	0.043	0.000	0.039	0.000	0.039	0.000	0.037	0.071	0.000
Mg	2.815	3.001	2.895	3.001	2.740	3.013	2.717	2.930	2.773	2.682	2.777	3.143	3.229	3.147	3.212	3.119
Ca	1.855	1.974	1.831	1.864	1.850	1.825	1.799	1.848	2.408	1.799	1.854	1.845	1.813	1.877	1.809	1.840
Na	0.348	0.249	0.274	0.262	0.277	0.312	0.345	0.299	0.238	0.368	0.369	0.225	0.251	0.207	0.261	0.242
K	0.189	0.138	0.153	0.133	0.229	0.166	0.218	0.146	0.157	0.217	0.194	0.103	0.116	0.141	0.171	0.139
X_{Mg}	0.67	0.66	0.69	0.70	0.68	0.70	0.68	0.69	0.59	0.69	0.64	0.73	0.74	0.72	0.75	0.72
Temp	557	615	586	591	614	574	581	445	445	584	583	--	599	--	--	570

4.6 MINOR MATRIX PHASES

The minor matrix phases within samples MC001/2/3 are composed of ilmenite, titanite and calcite with Mg and Fe. Other compositions include Rare Earth Elements (REE) as shown in BSE image (Figure 63). The phase that constitute REE occur as white, spot and elongate within the matrix (Figure 63).

REE are dominated by La_2O_3 and Ce_2O_3 accounting for over 50 wt%. There is presence of fluorine with less abundant oxides such as Nd_2O_3, Pr_2O_3 and Sm_2O_3. There are trace amounts of Fl, Fe, Ca and Si. The presence of fluorine would suggest hydrothermal REE transport system as fluoride complexes at high temperature and acidic conditions (Williams-Jones et al. 2000).

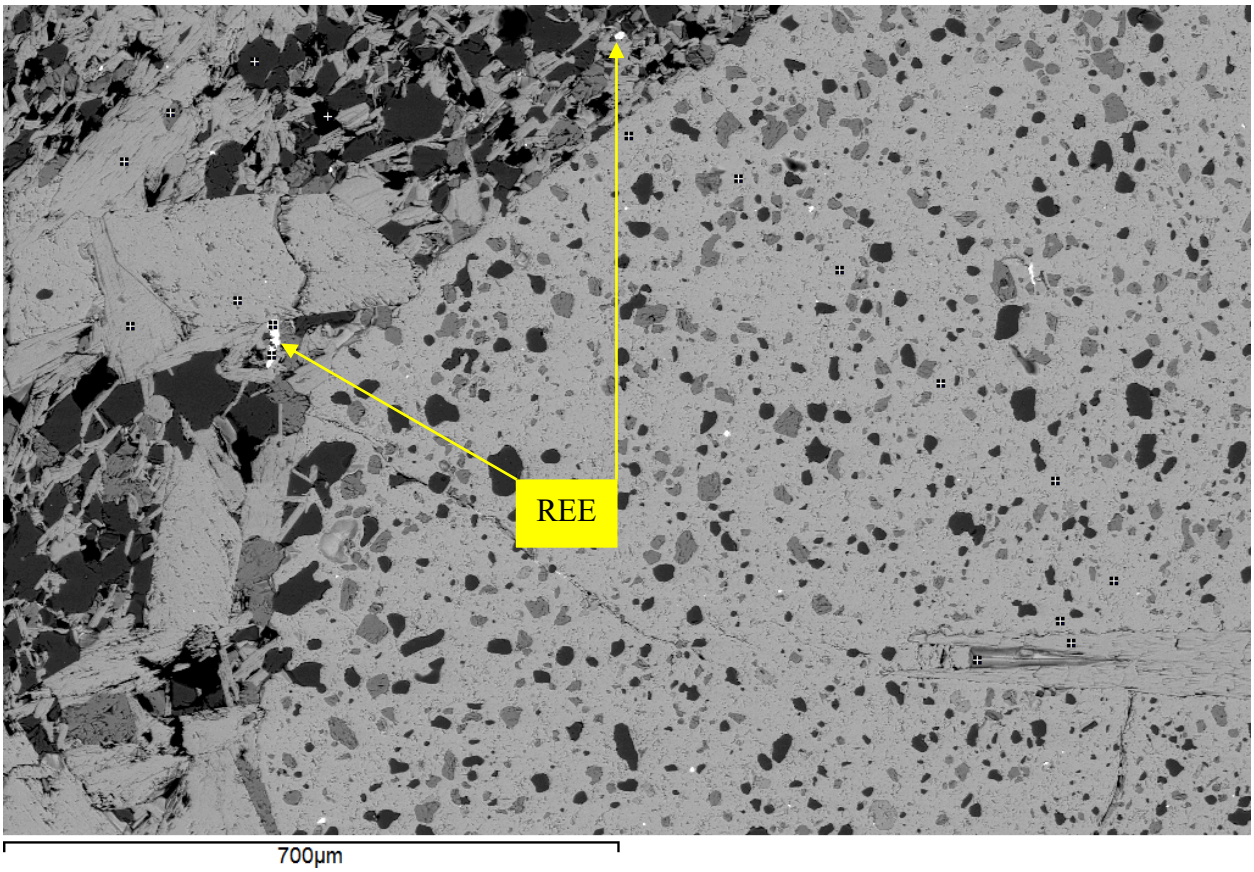

Figure 63: BSE image showing occurrence of REE within other matrix phases consisting of anthophyllite, bioitite, quartz and feldsparthe matrix. The phase with REE is white and randomly distributed

The major phases commonly consist of plagioclase, quartz, calcite, dolomite, biotite, garnet, anthophyllite. The carbonate constituent is commonly calcite and dolomite while ankerite is a minor phase which is more common in MC002.

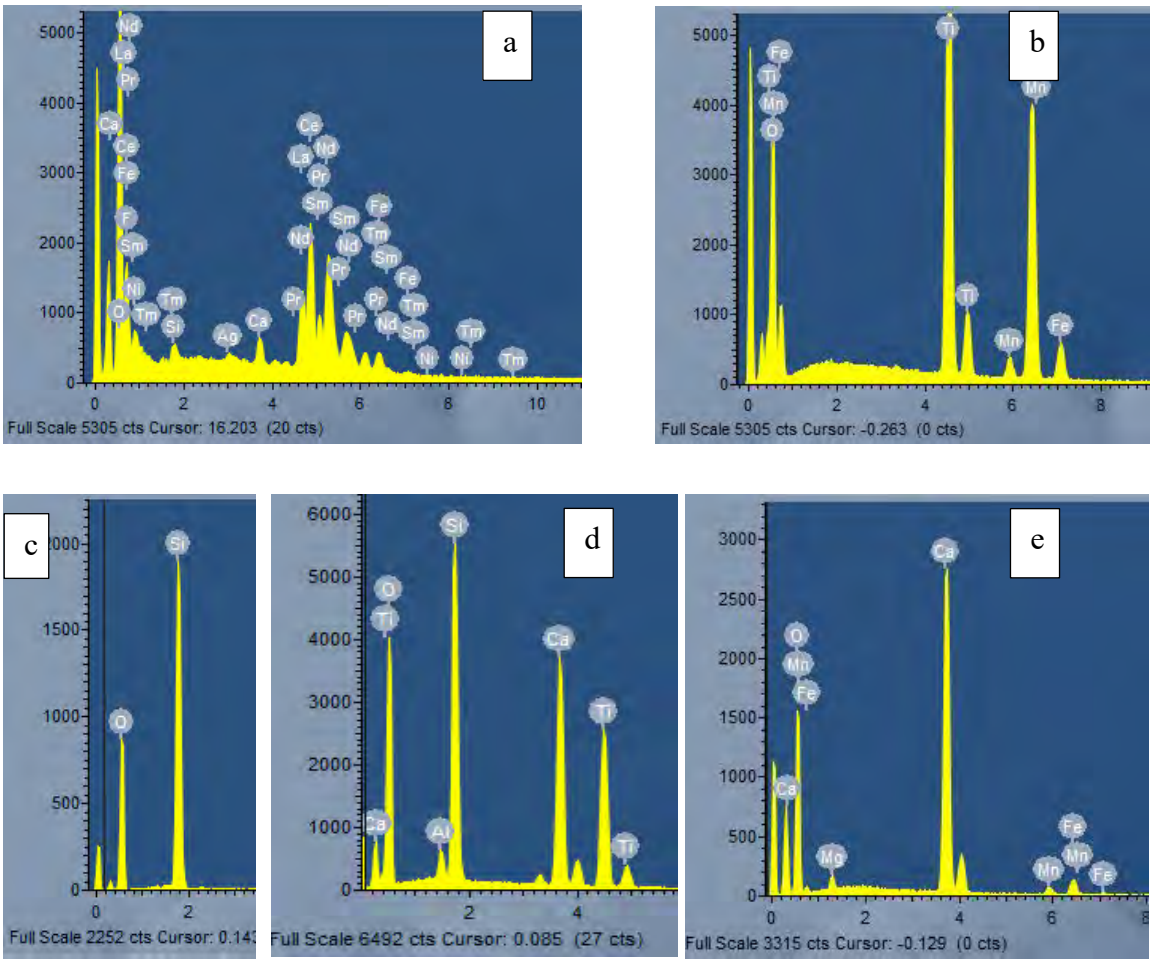

Figure 64: EDE spectra of some of the minor and major matrix phases. (a) Rare Earth Elements mixture, (b) Ilmenite, (c) Quartz, (d) Titanite and (e) Calcite with Mg and Fe.

The ACF diagram is plotted from molar proportion of the bulk rock composition (A=Al2O3 + Fe2O3 - (Na2O+ K2O), C=CaO - 3.3 P2O5; F=FeO + MgO (+ MnO)). The rocks from the Katanga Supergroup and those of the Basement Supergroup plot on different areas (Figure 65). The minerals in equilibrium from the Basement Supergroup are plotted on the ternary diagram which include biotite, hornblende and feldspar.

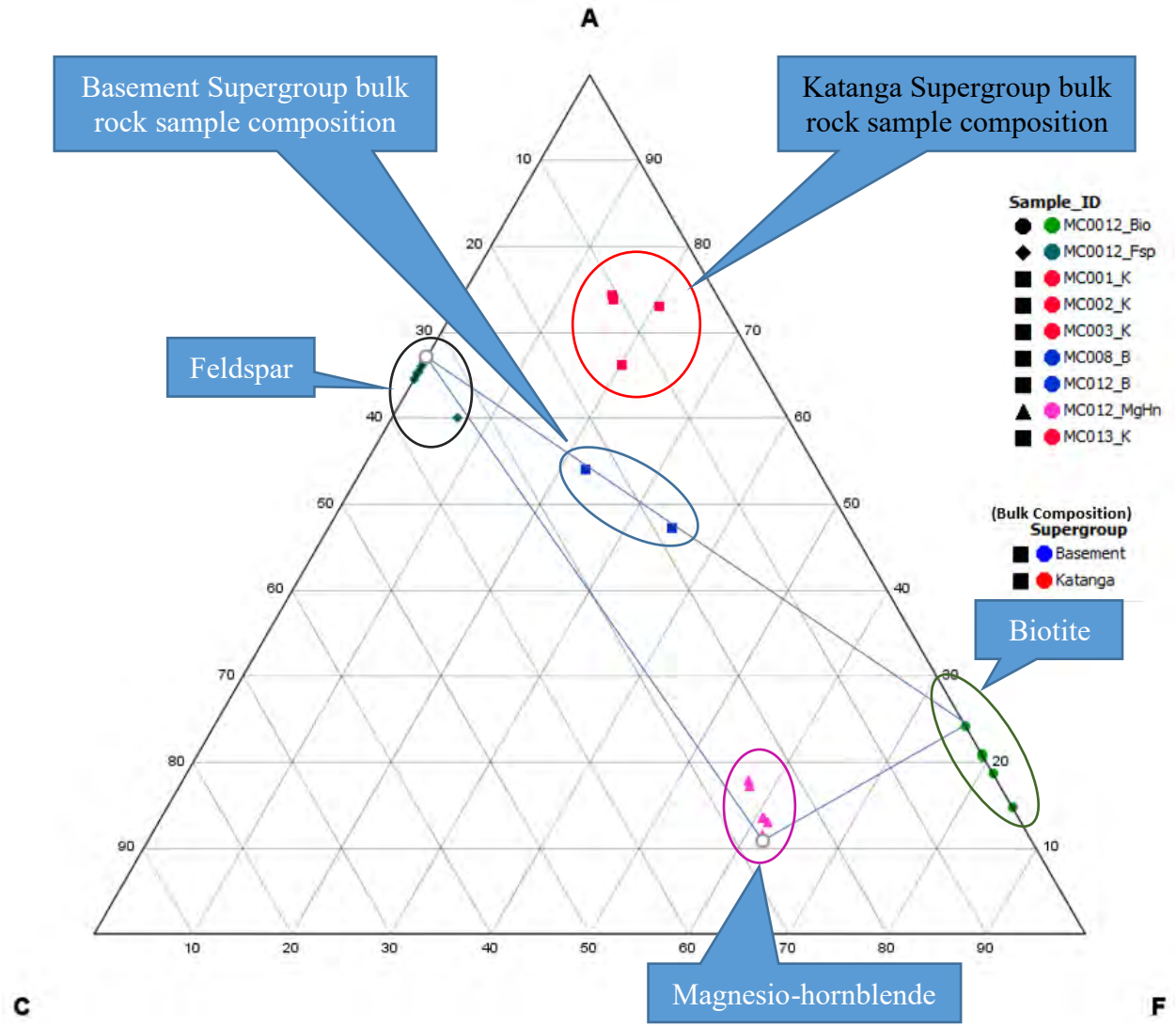

Figure 65: ACF diagram showing the bulk composition of the Basement and Katanga Supergroups plotted from mole proportions. The observed minerals in micropetrography include biotite, hornblende and feldspar. MC012_MgHn=magnesio-hornblende; MC012_Fsp=feldspar; MC012_Bio=biotite; MC001-3_K=Katangan bulk composition; MC008 and 12=Basement bulk composition; A=Al_2O_3 + Fe_2O_3 - (Na_2O+ K_2O), C=CaO - 3.3 P_2O_5; F=FeO + MgO (+ MnO)

The AFM diagram in Figure 66Figure 73 shows the bulk compositions of both the Katanga and Basement Supergroup rocks with different mineral assemblages. The AFM diagram shows compositions of both the pelitic and quartz-feldspathic rocks of the Katanga Supergroup and the Basement Supergroup respectively. The mineral phases in a ternary diagram from rocks of the Basement Supergroup consist of biotite, magnesio-hornblende and probably an aluminosilicate. The mineral phases from rocks of the Katanga Supergroup consist of biotite, garnet and anthophyllite.

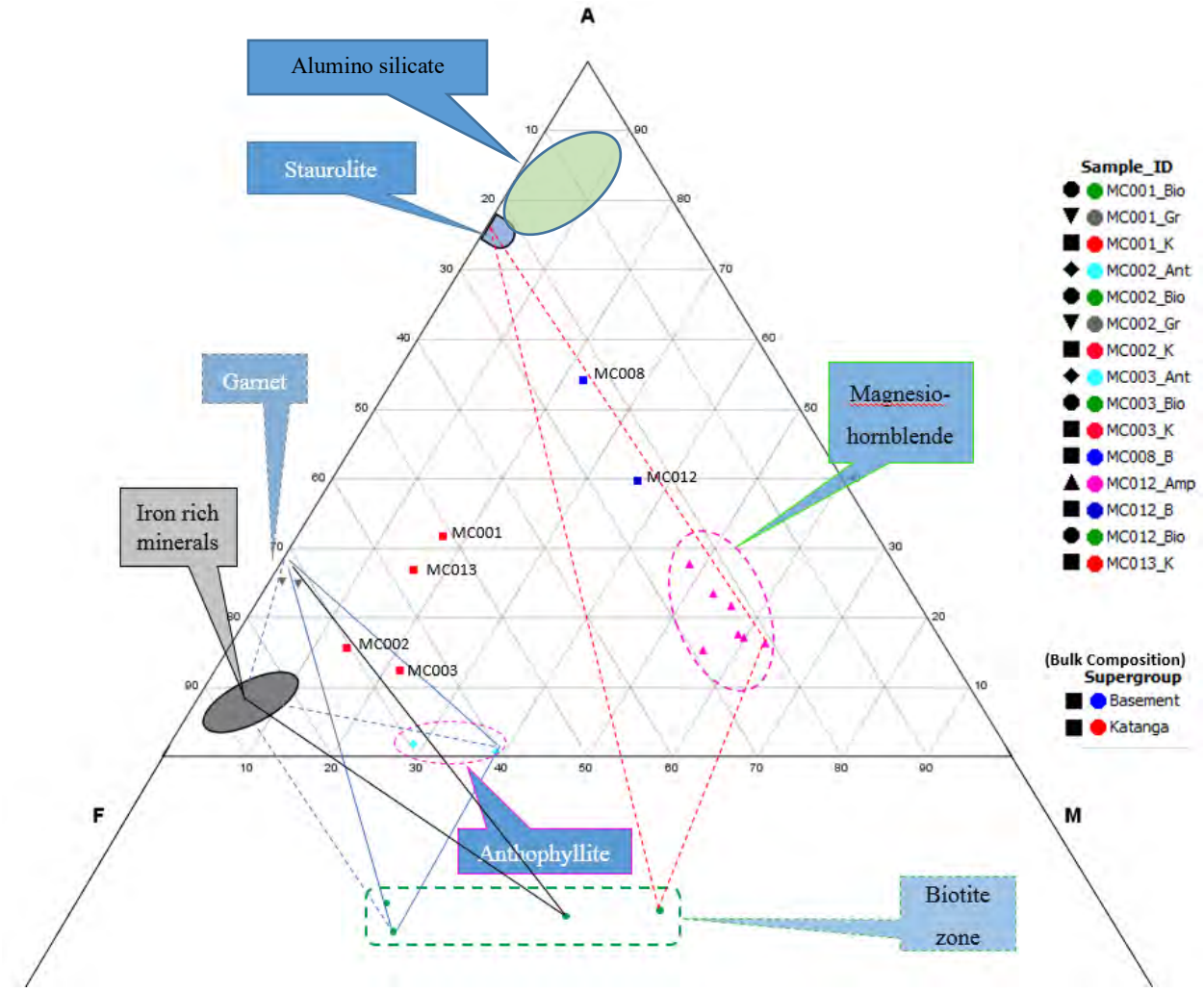

Figure 66: AFM diagram projected from muscovite representing bulk compositions of the Basement and Katanga Supergroup rock samples and mineral assemblages. The red square represents the bulk composition of samples from the Katanga Supergroup while those in blue represents bulk rock samples from the Basement Supergroup.

5. THERMOBAROMETRY

Six samples were selected for X-Ray Florescence (XRF) analysis, four of which were used for multiphase equilibrium to model pressure and temperature conditions during metamorphism. THERIAK/DOMINO software (de Capitani and Brown, 1987; v. 03.01.12) was used for calculating P-T equilibrium assemblage diagrams. Samples were selected from both the Katanga and the Basement Supergroups. Table 17 shows XRF results for six samples in weight percentages (wt%), these were converted to mol% proportions using the TD converter function of the Rock Maker MS Excel software by Büttner, (2012). The data was then used in THERIAK/DOMINO software for P-T equilibrium phases.

Representative XRF results for bulk samples used in thermodynamic modelling are shown in Table 17. The rock samples from the Basement Supergroup (MC008 and MC012) have some of the oxide contents (wt%) different from those of the Katanga Supergroup (MC001, MC002, MC003 and MC013). All samples are characterised by low to moderate MgO contents (3.45-7.29 wt%). Except for samples MC008 and MC012 (7.17 wt% Fe_2O_3 and 8.73 wt% Fe_2O_3 respectively), the Fe_2O_3 contents (20.59-32.44 wt%) are high. The contents of Al_2O_3 (7.72-13.65 wt%), CaO (2.56-6.01 wt%) are low to moderate. Generally, Na_2O (0.03-3.01 wt%), MnO (0.12-2.47 wt%) and K_2O (1.68-4.56 wt%) are relatively low.

The P-T diagrams were modelled according to different mineral phases for different bulk compositions. Biotite X_{Mg} isopleths were used for narrowing the stability peak metamorphic P-T conditions for the rocks. Similarly, garnet X_{Mg} and X_{Ca} were also used in two samples for estimating the P-T conditions.

Table 17: X-Ray Fluorescence analyses results of six samples (bdl=below detection limit)

Sample ID	Al_2O_3 (%)	CaO (%)	Cr_2O_3 (%)	Fe_2O_3 (%)	K_2O (%)	MgO (%)	MnO (%)	Na_2O (%)	P_2O_5 (%)	SiO_2 (%)	TiO_2 (%)	L.O.I. (%)	Total
MC001	12.16	2.56	bdl	20.59	2.87	3.86	2.47	0.04	0.10	53.45	0.72	0.27	99.09
MC002	7.72	5.25	bdl	32.44	2.38	3.58	1.65	0.05	0.34	40.59	0.55	4.92	99.47
MC003	8.27	5.72	0.01	25.00	4.56	4.62	0.70	0.17	0.38	39.98	0.74	8.90	99.05
MC008	13.65	5.93	0.02	7.17	1.68	3.88	0.12	3.01	0.08	62.05	0.63	1.10	99.32
MC012	13.33	6.01	0.07	8.73	2.95	7.29	0.14	2.21	0.26	56.19	0.66	1.17	99.01
MC013	9.32	4.42	bdl	21.68	1.90	3.45	0.55	0.03	0.31	52.51	0.68	4.21	99.06

Figure 67 shows a pseudo-binary diagram, different P-T assemblages and stability field of metamorphism for sample MC002. The observed mineral assemblages in sample MC002 are garnet, amphibole, biotite, quartz and calcite. The yellow polygon shows a region of stable mineral assemblages with stable P-T fields, has temperature ranging between ~270°C and 650°C with pressure >2.5 kbar. Garnet isopleths (green) have X_{Mg} ranging between 0.02 and 0.04 while X_{Ca} (blue) ranges between 0.5 and 0.8. The average garnet isopleths (X_{Mg} 0.03 and X_{Ca} 0.12) and that of biotite X_{Mg} (0.38) observed in sample MC002 intersect at ~470 (Figure 67). The P-T modelling using THERIAK DOMINO suggests a minimum metamorphic temperature of ~470°C with a pressure of 4.7 kbar. Thermometry on anthophyllite based on Holland and Blundy (1994) suggests an equilibration temperature of 445°C, which is similar to temperature modelled in THERIAK DOMINO from garnet and biotite isopleth (Figure 67). Both estimated temperatures are within the stability field of observed assemblages.

These estimates are in agreement with Grt-Bt thermometry using the method by Hodges and Spear 1982, yielding an equilibration temperature ranging between 435°C and 540°C. The results were estimated from garnet and biotite that are in contact with each other. Bhattacharya et al. (1992), garnet-biotite thermometry estimate metamorphism temperature ranging from 433°C to 488°C.

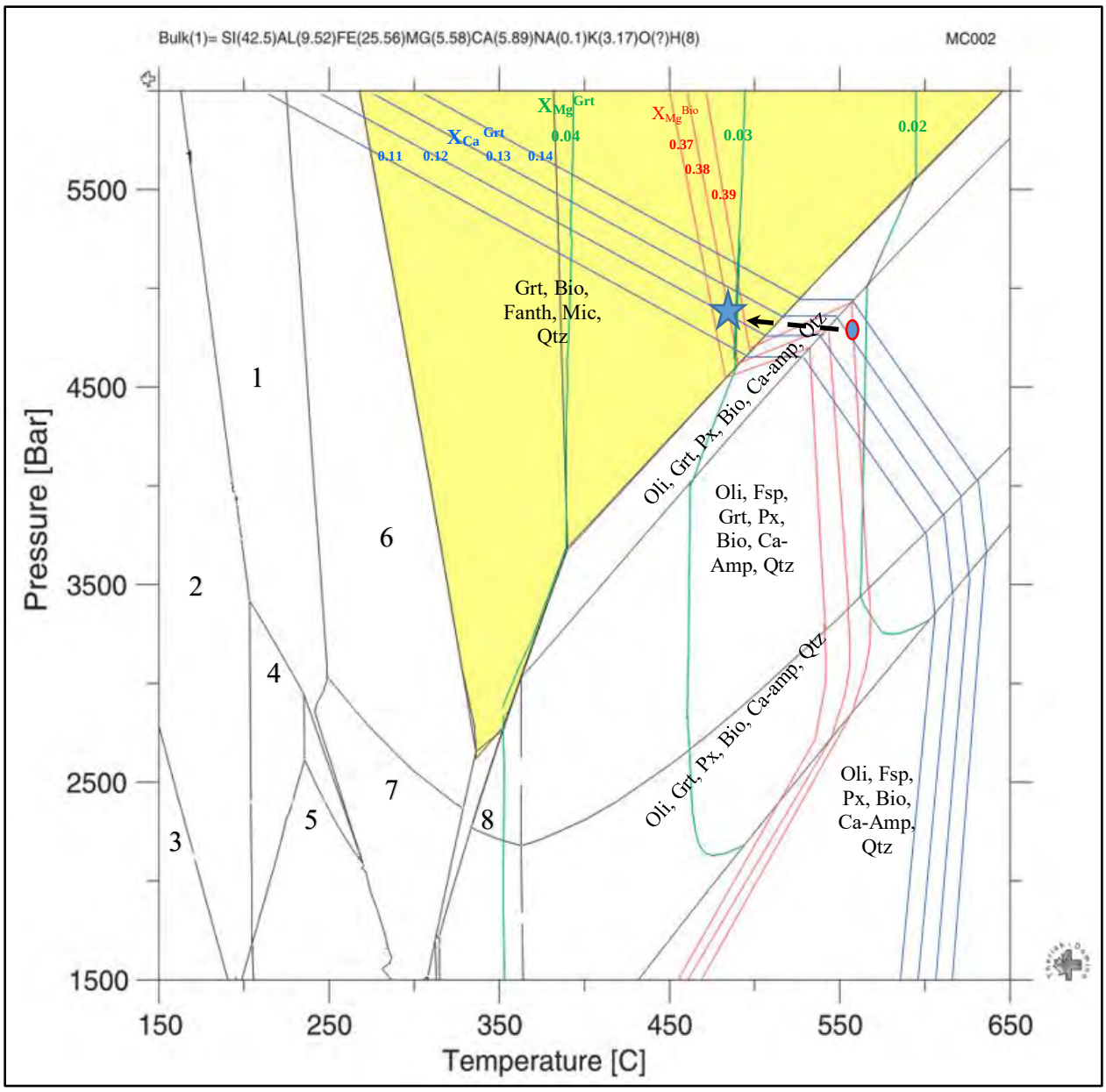

Key	
1= Grt, Bio, Ca-amp, Fanth, Mic, Qtz 2= Grt, Bio, Ca-amp, Fanth, Mic 3= Oli, Grt, Bio, Fanth, Mic 4= Grt, Bio, Ca-amp(2), Fanth, Mic,	5= Grt, Bio,Ca-amp, Fanth, Mic, Qtz 6= Grt, Bio, Ca-amp, Fanth, Mic, Qtz 7= Fsp, Grt, Bio, Ca-amp, Fanth, Mic, Qtz 8= Oli, Fsp, Grt, Bio, Ca-amp, Fanth, Qtz

Figure 67: Multiphase equilibrium assamblage modelling for sample MC002. The yellow polygon shows stabe peak metamorphic mineral assemblages within P-T fields of >2.5 kbar and ~270-650°C. The blue star indicates the peak metamorphic P-T conditions with temperature of 470°C and 4.7 kbar pressure. Green and red contour lines show garnet and biotite X_{Mg} isopleths respectively. The possible P-T path for the sample is indicated by black haseh arrow. Grt=garnet, Px=pyroxene, Bio=Biotite, Mic=microcline, Fanth=ferro-anthophyllite, Oli=olivine, Ca-amp=calcic amphibole, Qtz=quartz, Fsp=feldspar

The P-T condition of metamorphism for sample MC003 is shown in Figure 68. The observed mineral assemblages in sample MC003 are amphibole and garnet porphyroblasts within biotite, quartz, feldspar and minor carbonate matrix which might be secondary phase. There was no pyroxene observed in sample MC003, the pyroxene in the pseudo-section could be too small or uncommon to be observed in micropetrography. The yellow polygon shows a region of stable mineral assemblage within a P-T field of ~440°C to 700°C and >3.0 kbar. The X_{Mg} contours of biotite (X_{Mg} = 0.34-0.37) is marked by red lines and the coresponding average biotite X_{Mg} is 0.37. The X_{Ca} contours of garnet (X_{Ca} = 0.10-0.14) is marked by blue lines and the coresponding average garnet X_{Ca} is 0.12. The X_{Mg} isopleths of biotite and X_{Ca} isopleths of garnet intersect in the moderate temperature and pressure of ~630°C and ~4.5 kbar respectively (Figure 68). This shows an estimated temperature at 630°C which is a peak metamorphism though the garnet isopleths (X_{Ca}) used are for sample MC002. Anthophyllite thermometry based on Holland and Blundy. (1994) suggest a lower temperature of formation at ~445°C (Table 12).

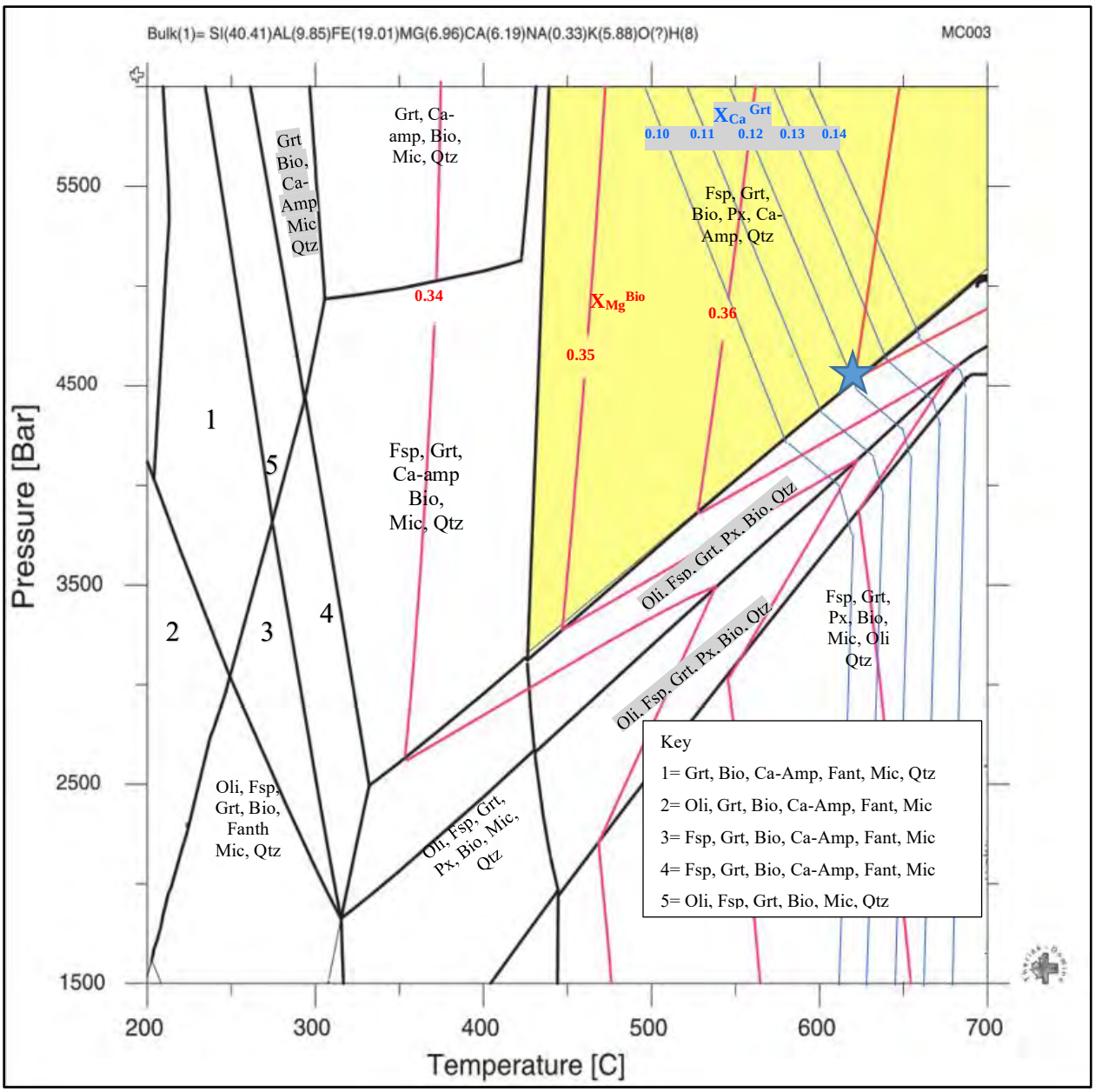

Figure 68: Multi-phase equilibria diagrams for sample MC003. The highlighted yellow polygon shows the observed stable mineral assemblage except for pyroxene. Black lines are boundaries for different assemblages. The blue star shows the peak metamorphic P-T conditions, red contours are biotite (X_{Mg}) isopleths while blue contours are garnet (X_{Ca}) isopleths. The estimated temperature and pressure are ~630°C and ~4.5 kbar respectively

Figure 69 shows a pseudo-binary diagram predicting the P-T condition of metamorphism for sample MC013. The yellow polygon represents a region of TD predictable mineral assemblages which are similar to the observed mineral assemblages in sample MC013. The observed

assemblage in micropetrography consist of garnet, biotite, feldspar and quartz which is stable at temperature and pressure greater than 440°C and 2 kbar respectively.

The two mineral phases biotite and garnet where in equilibrium with Fe and Mg exchange between them. This paragenesis was used for thermobarometry of sample MC013. Biotite X_{Mg} isopleths are between 0.41 and 0.46 while garnet X_{Mg} isopleths are within the range of 0.03 and 0.08. Metamorphic peak was at 580°C with pressure of 3.5 kbar determined from X_{Mg} of biotite and garnet contour intersections within the stability field. The unit underwent a prograde metamorphism which involved the following reaction chlorite/biotite + muscovite + quartz + plagioclase = garnet + biotite + plagioclase2 + H2O. Prograde metamorphism is observed in micropetrography of sample MC013 which show garnet porphyroblasts containing inclusions of biotite and quartz from which the garnet grew.

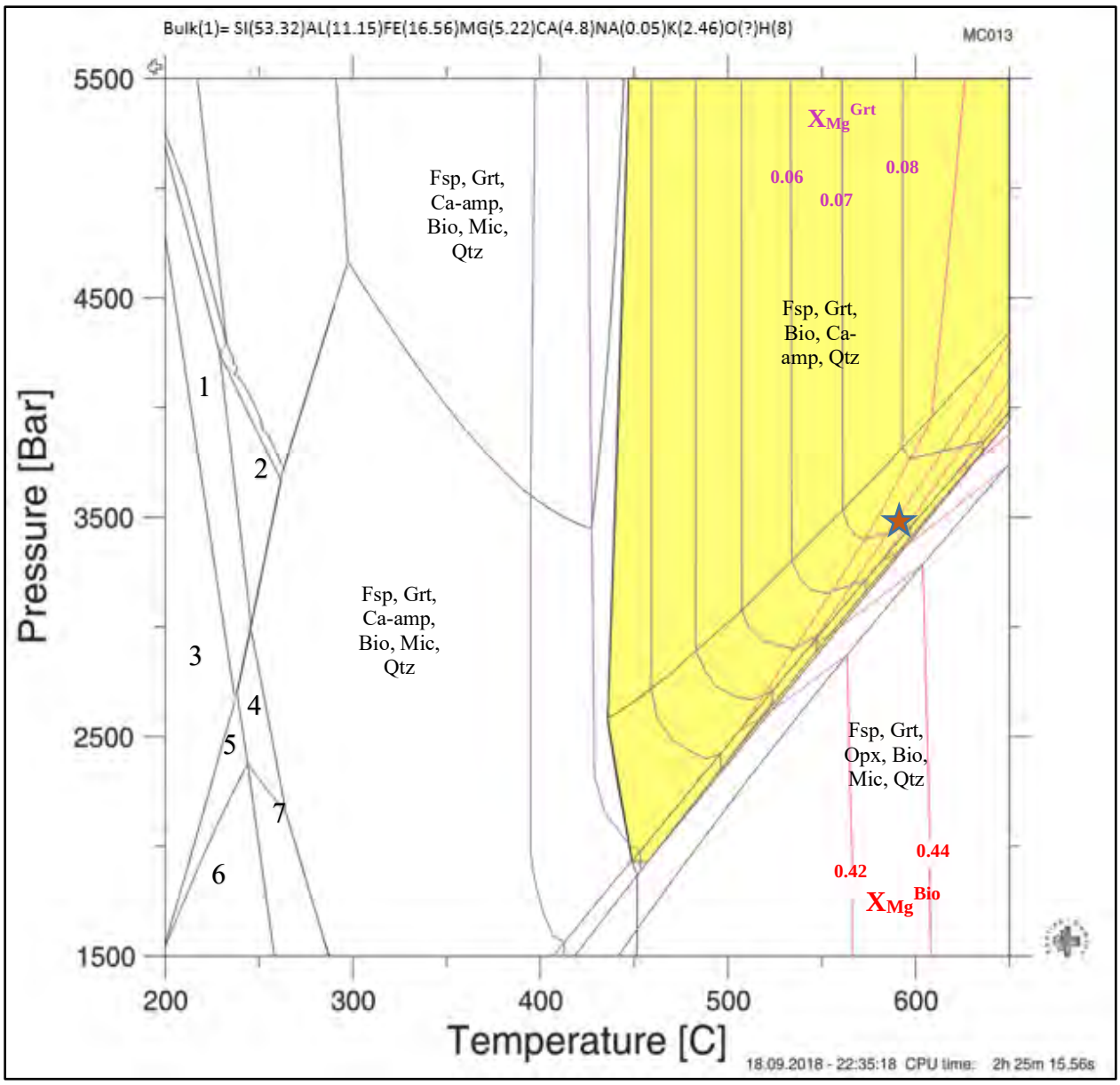

Key	
1= Grt, Bio, Ca-Amp, Mic, Qtz	4= Fsp, Grt, Chl, Bio, Mic, Qtz
2= Grt, Bio, Ca-Amp, Qtz	5= Fsp, Grt, Opx, Bio, Fanth, Mic, Qtz
3= Grt, Bio, Ca-Amp, Fanth, Mic, Qtz	6= Fsp, Grt, Opx, Bio, Ca-Amp, Fanth, Mic, Qtz
	7= Fsp, Grt, Opx, Bio, Ca-Amp, Mic, Qtz

Figure 69: Multi-phase equilibria diagrams for MC013. The highlighted yellow polygon shows peak metamorphic assemblages while black are boundaries for different assemblages. The blue star shows the peak metamorphic P-T conditions, the red lines show isopleths for biotite while garnet ones are lilac. Temperature of equilibration is 580°C with pressure at 3.5 kbar.

Figure 70 shows peak P-T metamorphic condition for MC012. The yellow outline shows a region with stable mineral assemblages. Biotite isopleth are indicated by red lines while the green lines shows anorthite isopleths. Biotite X_{Mg} isopleths are between 0.63 and 0.69 while plagioclase_anorthite isopleths are within the range of 0.18 and 0.23. The temperature and pressure

are based on Anorthite (X_{An}) and biotite X_{Mg} isopleth intersection determined by THERIAK DOMINO multiphase equilibria diagram (Figure 70). The low temperature and pressure being 270˚C and 3.4 kbar respectively are anorthite XAn and biotite XMg isopleth intersection. The temperature and pressure are very low to assume any equilibration. The estimated Temperature and Pressure of 270°C and 3.4 kbar respectively are invalid, biotite and anorthite were not in equilibrium at very low pressure while garnet was not observed.

The thermometry results (Table 15 and Table 16) show wide temperature range from 445°C to 615°C (Holland and Blundy, 1994). Amphibole-feldspar thermometry results were based on Holland and Blundy (1994) Metamorphic peak temperature was between 570°C and 610°C with an estimated pressure of 4.3 kbar.

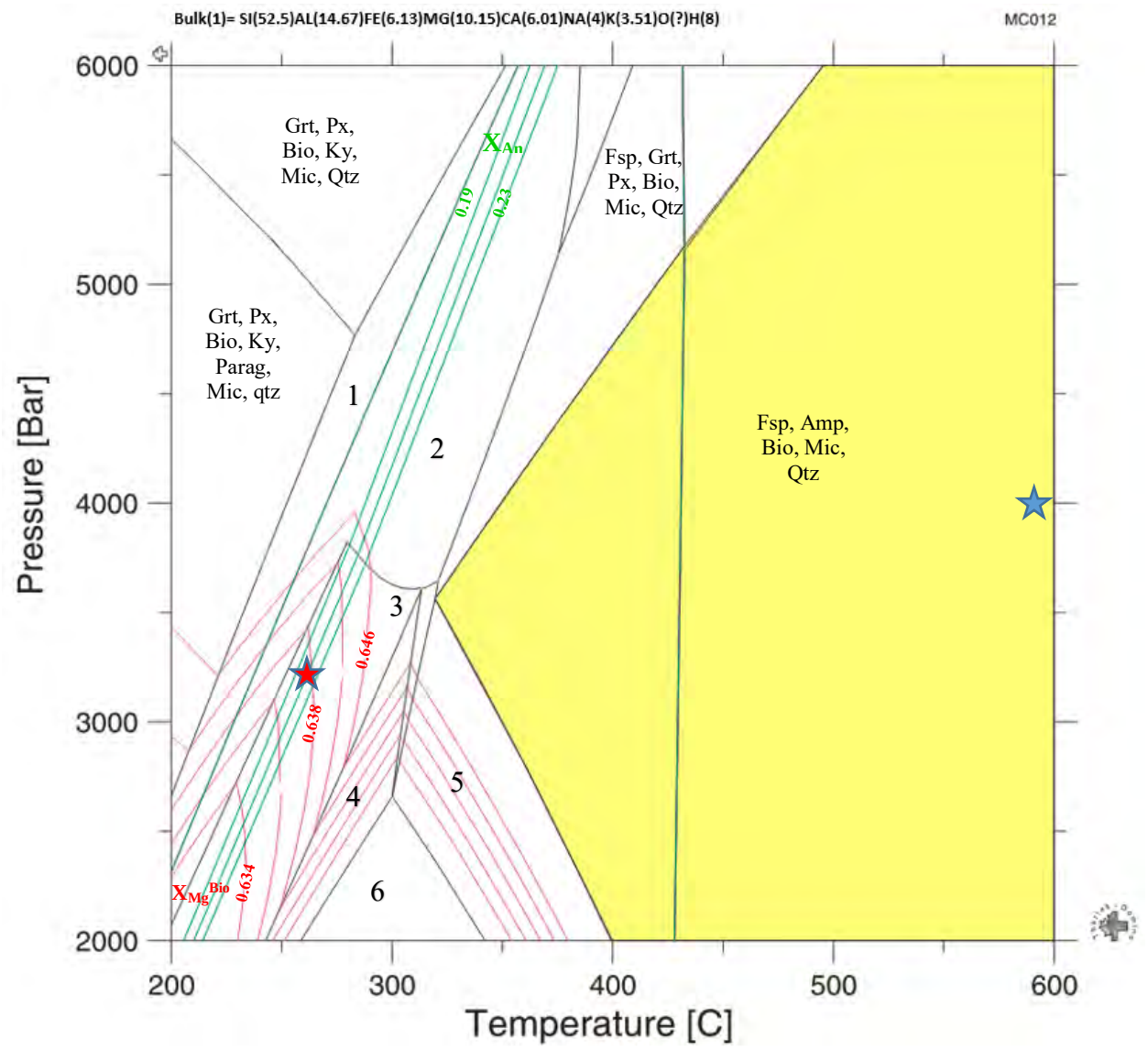

Key	
1= Grt, Bio, Ky, parg, mic, qtz	4= Fsp, Parg, Grt, Bio, Ca-Amp, Mic, Qtz
2=Fsp, Grt, Bio, Parg, mic, qtz	5= Fsp, Px, Bio, Ca-Amp, Mic, Qtz
3=Fsp, Grt, Bio, Ca-Amp, parg, Mic, Qtz	6= Fsp, Px, Bio, Mic, Qtz

Figure 70: Multiphase equilibria diagram for sample MC012. The yellow polygon shows observed peak metamorphic assemblages based on micropetrography. The blue star indicates the peak metamorphic P-T conditions with the temperature of equilibration being between 570°C and 610°C and estimated pressure of 4 kbar based on Holland and Blundy (1994). The red lines show isopleths for biotite while anorthite are in lilac intersecting at pressure and temperature of 270°C and 3.4 kbar respectively.

6. DISCUSSION

6.1 STRATIGRAPHY

The Domes Region in the Zambezi area is characterised by rocks of the Basement and Katanga Supergroups. The Basement Supergroup units include feldspathic quartzites, gneisses, meta-granites and schists which underlie the Katanga Supergroup. The outcrop geometry of the Basement Supergroup is in agreement with the dome-like structure of the Domes Region on the eastern Lufilian Arc. The contact between the Katanga and Basement Supergroups are marked by thrust faults and abrupt lithological changes. Thrusting within the Zambezi area is commonly identified by repetition of units and zones marked by brecciated rocks and massive ironstones. The Lower and Upper Roan Groups overlie the Basement Supergroup. These are commonly thin, or absent, unlike in the eastern and central Lufilian Arc, where they are thicker and more consistently present. Other stratigraphic units overlying the Basement Supergroup are the Grand Conglomerate Formation and the Mwashia Group.

The Grand Conglomerate Formation and the Mwashia Group are the most extensive and could be the thickest of the Katanga stratigraphic units in the Zambezi area (Figure 14). However, the true thickness of the Grand Conglomerate Formation is difficult to establish as it lacks primary structures and has gradational contacts. The apparent thickness of the Grand Conglomerate in the Zambezi area of ~400 m (Table 2) is similar to what has been reported in some of the areas in Democratic Republic of Congo (Wendorff, 2009). This is not the case of the eastern Lufilian Arc where the Grand Conglomerate Formation is thinner and has thicknesses ranging from 10 to 100 m (Selley et al. 2005; Wendorff and Key, 2009; Wendorff, 2009).

The Grand Conglomerate Formation is a key stratigraphic marker and was used in placement of other stratigraphic units. Understanding and placement of other stratigraphic units was based on identifying marker units such as the extensive Grand Conglomerate Formation and ironstones. All other stratigraphic units are placed below and above marker units. The stratigraphic levels as observed in KAY001 and NDD006 (Table 3 and Table 4) imply that towards the centre of basement domes stratigraphic units tend to be thinner.

The stratigraphic succession of the Zambezi area and that of the eastern and central Lufilian Arc are similar. The observed rocks in the Zambezi area comprise of both those of the Basement and

Katanga Supergroups. The rocks of the Basement Supergroup are gneisses and meta-granites (Figure 71). The rocks of the Lower Roan Group in the Zambezi area and those of eastern copperbelt have hematite bands with alteration minerals such as phlogopite. The upper stratigraphic units are similar (Figure 71). However, those of the Zambezi area have abundant phlogopite, biotite amphiboles and garnet commonly in the Grand Conglomerate Formation and the Mwashia Group.

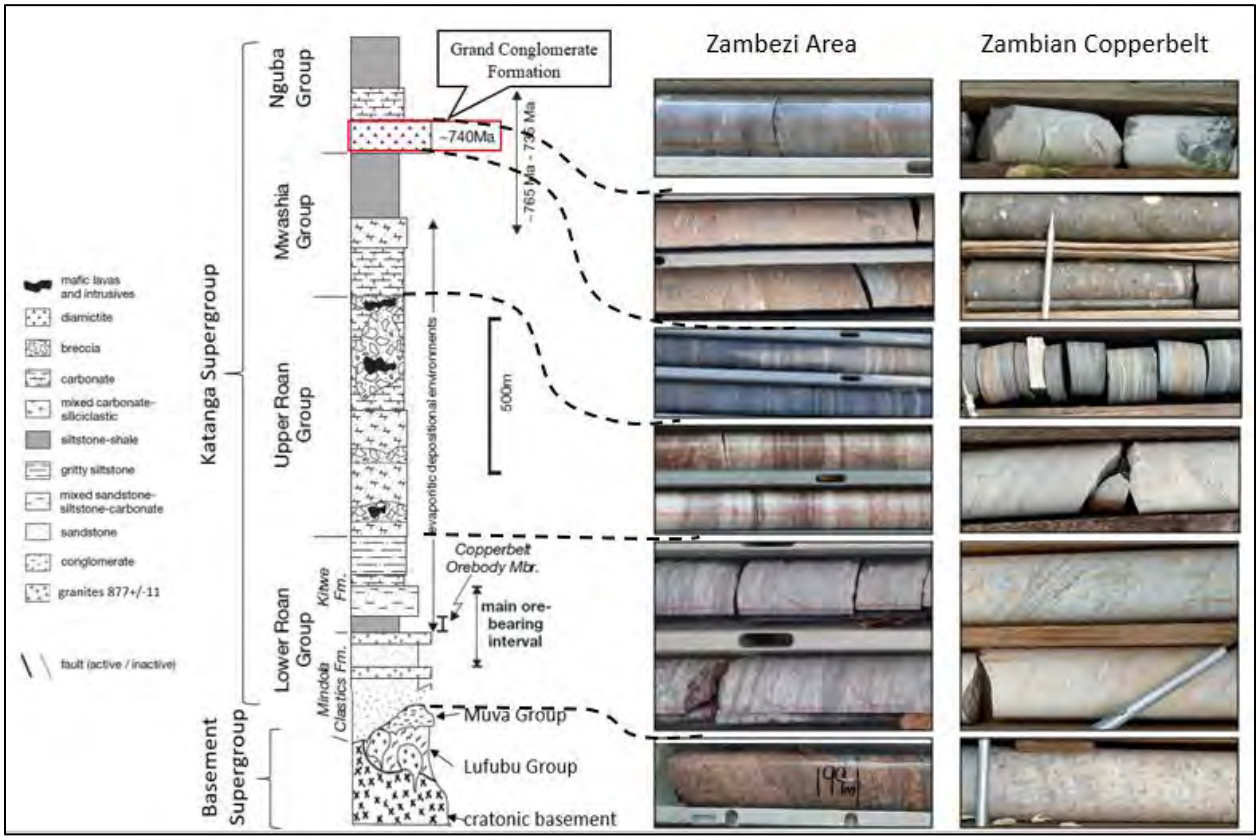

Figure 71: Stratigraphic succession of the Katanga Supergroup and the basement with corelating photographs of the Zambezi area and the eastern and central Zambian Copperbelt (modified after Selley et al., 2005).

6.2 DEFORMATION AND METAMORPHISM

Rock units within the Zambezi area have been sheared, faulted and folded with multiple deformation phases. Within units of the Katanga, there are a minimum of two phases of deformation identified in core and petrography attributed to the Lufilian Orogeny as observed also by Kampunzu and Cailteux. (1999). D1 is marked by the S1 foliation of muscovite and chlorite in MC004 though rarely marked by biotite in some units (Figure 25). D1 was likely responsible for

the development of the large-scale map patterns. D1 was probably associated with an event that formed the northeast-southwest trend within western arm of the Lufilian Arc (Kampuzu and Cailteux, 1999). A post D1 brecciation mostly within the Upper Roan Group is characterised randomly oriented fragments. S1 fabric is present in the fragments, but this internal foliation has random orientations which is due to brecciation. Accordingly, the brecciation post-dated the formation of S1 fabric.

The S1 foliation is also preserved as internal trails within garnets, which indicates the presence of S1 prior and during garnet growth (Figure 45, Figure 46 and Figure 58). The younger helicitic texture in garnet indicates syn kinematic growth. In the current case there might be a younger overprint that rotated the garnet with its inclusion trails. This is consistent with the observation of Turlin et al. (2016). Turlin et al. (2016) further suggests cleavage planes wrapped around late-D1 porphyroblasts being associated to the late phase of D1.

Within the drill core, there were neither lineation measured nor hinge line orientations obtained from fold closures. Hence, the geometry and associated transport directions related to D1 have not been determined.

The most significant sulphide mineralisation is pyrite and pyrrhotite which is spatially associated with S1 foliations. Sulphides occur along the S1 foliation trend as stringers and disseminations (Table 1) but are not observed along S0 planes. This suggests a post-diagenetic precipitation or remobilisation of sulphide mineralisation during D1. Within the Lumwana area, foliation delineated by oriented mineral inclusions of micas, graphite and Cu-sulphides such as bornite and chalcopyrite assemblages is interpreted to represent the metamorphic paragenesis developed during the prograde part of the P–T path (Turlin et al. 2016). The observed sulphides associated to D1 event in the Zambezi area are different from those in the Lumwana area which contains Cu and though associated to the same event.

The second deformation event is marked by S2 foliations, which are predominantly defined by aligned biotite and plagioclase. The S2 foliation is sub-parallel to F2 fold hinge surface (Figure 25) suggesting both to be related to D2. Clasts within the Grand Conglomerate are stretched along S1 and are commonly offset along S2 foliations as shown in Figure 25. Stretched and folded clasts within the GC accounts for D1 and D2 events respectively. The S2 foliation, folding and thrusting

within the Zambezi area are associated to D2 which is related to Pan African event that is responsible for folding, refolding and thrusting within the Lufilian Arc (Key et al, 2001; Kampuzu and Cailteux, 1999). There are other features associated with D2, which include asymmetric folds within KAY001. These folds commonly have high amplitude fold closures (Figure 26). Folds in KAY001 have NE-plunging fold hinge lines, which suggest syn- or post- D2 event.

Quartz-carbonate veins with or without pyrite commonly cut across the S1 fabric which suggests being post S1 development. Since veins crosscut S1 but get deformed and disrupted during D2 (Figure 28). Undeformed veins are also observed cross cutting D2 fabric. Hence, most veins and pods were emplaced post D1 episodes. Flattening and stretching of veins also formed pinch-and-swell structures of veins (Figure 29). Hydrothermal veining within the rocks might have taken place in multiple episodes or over longer time intervals, starting during the prograde heating and lasting until the retrograde stage.

Anthophyllite porphyroblasts in MC003 is as the result of post-D2 event, it is characterised by S2 biotite foliation inclusions within the porphyroblasts (Figure 37). Anthophyllite grew when initial S2 foliation was already present. Anthophyllite is most likely to have grown as the result of retrograde metamorphism of the garnet biotite dolomite schist of the Grand Conglomerate. Within the same rock sample, garnets are also post-D2 event marked by concordant matrix material with those in the porphyroblasts (Figure 38). Katangan amphiboles are mostly anthophyllite and are post-tectonic, whereas garnets are commonly syn and post-tectonic (Figure 46 and Figure 58).

The D3 deformation fabric which is hardly described elsewhere on the Lufilian Arc was not observed on the rocks within the Zambezi area. The last deformation phase D3 is not well developed on the eastern and central Lufilian Arc, however, it is associated to transversal folding (Kampuzu and Cailteux, 1999). The D3 event probably did not affect much of the structural geometry of Zambezi area and could not be identified in rocks. Post-D2 event might be responsible for retrograde metamorphism of the Katanga and the Basement Supergroup units to greenschist facies with foliation characterised by chlorite and retrogressed garnet to biotite (Figure 42).

6.3 MINERAL AND BULK COMPOSITIONS

The macro and micro-petrographic studies are summarised in the ternary diagrams that characterise bulk rock compositions and metamorphic mineral assemblages varying as a function

of rock composition (Figure 72 and Figure 73). The ACF diagram is plotted from molar proportion of the bulk rock composition, it suggests the rocks from the Katanga Supergroup being more pelitic while those of the Basement Supergroup are quartz-feldspathic with minor pelitic composition (Figure 72). The minerals in equilibrium from the Basement Supergroup are plotted on the ternary diagram which include biotite, hornblende and feldspar. However, there are other minerals observed in petrographic analysis but were not analysed by EDS to determine the mineral chemistry. There are presence of minor muscovite, chlorite and quartz (Figure 60) in the Basement Supergroup rocks which most likely reacted to form biotite and amphibole.

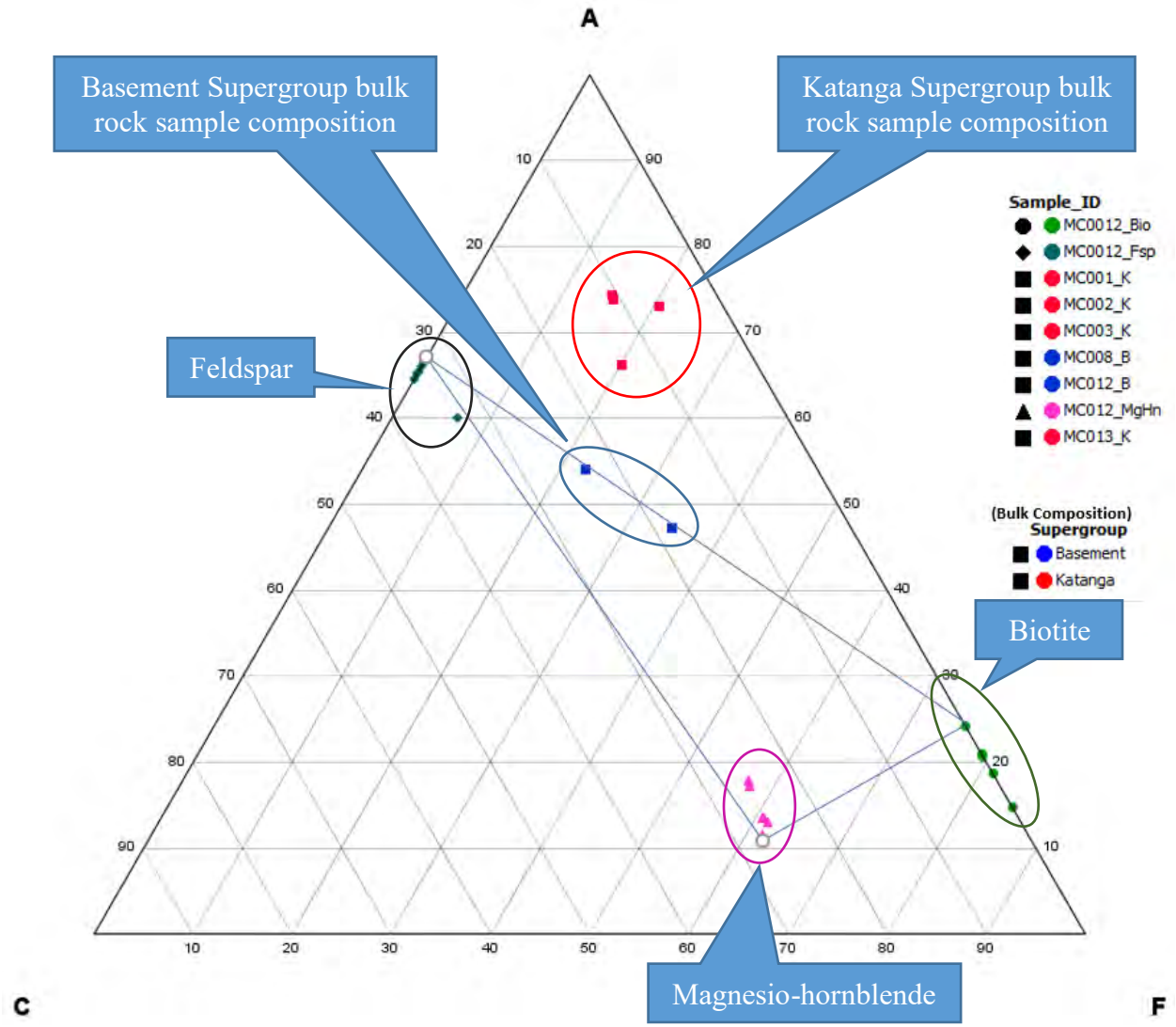

Figure 72: ACF diagram showing the bulk composition of the Basement and Katanga Supergroups plotted from mole proportions. The Katanga Supergroup samples represented by red points are more pelitic while those of the Basement Supergroup which are represented by blue points are quartz-feldspathic with minor pelitic. The mineral assemblages in equilibrium are those from the Basement Supergroup. The amphibolite facies mineral phases present and are in equilibrium are those observed in micropetrography include biotite, hornblende and feldspar. MC012_MgHn=magnesio-hornblende; MC012_Fsp=feldspar; MC012_Bio=biotite; MC001-3_K=Katangan bulk composition; MC008 and 12=Basement bulk composition; A=Al_2O_3 + Fe_2O_3 - (Na_2O+ K_2O), C=CaO - 3.3 P_2O_5; F=FeO + MgO (+ MnO)

The AFM diagram in Figure 73 shows the bulk compositions of both the Katanga and Basement Supergroup rocks with different mineral assemblages. The AFM diagram has been used to illustrate compositions of both the pelitic and quartz-feldspathic rocks of the Katanga Supergroup and the Basement Supergroup respectively. These are plotted on the same AFM diagram because

of the similar metamorphic conditions that the rocks underwent. The mineral phases in a ternary diagram from rocks of the Basement Supergroup consist of biotite, magnesio-hornblende and probably an aluminosilicate. The mineral phases from rocks of the Katanga Supergroup consist of biotite, garnet and anthophyllite.

Staurolite was only observed in micropetrography (Figure 56) with its element concentrations not measured. There could be aluminosilicate as suggested by the AFM diagram where by it was in equilibrium with biotite and magnesio-hornblende. However, magnesio-hornblende is a more dominant observed phase within the Basement Supergroup rocks.

The phases that represent the Katanga Supergroup bulk rock compositions are garnet, biotite and iron rich phases such as hematite (Figure 73). These mineral phases in equilibrium were in similar proportions for samples MC002 and MC003 while samples MC001 and MC013 are biotite and garnet rich.

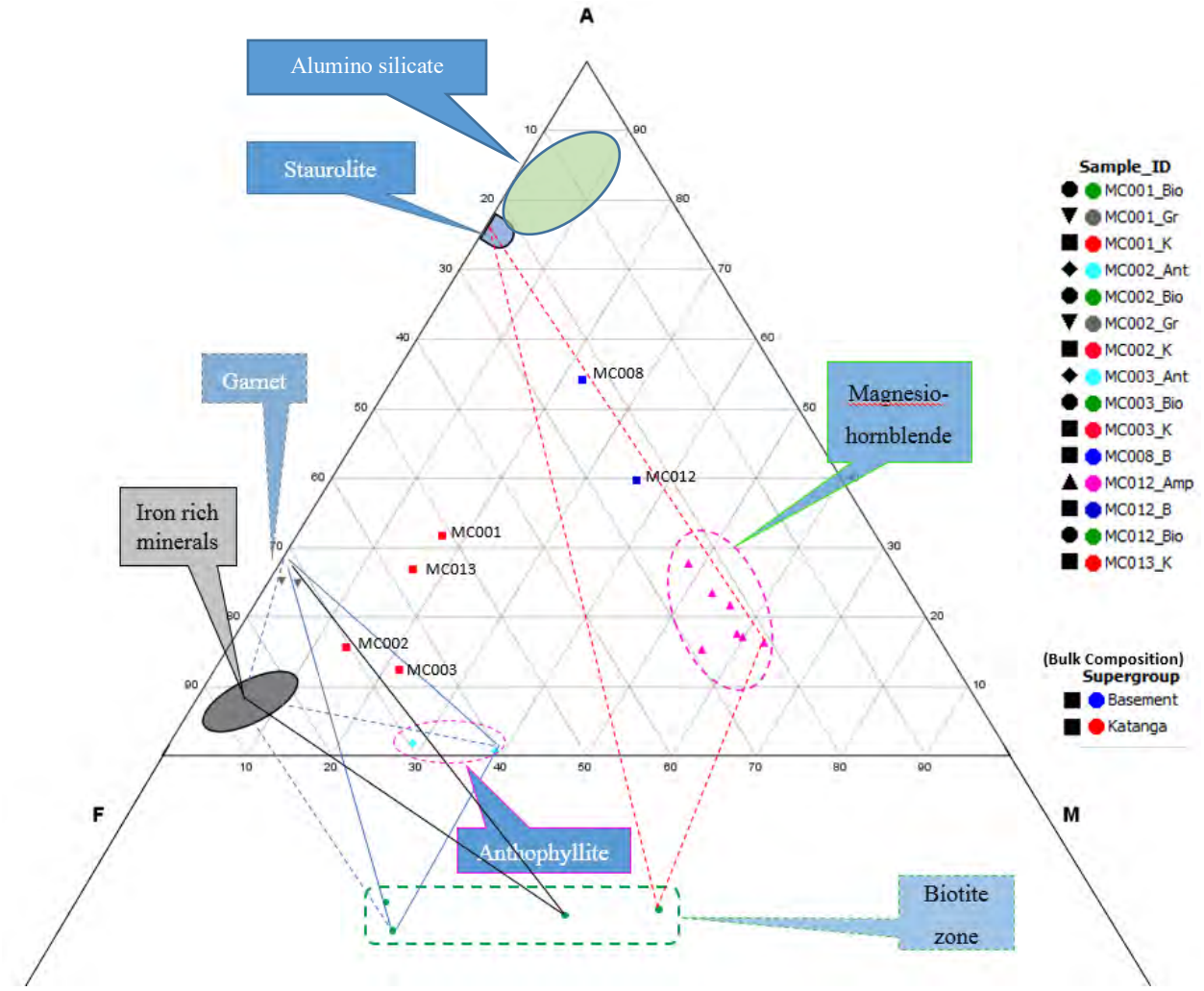

Figure 73: AFM diagram projected from muscovite representing bulk compositions of the Basement and Katanga Supergroup rock samples and mineral assemblages. The red square represents the bulk composition of samples from the Katanga Supergroup while those in blue represents bulk rock samples from the Basement Supergroup. The red triangle shows staurolite, biotite and amphibole equilibrium assemblages in amphibolite facies with temperature between 550°C and 600°C at an average pressure of ~4.3 kbar. The solid blue triangle represents variable tri-variant equilibrium mineral assemblages for most likely prograde metamorphic mineral reactions. The prograde metamorphism to form garnet and biotite is indicated by blue hashed lines involving garnet, biotite and iron rich minerals. The retrograde reaction of biotite to form anthophyllite at low temperature of 445°C is represented by blue triangle with solid and hashed lines.

The mineral assemblages in equilibrium have preserved material that reveal more details about mineral growth and their chemistry. It is observed that the sample MC002 consist of carbonate that occur as inclusions in both amphibole and garnet porphyroblasts. Since these porphyroblasts are formed at higher temperature and pressure to accommodate carbonate minerals, it can be inferred

that carbonatisation was an earlier event which could be from hydrothermal processes or the carbonate was primary. However, garnet has more carbonate inclusions than amphibole.

Garnet growth history can be deduced from its zonation, inclusions and composition (Finlay and Kerr, 1979). Mn zoning in garnet with depleted rim and increased concentration towards the core forming a bell shape (Figure 61) was earlier described by Hollister (1966) as a continuous Rayleigh fractionation during garnet growth. However, Mn content in garnet of sample MC001 decrease towards the rim and is mirrored by increasing Fe (Table 9), this has been described as a common prograde zonation (Andersen, 1984). Ca generally shows either slight increase from the core to the rim of the garnet (Figure 61) or a constant concentration (Table 9). Mg contents decreases slightly from the rim to the core of the garnet (Table 9). There was neither further subsequent equilibration nor crystallisation of the garnet as suggested by its zonation. MC001 shows to be a prograde growth zonation with core being spessartine. The most probable prograde reaction involved chlorite + muscovite + quartz + plagioclase to form garnet + biotite + plagioclase2 + H_2O as suggested by Andersen (1984) and the mineral assemblage observed in Figure 35.

Generally, garnets are high in iron contents which is common in metapelites and as such, almandine is the common solid solution phase (Figure 74). Within MC001, spessartine and almandine content in garnet core is similar which was the initial solid solution, further garnet growth resulted in depleted spessartine content and higher almandine. Grossular content was on average similar and attributed to continuous flow of calcic metasomatic fluid or presence of calcite during growth which is also observed as carbonate inclusions in element map (Figure 61). There is no observed garnet zonation in sample MC003 (Figure 36 and Figure 62). The element distribution in garnet from the core to the rim (Figure 62) is similar suggesting a single stage garnet growth for sample MC003.

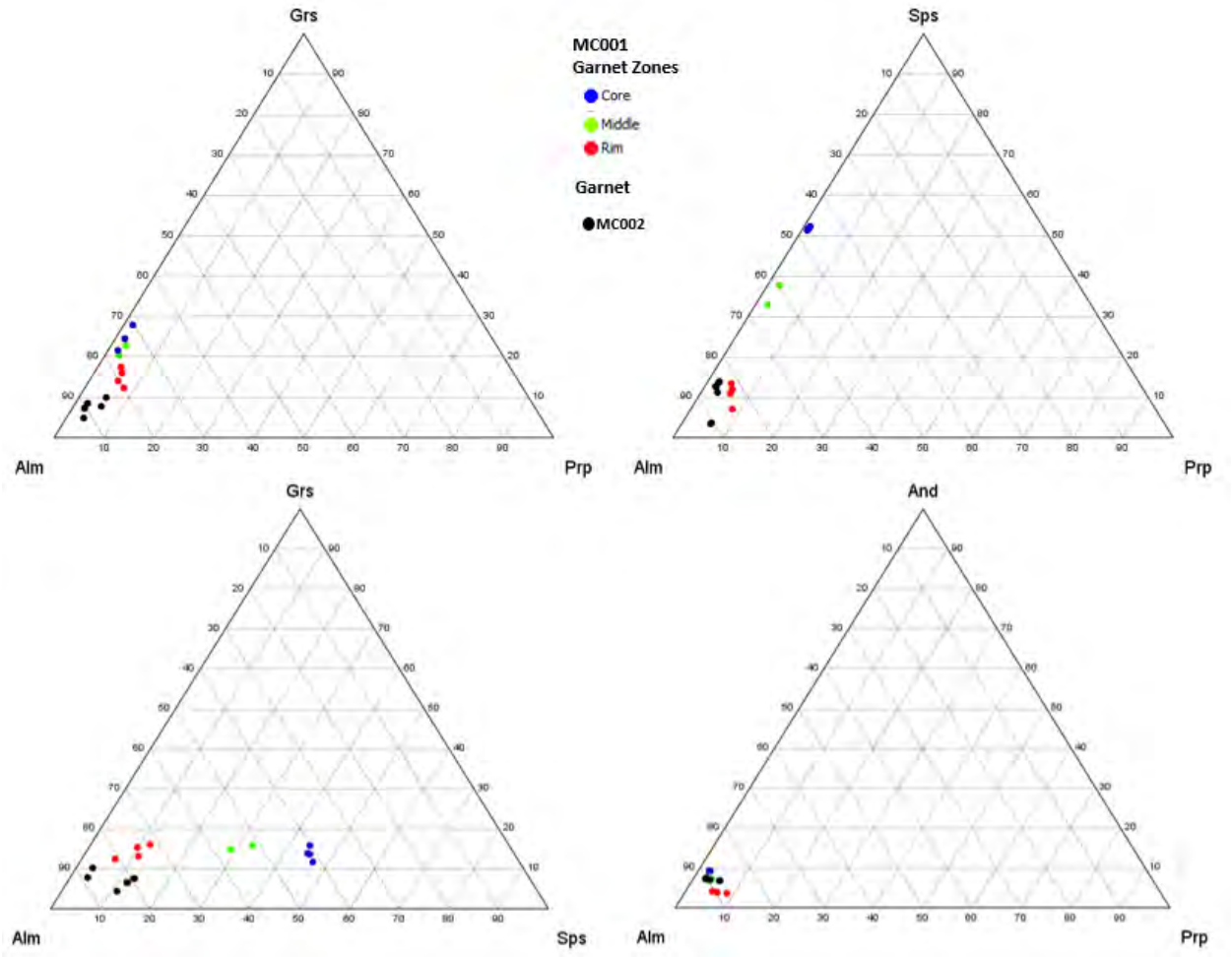

Figure 74: Ternary plots of garnet endmembers for samples MC001 and MC002. Almandine is the dominant solid solution phase in sample MC002 and the core of MC001. Garnet from sample MC001 is zoned and each zone has variable endmember contents. Towards the rim of garnet in sample MC001, spessartine and grossular contents gradually increase relative to pyrope contents.

Mineral phases in Katangan stratigraphy are mostly higher in Fe. Biotite from both the Katanga and Basement Supergroups plot within the re-equilibrated biotite suggesting all biotite to be metamorphic origin (Figure 75). Generally, annite content in biotite is high except for MC001 where annite is 50 and phlogopite is also 50. MC002 phlogopite content is 30 and annite 70. Within MC003 phlogopite is 40 and annite is 60 which is similar to MC013 with phlogopite being 35 while annite is 65. The trend of higher Fe content in garnet and biotite is also observed in anthophyllite. This is the common trend for Fe rich metapelites such as the Mwashia Group and the Grand Conglomerate Formation.

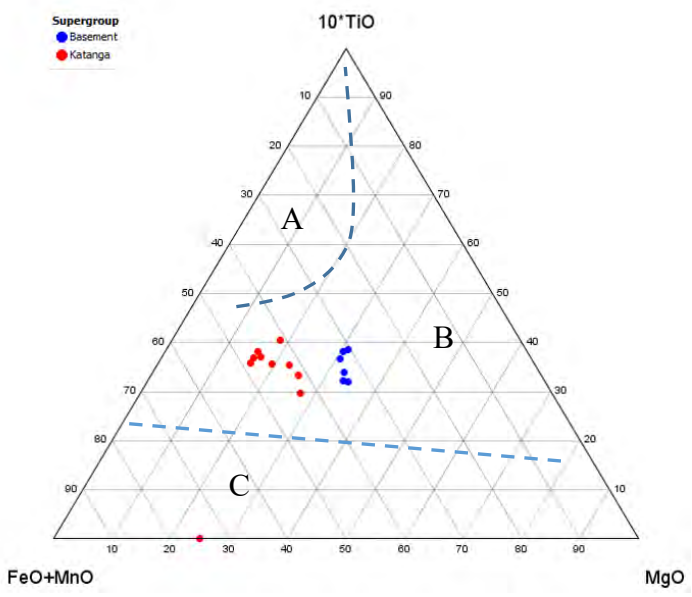

Figure 75: Biotite composition in the 10xTiO_2, FeO+MnO and MgO ternary plot. Limits of the domain, A=primary magmatic biotite, B=re-equilibrated biotite and C=secondary biotite (after Nachit et al. 2005). MnO are very low for all samples being <0.40 wt(%).

Biotite analysed from the Katanga Supergroup except two samples have X_{Mg} ratio less than 0.5 (Table 13). In contrast, analysis of biotite at Lumwana by Turlin et al. (2016), X_{Mg} are greater than 0.55 making the biotite at Lumwana Mg rich and classified more as phlogopite. The absolute Fe contents in biotite of the Katanga Supergroup at the Zambezi area show that it is twice the abundance of Mg in the Lumwana area. The biotite from the Basement Supergroup rocks in the Zambezi area has similar Fe content to that of the Lumwana area. The Ti content in the Zambezi area is approximately 25% more abundant than that of Lumwana. The conditions under which Katanga Supergroup biotite formed at the Zambezi area would appear to be significantly different from that of the Lumwana area. Similarly, the garnet analysed from the Katanga Supergroup in the Zambezi area has high Fe oxide total contents ranging between 32% and 35% while that of Lumwana area ranges between 30% and 32% (Turlin et al., 2016). The variation in biotite and garnet Mg content affects the biotite-garnet thermometry results.

The chemistry of amphibole is distinct for each stratigraphic zone, Katangan anthophyllite are Mg poor (Table 12) while the Basement Supergroup magnesio-hornblende (Table 16) are Mg rich. This is because of variable protolith composition. Amphiboles within the schists of the Grand Conglomerate have low X_{Mg} ratios ranging between 0.20 and 0.36.

6.4 P-T CONDITIONS

The general metamorphic P-T condition within the Zambezi Area shows that both the Katanga (MC003 and MC013) and the Basement Supergroup (MC012) rocks to have reached the amphibolite facies (Figure 76). The Katanga Supergroup rocks were retrogressed to greenschist facies with average pressure of 4.5 kbar during an isobaric cooling. It is very common that the retrogressed metamorphic pressure condition is similar to that of the metamorphic peak condition. Figure 76 shows the general thermobarometry observation using THERIAK/DOMINO and other modelling approach. There are three clusters of P-T conditions observed in the rocks with the highest being greenschist and amphibolite facies (Figure 76).

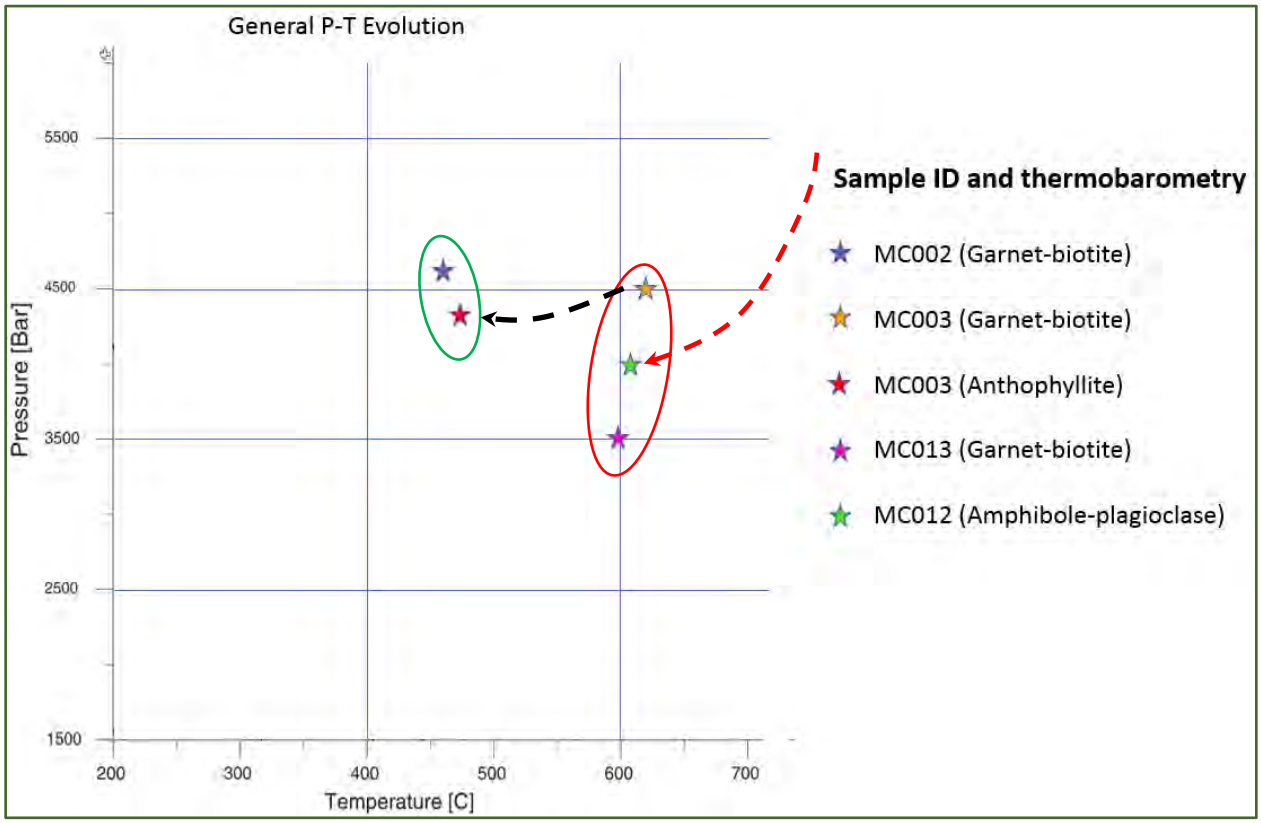

Figure 76: Reconstructed metamorphic P-T condition of the Zambezi area. The rocks from the Basement Supergroup (MC012) and those of the Katanga Supergroup (MC003 and MC013) have similar metamorphic temperature condition but slight variation in pressure conditions. Both the Basement and the Katanga Supergroup rocks reached the amphibolite facies with retrogressive metamorphism observed in Katangan Rocks indicated by black hashed line. The red hashed line shows hypothetical retrogressive P-T path of the Basement Supergroup not observed.

The Grand Conglomerate Formation within drill hole KAY001 (Table 3) underwent to upper greenschist facies estimated by THERIAK/DOMINO P-T equilibrium phases. In sample MC002

from drill hole KAY001, the temperature of metamorphism is estimated at 470°C with a pressure of ~4.7 kbar. It is observed that slight variation in X_{Mg} shifts the equilibrium phases, and this could be attributed to very low X_{Mg} in the garnet. The variation in slight X_{Mg} concentration could have affected the thermometry results and variation in results obtained by different thermobarometry methods. X_{Ca} is higher than $X_{Mg,}$ in garnets, X_{Ca} isopleths were used in THERIAK/DOMINO P-T analysis, which narrowed the P-T window and produced better results.

Temperature estimate using garnet-biotite thermometry by Hodges and Spear. (1982), metamorphic temperature range of sample MC002 is between 435°C and 540°C. However, the closest results to the THERIAK/DOMINO thermodynamic modelling is applying (Bhattacharya, et al., 1992) garnet-biotite thermometry with temperature ranging from 433°C to 488°C. The variable temperature range by comparing different methods is attributed to methods and assumptions used for equilibrium reactions. Generally, all three methods suggest a temperature range defined within the method by Hodges and Spear (1982).

Anthophyllite thermometry estimate of sample MC003 based on Holland and Blundy (1994) suggests a temperature of 445°C. This is lower than that of biotite and garnet thermobarometry determined by THERIAK/DOMINO (Figure 68) which suggest a temperature of formation at ~630°C. Anthophyllite grew after D2 (Figure 37) at the lower temperature of metamorphism than the D2 mineral assemblages such as garnet and prograde biotite.

The stable field equilibrium assemblages estimated by THERIAK/DOMINO (Figure 68) have pyroxene, this could have been replaced by amphiboles during retrograde hydration reaction although this was not observed in micropetrography. The assumption is that the remaining pyroxene might have been too small or uncommon to be identified in micro-petrography.

MC013 underwent a lower metamorphic grade than MC003. The peak temperature for MC013 was ~580°C with a very low pressure of 3.4 kbar. MC013 was sampled from a drill hole (NDD0010) located near the Basement Supergroup dome and basalt (Figure 14).

Sample MC003 shows both the amphibolite facies and upper greenschist facies which is observed in MC013 and MC002 respectively. The Katangan rocks in two different areas show different conditions of metamorphism. On the eastern within drill hole number KAY001 appears to show

retrograde upper greenschist facies condition of ~470°C at a pressure between 4.0 and 4.5 kbar. The other area around drill hole NDD0010 records a peak metamorphism up to mid amphibolite facies with temperatures between 570°C and 630°C and pressure of 4.8 kbar. Metamorphic temperatures recorded in the Lumwana area in Zambia within the central Lufilian Arc during development of the D2 paragenesis are similar, between 580 and 620 ± 50 °C (Turlin et al., 2016). The peak metamorphic conditions estimated in Sample MC003 around the Zambezi area and those around the Lumwana area are similar.

The peak assemblage of the Basement Supergroup is mid amphibolite facies reaching temperature of ~600°C at a pressure of ~4.3 kbar. The X_{Mg} ratios for amphibole are high, ranging from 0.59 to 0.70, which is common for rocks within mid to high amphibolite facies. The Basement Supergroup and the Katanga Supergroup were metamorphosed to a similar extent, however retrograde metamorphism is observed within both the Katanga and the Basement Supergroups.

The highest temperature of metamorphism (620 ± 50°C) within the central Lufilian Arc (Figure 77) are those recorded by Turlin et al. (2016). This is similar to the slightly higher temperature of formation (~630°C) in the Katanga Supergroup rocks of the Zambezi area (Figure 77). Generally, the extent of metamorphism increases from the east to the west and remains constant from the central to the western Lufilian Arc in the Zambezi area.

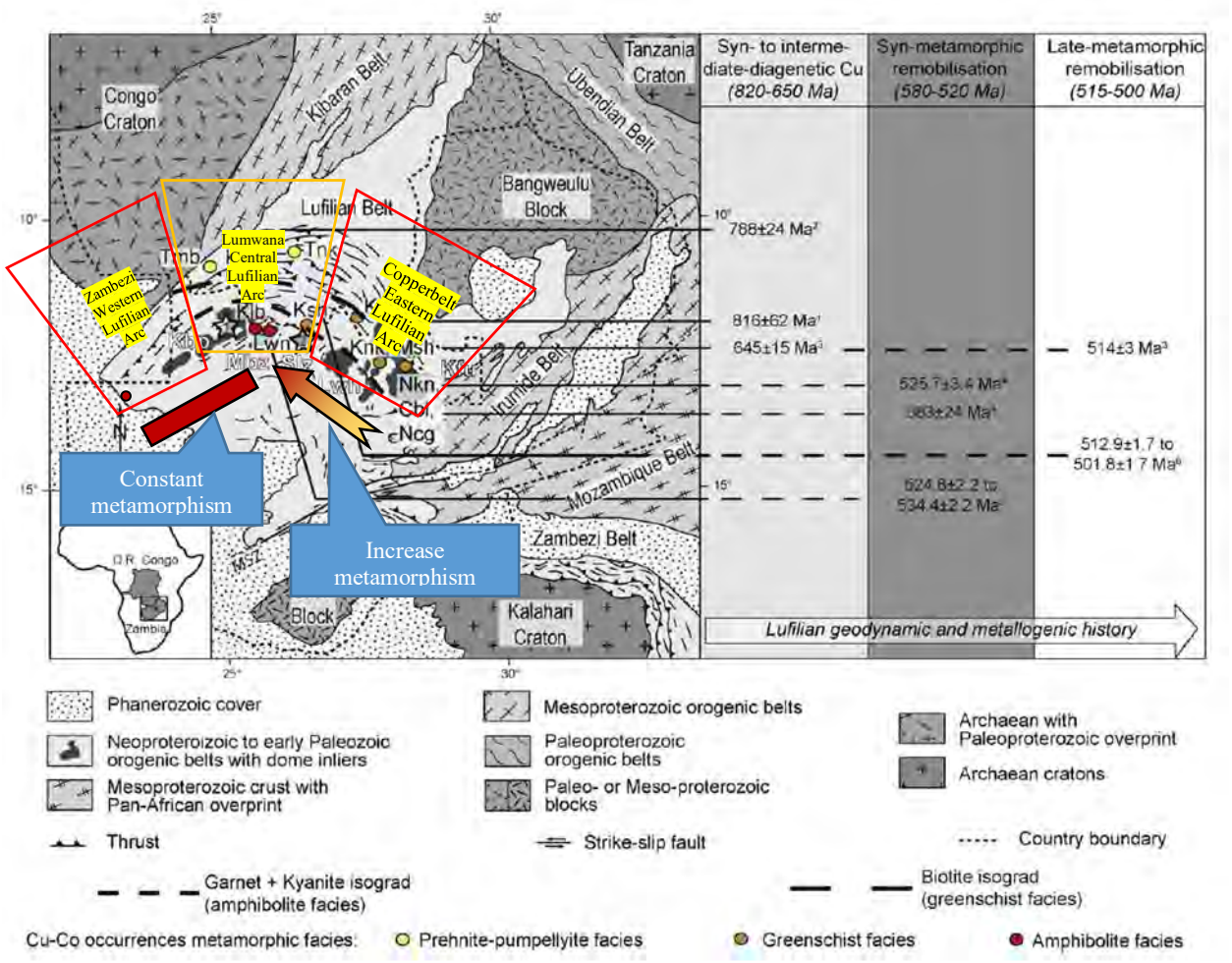

Figure 77: Lufilian Arc, other Pan-African mobile belts, cratons, associated geology, metamorphic facies and geochronological constraints, Cu-Co occurrences and their interpreted stage of emplacement. Lufilian arc divided into eastern, central and western part with increase in metamorphism from eastern to central and constant from central to western (modified after Turlin et al., 2016).

7. CONCLUSION

The Zambezi area is underlain by the extensive and thick Grand Conglomerate Formation and Mwashia Group of the Katangan Supergroup. The Basement Supergroup units occur as dome features wrapped by metamorphosed Katanga Supergroup. The rocks from the Katanga Supergroup more pelitic consisting of biotite, anthophyllite and quartz while those of the Basement Supergroup are quartz-feldspathic with minor pelitic composition.

The rocks in the Zambei area were affected by D1 which is associated with an event that formed the northeast-southwest trend within western arm of the Lufilian Arc. The D2 later event is responsible for the formation of S2 foliation, folding and thrusting within the Zambezi area. This is associated to the Pan African event that is responsible for folding, refolding and thrusting within the Lufilian Arc. The D3 event did not affect much of the structural geometry of Zambezi area and could not be identified in rocks of the western Lufilian Arc in the Zambezi area.

Modelling using of THERIAK/DOMINO, the metamorphism reached up to upper greenschist and the peak mid amphibolite facies (MC003, MC012 and MC013). The retrograde greenschist facies temperature conditions is ~470°C and pressure of 4.7 kbar (MC002) while the amphibolite facies reached temperatures between 590°C and 630°C with average pressure of 4.0 kbar. Different thermometry methods for biotite-garnet suggests a wider range of temperature between 430 °C and 630 °C.

The Basement Supergroup has reached the amphibolite facies with peak metamorphism between 570 °C and 610 °C at a pressure of 4.3 kbar. Biotite, anthophyllite and garnet phases are mostly iron rich and range from ~15% to 36% FeO total.

Generally, the extent of metamorphism within the Lufilian Arc increases from the east to the central and remains constant from the central to the western Lufilian Arc in the Zambezi area

Further work that would add value would be:

- To do more petrographic studies that would give further details of other mineral assemblages that might be similar to those of the central Lufilian Arc and compare the mineral chemistry.

- To do a detailed stratigraphic study on new drill cores and generate a detailed stratigraphic map that would be very useful to understand the stratigraphy such as other Groups and Formation within the western Lufilian Arc. Isotope geochemistry would be very useful to correlate carbonate rocks as carbon and oxygen isotopes are distinct for each carbonate rich Group within the Katanga Supergroup.
- To determine the metamorphic ages so that key events are correlated with regional metamorphic events of the Lufilian Arc in Zambezi area.
- To conduct detailed structural measurements within inclined holes that intersects the Katanga Supergroup. This would be very useful to generate the structural geometry of the area

REFERENCES

Andersen, T. B., 1984. Inclusion patterns in zoned garnets from Magerøy, north Norway. Mineralogical Magazine, v. 48, p. 21–26.

Anthony, J. W., Bideaux, B. A., Bladh, K. W., and Nichols, M. C., 2005. Eds., Handbook of Mineralogy, Mineralogical Society of America, Chantilly, VA 20151–1110, USA. http://www.handbookofmineralogy.org/ (Accessed from January 2017 to May 2019).

Armstrong, R. A., Robb, L. J., Master, S., Kruger, F. J., and Mumba, P. A. C. C., 1999. New U-Pb age constraints on the Katangan Sequence, Central African Copperbelt: Journal of African Earth Sciences, Special Abstracts Issue, GSA 11: Earth Resources for Africa, v. 28, p. 6–7.

Armstrong, R., Master, S., and Robb, L., 2005. Geochronology of the Nchanga granite, and constraints on the maximum age of the Katanga Supergroup, Zambian Copperbelt. Journal of African Earth Sciences, v .42(1), p. 32–40.

Batumike, J. M., Cailteux, J., and Kampunzu, A. B., 2006. Petrology and geochemistry of the Neoproterozoic Nguba and Kundelungu Groups, Katangan Supergroup, southeast Congo: Implications for provenance, paleoweathering and geotectonic setting. Journal of African Earth Sciences v. 44 p. 97–115

Bhattacharya, A., Mohanty, L., Maji, A., Sen, S. K., and Raith, M., 1992. Non-ideal mixing in the phlogopite-annite binary: constraints from experimental data on Mg−Fe partitioning and a reformulation of the biotite-garnet geothermometer. Contributions to Mineralogy and Petrology, v. 111, Issue 1, p 87–93.

Binda, P. L., 1994. Stratigraphy of Zambian Copperbelt orebodies: Journal African Earth Sciences. v. 19, p. 251–264.

Binda, P. L., and van Eden, J. G., 1972. Sedimentological evidence on the origin of the Precambrian Great Conglomerate (Kundelungu Tillite), Zambia: Palaeogeography, Palaeoclimatology, Palaeoecology, v. 12, p. 151–168.

Bodiselitsch, B., Koeberl, C., Master, S. and Reimold, W. U., 2005. Estimating Duration and Intensity of Neoproterozoic Snowball Glaciations from Ir Anomalies: Science, v. 308, p. 239–242.

Bull, S., Selley, D., Broughton, D., Hitzman, M., Cailteux, J., Large, R., and McGoldrick, P., 2011. Sequence and carbon isotopic stratigraphy of the Neoproterozoic Roan Group strata of the Zambian copperbelt. Precambrian Research 190 (2011) p. 70– 89.

Bumby, A. J., and Guiraud, R., 2005. The geodynamic setting of the Phanerozoic basins of Africa. Journal African Earth Sciences v 43 p. 1–12.

Büttner, S. H., 2012. Rock Maker: an MS Excel spreadsheet for the calculation of rock compositions from proportional whole rock analyses, mineral compositions, and modal abundance. Mineral. Petrol. v. 104, p. 129–135.

Cailteux, J., Binda, P., Katekesha, W. M., Kampunzu, A. B., Intiomale, M. M., Kapenda, D., Kaunda, C., Ngongo, K., Tshiauka, T. and Wendorff, M. 1994. Lithostratigraphic correlation of the Neoproterozoic Roan Supergroup from Shaba (Zaire) and Zambia, in the central African copper-cobalt metallogenic province: Journal of African Earth Sciences, v. 19, p. 265–278.

Cosi, M., De Bonis, A., Gosso, G., Hunziker, J., Martinotti, G., Moratto, S., Robert, J. P., and Ruhlman, F., 1992. Late Proterozoic thrust tectonics, high-pressure metamorphism and uranium mineralization in the Domes area, Lufilian arc, northwestern Zambia: Precambrian Research, v. 58, p. 215–240.

Daly, M. C., Chakraborty, S. K., Kasolo, P., Musiwa, M., Mumba, P., Naidu, B., Nameteba, C., Ngambi, O., and Coward, M. P., 1984. The Lufilian arc and Irumide belt of Zambia: Results of a geotraverse across their intersection: Journal of African Earth Sciences, v. 2. p. 311–318.

Daly, M., 1986. Crustal shear zones and thrust belts: Their geometry and continuity in Central Africa. Royal Society of London Philosophical Transactions Series A, 317, p. 111–127.

de Capitani, C., and Brown, T. H., 1987. The computation of chemical equilibrium in complex systems containing non-ideal solutions. Geochim. Cosmochim. Acta 51,2639–2652.

De Waele, B., and Fitzsimons, I. C., 2004. The age and detrital fingerprint of the Muva Supergroup of Zambia: Molassic deposition to the southwest of the Ubendian Belt. Conference abstract, Geoscience Africa 2004, Johannesburg, South Africa, p. 162−163.

Downie, J. R., 1968. Prospecting Operations in the Balovale Concession. Chartered Exploration Limited. Occasional Report Number 34.

Finlay, C. A., and Kerr, A. 1979. Garnet growth in metapelite from Moinian rocks of northern Sutherland, Scotland. Contribution to Mineralogy and Petrology. v. 71, p. 185–91.

Fleischer, V., 1984. Discovery, geology and genesis of copper-cobalt mineralization at Chambeshi southeast Prospect, Zambia. Precambrian Research, v. 25(1), p. 119–133.

Garlick, W. G., 1961. Muva System, in Mendelsohn, F., ed., The Geology of the Northern Rhodesian Copperbelt, London, MacDonald, p. 523.

Hancock, P. L., 1994. Continental deformation: Oxford, Pergamon, ix, p. 421.

Hanson, R. E., 2003. Proterozoic geochronology and tectonic evolution of southern Africa: Geological Society of London Special Publication, v. 206, p. 427–463.

Hanson, R. E., Wardlaw, M. S., Wilson, T. J., & Mwale, G. 1993. U-Pb zircon ages from the hook granite massif and mwembeshi dislocation: Constraints on pan-African deformation, plutonism, and transcurrent shearing in central Zambia. Precambrian Research, v. 63(3). p. 189–209.

Hanson, R. E., Wilson, T. J., and Munyanyiwa, H., 1994. Geologic evolution of the Neoproterozoic Zambezi orogenic belt in Zambia: Journal of African Earth Sciences, v. 18, p. 135–150.

Hitzman, M. W., Broughton, D. W., Selley, D., Woodhead, J., Wood, D. and Bull, S., 2012. The Central African Copperbelt: Diverse Stratigraphic, Structural and Temporal Settings in the World's Largest Sedimentary Copper District. Society of Economic Geologists, Inc, Special Publications 16, p. 487–514.

Hitzman, M., Kirkham, R., Broughton, D., Thorson, J., and Selley, D., 2005. The sediment-hosted stratiform copper ore system. Society of Economic Geologists, 100th Anniversary Volume, p. 609–642.

Hodges, K. V., Spear, F. S., 1982. Geothermometry, geobarometry and the Al2SiO5 triple point at Mt. Moosilauke, New Hampshire. Mineralogical Society of America American Mineralogist. v. 67 p. 1118–1134.

Holland, T. and Blundy, J., 1994. Non-ideal interactions in calcic amphiboles and their bearing on amphibole-plagioclase thermometry. Contribution to Mineralogy and Petrology. v. 116, p, 433–-47.

Holland, T. and Powell, R., 2011. An improved and extended internally consistent thermodynamic dataset for phases of petrological interest, involving a new equation of state for solids. Journal of Metamorphic Geology, v. 29, p. 333–383.

Hollister, L.S., 1966. Garnet zoning: An interpretation based on the Rayleigh fractionation model. Science, v. 154, p. 1647–1651.

Jackson, M. P. A., Warin, O. N., Woad, G. M., and Hudec, M. R., 2003. Neoproterozoic allochthonous salt tectonics during the Lufilian orogeny in the Katangan Copperbelt, central Africa: Geological Society of America Bulletin, v. 115, p. 314–330.

John, T., Schenk, V., Mezger, K., and Tembo, F., 2004. Timing and P-T evolution of whiteschist metamorphism in the Lufilian arc-Zambezi belt orogeny (Zambia): Implications for the assembly of Gondwana: Journal of Geology. v. 122, p. 71–90.

Johnson, S. P., De Waele, B., Evans, D., Banda, W., Tembo, F., Milton, J. A., and Tani, K., 2007. Geochronology of the Zambezi supracrustal sequence, southern Zambia: a record of Neoproterozoic divergent processes along the southern margin of the Congo Craton. Journal of Geology. v. 115. p. 355–374.

Kampunzu, A. B., and Cailteux, J., 1999. Tectonic evolution of the Lufilian Arc central Africa Copperbelt during Neoproterozoic pan African orogenesis. Gondwana Research, p. 2401–2421.

Key, R. M., Liyungu, A. K., Njamu, F. M., Somwe, V., Banda, J., Mosley, P. N., and Armstrong, R. A., 2001. The western arm of the Lufilian arc in NW Zambia and its potential for copper mineralization: Journal of African Earth Sciences, v. 33, p. 503–528.

Loughlin, W., 1979. The geology of the Luma river area. Rep. Geol. Surv. Zambia, No. 87.

Master, S., and Wendorff, M., 2011. Neoproterozoic glaciogenic diamictites of the Katanga Supergroup, Central Africa. Geological Society, London, Memoirs 2011; v. 36; p. 173–184.

Master, S., Rainaud, C., Armstrong, R. A., Phillips, D., and Robb, L. J., 2005. Provenance ages of the Neoproterozoic Katanga Supergroup (Central African Copperbelt), with implication of basin evolution. Journal of African Earth Sciences, 42, p. 41–60.

Mendelsohn, F., ed., 1961. The geology of the Northern Rhodesian Copperbelt: London, MacDonald.

Nachit, H., Ibhi, A.B., EI.-H., and Ben Ohoud, M., 2005. Discrimination between primary magmatic biotite, reequilibrated biotites, and neoformed biotites: Cmptes Rendus Gésciences, v. 337, p. 1415–1420.

Porada, H., 1989. Pan-African rifting and orogenesis in Southern to Equatorial Africa and Eastern Brazil: Precambrian Research. p. 103–136.

Porada, H., and Berhorst, V., 2000. Towards a new understanding of the Neoproterozoic-early Palaeozoic Lufilian and northern Zambezi belts in Zambia and the Democratic Republic of Congo: Journal of African Earth Sciences, v. 30, p. 727–771.

Rainaud, C., Master, S., Armstrong, R. A., and Robb, L. J., 2005. Geochronology and nature of the Palaeoproterozoic basement in the Central African Copperbelt (Zambia and the Democratic Republic of Congo), with regional implications. Journal of African Earth Sciences, v. 42, p. 1–31.

Selley, D., Broughton, D., Scott, R., Hitzman, M., Bull, S., Large, R., McGoldrick, P., Croaker, M., Pollington, N., and Barra, F., 2005. A New Look at the Geology of the Zambian Copperbelt. Economic Geologists. 100th Anniversary Volume, p. 965–1000.

Torrealday, H. I., Hitzman, M. W., Stein, H. J., Markley, R. J., Armstrong, R., and Broughton, D., (2000). Re-Os and U-Pb Dating of the Vein-Hosted Mineralization at the Kansanshi Copper Deposit, Northern Zambia: Economic Geology, v. 95, p. 1165–1170.

Turlin, F., Eglinger, A., Vanderhaeghe, O., Andre-Mayer, A., Poujol, M., Marcadier, J., and Bartlett, R., 2016. Synmetamorphic Cu remobilization during the Pan-African orogeny: Microstructural, petrological and geochronological data on the kyanite-micaschists hosting the Cu–U Lumwana deposit in the Western Zambian Copperbelt of the Lufilian belt. Ore Geology Reviews v. 75 p. 52–75.

Wendorff, M., 2003. Stratigraphy of the Fungurume Group–evolving foreland basin succession in the Lufilian fold-thrust belt, Neoproterozoic–Lower Palaeozoic, Democratic Republic of Congo. South African Journal of Geology, v. 106, p. 17–34.

Wendorff, M., 2005. Sedimentary genesis and lithostratigraphy of Neoproterozoic megabreccia from Mufulira, Copperbelt of Zambia. Journal of African Earth Sciences. v. 42. p. 61–81.

Wendorff, M., and Key, R. M., 2009. The relevance of the sedimentary history of the Grand Conglomerate Formation (Central Africa) to the interpretation of the climate during a major Cryogenian glacial event. Precambrian Research 172 p. 127–142

Williams-Jones, A. E., Samson, I. M., and Olivo G. R., 2000. The genesis of hydrothermal fluorite-REE deposits in the Gallinas Mountains, New Mexico. Economic Geology. v. 95, p. 327–341.